

# **PARTICULATE SYSTEMS FOR FLUORESCENCE IMAGING AND DRUG DELIVERY**

**Dissertation zur Erlangung des Doktorgrades der  
Naturwissenschaften (Dr. rer. nat)**

**an der Naturwissenschaftlichen Fakultät IV  
– Chemie und Pharmazie –  
der Universität Regensburg**



**vorgelegt von Cornelia Rose**

**Oktober 2010**







Diese Doktorarbeit entstand in der Zeit von Oktober 2005 bis Oktober 2009 am Lehrstuhl für Pharmazeutische Technologie der Universität Regensburg.

Die Arbeit wurde angeleitet von Prof. Dr. Achim Göpferich.

Promotionsgesuch eingereicht am: 12. Oktober 2010

Mündliche Prüfung am: 03. Dezember 2010

Prüfungsausschuss:	Prof. Dr. S. Elz	(Vorsitzender)
	Prof. Dr. A. Göpferich	(Erstgutachter)
	Prof. Dr. Torsten Blunk	(Zweitgutachter)
	Prof. Dr. J. Heilmann	(Drittprüfer)

*„Das tragische an jeder Erfahrung ist, dass man sie erst macht, nachdem man sie gebraucht hätte.“*

Friedrich Wilhelm Nietzsche, Philosoph (1844-1900)

## Table of Contents

Abbreviations	6
Variables and units	7
 <b>Chapter 1 Introduction</b>	
1. Particulate Drug Delivery Systems	11
2. Imaging of Drug Delivery Systems	14
2.1 Principals of Fluorescence	14
2.2 The Fluorescence Probe	15
2.3 Fluorescence Imaging Techniques	17
2.4 Fluorescence Imaging of Drug Delivery Systems	18
3. Goals of the thesis	20
4. References	22
 <b>Chapter 2 Nanoprecipitation – Preparation of monodisperse polymeric nanoparticles</b>	
1. Introduction	31
2. Materials and Methods	33
2.1 Materials	33
2.1.1 Synthesis and characterization of biodegradable copolymers	33
2.1.2 Preparation and characterization of polymeric nanoparticles	33
2.1.3 Cell culture	33
2.2 Methods	34
2.2.1 Synthesis of diblock copolymer	34
2.2.2 Characterization of diblock copolymers	35
2.2.3 Preparation of polymeric nanoparticles	35
2.2.4 Freeze – thawing / freeze-drying experiments	36
2.2.5 Determination of particle size	37
2.2.6 Determination of zeta potential	37
2.2.7 Morphology of polymeric nanoparticles	37
2.2.8 Cell culture	38
2.2.9 Biocompatibility of polymeric nanoparticles	38
3. Results	40
3.1 Stabilization of colloidal systems during freeze-drying	40
3.2 The nanoprecipitation process – Investigation of process conditions	44
3.2.1 Impact of precipitation system	44
3.2.2 Impact of polymer concentration	45
3.2.3 Impact of ratio of volumes of polymer solution to external phase	46
3.2.4 Impact of stabilizer	46
3.2.5 Measurement of zeta potential	47

3.2.6	Morphology of nanoparticles – impact of precipitation system	48
3.2.7	Measuring particle size – impact of analytical method	49
3.2.8	Biocompatibility of polymeric nanoparticles	50
4.	Discussion	51
4.1	Stabilization of colloidal formulations during freeze-drying	51
4.2	The nanoprecipitation process – Investigation of process conditions	53
4.3	Particle cytotoxicity	57
5.	Summary and Conclusion	58
6.	References	59

### **Chapter 3    Fluorescing nanoparticles for imaging applications in cell culture and *in-vivo* animal experiments**

1.	Introduction	65
2.	Materials and Methods	66
2.1	Materials	66
2.1.2	Preparation and characterization of nanoparticles	66
2.1.2	Cell culture	66
2.1.3	<i>In-vivo</i> imaging	66
2.2	Methods	67
2.2.1	Preparation of fluorescing nanoparticles	67
2.2.2	Determination of particle concentration	67
2.2.3	Fluorescence spectroscopic analysis	67
2.2.4	Determination of particle size	68
2.2.5	Determination of zeta potential	68
2.2.6	Cell culture	68
2.2.7	Determination of biocompatibility	68
2.2.8	Imaging of cellular uptake of fluorescently labelled nanoparticles	69
2.2.9	<i>In-vivo</i> imaging of fluorescently labelled nanoparticles	69
3.	Results	72
3.1	Nile red loaded nanoparticles – PLGA	72
3.1.1	Effect of Nile red loading	72
3.1.2	Effect of the nanoprecipitation system	73
3.2	Nile red loaded nanoparticles – diblock copolymers	73
3.3	Biocompatibility of fluorescently labelled nanoparticles	75
3.4	Imaging of cellular uptake	77
3.5	<i>In-vivo</i> imaging	78
4.	Discussion	80
5.	Summary and Conclusion	88
6.	References	89



**Chapter 4     Synthesis and characterization of CdSe Quantum Dots  
as stable particulate fluorescence markers**

1.	Introduction	95
2.	Materials and Methods	97
2.1	Materials	97
2.2	Methods	97
2.2.1	Synthesis of CdSe Quantum Dots	97
2.2.2	Coating of CdSe Quantum Dots	97
2.2.3	Purification of the Quantum Dot dispersion	98
2.2.4	Spectroscopic analysis	99
2.2.5	Determination of nanocrystals size and molar concentration	99
2.2.6	Calculation of theoretical – UV-based amount of Cd and Se	101
2.2.7	Determination of real elemental Quantum Dot composition	101
2.2.8	Investigation of Quantum Dot morphology	102
3.	Results	103
3.1	Synthesis and characterization of CdSe Quantum Dots	103
3.2	Purification of CdSe Quantum Dots	105
3.3	Lipophilic coating of CdSe Quantum Dots	107
3.4	Quantification of CdSe Quantum Dots	108
4.	Discussion	111
5.	Summary and Conclusion	116
6.	References	117

**Chapter 5     Non-aqueous nanoprecipitation – A promising technique  
for the encapsulation of lipophilic Quantum Dots?**

1.	Introduction	123
2.	Materials and Methods	125
2.1	Materials	125
2.2	Methods	125
2.2.1	Preparation and characterization of CdSe Quantum Dot stock dispersion	125
2.2.2	Preparation and characterization of the QDot® 800 stock dispersion	125
2.2.3	Precipitation of Quantum Dot loaded nanoparticles	126
2.2.4	Determination of particle concentration	126
2.2.5	Fluorescence spectroscopic analysis of the nanoparticles	127
2.2.6	Determination of particles loading with CdSe Quantum Dots	127
2.2.7	Determination of particle sizes	128
2.2.8	Morphologic analysis of Quantum Dot loaded nanoparticles	128
3.	Results	129
3.1	PLGA based nanoparticles – the effect of loading	129
3.2	PLGA based nanoparticles – the effect of Quantum Dot coating	132

3.3	The effect of matrix material	133
3.4	Encapsulation of Qdot® 800	136
4.	Discussion	137
5.	Summary and Discussion	142
6.	References	143

## **Chapter 6     Quantum Dots as fluorescent marker for microparticulate drug delivery systems**

1.	Introduction	147
2.	Materials and Methods	149
2.1	Materials	149
2.1.1	Preparation and characterization of microparticles	149
2.1.2	Cell culture	149
2.2	Methods	150
2.2.1	Preparation and characterization of CdSe Quantum Dot stock dispersion	150
2.2.2	Standard preparation of polymeric microparticles	150
2.2.3	Standard preparation of lipid microparticles	151
2.2.4	Particle size determination	151
2.2.5	Imaging of particles surface morphology	151
2.2.6	Determination of loading with Quantum Dots	151
2.2.7	Confocal imaging of Quantum Dot loaded microparticles	153
2.2.8	Fluorescence spectroscopic analyses	153
2.2.9	Microparticles embedded in polymeric hydrogels	153
2.2.10	Cell culture	154
2.2.11	Biocompatibility of polymeric microparticles	154
3.	Results	155
3.1	Tailoring the particle size	155
3.2	Determination of encapsulation efficiency	156
3.3	Optical properties of Quantum Dot loaded microparticles	156
3.4	Morphologic characterization of Quantum Dot loaded microparticles	159
3.5	Biocompatibility of Quantum Dot loaded microparticles	160
4.	Discussion	162
5.	Summary and Conclusion	167
6.	References	168

## **Chapter 7     Overall summary and conclusions**

1.	Overall summary	173
2.	Conclusions and Outlook	175
3.	References	177

**Appendices**

<b>Appendix A</b>	Characterization of biodegradable copolymers	181
<b>Appendix B</b>	Characterization of dispersion media	189
<b>Appendix C</b>	Curriculum Vitae	195
	List of Publications	197
	Acknowledgements	199

**Erklärung**

## Abbreviations

ANOVA	Analysis of variances
API	Active pharmaceutical ingredient
APS	Ammonium persulfate
CCD	Charge-coupled Device
CEFB	p-(carboxyethylformamido)benzoic acid
CH <sub>2</sub> Cl <sub>2</sub>	Methylene chloride
CHCl <sub>3</sub>	Chloroform
CHO	Chinese hamster ovarien
CLSM	Confocal Laser Scanning Microscopy
CdO	Cadmium oxide
CdSe	Cadmium selenide
CdTe	Cadmium telluride
DDA	Dodecylamine
DDS	Drug Delivery System
DiR	1,1'-Diocadecyl-3,3',3'-tetramethylindotricarboyanine iodide
DMPC	Dimyristoyl-glycero-phosphocholine
DNA	Desoxyribonucleic acid
CO <sub>2</sub>	Carbon dioxide
e.g.	exempli grati
EMEM	Eagle's minimum essential medium
etc.	et cetera
FBS	Fetal bovine serum
Fig.	Figure
FITC	Fluoresceinisothiocyanat
ICP-OES	Inductively coupled plasma optical emission spectroscopy
i.e.	item est
i.v.	intravenous
LED	Light Emitting Diode
HNO <sub>3</sub>	Nitric acid
MCF-7	Michigan Cancer Foundation – 7 (breast cancer cell line)
MW / MW <sub>exp</sub>	Molecular weight / experimental determined molecular weight
MTT	3-[4,5-Dimethylthiazol-2-yl]-2,5- diphenyltetrazolium bromide
mPEG	Poly (ethylene glycol) monomethylether
N <sub>2</sub>	Nitrogen
NH <sub>2</sub> -PEG	Amine group terminated poly(ethylene glycol)
NIR	Near-infrared
NP	Nanoparticle
OA	Oleylamine
OPF	Oligo(poly(ethylene glycol)) fumarate
O/W	Oil/water emulsion

RES	Reticuloendothelial system
RITC	Rhodamine Isothiocyanate
p.a.	pro analysi / post administrationem (chapter 2)
PBS	Phosphate buffered saline
PC	Phosphatidylcholine
PCS	Photon correlation spectroscopy
PEG	Poly(ethylene glycol)-poly(lactic acid)
PI	Polydispersity index
PL	Photoluminescence
PLA	Poly(lactic acid)
PLGA	Poly(lactic acid co glycolic acid)
PVA	Polyvinylalcohol
QD/QDots	Quantum dots
QY	Quantum yield
SD	Standard deviation
SDS	Sodium dodecyl sulfate
SEM	Scanning electron microscopy
Tab.	Table
TAMRA-ANP	5,6-carboxytetramethylrhodamine labelled atrial natriuretic peptide
techn.	technical grade
TEM	Transmission electron microscopy
TEMED	N,N,N',N'-Tetramethylethylenediamine
TFA	Trifluoro acetic anhydride
THF	Tetrahydrofuran
TOP / TOPO	Trioctylphosphine / trioctylphosphine oxide
UV	Ultraviolet
vs.	versus
W/O(W)	Water/oil(/water) emulsion
ZnS	Zinc sulphide

## Symbols and units

A	Absorption
Å	Angstrom
a.u.	Arbitrary units
c	Concentration
°C	Degree Celsius
<i>d</i>	Diameter
Da	Dalton
$\epsilon_0$	Dielectric constant

## Abbreviations

---

$\epsilon_{ab}$	Decadic molar absorbance coefficient
$\lambda_a$	Lowest energy excitonic peak
$\lambda_{ab}$	Maximum absorption wavelength of organic fluorescence dyes
$\lambda_{em}$	Maximum emission wavelength
$h\nu_{EM}/h\nu_{EX}$	Emission/excitation light energy
K	Kelvin
kV	Kilovolt
$\mu$ l	Microliter
$\mu$ m	Micrometer
ml	Mililiter
mm	Milimeter
mmol	Milimol
min	Minutes
mPas	Mili pascal-second
nm	Nanometer
%	Percent
rpm	Rounds per minute
$\Phi$	Quantum yield
ppb	Part per billion
ppm	Parts per million
$T_G$	Glass transition temperature

# **Chapter 1**

## **Fluorescence based investigations of particulate drug delivery systems**

-

### **Introduction and Goals**





# 1. Particulate Drug Delivery Systems

The term 'particulate drug delivery system' is not exactly defined; moreover, it is used in association with a wide range of different systems with pronounced structural differences (**Fig. 1**). They could be categorized based on their internal and external structure (e.g. dissolved/dispersed drug molecules, solid or fluid particulate character) as well as the apparent size of the individual delivery system.

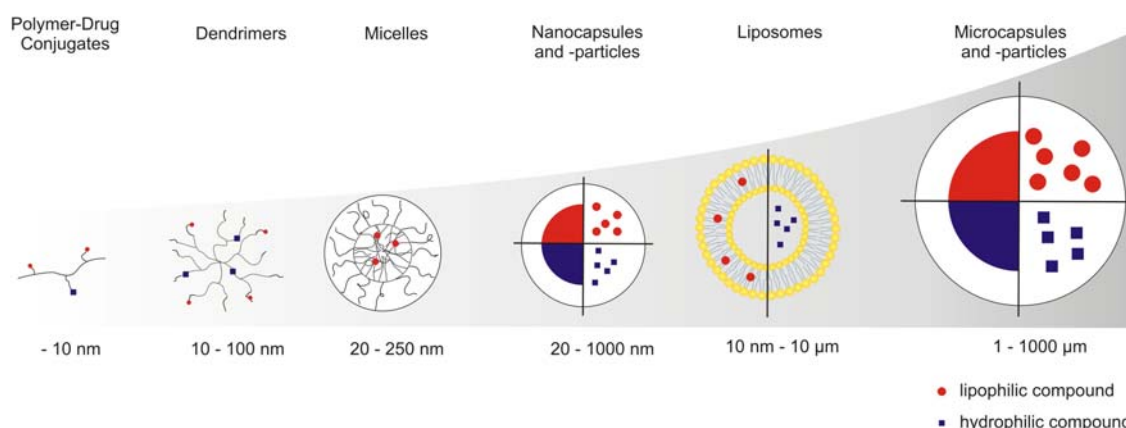


**Fig. 1:** Classification of particulate drug delivery systems

Particulate drug carriers are intended for the controlled delivery of active substances and the enhancement of their therapeutic performance, by tailoring either the release profile from the carrier, the carriers' biodistribution as well as the carrier uptake into certain tissues or cells [1-3]. They are used in oral, parenteral and also varying localized delivery applications (e.g. dermal, pulmonary, ocular or nasal) [1; 4-6]. From the huge variety of particulate systems the current overview will predominantly focus on solid micro- and nanoparticles based on organic compounds.

## Solid particulate carriers

The most versatile group of carriers are the solid DDS. Based on organic materials, such as polymers or lipids, they are termed micro- or nanoparticles irrespective of their exact interior and exterior structure [7]. However, in most cases the micro-/nanoparticles are delivery systems, where the active ingredient is more or less homogeneously distributed within the matrix material (either as solid solution or dispersed in individual crystals). The term 'micro-' or 'nanosphere' is thereby often used interchangeably, but would actually be restricted to strictly spherical systems. Particular systems (certain kind of subclass) are called 'micro-' or 'nanocapsules', where a single domain of an active ingredient is surrounded by the matrix material in a core-shell like structure [7] (**Fig. 1**).

Numerous scientific papers (including various reviews) deal with micro- and nanoparticles and their applications in different drug delivery approaches [3; 7-9]. Since the materials and methods used are quite similar for the preparation of both particle systems, the finally obtained size is predominantly determined by the applied process parameters such as the phase volume ratios or the homogenization of the intermediate emulsions.

Commonly used matrix materials (**Tab. 1**) are either of natural or synthetic origin and the choice of material will predominantly depend on the desired properties of the final product, but also on the compatibility of the used material with the encapsulated drug substance as well as the preparation process.

**Tab. 1:** Commonly used matrix materials for solid particles

Classification	Examples	
<u>Natural polymers</u>	Chitosan, sodium alginate, gelatine, albumine	[10-17]
<u>Synthetic biodegradable polymers</u>		
Polyesters and derivatives	Poly(lactic acid); poly(lactic acid-co-glycolic acid), poly( $\epsilon$ -caprolactone); copolymers and derivatives; poly(phosphor esters)	[4; 18-22]
Polyanhydrides	Poly (maleic acid), poly (fumaric anhydride-co-isophthalmic anhydride)	[23; 24]
Poly(phosphazenes)	Polydichlorophosphazene, poly [(p-methyl-phenoxy) (ethyl glycinate) phosphazene]	[25; 26]
Others	Poly (cyanoacrylate)	[27; 28]
<u>Synthetic non-biodegradable polymers</u>		
Acrylic polymers	N-isopropylacrylamide; copolymers of methacrylic acid and ethacrylic acid	[28-30]
Cellulose-based	Hydroxypropylmethylcellulose; ethylcellulose	[31; 32]
<u>Lipids</u>		
Esters of glycerol	Glycerol tripalmitate; glycerol trimyristate; glycerol behenate; glycerol monostearate	[33-35]
Fatty acids	Stearic acid; palmitic acid	[35; 36]

The applied preparation process will not only determine the resulting particle size, but moreover the achieved entrapment and release characteristics of the prepared DDS. Numerous different preparation procedures are available, which are usually optimized on a certain drug – matrix combination for a desired release kinetic [37].

The most frequently used methods are emulsion-based solvent evaporation processes, which combine a variety of different preparation stages generally including the formation of either a single (O/W or W/O) or different multiple emulsions (W/O/W etc.), which again strongly depend on the characteristics of the used matrix material and the encapsulated active substance [7; 38; 39].

Especially the applied emulsification technique (e.g. propeller or paddle stirrer, high shear homogenizer, high pressure homogenizer or ultrasound) will primarily determine the final particle size following the simple rule – the higher the applied shear stress the smaller the droplet and thus consequently the obtained particles, which is usually accompanied by a tightened particle size distribution [40-44]. Due to the variability and complexity of these technological procedures numerous factors affect the resulting particle properties (i.e. size, morphology, drug loading, internal drug distribution) and also the subsequent behaviour of the DDS (release, degradation). Some of the factors, described in literature, include: viscosity of the dissolved polymer phase (predominantly determined by molecular weight and concentration of the matrix material), initial loading with the active compound, the ratio of internal and external phase of the emulsion, the type and concentration of the used emulsion stabilizer in the external phase, the technique of solvent removal (determining the rate of solvent removal and the subsequent particles solidification) [35; 38; 40; 45-50].

Alternatively phase separation methods are used for the preparation of polymeric particles and include the frequently used manufacturing procedures, coacervation [51] and nanoprecipitation [52]. The essential phase separation and thus the precipitation of the polymer could be ideally achieved by changes of the solution pH, the addition of multivalent electrolytes or the interaction with oppositely charged polymers in case of hydrophilic polymers [53-56] or by thoroughly mixing an organic polymer solution with an appropriate miscible polymer non-solvent [37; 57]. The here described impact factors are the used polymer type, the viscosity of the non-solvent, the ratio of non-solvent to the internal polymer solution, the order of mixing and, if applicable, the applied stirring rate [32; 57-60].

Numerous other preparation methods have been developed for other DDSs, including for example spray drying [61; 62] and spray congealing [33], salting out of polymer precipitates [63], processes based on supercritical fluids [34], the emulsion polymerization of individual monomers [64], breaking down of bigger aggregates (e.g. by jet-milling) [65] or various so-called printing methods based on small volume droplet generators known from commercial inkjet printers [66; 67].

## 2. Imaging of Drug Delivery Systems

In general imaging is frequently used during development and characterization of new drug delivery systems. Moreover the still raising impact also becomes apparent in a current issue of the European Journal of Pharmaceutics and Biopharmaceutics on “Imaging techniques in Drug Development” [68]. The editors highlighted imaging techniques, allowing spatial and temporal analyses, as tools for the drug development, which enable researchers to “see and measure and not just believe” [69].

Available analytical methods differ basically in their signal used for the detection. The most frequently used optical imaging techniques are generally based on the interaction of electromagnetic radiation with a certain sample, resulting in changes in light properties, which are detectable as image contrast. In conventional light microscopes this contrast arises from variations of phase, absorbance, scattering, reflection or refraction of light by the sample [70]. Despite several approaches for further contrast enhancement (e.g. phase contrast, darkfield illumination) some drawbacks still limit the application of light microscopy [70]:

- Signal to background contrast often is quite low;
- Mapping of certain functional or even structural aspects is usually difficult;
- Lack of chemical specificity result in broad non-specific spectra.

By introducing more specific photochemical probes such limitations could be overcome. On the one hand contrast is enhanced by an increased interaction of the probe with the excitation light and furthermore, using probes with desirable high affinity to certain structures allow the mapping of specific features or processes of interest.

### 2.1 Principles of fluorescence

In this context, fluorescence is by far the most commonly used and versatile probe signal, resulting from a multistep process – the radiative de-activation of the lowest electronically excited singlet state (**Fig 2**) [70; 71].

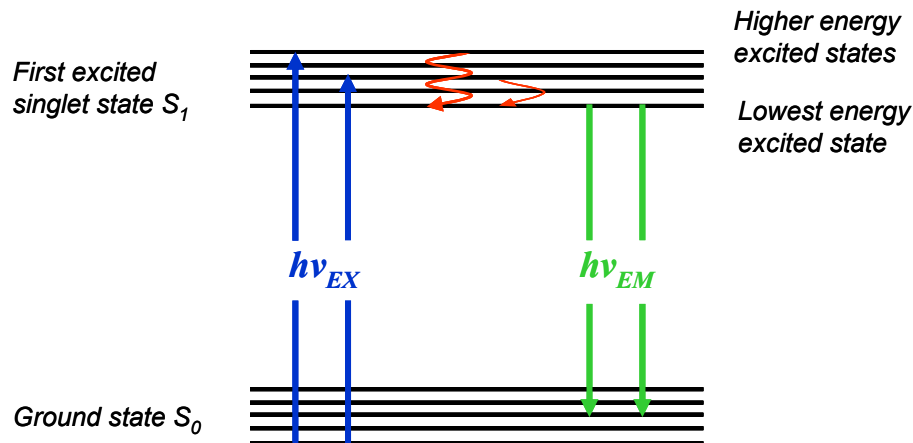


**Fig. 2:** Simplified Jablonski scheme illustrating the electron transitions during the fluorescence process

By absorption of a certain quantum of energy (e.g. light of specific wavelength;  $h\nu_{EX}$ ) molecules are excited in their electronic state from the lowest present energy level, the ground state  $S_0$ , to several excited singlet states,  $S_1$  levels. The absorbed energy is not retained by the molecules, but will be released within different time intervals. Immediately, non-radiative, rotational and vibrational, transitions occur to the lowest energy excited state. The following return into the ground state  $S_0$  is accompanied by the later emission of light ( $h\nu_{EM}$ ) of lower energy and therefore longer wavelengths than the light absorbed. This increase in the wavelength between absorbed and emitted light is the so-called Stoke's shift of the used fluorophor [70].

## 2.2 Fluorescence imaging techniques

There are numerous differing instruments described for fluorescence imaging. However, basically all are composed of only few fundamental components: (1) an excitation unit (e.g. incandescent lamps, lasers, LEDs), (2) a contrast enhancement unit (e.g. filters) and (3) a detection unit (e.g. photo-detectors, diode or CCD arrays) [70]. Based on their image acquisition mode most of the available imaging instruments could be classified in two groups:

### Wide-field fluorescence microscopy

Wide-field microscopes are most frequently used for fluorescence imaging. A specimen is fully illuminated by light of a certain wavelength, normally generated using mercury or xenon lamps in combination with certain excitation filters. Emitted fluorescence light is collected from the sample across a large depth, including light from areas outside of the focal plane leading to a limited axial resolution, which is about 1  $\mu\text{m}$  in a standard wide-field instrument [72].

### Scanning fluorescence microscopy

Scanning fluorescence microscopes comprises a variety of different instrumentations, all have in common that images are build-up in a scanning mode. By reducing the illumination aperture of a conventional microscope, excitation light is centred to a single point of the specimen. Both, excitation of the sample and collection of the fluorescence light occur successively for small single areas of the specimen. There are several scanning modes described in literature, including beam scanning, stage scanning or acusto-optical scanning; however, confocal laser scanning microscopy (CLSM) has by far the highest impact in biomedical research and characterization of pharmaceutical dosage forms [70].

Since spatial resolution of a CLSM is increased only marginally compared to a conventional wide-field fluorescence microscope (by factor of 0.4 to 2), the apparent contrast enhancement is based on the exclusion of secondary fluorescence from out-of-focus planes [73]. Moreover the achieved image resolution is still limited. Actually several approaches have been developed to “break the diffraction limit”, for example by multiphoton microscopy, near-field techniques,  $4\pi$ -microscopy or stipulated-fluorescence-depletion fluorescence microscopy all summarized by Patterson et al. [74].

Although the emitted light is the main primary detection signal there are several measurable parameters used to further characterize the occurring fluorescence process [70], e.g.

- Fluorescence intensity
- Emission or excitation spectra
- Fluorescence lifetime
- Polarization of the fluorescence light
- Photobleaching and photoactivation
- Fluorescence correlation.

Thus, there are numerous different fluorescence based imaging techniques, which have been thoroughly reviewed and summarized elsewhere [70; 72; 73]. An overview about commonly used techniques is given in the **table 2**.

**Tab. 2:** Fluorescence imaging techniques – principles and applications [71; 72]

Technique	Characteristics
FRAP	Fluorescence Recovery After Photobleaching - return of fluorescence signal in certain area of sample following photobleaching → mobility determination of fluorescence probes
FLIP	Fluorescence Loss In Photobleaching - fluorescence loss in the whole sample, following bleaching of specified area → structural analyses, mobility
FRET	Fluorescence Resonance Energy Transfer - energy transfer from an excited fluorophore (donor) to second fluorophore (acceptor) → analyses of molecular proximity and intermolecular interactions
FLIM	Fluorescence Lifetime Imaging - the lifetime of the excited state / decay of the fluorescence signal → analyses of molecular proximity (signal depends on local pH, ion concentration etc.)
FCS-Imaging	Fluorescence Correlation Spectroscopy Imaging - fluctuation in the fluorescence signal → analyses of molecular mobility, chemical reactions

## 2.3 The fluorescence probe

The presence of a photochemical active compound is generally essential for the fluorescence based analyses of particulate systems. Usually the fluorophore comprises a certain part of an organic molecule, which is able to absorb light of a certain wavelength and re-emit this energy as light with a different wavelength. Each fluorophore is characterized by specific excitation and emission spectra. Typically, resulting from the characteristics of the fluorescence process (**Fig. 2**) the maximum emission wavelength  $\lambda_{em}$  is slightly shifted into the red region of lower energy, compared to the maximum absorption wavelength  $\lambda_{ab}$ . The brightness of a fluorescence dye is expressed by the so-called fluorescence quantum yield, which represents the number of fluorescence photons emitted per absorbed excitation photons [75].

For the characterization of particulate systems one can choose from a huge variety of different organic fluorophores, differing for example in their optical properties, photostability, lipophilicity or reactivity. Choosing the appropriate fluorescence probe is challenging but will be crucial for the success of an investigation. Several factors need to be considered comprising fundamentals such as: the information one is interested in, the composition and properties of the system to be investigated, the used imaging techniques and available instrumental conditions. Strongly depending on the intended application, there are several technical approaches for the introduction of the desired fluorescence

probe into the particulate DDS. The most comfortable way is the use of the intrinsic fluorescence of the encapsulated active pharmaceutical ingredient (API). However, since this is immediately linked to suitable optical properties of the API, this approach is usually applicable only in limited cases. Instead of the API most commonly organic fluorescence dyes are used. These could be either covalently conjugated to certain functional groups of the API, usually done in case of higher molecular weight drugs (e.g. proteins, peptides, DNA), co-encapsulated with the desired API or most frequently be used as model drugs, thus completely replacing the API. Besides the encapsulated compound also the matrix material can be varied in order to obtain a fluorescing system – either also by labelling of the matrix molecules with appropriate fluorophores or in single case by using matrix materials with intrinsic fluorescence. An additional opportunity offers the association of fluorescence labels with the surface of DDS, e.g. by biotin-streptavidin conjunction [76; 77]. Examples for the above described possibilities are presented in **table 3**.

**Tab. 3:** Approaches for introduction of fluorescence probes into particulate DDS

Technique	Examples	
<i>APIs with intrinsic fluorescence</i>	Minocyclin-HCl; riboflavin; topotecan; pheophorbide; dipyrindamol	[78-81]
<i>Organic fluorescence dye</i>	Fluorescein salts, coumarin-6; congo red, Nile red, rhodamine dyes	[54; 82-85]
<i>Fluorescently labelled API</i>	FITC-peptides/dextrans; RITC-lysozyme; TAMRA-ANP	[11; 54; 86; 87]
<i>Matrix materials with intrinsic fluorescence</i>	CEFB	[88]
<i>Fluorescently labelled matrix materials</i>	Rhodamine-DMPC; FITC-PAH; FITC-gelatine; Bodipy-DOPA; CEFB-PLGA	[54; 88-90]

## 2.4 Application of fluorescence imaging

Especially in the field of solid particulate DDS (nano- and microparticles) research without fluorescence imaging is hardly to imagine and numerous applications have been found in literature. State of the art is the characterization of systems subsequent to their preparation by CLSM analyses. Especially it is used to proof and visualize either the successful encapsulation [87; 91] or an applied surface coating and functionalization by conjugation with fluorescent compounds [76; 77; 92]. Furthermore it deals for mapping the APIs' distribution within the DDS [15; 86; 89; 93] as well as structural composition of complex matrices or DDS [93; 94]. Internal drug distribution and matrix structure belong to the main determinants of drug release characteristics of a system [95; 96]. The correlation of individual release profiles and the fluorescence maps of the DDS allows the



comparison of impact for completely different preparation methods and varying preparation parameters and moreover increase the comprehension of apparent mechanisms [79; 97-99]. Thus the properties of DDS might be optimized and tailored for each specific application.

Additionally fluorescence imaging is commonly applied for the characterization/elucidation of the DDS's performance during their *in-vitro* or *in-vivo* application. Visualization and measuring of the mobility of fluorescing compounds, either originally encapsulated in the matrix or taken up from the enclosed medium, allows the characterization of release behaviour and mechanisms [78; 81; 100-102]. Microparticles' degradation characteristics were investigated by mapping the development of internal pH distribution, the so-called microclimate pH [103-105], additionally allowing conclusions to be drawn on the stability of an encapsulated API. Investigation, especially of the nanoscaled systems, in cellular context is widely used for the determination of their properties in terms of drug targeting ability and/or toxicity. Using *in-vitro* cell culture systems, particle interaction with cells (frequently cancer cell lines) and their uptake into the cells as well as their intracellular tracking enable research to easily assess particles' therapeutic capabilities and characterize the underlying uptake mechanisms [106-110]. Successful *in-vivo* targeting might be proofed subsequently by imaging of tissues isolated from animals following application of the DDS [110-113].

Finally fluorescence imaging is also applied for *in-vivo* investigations of DDS. The investigation of each developed system *in-vivo* generally is essential, as the living organism is much more complex than any available *in-vitro* experimental set-up. Optical imaging offers a non-invasive method for evaluation and possibly even verification of the knowledge gained in the several *in-vitro* experiments. However, unfortunately application is challenging and limited especially by the interaction of the excitation as well as the emitted light with the surrounding tissue components. Strongly depending on the system and especially requiring an appropriate fluorescence probe, it allows the *in-vivo* tracking of nanoparticles following subcutaneous or intravenous administration in small animals (mice, rats). Most common application is the visualization of drug targeting – passive or active, drug release as well as the subsequent therapeutic efficacy of the system [86; 114-117].

### 3. Goals of the thesis

Fluorescence imaging is ubiquitously used and irreplaceable in biomedical and pharmaceutical research. This outstanding position is especially founded on the numerous available detection techniques and therefore very versatile imaging capabilities. There is hardly any scientific question, which might not be addressed using fluorescence based analytics and where these investigations can significantly improve understanding of the underlying problems.

Since only few APIs or matrix systems exhibit the necessary intrinsic fluorescence, the use of appropriate model compounds or the chemical modification of the API is indispensable. This can be seen as the main limitation of fluorescence imaging, as particulate systems are sensitive to almost every minute alteration of process parameters, which further complicates the interchangeable transfer of knowledge from one specific study to another. Especially the *in-vivo* performance, release and degradation behaviour of therapeutic systems, were shown to be highly sensitive to its composition, which might be already altered by varying excipients, preparation methods or even by only slightly differing preparation parameters. Basically a thorough knowledge of the DDS and its respective model system as well as their dependence on varying impact factors is essential to understand and transfer the results obtained from the imaging experiments.

In this context the overall aim of this work, was the establishment of versatile particulate detection systems, capable for a variety of further applications, in particular the tracking of particles *in-vitro* or *in-vivo*, with special focus on the evaluation of potential impact factors on the particles' characteristics.

Based on a single preparation method, namely nanoprecipitation, a suitably sized nanoparticulate delivery system was established. To allow on-demand tailoring of specific particle properties for a particular application the influence of variations in single preparation parameters was investigated using plain particles prepared from different biodegradable polymers (**Chapter 2**). The application of the established particulate system for fluorescence imaging purposes further requires the introduction of a fluorescent label, which however might alter the processes during particle preparation and therefore the resulting particle properties. The impact of loading was evaluated using lipophilic organic fluorescent dyes as model compounds. Following thorough *in-vitro* characterization the *in-vivo* performance of different, fluorescently labelled systems was visualized by *in-vivo* small animal imaging (**Chapter 3**).

In the second part of this thesis quantum dots, fluorescing semiconductor nanocrystals, should be established as additional fluorescent marker of particulate systems. With their bright and stable photoluminescence they were assumed to offer an attractive alternative

for commonly used organic fluorescence dyes and overcome their drawbacks (e.g. leakage from the matrix, photobleaching), which are problematic especially in case of long-term imaging applications. First of all CdSe nanocrystals, appropriate for *in-vitro* and *in-vivo* investigations, were synthesized using a simple one-step synthesis route. Several post-synthesis treatments were evaluated with respect to their potential to improve optical properties of the quantum dots and to enhance stability for further encapsulation (**Chapter 4**). Encapsulation of these CdSe quantum dots into polymeric nanoparticles using the prior established nanoprecipitation method was assumed to be well-suited to preserve the QDs optical properties due to the absence of mechanical high-shear processes and therefore allow the preparation of bright fluorescing, stable and monodisperse particles. The encapsulation process was investigated to elucidate critical steps, allowing further improvement of the particulate detection system (**Chapter 5**). Finally quantum dots were evaluated also as fluorescent label for larger polymeric microparticles. The impact of quantum dot properties and the matrix system on the overall characteristics of the microparticulate system and their potential use for imaging purposes was investigated (**Chapter 6**).

## 4. References

- [1] Allen, T.M. et al.: "Drug Delivery Systems: Entering the Mainstream", **Science** 303 (2004) pp. 1818-1822.
- [2] Coombes, A.G.A.: "Design of Nano- and Microparticulate Controlled Release Systems", **The Drug Delivery Companies Report** 2001/02 (2001) pp. 44-47.
- [3] Hans, M.L. et al.: "Biodegradable nanoparticles for drug delivery and targeting", **Current Opinion in Solid State and Materials Science** 6 (2002) pp. 319-327.
- [4] Benoit, M.A. et al.: "Preparation and characterization of protein-loaded poly( $\epsilon$ -caprolactone) microparticles for oral vaccine delivery", **International Journal of Pharmaceutics** 184 (1999) pp. 73-84.
- [5] Chen, H. et al.: "Oral particulate delivery: status and future trends", **Advanced Drug Delivery Reviews** 34 (1998) pp. 339-350.
- [6] Zimmer, A. et al.: "Microspheres and nanoparticles used in ocular delivery systems", **Advanced Drug Delivery Reviews** 16 (1995) pp. 61-73.
- [7] Birnbaum, D.T. & Brannon-Peppas, L., "Microparticle Drug Delivery Systems," in **Drug Delivery Systems in Cancer Therapy** (2003) pp. 117-135.
- [8] Soppimath, K.S. et al.: "Biodegradable polymeric nanoparticles as drug delivery devices", **Journal of Controlled Release** 70 (2001) pp. 1-20.
- [9] Brannon-Peppas, L. et al.: "Nanoparticle and targeted systems for cancer therapy", **Advanced Drug Delivery Reviews** 56 (2004) pp. 1649-1659.
- [10] Bugamelli, F. et al.: "Controlled insulin release from chitosan microparticles", **Archiv der Pharmazie** 331 (1998) pp. 133-138.
- [11] Maculotti, K. et al.: "Preparation and in Vitro Evaluation of Thiolated Chitosan Microparticles", **Journal of Microencapsulation** 22 (2005) pp. 459-470.
- [12] Tan, W.B. et al.: "Surface modification of gold and quantum dot nanoparticles with chitosan for bioapplications", **Journal of Biomedical Materials Research, Part A** 75A (2005) pp. 56-62.
- [13] Coppi, G. et al.: "Ex-vivo evaluation of alginate microparticles for Polymyxin B oral administration", **Journal of Drug Targeting** 14 (2006) pp. 599-606.
- [14] Motwani, S.K. et al.: "Chitosan-sodium alginate nanoparticles as submicroscopic reservoirs for ocular delivery: Formulation, optimisation and in vitro characterisation", **European Journal of Pharmaceutics and Biopharmaceutics** 68 (2008) pp. 513-525.
- [15] Lamprecht, A. et al.: "Visualization and quantification of polymer distribution in microcapsules by confocal laser scanning microscopy (CLSM)", **International Journal of Pharmaceutics** 196 (2000) pp. 223-226.
- [16] Katti, D.: "Preparation of albumin microspheres by an improved process", **Journal of Microencapsulation** 16 (1999) pp. 231-242.
- [17] Palmieri, G.F. et al.: "Methoxybutropate microencapsulation by gelatin-acacia complex coacervation", **Drug development and industrial pharmacy** 25 (1999) pp. 399-407.
- [18] Bramwell, V.W. et al.: "Particulate delivery systems for biodefense subunit vaccines", **Advanced Drug Delivery Reviews** 57 (2005) pp. 1247-1265.

- [19] Chung, Y.Y.H.: "Microencapsulation of gentamicin in biodegradable PLA and/or PLA/PEG copolymer", **Journal of Microencapsulation** 18 (2001) pp. 457-465.
- [20] Xie, J. et al.: "Biodegradable microparticles and fiber fabrics for sustained delivery of cisplatin to treat C6 glioma in vitro", **Journal of Biomedical Materials Research Part A** 85A (2008) pp. 897-908.
- [21] Gref, R. et al.: "Polyoxyethylene-coated nanospheres: effect of coating on zeta potential and phagocytosis", **SO: Polymer International** 48 (1999) pp. 251-256.
- [22] Chawla, J.S. et al.: "Biodegradable poly(epsilon-caprolactone) nanoparticles for tumor-targeted delivery of tamoxifen", **International Journal of Pharmaceutics** 249 (2002) pp. 127-138.
- [23] Göpferich, A. et al.: "Polyanhydride degradation and erosion", **Advanced Drug Delivery Reviews** 54 (2002) pp. 911-931.
- [24] Ebrahim, V.F. et al.: "Hydrophilic drug release from bioerodible polyanhydride microspheres", **SO: Journal of Applied Polymer Science** 83 (2002) pp. 1457-1464.
- [25] Veronese, F.M. et al.: "Polyorganophosphazene microspheres for drug release: polymer synthesis, microsphere preparation, in vitro and in vivo naproxen release", **Journal of Controlled Release** 52 (1998) pp. 227-237.
- [26] Ibim, S.M. et al.: "Controlled macromolecule release from poly(phosphazene) matrices", **Journal of Controlled Release** 40 (1996) pp. 31-39.
- [27] Douglas, S.J. et al.: "Poly(butyl 2-cyanoacrylate) nanoparticles with differing surface charges", **Journal of Controlled Release** 3 (1986) pp. 15-23.
- [28] Stella, B. et al.: "Encapsulation of gemcitabine lipophilic derivatives into polycyanoacrylate nanospheres and nanocapsules", **International Journal of Pharmaceutics** 344 (2007) pp. 71-77.
- [29] Shinichi, S. et al.: "In Vitro Studies on a New Method for Islet Microencapsulation Using a Thermoreversible Gelation Polymer, N-Isopropylacrylamide-Based Copolymer", **SO: Artificial Organs** 20 (1996) pp. 1232-1237.
- [30] Obeidat, W.M. et al.: "Preparation and in Vitro Evaluation of Propylthiouracil Microspheres Made of Eudragit RL 100 and Cellulose Acetate Butyrate Polymers Using the Emulsion-Solvent Evaporation Method", **Journal of Microencapsulation** 22 (2005) pp. 281-289.
- [31] Kentepozidou, A. et al.: "Production of Water-Containing Polymer Microcapsules by the Complex Emulsion/Solvent Evaporation Technique. Effect of Process Variables on the Microcapsule Size Distribution", **Journal of Microencapsulation** 12 (1995) pp. 627-638.
- [32] Thioune, O. et al.: "Preparation of pseudolatex by nanoprecipitation: Influence of the solvent nature on intrinsic viscosity and interaction constant", **International Journal of Pharmaceutics** 146 (1997) pp. 233-238.
- [33] Maschke, A. et al.: "Development of a spray congealing process for the preparation of insulin-loaded lipid microparticles and characterization thereof", **European Journal of Pharmaceutics and Biopharmaceutics** 65 (2007) pp. 175-187.
- [34] Ribeiro Dos Santos, I. et al.: "Microencapsulation of protein particles within lipids using a novel supercritical fluid process", **International Journal of Pharmaceutics** 242 (2002) pp. 69-78.

- [35] Mehnert, W. et al.: "Solid lipid nanoparticles: Production, characterization and applications", **Advanced Drug Delivery Reviews** 47 (2001) pp. 165-196.
- [36] Cavalli, R. et al.: "Solid lipid nanoparticles as carriers of hydrocortisone and progesterone complexes with  $\beta$ -cyclodextrins", **International Journal of Pharmaceutics** 182 (1999) pp. 59-69.
- [37] Park, J et al.: "Biodegradable polymers for microencapsulation of drugs", **Molecules** 10 (2005) pp. 146-161.
- [38] O'Donnell, P.B. et al.: "Preparation of microspheres by the solvent evaporation technique", **Advanced Drug Delivery Reviews** 28 (1997) pp. 25-42.
- [39] Bodmeier, R. et al.: "Solvent selection in the preparation of poly(-lactide) microspheres prepared by the solvent evaporation method", **International Journal of Pharmaceutics** 43 (1988) pp. 179-186.
- [40] Sansdrap, P. et al.: "Influence of manufacturing parameters on the size characteristics and the release profiles of nifedipine from poly(DL-lactide-co-glycolide) microspheres", **International Journal of Pharmaceutics** 98 (1993) pp. 157-164.
- [41] Benita, S. et al.: "Characterization of drug-loaded poly(d,l-lactide) microspheres", **SO: Journal of Pharmaceutical Sciences** 73 (1984) pp. 1721-1724.
- [42] Yadav, K.S. et al.: "Formulation Optimization of Etoposide Loaded PLGA Nanoparticles by Double Factorial Design and their Evaluation", **Current Drug Delivery** (2009).
- [43] Liu, J. et al.: "Poly(omega-pentadecalactone-co-butylene-co-succinate) nanoparticles as biodegradable carriers for camptothecin delivery", **Biomaterials** 30 (2009) pp. 5707-5719.
- [44] Freitas, S. et al.: "Solvent extraction employing a static micromixer: a simple, robust and versatile technology for the microencapsulation of proteins", **Journal of Microencapsulation** 20 (2003) pp. 67-85.
- [45] Lin, S.Y. et al.: "In vitro degradation and dissolution behaviours of microspheres prepared by three low molecular weight polyesters", **Journal of Microencapsulation** 17 (2000) pp. 577-586.
- [46] Sato, T. et al.: "Porous Biodegradable Microspheres for Controlled Drug Delivery. I. Assessment of Processing Conditions and Solvent Removal Techniques", **Pharmaceutical Research** 5 (1988) pp. 21-30.
- [47] Jeyanthi, R. et al.: "Effect of solvent removal technique on the matrix characteristics of polylactide/glycolide microspheres for peptide delivery", **Journal of Controlled Release** 38 (1996) pp. 235-244.
- [48] Zambaux, M.F. et al.: "Influence of experimental parameters on the characteristics of poly(lactic acid) nanoparticles prepared by a double emulsion method", **Journal of Controlled Release** 50 (1998) pp. 31-40.
- [49] Saito, N. et al.: "Effect of Colloidal Stabilizer on the Shape of Polystyrene/Poly(Methyl Methacrylate) Composite Particles Prepared in Aqueous Medium by the Solvent Evaporation Method", **Langmuir** 22 (2006) pp. 9397-9402.
- [50] Müller, R.H. et al.: "Solid lipid nanoparticles (SLN) for controlled drug delivery - a review of the state of the art", **European Journal of Pharmaceutics and Biopharmaceutics** 50 (2000) pp. 161-177.

- 
- [51] Reza, A.: "Microspheres and microcapsules, a survey of manufacturing techniques Part II: Coacervation", **SO: Polymer Engineering & Science** 30 (1990) pp. 905-914.
- [52] Barichello, J.M. et al.: "Encapsulation of Hydrophilic and Lipophilic Drugs in PLGA Nanoparticles by the Nanoprecipitation Method", **Drug development and industrial pharmacy** 25 (1999) pp. 471-476.
- [53] Guliyeva, Ü. et al.: "Chitosan microparticles containing plasmid DNA as potential oral gene delivery system", **European Journal of Pharmaceutics and Biopharmaceutics** 62 (2006) pp. 17-25.
- [54] Lamprecht, A. et al.: "Structural analysis of microparticles by confocal laser scanning microscopy", **AAPS PharmSciTech** 1 (2000) pp. 10-19.
- [55] Amiet-Charpentier, C. et al.: "Preparation of rhizobacteria-containing polymer microparticles using a complex coacervation method", **Colloids and Surfaces A: Physicochemical and Engineering Aspects** 144 (1998) pp. 179-190.
- [56] Mao, H.Q. et al.: "Chitosan-DNA nanoparticles as gene carriers: synthesis, characterization and transfection efficiency", **Journal of Controlled Release** 70 (2001) pp. 399-421.
- [57] Bilati, U. et al.: "Development of a nanoprecipitation method intended for the entrapment of hydrophilic drugs into nanoparticles", **European Journal of Pharmaceutical Sciences** 24 (2005) pp. 67-75.
- [58] Nihant, N. et al.: "Microencapsulation by coacervation of poly(lactide-co-glycolide) IV. Effect of the processing parameters on coacervation and encapsulation", **Journal of Controlled Release** 35 (1995) pp. 117-125.
- [59] Ruiz, J.M. et al.: "Influence of Average Molecular Weights of Poly(DL-Lactic Acid-Co-Glycolic Acid) Copolymers 50/50 on Phase Separation and in Vitro Drug Release from Microspheres", **Pharmaceutical Research** 7 (1990) pp. 928-934.
- [60] Mallarde, D. et al.: "PLGA-PEG microspheres of teverelix: influence of polymer type on microsphere characteristics and on teverelix in vitro release", **International Journal of Pharmaceutics** 261 (2003) pp. 69-80.
- [61] Bruschi, M.L. et al.: "Gelatin microparticles containing propolis obtained by spray-drying technique: preparation and characterization", **International Journal of Pharmaceutics** 264 (2003) pp. 45-55.
- [62] Mok, H. et al.: "Water-free microencapsulation of proteins within PLGA microparticles by spray drying using PEG-assisted protein solubilization technique in organic solvent", **European Journal of Pharmaceutics and Biopharmaceutics** 70 (2008) pp. 137-144.
- [63] Zweers, M.L.T. et al.: "In vitro degradation of nanoparticles prepared from polymers based on DL-lactide, glycolide and poly(ethylene oxide)", **Journal of Controlled Release** 100 (2004) pp. 347-356.
- [64] Kriwet, B. et al.: "Synthesis of bioadhesive poly(acrylic acid) nano- and microparticles using an inverse emulsion polymerization method for the entrapment of hydrophilic drug candidates", **Journal of Controlled Release** 56 (1998) pp. 149-158.
- [65] Nykamp, G. et al.: "Jet milling-a new technique for microparticle preparation", **International Journal of Pharmaceutics** 242 (2002) pp. 79-86.
- [66] DeSimone, J.M.: "Fabrication of monodisperse, shape-specific nanoparticles: Particle replication in non-wetting templates (PRINT)", **Abstracts of Papers**,
-

- 230th ACS National Meeting, Washington, DC, United States, Aug 28-Sept 1, 2005** (2005) p. MSE-468.
- [67] Katstra, W.E. et al.: "Oral dosage forms fabricated by Three Dimensional Printing(TM)", **Journal of Controlled Release** 66 (2000) pp. 1-9.
  - [68] Maeder, K. et al.: "Imaging Techniques in Drug Development", **European Journal of Pharmaceutics and Biopharmaceutics** 74 (2010) pp. 1-126.
  - [69] Gurny, R. et al.: "Imaging tools for pharmaceutical development", **European Journal of Pharmaceutics and Biopharmaceutics** 74 (2010) p. 1.
  - [70] White, N.S. et al.: "Fluorescence techniques for drug delivery research: theory and practice", **Advanced Drug Delivery Reviews** 57 (2005) pp. 17-42.
  - [71] Festy, F. et al.: "Imaging proteins in vivo using fluorescence lifetime microscopy", **Molecular BioSystems** 3 (2007) pp. 381-391.
  - [72] Gumbleton, M. et al.: "Coming out of the dark: the evolving role of fluorescence imaging in drug delivery research", **Advanced Drug Delivery Reviews** 57 (2005) pp. 5-15.
  - [73] Pygall, Samuel R. et al.: "Pharmaceutical applications of confocal laser scanning microscopy: The physical characterisation of pharmaceutical systems", **Advanced Drug Delivery Reviews** 59 (2007) pp. 1434-1452.
  - [74] Patterson, G. H.: "Fluorescence microscopy below the diffraction limit", **Seminars in Cell and Developmental Biology** 20 (2009) pp. 886-893.
  - [75] Molecular Probes: "The Handbook - A Guide to fluorescent probes and labeling technologies",
  - [76] Fischer, S. et al.: "One-step preparation of polyelectrolyte-coated PLGA microparticles and their functionalization with model ligands", **Journal of Controlled Release** 111 (2006) pp. 135-144.
  - [77] Rigler, P. et al.: "Encapsulation of Fluorescent Molecules by Functionalized Polymeric Nanocontainers: Investigation by Confocal Fluorescence Imaging and Fluorescence Correlation Spectroscopy", **Journal of the American Chemical Society** 128 (2005) pp. 367-373.
  - [78] Cutts, L.S. et al.: "Characterizing Drug Release Processes Within Controlled Release Dosage Forms Using the Confocal Laser Scanning Microscope", **Journal of Controlled Release** 42 (1996) pp. 115-124.
  - [79] Nilkumhang, S. et al.: "Drug distribution in enteric microparticles", **International Journal of Pharmaceutics** 379 (2009) pp. 1-8.
  - [80] Errington, R.J. et al.: "Advanced Microscopy Solutions for Monitoring the Kinetics and Dynamics of Drug-DNA Targeting in Living Cells", **Advanced Drug Delivery Reviews** 57 (2005) pp. 153-167.
  - [81] Chen, K. et al.: "Novel Photosensitizer-Protein Nanoparticles for Photodynamic Therapy: Photophysical Characterization and in Vitro Investigations", **Journal of Photochemistry and Photobiology B: Biology** 96 (2009) pp. 66-74.
  - [82] Bastian, P. et al.: "Chemo-Embolization of Experimental Liver Metastases. Part 1. Distribution of Biodegradable Microspheres of Different Sizes in an Animal Model for the Locoregional Therapy", **European Journal of Pharmaceutics and Biopharmaceutics** 46 (1998) pp. 243-254.



- 
- [83] Morgan, T.T. et al.: "Encapsulation of Organic Molecules in Calcium Phosphate Nanocomposite Particles for Intracellular Imaging and Drug Delivery", **Nano Letters** 8 (2008) pp. 4108-4115.
- [84] Prabu, P. et al.: "In Vitro Evaluation of Poly(Caprolactone) Grafted Dextran (PGD) Nanoparticles With Cancer Cell", **Journal of Materials Science: Materials in Medicine** 19 (2008) pp. 2157-2163.
- [85] Wang, F. et al.: "Formulation of Nano and Micro PLGA Particles of the Model Peptide Insulin: Preparation, Characterization, Stability and Deposition in Human Skin", **Open Drug Delivery Journal** 2 (2008) pp. 1-9.
- [86] Lee, E.S. et al.: "Protein Complexed With Chondroitin Sulfate in Poly(Lactide-Co-Glycolide) Microspheres", **Biomaterials** 28 (2007) pp. 2754-2762.
- [87] Brunner, A. et al.: "Labelling peptides with fluorescent probes for incorporation into degradable polymers", **European Journal of Pharmaceutics and Biopharmaceutics** 45 (1998) pp. 265-273.
- [88] Jiang, H.L. et al.: "Bioadhesive Fluorescent Microspheres As Visible Carriers for Local Delivery of Drugs. I: Preparation and Characterization of Insulin-Loaded PCEFB/PLGA Microspheres", **Journal of Microencapsulation** 19 (2002) pp. 451-461.
- [89] Bershteyn, A. et al.: "Polymer-supported lipid shells, onions, and flowers", **Soft Matter** 4 (2008) pp. 1787-1791.
- [90] De Geest, B.G. et al.: "Self-Exploding Lipid-Coated Microgels", **Biomacromolecules** 7 (2006) pp. 373-379.
- [91] Frangione-Beebe, M.: "Microencapsulation of a synthetic peptide epitope for HTLV-1 in biodegradable poly(D,L-lactide-co-glycolide) microspheres using a novel encapsulation technique", **Journal of Microencapsulation** 18 (2001) pp. 663-677.
- [92] Elmas, B. et al.: "Synthesis of Uniform, Fluorescent Polyglycidyl Methacrylate Based Particles and Their Characterization by Confocal Laser Scanning Microscopy", **Colloids and Surfaces, A** 269 (2005) pp. 125-134.
- [93] Lamprecht, A. et al.: "Structural Analysis of Microparticles by Confocal Laser Scanning Microscopy", **AAPS PharmSciTec** 1 (2000) pp. 10-19.
- [94] Liu, X. et al.: "Composite Hydrogels for Sustained Release of Therapeutic Agents", **Soft Materials** 1 (2003) pp. 393-408.
- [95] Yang, Yi Y. et al.: "Morphology, drug distribution, and in vitro release profiles of biodegradable polymeric microspheres containing protein fabricated by double-emulsion solvent extraction/evaporation method", **Biomaterials** 22 (2001) pp. 231-241.
- [96] Berkland, C. et al.: "Microsphere size, precipitation kinetics and drug distribution control drug release from biodegradable polyanhydride microspheres", **Journal of Controlled Release** 94 (2004) pp. 129-141.
- [97] Alvarez, M. et al.: "Rapid Production of Protein-Loaded Biodegradable Microparticles Using Surface Acoustic Waves", **Biomicrofluidics** 3 (2009) pp. 14102.
- [98] Leo, E. et al.: "PLA-microparticles formulated by means a thermoreversible gel able to modify protein encapsulation and release without being co-encapsulated", **International Journal of Pharmaceutics** 323 (2006) pp. 131-138.
-

- [99] Wischke, C. et al.: "Influence of the Primary Emulsification Procedure on the Characteristics of Small Protein-Loaded PLGA Microparticles for Antigen Delivery", ***Journal of Microencapsulation*** 23 (2006) pp. 435-448.
- [100] Barnes, M.D. et al.: "Fluorescence imaging of single molecules in polymer microspheres", ***Cytometry*** 36 (1999) pp. 169-175.
- [101] Kang, J. et al.: "Determination of Diffusion Coefficient of a Small Hydrophobic Probe in Poly(Lactide-Co-Glycolide) Microparticles by Laser Scanning Confocal Microscopy", ***Macromolecules*** 36 (2003) pp. 1324-1330.
- [102] Kang, J. et al.: "Pore Closing and Opening in Biodegradable Polymers and Their Effect on the Controlled Release of Proteins", ***Molecular Pharmaceutics*** 4 (2007) pp. 104-118.
- [103] Shenderova, A. et al.: "The Acidic Microclimate in Poly(Lactide-Co-Glycolide) Microspheres Stabilizes Camptothecins", ***Pharmaceutical Research*** 16 (1999) pp. 241-248.
- [104] Li, L. et al.: "Mapping neutral microclimate pH in PLGA microspheres", ***Journal of Controlled Release*** 101 (2005) pp. 163-173.
- [105] Ding, A.G. et al.: "Acidic Microclimate PH Distribution in PLGA Microspheres Monitored by Confocal Laser Scanning Microscopy", ***Pharmaceutical Research***, 25 (2008) pp. 2041-2052.
- [106] Butoescu, N. et al.: "Dexamethasone-containing PLGA superparamagnetic microparticles as carriers for the local treatment of arthritis", ***Biomaterials*** 30 (2009) pp. 1772-1780.
- [107] Dailey, L.A. et al.: "Surfactant-Free, Biodegradable Nanoparticles for Aerosol Therapy Based on the Branched Polyesters, DEAPA-PVAL-g-PLGA", ***Pharmaceutical Research*** 20 (2003) pp. 2011-2020.
- [108] Denis-Mize, K.S. et al.: "Plasmid DNA Adsorbed Onto Cationic Microparticles Mediates Target Gene Expression and Antigen Presentation by Dendritic Cells", ***Gene Therapy*** 7 (2000) pp. 2105-2112.
- [109] Lee, E.S. et al.: "Tumor pH-responsive flower-like micelles of poly(l-lactic acid)-b-poly(ethylene glycol)-b-poly(l-histidine)", ***Journal of Controlled Release*** 123 (2007) pp. 19-26.
- [110] Cheng, F.Y. et al.: "Stabilizer-free poly(lactide-co-glycolide) nanoparticles for multimodal biomedical probes", ***Biomaterials*** 29 (2008) pp. 2104-2112.
- [111] Vila, A. et al.: "Transport of PLA-PEG particles across the nasal mucosa: effect of particle size and PEG coating density", ***Journal of Controlled Release*** 98 (2004) pp. 231-244.
- [112] Hu, K. et al.: "Lactoferrin-conjugated PEG-PLA nanoparticles with improved brain delivery: In vitro and in vivo evaluations", ***Journal of Controlled Release*** 134 (2009) pp. 55-61.
- [113] Kim, J. et al.: "Multifunctional Uniform Nanoparticles Composed of a Magnetite Nanocrystal Core and a Mesoporous Silica Shell for Magnetic Resonance and Fluorescence Imaging and for Drug Delivery", ***Angewandte Chemie, International Edition*** 47 (2008) pp. 8438-8441.
- [114] Ishihara, T. et al.: "Prolonging the In Vivo Residence Time of Prostaglandin E1 with Biodegradable Nanoparticles", ***Pharmaceutical Research*** 25 (2008) pp. 1686-1695.

- [115] He, X. et al.: "In Vivo Study of Biodistribution and Urinary Excretion of Surface-Modified Silica Nanoparticles", ***Analytical Chemistry*** 80 (2008) pp. 9597-9603.
- [116] Park, K. et al.: "Effect of polymer molecular weight on the tumor targeting characteristics of self-assembled glycol chitosan nanoparticles", ***Journal of Controlled Release*** 122 (2007) pp. 305-314.
- [117] Medarova, Z. et al.: "In vivo imaging of siRNA delivery and silencing in tumors", ***Nature Medicine*** 13 (2007) pp. 372-377.



# **Chapter 2**

## **Nanoprecipitation**

—

### **Preparation of monodisperse polymeric nanoparticles**



## 1. Introduction

Despite enormous developments during the last 30 years [1-3], the field of nanoparticulate systems is still growing, understandable regarding their multiple applications including targeted and controlled drug delivery following parenteral, oral or local administration [4-6] as well as for different imaging purposes [7; 8]. Nowadays one can choose from a pool of different materials and preparation methods, tailoring the optimal preparation conditions and product properties for the intended application [2; 3].

Offering in general very desirable properties – biocompatibility and biodegradability – polymers based on poly-(lactic acid), including various copolymers and derivatives are the most commonly investigated building blocks [3]. However, also natural polymers, such as chitosan or sodium alginate, have been described [9; 10]. The varying already established preparation processes basically could be classified into two different groups [2]: using either the polymerization of monomers, which directly leads to the particulate systems, or alternatively the dispersion of already preformed polymers to particulates of nanometre size by appropriate dispersion techniques. The latter group contains several different procedures including emulsion-based solvent-evaporation methods, salting out of the used polymers or their nanoprecipitation, thoroughly reviewed elsewhere [2]. The chosen combination of the particle forming polymer, a certain preparation method and the applied process conditions obviously has an enormous impact on the resulting particle characteristics, including release behaviour, bio-distribution and tissue accumulation or cell-uptake [11]. Therefore a detailed knowledge of potential impact factors is generally essential in order to predict the fate of the developed drug delivery system.

In the current work the technique of nanoprecipitation, first described by Fessi et al. [12], has been chosen as the desirable preparation method due to its characteristics, which allow an one-step preparation of small, nearly monodisperse particles [13], without the application of additional high-shear stress processes as for example microfluidization or ultrasound [14], which would further harm sensitive substances, like for example quantum dots.

To provide a highly versatile system, suited for a wide range of applications several factors have been investigated with respect to their effect on the colloidal systems' quality, predominantly determined by the achieved particle size and size distributions. The intended particle sizes for imaging applications were defined to be below 300 nm, which should provide sufficient diffusivity in the blood stream or within tissues of particles in subsequent *in-vivo* imaging applications. Aqueous as well as non-aqueous systems were established to allow also processing of hydrophilic or water-sensitive compounds by avoiding an aqueous phase. The chosen polymers were well-established for the

preparation of biodegradable particulate drug delivery systems [DDS] and differed in their lipophilicity, which should affect the surface properties of the resulting particles.



## **2. Materials and Methods**

### **2.1 Materials**

#### **2.1.1 Synthesis and characterization of biodegradable copolymers**

Ethylene oxide (>98.8 %), potassium bis(trimethylsilyl) amide (0.5 M in toluene), 3,6-dimethyl-1,4-dioxan [D,L-lactide], poly(ethylene glycol) monomethyl ether [mPEG<sub>2</sub>; MW=2000 Da], stannous 2-ethylhexanoate (>95 %) and trifluoro acetic anhydride [TFA] were obtained from Sigma-Aldrich (Sigma-Aldrich Chemie GmbH, Taufkirchen, Germany). Acetic acid (99 %) [glacial acid] was purchased from Merck (Merck KGaA, Darmstadt, Germany). Tetrahydrofuran [THF], diethyl ether, methylene chloride (p.a.), acetone (p.a.) were obtained at Acros (Acros Organics, Fischer Scientific GmbH, Nidderau, Germany). Chloroform [CHCl<sub>3</sub>] (HPLC grade) was provided by Carl ROTH (Carl ROTH GmbH, Karlsruhe, Germany). Deuterated chloroform [Chloroform-d<sub>1</sub>; CDCl<sub>3</sub>] was purchased from Deutero (Deutero GmbH, Kastellaun, Germany).

#### **2.1.2 Preparation and characterization of polymeric nanoparticles**

PLGA 75:25 (Resomer<sup>®</sup> 756) was obtained as kind gift of Boehringer Ingelheim (Boehringer Ingelheim AG, Biberach, Germany). Biodegradable copolymers PEG<sub>2</sub>PLA<sub>Y</sub> and NH<sub>2</sub>PEG<sub>2</sub>PLA<sub>Y</sub> (Y=20 or 40) were custom made following an established method as described. Pluronic<sup>®</sup> F68, sodium cholate hydrate (98 %), phosphotungstic acid (reagent grade) and poly(vinylalcohol) [PVA] (Mowiol 40-88) were obtained from Sigma-Aldrich (Sigma-Aldrich Chemie GmbH, Taufkirchen, Germany). Sodium dodecyl sulfate [SDS], sucrose and glucose were purchased from Merck (Merck KGaA, Darmstadt, Germany). Chloroform (p.a.) and acetone (p.a.) were obtained from Acros (Acros Organics, Fischer Scientific GmbH, Nidderau, Germany). Ethanol (p.a.) was provided from Merck (Merck KGaA, Darmstadt, Germany).

#### **2.1.3 Cell culture**

The L929 mouse fibroblast cell line and the CHO-K1 cell line (ATTC code No. CCL-61) were kind gifts from the Department of Pharmaceutical Chemistry, University of Regensburg. Fetal bovine serum [FBS] was purchased from Biochrom (Biochrom KG, Berlin, Germany). Trypsin-EDTA 0.25 % and Dulbecco's phosphate buffered saline [PBS] were obtained from Invitrogen (Invitrogen GmbH, Karlsruhe, Germany). 3-[4,5-Dimethylthiazol-2-yl]-2,5-diphenyltetrazolium bromide [MTT] was purchased from AppliChem (AppliChem GmbH Darmstadt, Germany). Eagle's minimum essential medium

[EMEM] and nutrient mixture HAM's F-12 were obtained from Sigma-Aldrich (Sigma-Aldrich Chemie GmbH, Taufkirchen, Germany). Triton-X (p.a.) was obtained from Merck (Merck KGaA, Darmstadt, Germany).

## **2.2 Methods**

### **2.2.1 Synthesis of diblock copolymer**

#### **Synthesis of Poly(ethylene glycol)-mono amine ( $\text{NH}_2\text{-PEG}_2\text{-OH}$ )**

Poly(ethylene glycol)-mono amine with a molecular weight of 2,000 Da (2 kDa) was synthesized following a modified synthesis route, previously described by Tessmar et al. [15]. Briefly, 22 ml ethylene oxide (500.5 mmol) were dissolved in 150 ml THF (cooled at  $-79\text{ }^\circ\text{C}$ ). After slow addition of 22 ml of a 0.5 M potassium bis(trimethylsilyl)-amide solution in toluene (11 mmol), the mixture was stirred for 36 h. In the following the THF was evaporated using a rotary evaporator (Heidolph Instruments GmbH, Schwabach, Germany) and the solution was concentrated until a viscous polymer solution was obtained. For purification the product was dissolved in methylene chloride and precipitated in four portions of 500 ml diethyl ether. The precipitated polymer was dried under reduced pressure for at least 48 h.

#### **Synthesis of diblock copolymers $\text{mPEG}_2\text{PLA}_Y/\text{NH}_2\text{PEG}_2\text{PLA}_Y$ ( $Y=20/40$ )**

Two kinds of diblock copolymers, each with two different molecular weights, were synthesized. The hydrophilic block consisted either of poly(ethylene glycol)-monomethyl ether [mPEG] or poly(ethylene glycol)-mono amine [ $\text{NH}_2\text{PEG}$ ] each with a molecular weight of 2 kDa. The second, lipophilic block consisted of a poly(lactic acid) [PLA] part, where Y refers to the molecular weight of the PLA block, which was either 20 kDa or 40 kDa. The PLA part was attached to the PEG part by a ring-opening polymerization of D,L-dilactide using stannous 2-ethyl hexanoate as catalyst [16]. First of all, any trace amounts of water were removed from the educts. Therefore about 2 g of the PEG component were dissolved in 100 ml toluene in a three neck round bottom flask. Heated to reflux, 50 ml of toluene were distilled off using a water separator. The D,L-dilactide (20 g and 40 g, respectively) and further 100 ml toluene were added and again 50 ml solvent were distilled off. The final volume of toluene did not exceed 100 ml. After addition of 500  $\mu\text{l}$  glacial acid and about 400 mg of the catalyst the mixture was refluxed for at least 8 h under nitrogen atmosphere. Afterwards toluene was removed by repeated distillation with 200 ml methylene chloride and acetone using a rotary evaporator. Finally, the polymer dissolved in acetone was precipitated by slow dropwise addition to water. The

precipitate was separated, frozen at -80 °C and dried under vacuum. Until usage the polymers were kept under vacuum in a desiccator.

### **2.2.2 Characterization of diblock copolymers**

To prove their successful synthesis, polymers have been characterized by determination of their molecular weight and thermal behaviour. Description of the used methods as well as the respective results will be presented in **Appendix A**.

### **2.2.3 Preparation of polymeric nanoparticles**

Polymeric nanoparticles were prepared following a modified nanoprecipitation method (also called solvent displacement) first described by Fessi et al. [12], using a lipophilic organic solvent for the polymer and an excess of an external phase, which is a non-solvent for the polymer, but miscible with the polymer-solvent. Two differing procedures were established to enable the use for a broad spectrum of encapsulated substances: **(A)** a non-aqueous procedure with chloroform as polymer-solvent and ethanol as external phase (non-solvent) and **(B)** an aqueous system composed of acetone and water, respectively. Generally 10 ml of a 1 % solution of the polymer in the respective solvent was added dropwise to 40 ml of the external phase, partially containing additional stabilizers, with a drop-rate of about 2 ml per minute. The organic solvent was then allowed to evaporate over the required time, either avoiding agitation in case of the non-aqueous system or under permanent stirring with about 550 rpm. In case of the non-aqueous system the ethanol was afterwards removed by dialysis using a Nadir<sup>®</sup> dialysis membrane (cut-off of 10 to 20 kDa; Carl ROTH GmbH, Karlsruhe, Germany). Ethanol was exchanged by an aqueous solution of 0.1 % Pluronic F68.

From the aqueous dispersions the particles were recovered by centrifugation (12,500 g, at least 30 min, 10 °C; Avanti JE centrifuge; Beckman Coulter GmbH, Krefeld, Germany), re-dispersed in a solution of an appropriate protectant and subsequently freeze-dried.

### **Variations of preparation process**

Based on the above described standard process several parameters were varied to determine their impact on the properties and quality of the resulting nanoparticles. An overview of the applied variations is given in **table 1**.

**Tab. 1:** Summarized variations of the standard preparation process

Process factor	Investigated conditions	Standard
Concentration of polymer in solution	0.01–2 %	1 %
Ratio of volumes of solvent to non-solvent	1:2; 1:4; 1:8	1:4
Concentration of Pluronic F68 in non-solvent	0.1– 0.5 %	0.5 %
Type of stabilizer in non-solvent	Pluronic F68 Sodium dodecyl sulfate Sodium cholate	Pluronic F68

### 2.2.4 Freeze – thawing / freeze-drying experiments

The effect of four different cryo/lyo-protectants, described in literature [17; 18], on the stability of the freeze-dried dispersions of polymeric nanoparticles was investigated at varying concentrations. Sucrose and glucose were used at concentrations of 0.5, 5.0, 10 and 20 %; Pluronic F68 in concentrations of 0.1, 0.5, 1.0 and 1.5 % and additionally PVA in concentrations of 1.0, 1.5 and 2.5 %.

Following centrifugation (2.2.3) nanoparticles were re-dispersed in about 10 ml of the protectant solution. 3 ml of each dispersion were transferred into glass vials and frozen either at -196 °C over 1 h, -80 °C over 24 h or -20 °C over 48 h. In the following, frozen samples were either thawed at room temperature to assess the particle protection during the freezing process or lyophilised using a lab-scale freeze-dryer (Martin Christ Gefriertrocknungsanlagen, Osterode am Harz, Germany). The minimum shelf temperature at the beginning was set to -40 °C. Sublimation lasted at least 4 days at vacuum pressure of 0.125 mbar and a shelf temperature of 15 °C. Dried samples were subsequently sealed and stored until re-dispersion in the same volume of water.

Particle stability during freezing and freeze-drying was determined based on particle sizes and polydispersity indices [PI] prior and after freezing as well as after re-dispersion following lyophilisation. Results are presented either as directly measured particle size or as ratio of the obtained sizes (and PIs) determined after re-suspension and prior freezing, where a ratio of 1 indicated highest possible stability [19].

## **2.2.5 Determination of particle size**

### **Photon correlation spectroscopy**

Commonly photon correlation spectroscopy [PCS] was used to determine the hydrodynamic diameters and polydispersity indices of the prepared nanoparticles usually dispersed in 5 % sucrose solution. Measurements were performed at 20 °C with a Zetasizer 3000 A (Malvern Instruments Inc., Herrenberg, Germany). Results are presented as mean and relative standard deviation of three independent measurements.

The measurements were performed in different dispersion media, depending on the process step or the exact process conditions used. As PCS measurements are strongly influenced by the properties of dispersion media [20], refractive index and viscosity of each medium used was determined and results are summarized in **Appendix B**.

### **Transmission electron microscopy**

Transmission electron microscopic [TEM] images (**2.2.7**) were used to determine the apparent diameter of the polymeric particles. Size was determined by manually measuring the diameter of 100 particles, for each sample. Results are presented as mean and relative standard deviation.

## **2.2.6 Determination of zeta potential**

Zeta potential of nanoparticles, dispersed in water (pH ~6.7) was determined based on so-called laser Doppler electrophoresis using a Zetasizer 3000 A (Malvern Instruments Inc., Herrenberg, Germany). Measurements were performed at 20 °C.

## **2.2.7 Morphology of polymeric nanoparticles**

The morphology of nanoparticles was imaged by transmission electron microscopy. Samples were prepared by dropping diluted aqueous dispersions on 3.05 mm formvar/carbon coated copper grids (300 mesh) followed by negatively staining with phosphotungstic acid (2 % in water) for 30 s and subsequent drying under vacuum. Images were taken using a Zeiss EM C/CR (Carl Zeiss AG, Jena, Germany) with 60 kV operating voltage.

### 2.2.8 Cell culture

The L929 cells and CHO cells were cultured in EMEM and nutrient mixture HAM's F12, respectively, both supplemented with 10 % FBS. Standard cell culture conditions were 37°C, 95 % relative humidity and 5 % CO<sub>2</sub>. Growth medium was changed every third day.

### 2.2.9 Biocompatibility of polymeric nanoparticles

Biocompatibility of prepared particulate systems was investigated following an established procedure using the colorimetric MTT assay for quantitative assessment [21]. Acute toxicity of nanoparticles was assessed in a direct contact test [22]. Test dispersions of the particles were prepared by serial dilution with the respective cell culture medium, supplemented with 10 % FBS.

After seeding in a 96-well plate cells were grown to 80 to 90 % confluence. Medium was removed and the test samples (n=4, each concentration) were added. A solution of Triton X (0.5 % in PBS) was used as positive control (n=4), untreated cells with medium served as negative control (n=4) and blank values were obtained from medium without cells. After incubation at standard conditions for 4 h supernatants were aspirated and cells were washed once with PBS to remove any residuals. MTT solution (0.625 mg/ml in medium + 10 % FBS) was added and again cells were incubated for 4 h at standard conditions under exclusion of light. The water-soluble MTT is then converted into an insoluble formazan dye by mitochondrial dehydrogenase only present in still living cells (**Fig. 1**) [23].

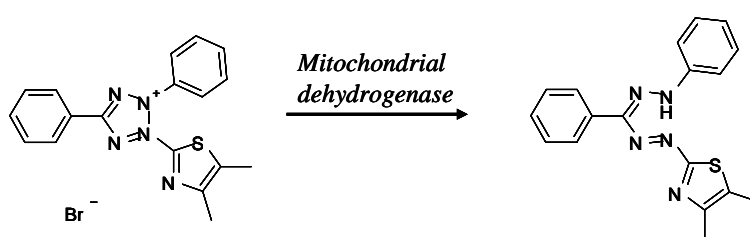


**Fig. 1:** Conversion of MTT to its insoluble formazan

Thereafter the excess MTT solution was removed and a solution of SDS (10 % in PBS) was added for cell lysis and dissolution of the precipitated formazan crystals over 24 h at room temperature under exclusion of light.

Subsequently, the formazan concentration was determined by measuring the optical density [OD] using an automatic microplate reader (TiterTek Plus; Friedrich S. Bartolomey Labortechnik, Germany) at 550 nm with a background correction at 630 nm. Cytotoxicity

was expressed as cell viability [%] of the treated cells relative to the untreated (negative control) calculated based on the following equation:

$$cell\ viability\ [\%] = \frac{OD\ test\ cells}{OD\ negative\ controll} * 100\ \% \quad (1)$$

All data were expressed as mean (N=4) and relative standard deviation. Statistic significance was assessed by one-way analysis of variances (ANOVA) in conjunction with Tukey's studentized range test using SigmaStat software.

### 3. Results

Nanoparticles are highly sensitive towards polymer degradation or aggregation during storage in aqueous dispersions. The transfer of the colloidal system into a storable dry form was achieved by lyophilisation. The results of development of a reproducible freeze-drying procedure ensuring conservation of nanoparticles properties will be presented in the first part, since all following particle characterizations (e.g. size measurements) during evaluation of several impact factors were performed following freeze-drying and re-dispersion.

#### 3.1 Stabilization of colloidal systems during freeze-drying

The impact of different protectants on the stability of polymeric nanoparticles during freezing and subsequent freeze-drying was thoroughly assessed using the PLGA particles, prepared via the non-aqueous system. A complete series of the obtained results, i.e. particle size prior freezing, after freezing at three different conditions and after re-dispersion following freeze-drying is exemplary presented for sucrose (**Fig. 2**). Results were generally found to be independent of the applied freezing conditions. No stabilization at all was obtained in pure, un-stabilized particle dispersions (values at 0 %) and aggregation could be easily detected by visual examination of the samples after thawing or re-suspension. Amounts, as low as 0.5 %, were sufficient for all protectants during freezing. However, aggregation of particles still occurred during subsequent freeze-drying, with the worst results obtained for the freezing temperature of -196 °C. For concentrations ranging between 5 and 20 %, no noteworthy changes either in mean particles sizes or in the obtained size distributions, indicated by the polydispersity indices of the measurements, were determined.



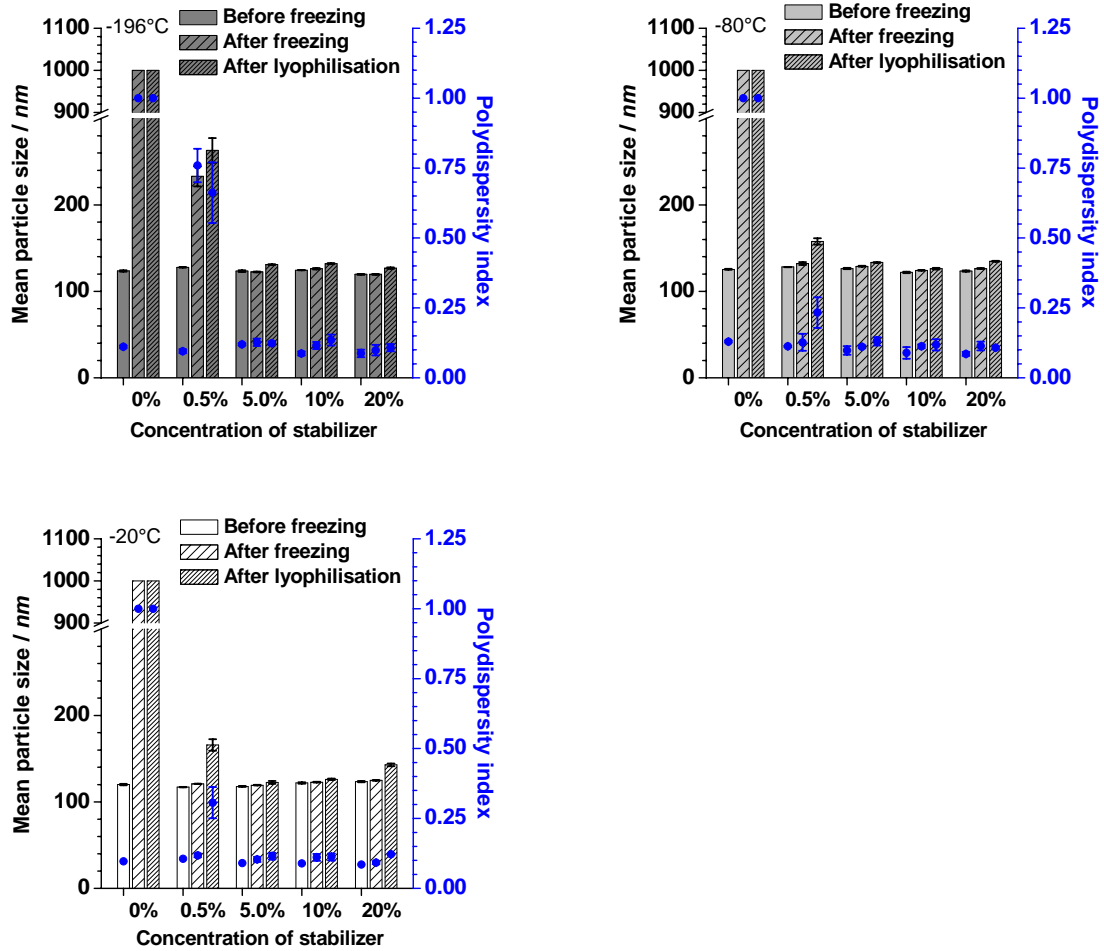


**Fig. 2:** Particle sizes [nm] and polydispersity indices of PLGA nanoparticles, prepared with non-aqueous system (+0.5 % F68) and stabilized with increasing concentrations of sucrose frozen at -196 °C (over 1 h), -80 °C (over 24 h) or -20 °C (over 48 h)

For all the further used protectants, the overall stability of the nanoparticles, is summarized using the respective ratios of mean particle sizes and PIs after freeze-drying to prior freezing (**Fig. 3**). Glucose stabilization generally gave results comparable to those of sucrose, with a sufficient effect at concentrations between 5 to 20 % independent of the applied freezing temperature.

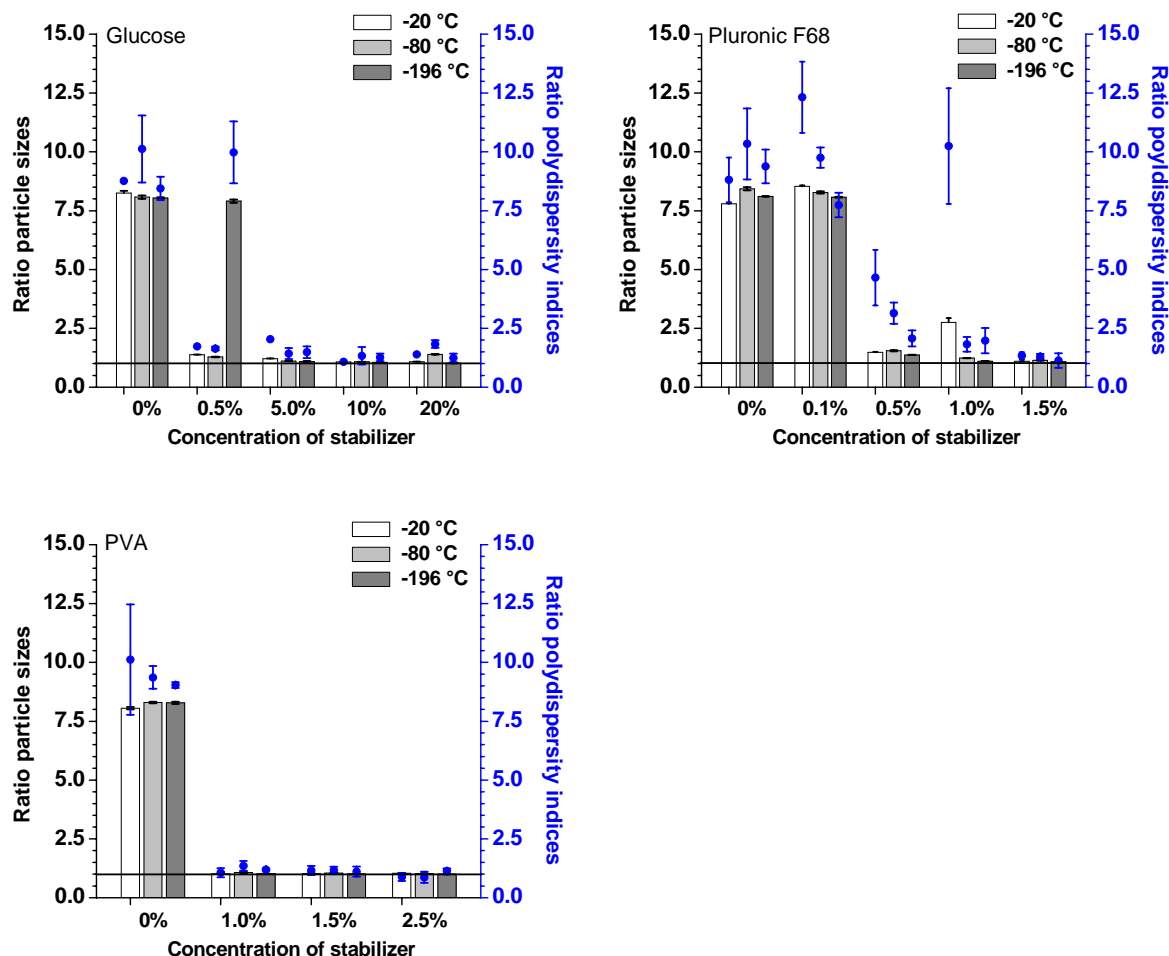


**Fig. 3:** Ratios of particle sizes and polydispersity indices of PLGA nanoparticles stabilized using different protectants (glucose, Pluronic F68 and PVA determined after and before freeze-drying)

In case of the surfactant Pluronic F68 the highest impact of the applied freezing temperature was found. While stable particle formulations were obtained even with the lower concentration of 0.5 % at a freezing temperature of -196 °C, 1 % was necessary in case of -80 °C and highest amounts were required at lowest freezing temperature. PVA overall showed the best particle stability at all concentrations used, independent of the used freezing step.

The time required for a quantitative re-dispersion of the lyophilisates (except apparent aggregates) also served as quality parameter and results are given in **table 2**.

**Tab. 2:** Re-dispersion times of lyophilisates containing increasing amounts of varying stabilizers

Sucrose		Glucose		Pluronic F68		PVA	
0.5 %	< 30 s	0.5 %	< 30 s	0.1 %	< 30 s	1 %	< 2 h
5 %	< 1 min	5 %	< 1 min	0.5 %	< 30 s	1.5 %	< 2 h
10 %	< 1 min	10 %	< 1 min	1 %	< 30 s	2.5 %	> 3 h
20 %	< 5 min	20 %	< 1 min	1.5 %	< 1 min		

Except for some occurring aggregates all lyophilisates could be quantitatively re-dispersed. However, the re-dispersion time was affected by the type of stabilizer and took up to several hours in case of PVA.

Subsequently the stability of nanoparticles prepared from the different diblock copolymers during the freeze-drying process was investigated exemplarily using 5 % sucrose as stabilizer and was found to be overall very high, indicated by the obtained size ratios near to one (**Fig. 4**). Only in case of the amine group containing polymer the size distribution became broader during drying, if frozen at -196 °C.

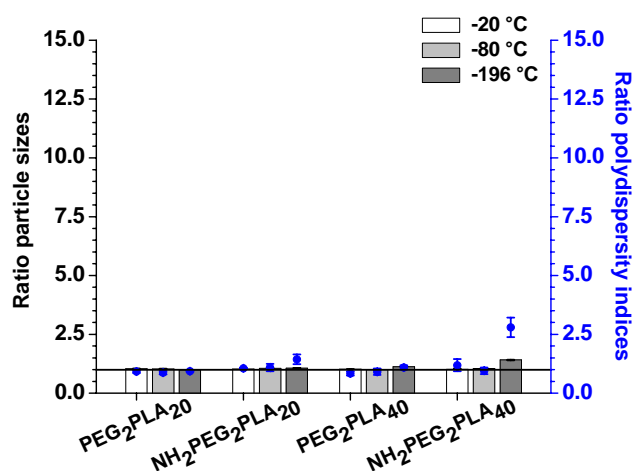


**Fig. 4:** Ratios of particle sizes and polydispersity indices of polymeric nanoparticles prepared of different copolymers stabilized with 5 % sucrose determined after and before freeze-drying

## 3.2 The nanoprecipitation process – Investigation of process conditions

### 3.2.1 Impact of precipitation system

The impact of the used precipitation system (non-aqueous or aqueous) should be investigated originally based on the described standard conditions. However, it was observed, that the preparation in non-aqueous environment failed in case of the diblock copolymers, if the external phase was supplemented with Pluronic F68, which was essential in case of PLGA. Therefore all precipitations of diblock copolymers in ethanol were performed in absence of any stabilizer.

The properties of the obtained particles, displayed by their particles size and size distribution, were found to strongly depend on the used polymers and moreover the used precipitation system (**Fig. 5**). Regarding the single polymers, particle sizes differed significantly between both preparation systems.

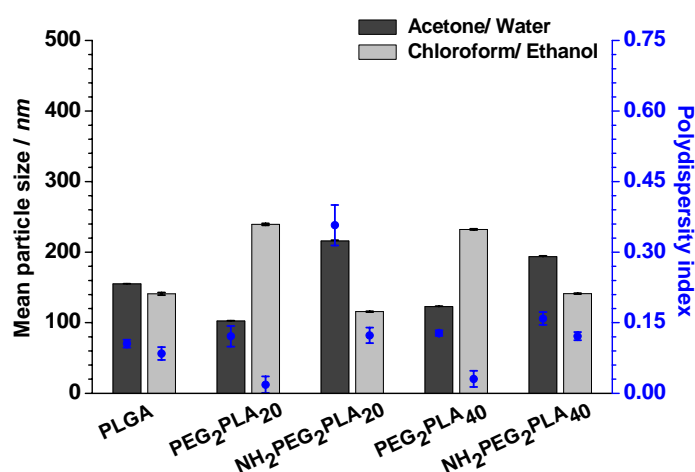


**Fig. 5:** Comparison of particle sizes [nm] and polydispersity indices of polymeric nanoparticles prepared via nanoprecipitation either using an aqueous or non-aqueous precipitation system

PLGA particles were almost unaffected by the used solvent – non-solvent system. Indeed, in case of the copolymers behaviour differed depending on the absence or presence of the amine group. While methoxy-PEG-derivatives, independent of their molecular weight, are characterized by a pronounced increase in the measured particles size when changing the solvent system to anhydrous, the results are the opposite in case of the amine-derivative. Here, particles prepared in the aqueous system are clearly bigger than in the non-aqueous system. Although PIs were generally low in most cases, which indicates narrow size distributions, the results obtained using the hydrous preparation

system were comparably bad and overall the higher values were determined for the  $\text{NH}_2\text{PEG}_2\text{PLA}_y$  based particles.

Since the general trend of the copolymers was found to be independent of their molecular weight, further investigations were done with only one polymer group, namely the  $\text{mPEG}_2\text{PLA}_{20}$  and  $\text{NH}_2\text{PEG}_2\text{PLA}_{20}$  derivatives.

### 3.2.2 Impact of polymer concentration

The polymer concentration in a fixed volume of organic solvent was found to strongly influence the resulting particle size only in case of the PLGA and  $\text{mPEG}_2\text{PLA}_{20}$  particles, where increasing polymer concentrations led to increasing particle sizes, independent of the used precipitation system (**Fig. 6**).

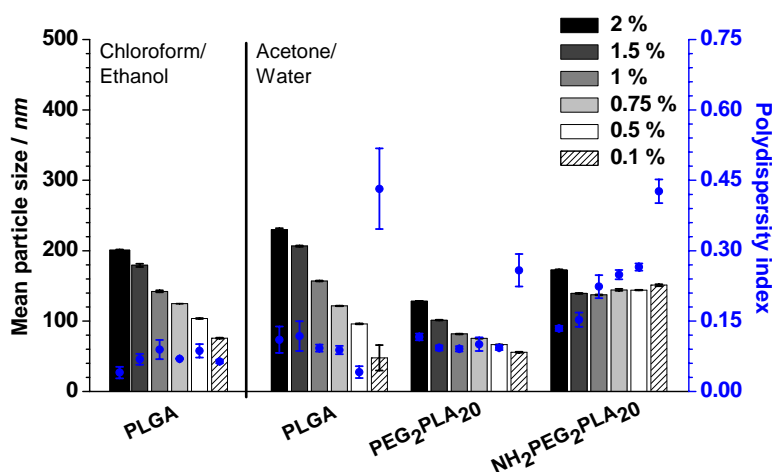


**Fig. 6:** Particle sizes [nm] and polydispersity indices of polymeric nanoparticles using decreasing polymer concentrations using aqueous system (ratio 1:4); in case of PLGA particles results for non-aqueous system are presented additionally

In contrast, the size of  $\text{NH}_2\text{PEG}_2\text{PLA}_{20}$  particles seemed to be almost not affected by the used polymer concentration in the organic phase, only the highest concentration led to a significant increase in size. The impact on size distributions was found to be more pronounced if the hydrous system was used, with an irregular increase in PI in case of lowest polymer concentrations, and overall broader distributions for the  $\text{NH}_2\text{PEG}_2\text{PLA}_{20}$  based particles.

### 3.2.3 Impact of ratio of volumes of polymer solution to external phase

With constant polymer concentrations in the organic phase, the ratios of polymer solution and external phase were varied by adding increasing volumes of polymer solution to a constant volume of external phase. Overall, the effect was comparably low (**Fig. 7**). No changes could be determined in case of mPEG<sub>2</sub>PLA<sub>20</sub>, whereas PLGA particles are characterized by a slight increase in size when a volume ratio of 1:2 and the anhydrous system was used for precipitation. The results found for NH<sub>2</sub>PEG<sub>2</sub>PLA<sub>20</sub> were differing with highest particle size in case of a ratio of 1:4 and similar values for both other ratios. Size distributions generally seemed to be slightly broader with decreasing ratios.

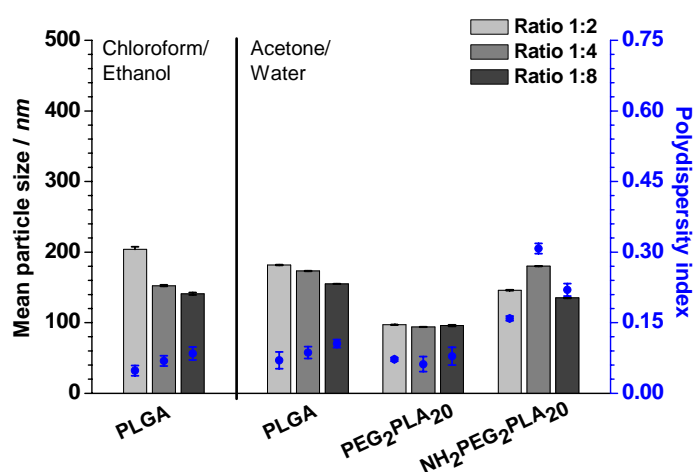


**Fig. 7:** Particle sizes [nm] and polydispersity indices of polymeric nanoparticles using decreasing ratios of polymer solution (internal phase) to external phase prepared using aqueous system; in case of PLGA particles results for non-aqueous system are presented additionally

### 3.2.4 Impact of stabilizer

The impact of the stabilizer addition to the external phase was investigated by varying either the stabilizer type at similar concentrations or the concentrations of one stabilizer, namely Pluronic F68, which was chosen as standard, prior to any investigation (**Fig. 8**). All investigations were exclusively performed using the aqueous system, since presence of alternative surfactants (other than Pluronic F68) in the external phase was found to cause complete aggregation during the evaporation in case of the anhydrous system and furthermore the other used stabilizers were not sufficiently soluble in ethanol. Regarding the different investigated stabilizer types, trends in the results were almost independent of the used polymer. However, their impact on mPEG<sub>2</sub>PLA<sub>20</sub> particles was almost negligible (**Fig. 8, left**). Smallest particles were obtained using sodium cholate, but accompanied of comparable high polydispersity indices. Lowest PIs, indicating narrow size distributions,

could be observed in case of Pluronic F68. Quality of particles prepared in presence of SDS was characterized by high particle sizes and broad size distributions.

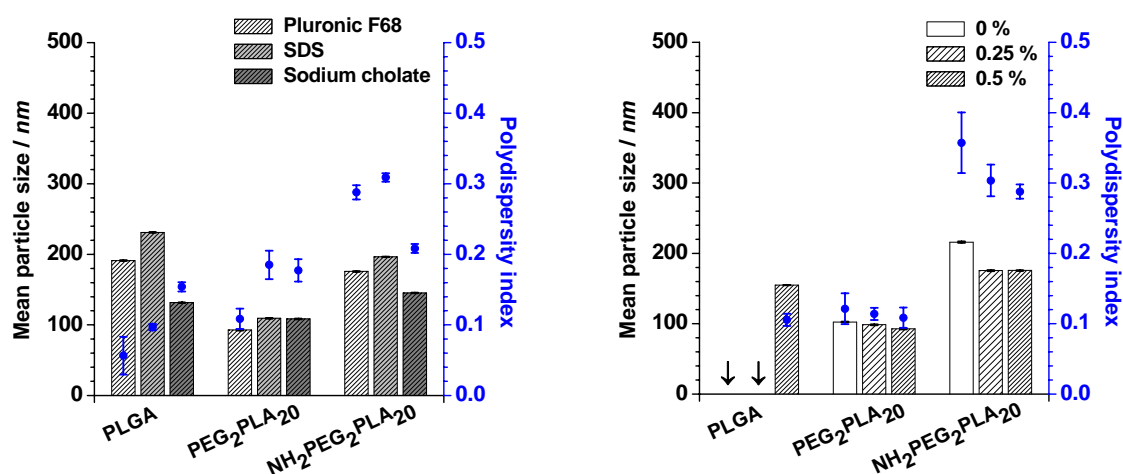


**Fig. 8:** Particle sizes [nm] and polydispersity indices of polymeric nanoparticles prepared using the aqueous system (1 % polymer; ratio 1:8) - (*left*) with different types of stabilizer in the external phase (all at 0.5 %); (*right*) with different concentrations of Pluronic F68 in the external phase; arrows indicate failure in preparation of stable nanoparticles

The effect of varying concentrations of Pluronic F68 generally differed between the lipophilic PLGA and the amphiphilic diblock copolymers (**Fig. 8, right**). For preparation of PLGA nanoparticles a stabilizer concentration of 0.5 % in the aqueous external phase was essential, otherwise aggregation occurred already during the precipitation step. In case of all PEG containing copolymers (mPEG, NH<sub>2</sub>PEG), a stable nanoprecipitation was possible in surfactant-free environment. Indeed, particle size was higher than in presence of any of the used amounts of Pluronic F68. Again, the impact was more pronounced in case of the NH<sub>2</sub>PEG-derivative.

### 3.2.5 Measurement of zeta potential

The zeta potential is a commonly used parameter to characterize particle surfaces. However, as the measured results differed strongly for the different polymers and preparation procedures and often very broad signal distributions were observed exact evaluation is complicated, wherefore only the main trends are schematically presented (**Fig. 9**). At first, measured potential was in the negative range in all cases. PLGA exhibited by far lowest surface potentials only less affected by changes in the preparation procedure. In contrast both PEG containing copolymers were characterized by overall higher zeta potentials and no influence of the amine group could be observed. However, different process parameters caused more pronounced changes.

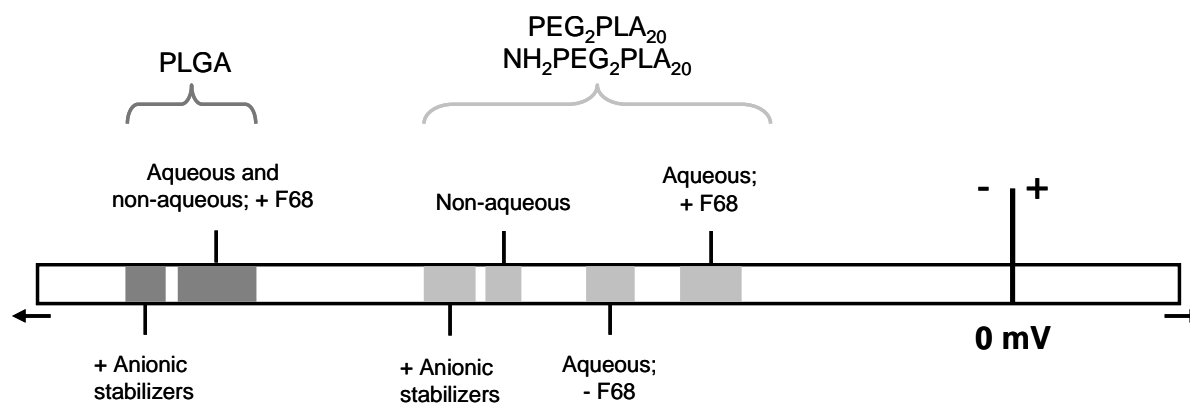


**Fig. 9:** Schematic demonstration of the position of nanoparticles zeta potential, depending on polymer and exact preparation conditions

### 3.2.6 Morphology of nanoparticles – impact of precipitation system

Nanoparticles prepared by nanoprecipitation appeared round shaped and smooth, independent of the used polymer type (**Fig. 10**). In case of the diblock copolymers also the precipitation method did not significantly alter the appearance of particles in TEM, indicated by the comparison of NH<sub>2</sub>PEG<sub>2</sub>PLA<sub>20</sub> prepared using non-aqueous (**Fig. 10, C**) or aqueous route (**Fig. 10, D**).

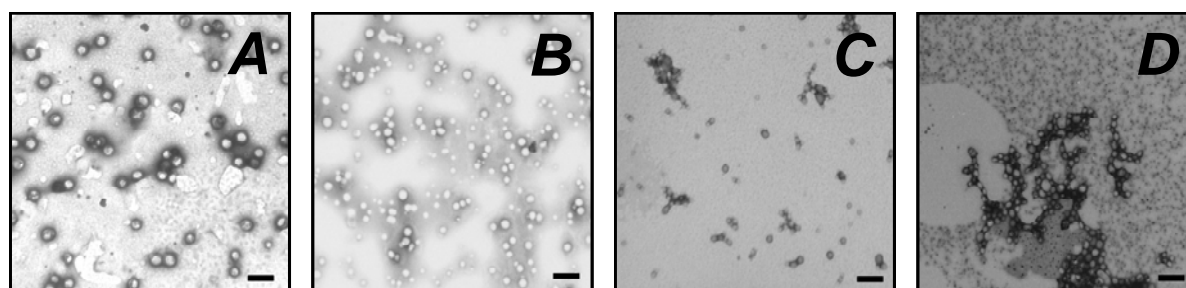


**Fig. 10:** TEM images of polymeric nanoparticles (**A**) PLGA in aqueous system (**B**) PEG<sub>2</sub>PLA<sub>20</sub> in aqueous system, (**C**) NH<sub>2</sub>PEG<sub>2</sub>PLA<sub>20</sub> in aqueous system and (**D**) NH<sub>2</sub>PEG<sub>2</sub>PLA<sub>20</sub> in non-aqueous; particles negatively stained with phosphotungstic acid; magnification: 8000x; scale bars correspond to 250 nm



### 3.2.7 Measuring particle size – impact of analytical method

For the above mentioned investigations PCS measurements have been used as standard method to determine particles size and size distributions. Results obtained were compared to a further, different method using TEM images. Generally particle sizes determined with TEM are smaller than the respective values of the PCS investigation (Fig. 11).

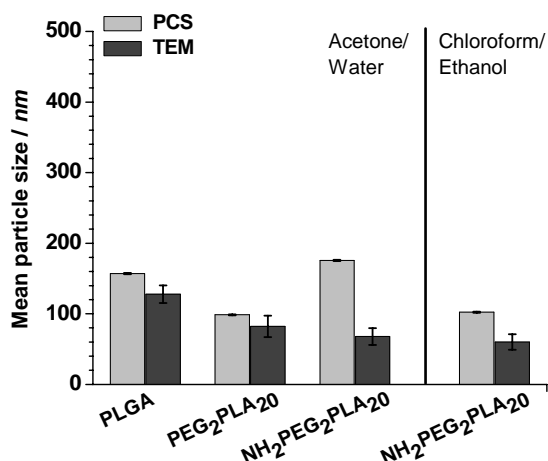


**Fig. 11:** Particle sizes [nm] of polymeric nanoparticles either measured with PCS (mean  $\pm$  SD of three measurements) or determined based on TEM images (mean  $\pm$  SD of 100 particles)

However, the most pronounced differences were found in case of the NH<sub>2</sub>PEG<sub>2</sub>PLA<sub>20</sub> particles. Moreover, the extents of differences depend on the used precipitation system. After preparation following the aqueous route particle sizes obtained by PCS were nearly twice as high as the respective results of the images analysis. In contrast to PCS results, TEM based particle sizes were almost equal for both types of diblock copolymers in both preparation methods.

### 3.2.8 Biocompatibility of polymeric nanoparticles

Cytotoxicity of various types of nanoparticles has been tested in L929 and CHO cells. The results are exemplarily presented for the single batches and, independent of the polymer type, no significant toxicity was detected in both cell lines (**Fig. 12**).

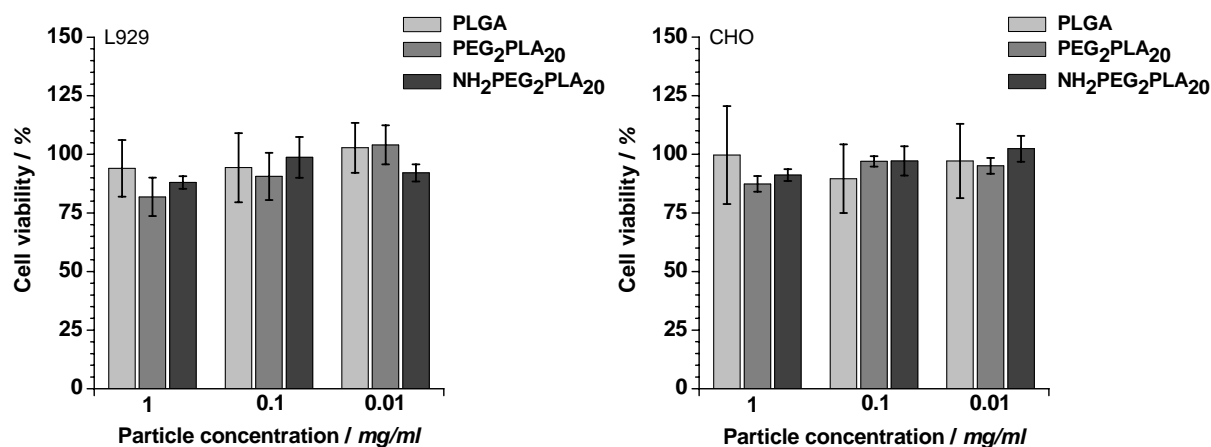


**Fig. 12:** Viability of L929 and CHO cells after incubation (4 h) with nanoparticles prepared from different biodegradable polymers, using the aqueous system (1 % polymer; ratio 1:8); star indicate significant toxicity compared to the respective negative control ( $p < 0.05$ )

## 4. Discussion

### 4.1 Stabilization of colloidal formulations during freeze-drying

As nanoparticulate systems gain more and more attention either as targeted DDS or for imaging purposes [3; 24], the storage of these colloidal systems until application is of rising importance in order to prevent physical instabilities due to particle aggregation or even fusion. Furthermore the hydrolysis of the matrix forming biodegradable polymer, or, in case of loaded nanoparticles, the leakage of encapsulated drug substance has to be prevented in an aqueous environment [17-19]. Lyophilisation was described as appropriate method to convert nanoparticle dispersions into long-term storable formulations preserving their quality. Since nanoparticles are exposed to several stress factors [24] and tend to aggregate during freezing and/or lyophilisation, impeding a quantitative reconstitution [19; 25; 26], the development of a suitable freeze-drying method was an essential step of this work. Sufficient stabilization of particle dispersions during freezing and desiccation could be achieved by addition of several protectants. Commonly the used stabilizers described in literature were several sugars or sugar alcohols and polymeric substances like PVA, PEG, gelatine or Pluronic F68 [17; 25-27]. However, the choice of the most appropriate substance strongly depends on the properties of the investigated nanoparticulate system and therefore has to be a case by case decision. Four frequently used protectants, each in several typical concentrations, were investigated regarding their effect on PLGA nanoparticles prepared by nanoprecipitation. As expected the supplementation of additional stabilizers was essential, since no un-stabilized sample was stable already during freezing. Generally all four substances (sucrose, glucose, Pluronic F68 and PVA) were found to sufficiently stabilize the system, but with different appropriate concentrations (**Fig. 1 and Fig. 2**). Besides the overall stability of the formulation, displayed by the ratios of size and PI of the product after and prior lyophilisation, the decision for an adequate substance depended on additional further aspects. Therefore, single results for particles of one batch are compared after dispersion in water or aqueous solutions of either sucrose (5 %), glucose (5 %), Pluronic F68 (1%) or PVA (1 %), reflecting the general behaviour of the investigated stabilizers on the resulting particle sizes (**Tab. 3**).

**Tab. 3:** Single results of particle sizes and polydispersity indices of nanoparticles in different dispersion media

Dispersion medium	Particle size ( $\pm$ SD) / nm	PI ( $\pm$ SD)
Water	122.6 (2.7)	0.102 (0.013)
Sucrose 5 %	117.7 (2.3)	0.105 (0.003)
Glucose 5 %	120.7 (0.9)	0.117 (0.176)
Pluronic F68 1 %	140.3 (3.2)	0.119 (0.016)
PVA 1 %	152.9 (2.3)	0.487 (0.012)

In case of both polymeric compounds (Pluronic F68 and PVA), an increase in the particle size following dispersion was observed, which can occur due to the adsorption of the macromolecules on the particles surface with a subsequent increase of the particles hydrodynamic diameters. Moreover the used PVA solutions exhibit comparable high viscosities (3.3 to 11.8 mPas), which could also interfere with the accuracy of the PCS measurements, leading to deviations of the polydispersity indices. Additionally the longest re-dispersion time of several hours are required, not desirable during application (**Tab. 2**). Additionally, the reproducibility was low in case of the non-ionic surfactant Pluronic F68, indicated by high standard deviations; especially for the polydispersity index (**Fig. 3**). Comparing the results of both sugar components generally similar stabilization capacity was observed. However, both differed strongly in stability or quality of the resulting lyophilisate (**Fig. 13**).

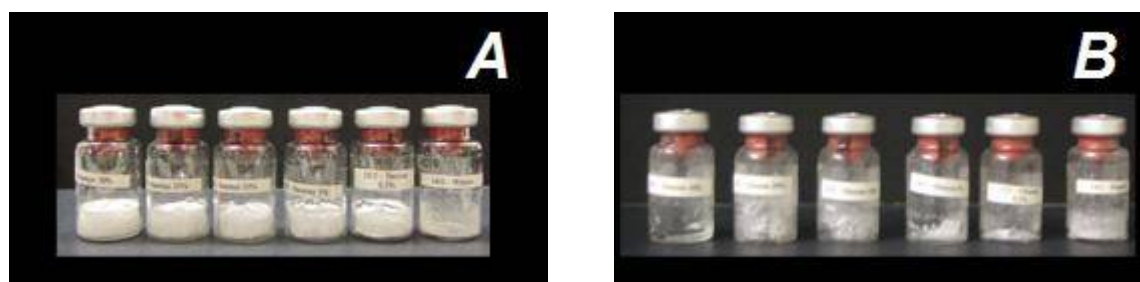


**Fig. 13:** Images of PLGA nanoparticles after freeze-drying (freezing at  $-196^{\circ}\text{C}$ ) stabilized with (**A**) sucrose and (**B**) glucose; each picture displays series starting with the highest concentration in left to the un-stabilized sample in the right

All samples containing glucose were extremely hygroscopic (**Fig. 13, B**), resulting in a pronounced uptake of water within several minutes directly after finishing the freeze-drying process. Considering all mentioned observations, and since the effect of freezing temperature was found to be almost negligible, standard conditions for all preparations were defined as: 5 % sucrose and freezing at  $-196^{\circ}\text{C}$  for one hour. These

conditions furthermore were proved to be appropriate also for the stabilization of particles prepared from the other polymers used during this work (**Fig. 4**).

## **4.2 The nanoprecipitation process – Investigation of process conditions**

During the development of DDS, the establishment of optimal process conditions generally requires the knowledge factors of potentially influencing the resulting product. This may be even more important in case of the herein used nanoprecipitation method, as particles sizes and size distributions are determined without the application of additional high-shear stress processes like microfluidization or ultrasound [14], but only depend on the chosen additives and process conditions, like solvent ratios or polymer concentrations. Despite the widespread use of this preparation method and several thorough investigations, the exact mechanistic background of the precipitation process is not conclusively elucidated [14; 28]. To simplify the process, it could be divided in two essential steps: During the addition of the organic polymer solution to a miscible non-solvent a spontaneous diffusion of the organic solvent into the non-solvent (eventually accompanied also by a certain flux of the non-solvent into the organic polymer phase) will lead to interfacial turbulences resulting in an immediate dispersion of polymer rich small sized nanodroplets. In intimate contact with the non-solvent the polymer precipitation is initiated and the final solidification is completed by a slow evaporation of the organic solvent [14; 29]. The main prerequisite is the application of an appropriate solvent combination of an organic phase with good solubility properties for the used polymer and on the other hand an external phase, which needs to be miscible with the organic solvent and essentially a non-solvent for the polymer [13]. Various combined systems are possible and have been already investigated [13; 30; 31], whereas water is the most commonly used external phase. In the current work two very different systems have been chosen. Besides the most frequently used combination of acetone and water, a anhydrous system should be additionally established, allowing the processing of highly water-soluble or water – sensitive compounds [32; 33]. Chloroform and ethanol were chosen based on the most promising results of initial screening experiments with several alternative combinations, like for example methylene chloride/ethanol, chloroform/ethanol and chloroform/heptane. Generally both systems were found to be appropriate for the nanoprecipitation of the three investigated polymers. Concluding from the above described experiments, the basic feature of nanoprecipitation – small particles with a narrow size distribution [13] – was fulfilled for most preparations, which is reflected by

particle sizes below 250 nm and PI values rarely exceeding 0.15, whereas values below 0.1 are commonly obtained for nearly monodisperse particle collectives [20; 34].

However, using ethanol as external phase raised some problems, leading to deviations in the preparation process (see **2.2.3**). In ethanolic environment soft polymer nanoprecipitates were formed and any further agitation during the evaporation of chloroform was found to provoke uncontrolled aggregation. Moreover a further dialysis step is required to remove the ethanol and transfer the particles into an aqueous environment, leading to the final solidification of the particles, which then allows their recovery via centrifugation.

Numerous factors already have been described to influence the resulting particles' properties - size, size distribution as well as the encapsulation efficiency and release characteristics for drug-loaded particles. Only few of them have been investigated in the current work, but single impact factors were found to differ in their degree of effect predominantly depending on both, the used polymer type and also the solvent – non-solvent system.

The exact composition of the used solvent – non-solvent system has been reported to strongly determine the particles properties (e.g. size and size distribution). However, comparison of the results from the different preparation procedures indicate that the general rule – the lower the polarity of the non-solvent (expressed by its dielectric constant  $\epsilon_0$ ), the higher the particle size [13; 30] – is not generally applicable for all polymers, except for particles made of mPEG<sub>2</sub>PLA<sub>y</sub>. While PLGA particles did hardly differ in size, NH<sub>2</sub>PEG<sub>2</sub>PLA<sub>y</sub> based NPs behave the other way round, yielding bigger particles in the more polar water ( $\epsilon_0=80.1$  [13]) compared to ethanol ( $\epsilon_0=24.6$  [13]). Moreover, despite its structural similarity to the mPEG<sub>2</sub>PLA<sub>y</sub> copolymers, this polymer type generally seems to exhibit a different behaviour (**Fig. 5-8**), which also will be discussed later.

Since the particle sizes were reported to be influenced also by the rate of diffusion of the solvent into the surrounding non-solvent [13], the impact of the used polymer as well as its concentration in the internal phase could significantly contribute to the viscosity of this organic polymer solution and consequently also the diffusion and exchange of the solvent [13; 35]. Considering the results of the aqueous system (**Fig. 5**), particle sizes increase at same polymer concentration with increasing molecular weight [MW] of the polymer, which obviously influences the solution's viscosity [36]: mPEG<sub>2</sub>PLA<sub>20</sub> (MW<sub>exp</sub>=24 kDa) < mPEG<sub>2</sub>PLA<sub>40</sub> (MW<sub>exp</sub>=45 kDa) << PLGA (Resomer<sup>®</sup> 756, MW=76-110 kDa [37]). While the impact of MW interestingly changed with exchanging the solvent – non-solvent system, the effect of polymer concentration was found to be independent of the used precipitation conditions (**Fig. 6**). Besides the viscosity mediated effect, the polymer concentration also determines the number of particle forming polymer molecules

(so-called aggregation number) and therefore the resulting particle size, which was thoroughly investigated for the similar mPEG<sub>5</sub>PLA<sub>45</sub> copolymers [35; 38].

Adjusting the polymer concentration between 2 and 0.1 % allows tailoring of particle sizes ranging between 220 nm and 50 nm. A further increase in concentration leads to the formation of irregular aggregates instead of defined particles. However, the decrease of particle size also reduces the quality of the particle collective, displayed by an erratic increase of the obtained PIs (**Fig. 6**). This might be due to the very low number of polymer molecules in solution, which is expected to move freely with very low interactions with each other. During the precipitation the distribution of the solvent in the external phase will take place almost immediately leading to an aggregation of neighbouring molecules, whose number may be absolutely arbitrary, thereof increasing the particle polydispersity. Interestingly this phenomenon could not be observed in the non-aqueous system, where the much slower solidification process may lead to a unification of the size distribution with time.

As diffusion processes are predominantly gradient driven, the volume ratios of solvent and non-solvent were expected to contribute significantly to particle size [13; 39], which indeed could be proven for the PLGA particles only, with a higher impact in the non-aqueous system. A decreased particles size of about 70 to 80 nm could be observed if the external phase was provided in four- or eight-fold excess (**Fig. 7**).

The addition of a stabilizer to the external phase was found to be essential in case of PLGA independent of the used system, in order to prevent the agglomeration or coalescence of the precipitate during solvent evaporation. In contrast, both PEG-PLA based systems were able to form stable dispersions also in absence of any surfactant, a characteristic behaviour of the amphiphilic diblock copolymers in polar solvents [38; 40]. The interaction of the hydrophilic PEG part with the surrounding environment can result in a predominant orientation of the PEG blocks to the aggregate surface, surrounding a PLA rich core. The resulting structure could also be described as micellar like [38] with the PEG chains providing a steric hindrance for the aggregation of the particles. The higher zeta potential of PEG-PLA based particles compared to those based on PLGA (**Fig. 9**) commonly proves the existence of less charged PEGylated surfaces [6; 41; 42]. Interestingly the surface potential of diblock copolymers decreased if the precipitation system was changed from the aqueous to the non-aqueous, which might indicate a reduced interaction of the PEG chains with the ethanol compared to water.

Unexpected was the failure of the nanoparticle formation in the non-aqueous environment in presence of only small amounts of Pluronic F68, which again might be explained by the changed hardening behaviour in ethanol. First of all, the non-ionic surfactant could interfere with the characteristic surface orientation of the PEG since it takes over the

surface stabilizing effect and the shielding to the polar environment, leading to a subsequent enrichment of PEG within the PLA core. Its well known plasticising properties [14; 43] accompanied by the softening of the particles due to the influx of ethanol could lead to a coalescence of the precipitate and finally to the formation of polymer films at the bottom of the beaker.

However, the addition of varying concentrations of Pluronic F68 did not alter the particle size obtained of PEG<sub>2</sub>PLA<sub>20</sub> in the aqueous solvent system (**Fig. 8, right**), which is in line with information from literature [41].

The exchange of the stabilizer type also alters particles sizes and size distributions (**Fig. 8, left**); but no clear trend could be determined as the negatively charged substances – SDS and sodium cholate – behave very contrary. Since both, in addition, resulted in a significant broadening of the size distribution, they were excluded as appropriate candidates for the desired nanoprecipitation system.

Besides the frequently used biodegradable PLGA and mPEG-PLA polymers nanoprecipitation was also investigated using amine group terminated PEG-PLA polymers. The basic idea behind was the preparation of amine group bearing biodegradable nanoparticles to offer a system, which allows for example targeted transport or cellular interaction/uptake via the attachment of suitable ligands [44]. Therefore the impact of the amine group on the preparation processes was investigated as well. Surprisingly, the particle properties (e.g. size and size distribution) of the structural very similar mPEG<sub>2</sub>PLA<sub>γ</sub> and NH<sub>2</sub>PEG<sub>2</sub>PLA<sub>γ</sub> displayed partially pronounced differences or even contrary behaviour, which was observed, comparing the different solvent – non-solvent systems (**Fig. 5**), the polymer concentrations (**Fig. 6**), the volume ratios (**Fig. 7**) as well as the used stabilization system (**Fig. 8**). However, the morphological analysis of the prepared particles could not prove the preceding differences in the sizes (**Fig. 10**). Moreover, a TEM-based size analysis of several particles (**Fig. 11**) instead verified the assumed similarity between mPEG<sub>2</sub>PLA<sub>γ</sub> and its amine derivative, as both showed almost same sizes. Indeed it can be concluded, that the observed differences between both polymer types appear to depend on the size determination method, where the different PEG derivatives seem to interfere with the analytical principle of PCS. The commonly used method for nanoparticle size determination, PCS, usually determines the so-called hydrodynamic diameter of particles, which obviously is sensitive to interactions of functional groups, e.g. amines, with the surrounding aqueous environment. In contrast, an image-based analysis provides an exact diameter, which in this case excludes the free diffusion of the contrast agent used for negative staining and which usually is slightly smaller than the corresponding PCS size [20; 45; 46]. In case of PEGylated nanoparticles it should also be considered, that the brush-like arrangement of



the PEG chains will predominantly affect the size in liquid dispersion, due to interactions with the polar media (PCS), and not in dried state (conventional TEM). The drying process could lead to a much thinner PEG film on the particle surface. Keeping in mind that the interaction with the surrounding environment will also influence the thickness of the attached water layer, the increased apparent particle size would be more reasonable for the hydrophilic, possibly charged primary amine end groups compared to the hydrophobic methoxy groups. Although no differences were observed in the surface potential (see **3.2.5**), which can be attributed to the additional water layer on the particles, further levelling occurring charges on the particle surfaces. In consequence, the observed reduction of the hydrodynamic diameter of  $\text{NH}_2\text{PEG}_2\text{PLA}_{20}$  particles in the anhydrous solvent system suggests a decreased interaction of the  $\text{NH}_2$ -group with ethanol, which subsequently could also lead to an altered surface arrangement of the  $\text{NH}_2\text{PEG}$ . The amine groups are probably not oriented straight away from the particle core, decreasing the interactions with the final aqueous dispersion also during PCS measurement. Although this phenomenon could not be completely elucidated based on the available information, the obtained results should sensibilise to a careful interpretation of particle size measurements, especially in case of nanoparticles, which show pronounced differences in their size dependent behaviour [20].

### **4.3 Particle cytotoxicity**

Finally, the cytotoxicity of the obtained nanoparticles was tested in different cell types to demonstrate the suitability of the prepared biodegradable nanoparticle system for applications as DDS or imaging tool. Although the results are only presented for a selected number of particle types (**Fig. 12**), all tested batches were found to be highly biocompatible, as significant toxicity appeared only in small number of experiment with individual samples, indicating no general impact of the particles tested.

## 5. Summary and Conclusion

Nanoprecipitation was found to be a well-suited simple method for the preparation of nearly monodisperse polymeric nanoparticles from three different polymer types. By varying factors such as polymers' molecular weight, polymer concentration and, to certain extent, also the ratio of solvent and non-solvent volumes tailoring of particle size within a size range of 50 to 250 nm was achieved. Depending on the used polymer type quite similar sizes were obtained in an aqueous and also a non-aqueous procedure, which was in contrast to already described investigations, but can be attributed to surface stabilizing effects of amphiphilic polymers. Therefore the established methods should be applicable for the encapsulation of both, lipophilic as well as highly water-soluble or water-sensitive compounds considering the same impact factors. Despite the successful establishment of an universal nanoprecipitation procedure, the current findings also reveal some limitations of the used analytical procedures for the particle size determination and the nanoparticle surface characteristics, especially obvious in case of the used diblock copolymers. Since the applied methods – PCS and electrophoretic mobility – are the most commonly used methods for nanoparticles characterization, these results should also sensibilise towards a critical interpretation of size measurements, which are in particular essential as *in-vivo* or *in-vitro* nanoparticle behaviour is strongly influenced by their apparent size as well as their zeta potential.

## 6. References

- [1] Brannon-Peppas, L.: "Recent advances on the use of biodegradable microparticles and nanoparticles in controlled drug delivery", ***International Journal of Pharmaceutics*** 116 (1995) pp. 1-9.
- [2] Soppimath, K.S. et al.: "Biodegradable polymeric nanoparticles as drug delivery devices", ***Journal of Controlled Release*** 70 (2001) pp. 1-20.
- [3] Hans, M.L. et al.: "Biodegradable nanoparticles for drug delivery and targeting", ***Current Opinion in Solid State and Materials Science*** 6 (2002) pp. 319-327.
- [4] Danhier, F. et al.: "Paclitaxel-loaded PEGylated PLGA-based nanoparticles: In vitro and in vivo evaluation", ***Journal of Controlled Release*** 133 (2009) pp. 11-17.
- [5] Delie, F.: "Evaluation of nano- and microparticle uptake by the gastrointestinal tract", ***Advanced Drug Delivery Reviews*** 34 (1998) pp. 221-233.
- [6] Vila, A. et al.: "Transport of PLA-PEG particles across the nasal mucosa: effect of particle size and PEG coating density", ***Journal of Controlled Release*** 98 (2004) pp. 231-244.
- [7] Doiron, A.L. et al.: "Poly(lactic-co-glycolic) acid as a carrier for imaging contrast agents", ***Pharmaceutical Research*** 26 (2009) pp. 674-682.
- [8] Kim, S. et al.: "Conjugated polymer nanoparticles for biomedical in vivo imaging", ***Chemical Communications*** 46 (2010) pp. 1617-1619.
- [9] Kim, J.H. et al.: "Hydrophobically modified glycol chitosan nanoparticles as carriers for paclitaxel", ***Journal of Controlled Release*** 111 (2006) pp. 228-234.
- [10] Motwani, S.K. et al.: "Chitosan-sodium alginate nanoparticles as submicroscopic reservoirs for ocular delivery: Formulation, optimisation and in vitro characterisation", ***European Journal of Pharmaceutics and Biopharmaceutics*** 68 (2008) pp. 513-525.
- [11] Galindo-Rodriguez, S. et al.: "Physicochemical Parameters Associated with Nanoparticle Formation in the Salting-Out, Emulsification-Diffusion, and Nanoprecipitation Methods", ***Pharmaceutical Research*** 21 (2004) pp. 1428-1439.
- [12] Fessi, H. et al.: "Nanocapsule formation by interfacial polymer deposition following solvent displacement", ***International Journal of Pharmaceutics*** 55 (1989) pp. R1-R4.
- [13] Bilati, U. et al.: "Development of a nanoprecipitation method intended for the entrapment of hydrophilic drugs into nanoparticles", ***European Journal of Pharmaceutical Sciences*** 24 (2005) pp. 67-75.
- [14] Ganachaud, F. et al.: "Nanoparticles and Nanocapsules Created Using the Ouzo Effect: Spontaneous Emulsification as an Alternative to Ultrasonic and High-Shear Devices", ***ChemPhysChem*** 6 (2005) pp. 209-216.
- [15] Tessmar, J.K. et al.: "Amine-Reactive Biodegradable Diblock Copolymers", ***Biomacromolecules*** 3 (2001) pp. 194-200.
- [16] Lucke, A. et al.: "Biodegradable poly(D,L-lactic acid)-poly(ethylene glycol)-monomethyl ether diblock copolymers: structures and surface properties relevant to their use as biomaterials", ***Biomaterials*** 21 (2000) pp. 2361-2370.

- [17] Abdelwahed, W. et al.: "Freeze-drying of nanoparticles: Formulation, process and storage considerations", **Advanced Drug Delivery Reviews** 58 (2006) pp. 1688-1713.
- [18] Young, I.J. et al.: "Surfactant-free nanoparticles of poly(DL-lactide-co-glycolide) prepared with poly(L-lactide)/ poly(ethylene glycol)", **SO: Journal of Applied Polymer Science** 89 (2003) pp. 1116-1123.
- [19] Chacón, M. et al.: "Stability and freeze-drying of cyclosporine loaded poly(D,L lactide-glycolide) carriers", **European Journal of Pharmaceutical Sciences** 8 (1999) pp. 99-107.
- [20] Gaumet, M. et al.: "Nanoparticles for drug delivery: The need for precision in reporting particle size parameters", **European Journal of Pharmaceutics and Biopharmaceutics** 69 (2008) pp. 1-9.
- [21] Westedt, U. et al.: "Poly(vinyl alcohol)-graft-poly(lactide-co-glycolide) nanoparticles for local delivery of paclitaxel for restenosis treatment", **Journal of Controlled Release** 119 (2007) pp. 41-51.
- [22] Zhang, Y. et al.: "Effect of poly(ethylene glycol)-block-poly(lactide) nanoparticles on hepatic cells of mouse: Low cytotoxicity, but efflux of the nanoparticles by ATP-binding cassette transporters", **European Journal of Pharmaceutics and Biopharmaceutics** 66 (2007) pp. 268-280.
- [23] Mosmann, T.: "Rapid colorimetric assay for cellular growth and survival: Application to proliferation and cytotoxicity assays", **Journal of Immunological Methods** 65 (1983) pp. 55-63.
- [24] Jose Alonso, M.: "Nanomedicines for overcoming biological barriers", **Biomedicine & Pharmacotherapy** 58 (2004) pp. 168-172.
- [25] Jeong, Y.I. et al.: "Effect of cryoprotectants on the reconstitution of surfactant-free nanoparticles of poly(DL-lactide-co-glycolide)", **Journal of Microencapsulation** 22 (2005) pp. 593-601.
- [26] Saez, A. et al.: "Freeze-drying of polycaprolactone and poly(-lactic-glycolic) nanoparticles induce minor particle size changes affecting the oral pharmacokinetics of loaded drugs", **European Journal of Pharmaceutics and Biopharmaceutics** 50 (2000) pp. 379-387.
- [27] Cavalli, R. et al.: "Sterilization and freeze-drying of drug-free and drug-loaded solid lipid nanoparticles", **International Journal of Pharmaceutics** 148 (1997) pp. 47-54.
- [28] Murakami, H. et al.: "Preparation of poly(-lactide-co-glycolide) nanoparticles by modified spontaneous emulsification solvent diffusion method", **International Journal of Pharmaceutics** 187 (1999) pp. 143-152.
- [29] Chorny, M. et al.: "Lipophilic drug loaded nanospheres prepared by nanoprecipitation: effect of formulation variables on size, drug recovery and release kinetics", **Journal of Controlled Release** 83 (2002) pp. 389-400.
- [30] Thioune, O. et al.: "Preparation of pseudolatex by nanoprecipitation: Influence of the solvent nature on intrinsic viscosity and interaction constant", **International Journal of Pharmaceutics** 146 (1997) pp. 233-238.
- [31] Ren, J. et al.: "Particle size and distribution of biodegradable poly-D,L-lactide-co-poly(ethylene glycol) block polymer nanoparticles prepared by nanoprecipitation", **Journal of Applied Polymer Science** 98 (2005) pp. 1884-1890.

- [32] Peltonen, L. et al.: "Improved entrapment efficiency of hydrophilic drug substance during nanoprecipitation of poly(l)lactide nanoparticles", **AAPS PharmSciTech** 5 (2004) pp. 115-120.
- [33] Bilati, U. et al.: "Nanoprecipitation versus emulsion-based techniques for the encapsulation of proteins into biodegradable nanoparticles and process-related stability issues", **AAPS PharmSciTech** 6 (2005) pp. E594-E604.
- [34] Zambaux, M.F. et al.: "Influence of experimental parameters on the characteristics of poly(lactic acid) nanoparticles prepared by a double emulsion method", **Journal of Controlled Release** 50 (1998) pp. 31-40.
- [35] Galindo-Rodriguez, S. et al.: "Physicochemical Parameters Associated with Nanoparticle Formation in the Salting-Out, Emulsification-Diffusion, and Nanoprecipitation Methods", **Pharmaceutical Research** 21 (2004) pp. 1428-1439.
- [36] Krigbaum, W.R. et al.: "Molecular weight dependence of the intrinsic viscosity of polymer solutions. II", **SO: Journal of Polymer Science** 11 (1953) pp. 37-51.
- [37] Sigma Aldrich Co.: "Biodegradable polymers: RESOMER materials by Boehringer Ingelheim", <http://www.sigmaaldrich.com/materials-science/polymer-science/resomer.html>. Date of access: 10-06-2010.
- [38] Riley, T. et al.: "Physicochemical Evaluation of Nanoparticles Assembled from Poly(lactic acid)-Poly(ethylene glycol) (PLA-PEG) Block Copolymers as Drug Delivery Vehicles", **Langmuir** 17 (2001) pp. 3168-3174.
- [39] Quintanar-Guerrero, D. et al.: "Preparation Techniques and Mechanisms of Formation of Biodegradable Nanoparticles from Preformed Polymers", **Drug development and industrial pharmacy** 24 (1998) pp. 1113-1128.
- [40] Gref, R. et al.: "Biodegradable long-circulating polymer nanospheres", **Science** 263 (1994) pp. 1600-1603.
- [41] Dong, Y. et al.: "Methoxy poly(ethylene glycol)-poly(lactide) (MPEG-PLA) nanoparticles for controlled delivery of anticancer drugs", **Biomaterials** 25 (2004) pp. 2843-2849.
- [42] Gref, R. et al.: "Polyoxyethylene-coated nanospheres: effect of coating on zeta potential and phagocytosis", **SO: Polymer International** 48 (1999) pp. 251-256.
- [43] Martin, O. et al.: "Poly(lactic acid): plasticization and properties of biodegradable multiphase systems", **Polymer** 42 (2001) pp. 6209-6219.
- [44] Stella, B. et al.: "Design of folic acid-conjugated nanoparticles for drug targeting", **SO: Journal of Pharmaceutical Sciences** 89 (2000) pp. 1452-1464.
- [45] Putaux, J.L. et al.: "Ultrastructural aspects of phytoglycogen from cryo-transmission electron microscopy and quasi-elastic light scattering data", **International Journal of Biological Macromolecules** 26 (1999) pp. 145-150.
- [46] Cheng, F.Y. et al.: "Stabilizer-free poly(lactide-co-glycolide) nanoparticles for multimodal biomedical probes", **Biomaterials** 29 (2008) pp. 2104-2112.



# **Chapter 3**

**Fluorescing nanoparticles for imaging  
applications in cell culture  
and *in-vivo* animal experiments**





## 1. Introduction

Fluorescence imaging using nanoparticulate systems is done either for diagnostic or detection purposes [1; 2] or during investigation and evaluation of the characteristic distribution behaviour of their respective drug loaded equivalents [3; 4]. Introduction of an appropriately detectable label is a prerequisite and could be done either by encapsulation of fluorescently labelled drug molecules [5; 6], the application of fluorescing matrix materials [7; 8] or by co-encapsulation of organic fluorescence dyes. The last method is the most frequently used one due to the ease of preparation and eventually the parallel applicability of unmodified drug molecules or the mere exchange of the labelling substance for the drug substance. Commonly used organic fluorophores reported in literature are for example coumarin 6, rhodamine 6G or Nile red, which are mainly chosen due to their fluorescence or solubility properties [9-13]. In general, the choice of an appropriate fluorescent label depends on the used particulate system, the intended application and the objective of the study as well as the used detection system.

In the current work Nile red has been chosen initially as desirable fluorescent probe due to several characteristics. By reason of its good solubility in organic solvents [14] and the very lipophilic nature, it was expected to allow an easy encapsulation into lipophilic and amphiphilic polymers with a high loading capacity, consequently leading to bright fluorescing particles. Various applications have been reported using Nile red as lipophilic fluorescent probe either as free dye (e.g. for direct staining of lipidic intracellular cell components [15; 16]) or in encapsulated form for *in-vitro* investigations in cell-culture [11; 17; 18] as well as isolated tissues [3; 19; 20]. With similar emission characteristics like other *in-vivo* applied fluorescent labels (e.g. CdSe quantum dots [21]) *in-vivo* applications of Nile red loaded nanoparticles may also be possible, which would make them a versatile and easily applicable tool.

Using the previously established nanoprecipitation system (**Chapter 2**), Nile red was encapsulated into several different biodegradable polymers, dealing as fluorescent probe and furthermore as lipophilic model drug. Impact of particle loading was investigated to identify possible alterations in the particle properties due to performed substance encapsulation. The applicability of different Nile red loaded nanoparticles was evaluated by imaging their behaviour in cellular context as well as after intravenous (i.v.) administration in nude mice. Finally the obtained *in-vivo* results were assessed by comparison with an additional fluorescence labelled system with longer emission wavelength in the near-infrared region.

## 2. Materials and Methods

### 2.1 Materials

#### 2.1.1 Preparation and characterization of nanoparticles

PLGA 75:25 (Resomer<sup>®</sup> 756) was obtained as kind gift from Boehringer Ingelheim (Boehringer Ingelheim AG, Biberach, Germany). Biodegradable copolymers PEG<sub>2</sub>PLA<sub>Y</sub> and NH<sub>2</sub>PEG<sub>2</sub>PLA<sub>Y</sub> (Y=20 and 40) were custom made following an established method as described in **chapter 2**. Nile red (nile blue A oxazone) and Pluronic<sup>®</sup> F68 were obtained from Sigma-Aldrich (Sigma-Aldrich Chemie GmbH, Taufkirchen, Germany). 1,1'-Diocetyl-3,3',3',3'-tetramethylindotricarbocyanine iodide [DiR] was purchased from Invitrogen (Invitrogen GmbH, Karlsruhe, Germany). Sucrose and ethanol (p.a.) were purchased from Merck (Merck KGaA, Darmstadt, Germany). Chloroform (p.a.) and acetone (p.a.) were obtained from Acros (Acros organics, Fischer scientific GmbH, Nidderau, Germany).

#### 2.1.2 Cell culture

The CHO-K1 cell line (ATTC code No. CCL-61), the L929 mouse fibroblasts and the MCF-7 human breast cancer cell lines were kind gifts of the Department of Pharmaceutical Chemistry, University of Regensburg. Fetal bovine serum [FBS] was purchased from Biochrom (Biochrom KG, Berlin, Germany). Trypsin-EDTA 0.25 %, Dulbecco's phosphate buffered saline [PBS] and Leibowitz medium L-15 were obtained from Invitrogen (Invitrogen GmbH, Karlsruhe, Germany). 3-[4,5-Dimethylthiazol-2-yl]-2,5-diphenyltetrazolium bromide [MTT] was purchased from AppliChem (AppliChem GmbH, Darmstadt, Germany). Monobasic sodium carbonate [Na<sub>2</sub>HCO<sub>3</sub>], HAM's F-12 and Eagle's minimum essential medium [EMEM] were obtained from Sigma-Aldrich (Sigma-Aldrich Chemie GmbH, Taufkirchen, Germany). Sodium pyruvate was purchased from Serva (Serva Electrophoresis GmbH, Heidelberg, Germany). Triton-X (p.a.) was obtained from Merck (Merck KGaA, Darmstadt, Germany).

#### 2.1.3 *In-vivo* imaging

Female hairless and immune competent SHK1-hr mice were obtained from Charles River (Charles River Laboratories Inc., Sulzfeld, Germany).

## **2.2 Methods**

### **2.2.1 Preparation of fluorescing nanoparticles**

Polymeric nanoparticles were prepared following modified nanoprecipitation methods [22] in detail established and discussed in **chapter 2**. Depending on the intended application, either the aqueous or the non-aqueous preparation route was used. Generally, a 1 % solution of the polymer was prepared in an organic solvent (either acetone or chloroform) and an aliquot of a stock solution of the fluorescent marker (either Nile red or DiR) in the same solvent was added (the amount was dependent on the intended loading). The final volume of the organic phase was generally adjusted to 5 ml. Afterwards this polymer solution was added dropwise to 40 ml of the external phase with an immediate formation of particles. The external phase differed depending on the used polymer solvent – ethanol in case of chloroform (non-aqueous system) and water in case of acetone (aqueous system). Afterwards the organic solvent was allowed to evaporate, followed by extended dialysis against an aqueous solution of Pluronic F68 (0.1 %) in case of the non-aqueous precipitation system. Recovery of the nanoparticles from the aqueous particle dispersions was performed via centrifugation (12,500 g, for at least 30 min, 10 °C; Avanti JE highspeed centrifuge; Beckman Coulter GmbH, Krefeld, Germany) and finally re-dispersion in 5 % sucrose. Microparticles and artefacts were removed via filtration (< 1 µm). Subsequently nanoparticles were freeze-dried using a lab-scale freeze-dryer (Martin Christ Gefriertrocknungsanlagen, Osterode am Harz, Germany). The used preparation parameters will be given, as required.

### **2.2.2 Determination of particle concentration**

Concentration of nanoparticles in dispersion was usually estimated semiquantitatively based on the solid content in an aliquot of the particle dispersions. For the determination one aliquot (usually 500 to 1000 µl) of the final dispersion was centrifuged (15,000 g, 45 min, 10 °C) and the residual sediment was freeze-dried and weighed to determine the particle content.

### **2.2.3 Fluorescence spectroscopic analysis**

Fluorescence spectra of the marker substances (in organic stock solutions) and the final particles (dispersed in aqueous solutions) were measured using a LS 55 spectrophotometer (PerkinElmer, Waltham, USA), equipped with a red-sensitive R928 photomultiplier in case of the DiR loaded samples. The measurement parameters differed depending on the used fluorescence label, as summarized in **table 1**.

**Tab. 1:** Instrumental settings for *in-vitro* fluorescence measurements

Marker	Excitation wavelength / nm	Spectrum range / nm	Detector voltage / V
Nile red	512	530-700	750
DiR	750	775-900	750

To allow a comparison of different particle batches, the measured intensities were subsequently normalized on the pre-determined particle concentration.

## 2.2.4 Determination of particle size

Photon correlation spectroscopy [PCS] was used to determine the hydrodynamic diameters and polydispersity indices of the prepared nanoparticles, usually dispersed in 5 % sucrose. Measurements were performed at 20 °C with a Zetasizer 3000 A (Malvern Instruments Inc., Herrenberg, Germany). Results are presented as mean and relative standard deviation of three independent measurements.

## 2.2.5 Determination of zeta potential

Zeta potential of nanoparticles, dispersed in water (pH ~6.7) was determined based on so-called laser Doppler electrophoresis using a Zetasizer 3000 A (Malvern Instruments Inc., Herrenberg, Germany). Measurements were performed at 20 °C and results are given as mean and relative standard deviation of six independent measurements.

## 2.2.6 Cell culture

The CHO cells were cultured in HAM's F-12 nutrient mixture, supplemented with 10 % FBS. The L929 cell line was cultured in EMEM medium supplemented with 10 % FBS. The MCF-7 cells were cultured in EMEM medium supplemented with 5 % FBS. Standard cell culture conditions were 37 °C, 95 % relative humidity and 5 % CO<sub>2</sub>. Growth medium was changed every third day.

## 2.2.7 Determination of biocompatibility

Investigation of biocompatibility followed an established procedure [23] using the colorimetric MTT assay for quantitative assessment. Acute toxicity of nanoparticles was investigated using a direct contact test. Three different cell lines were used, the CHO cells (animal derived endothelial cell line), the L929 cells (animal derived fibroblast cell line)

and a human cancer cell line, the MCF-7 cells. The general parameters of the assay in detail have been given in **chapter 2**.

All data were expressed as mean (N=4) and relative standard deviation. Statistic significance was assessed by one-way analysis of variances (ANOVA) in conjunction with Tukey's studentized range test using SigmaStat software.

### **2.2.8 Imaging of cellular uptake of fluorescently labelled nanoparticles**

Cellular uptake of fluorescently labelled nanoparticles was investigated using MCF-7 cell line. Cells were seeded in an 8-well Lab-Tek™ Chambered Coverglass (Nunc, Thermo Fisher Scientific, Langenselbold, Germany) with an initial density of 5,000 cells per well and grown for 48 h under standard cell culture conditions (given in **2.2.6**). Dispersions of Nile red loaded particles were prepared by re-suspending the lyophilisate with Leibowitz medium and the particle concentration was adjusted to 0.2 mg/ml. After aspiration of the supernatant from the seeded cells, 150 µl of the each dispersion was added to one chamber, followed by incubation for 30 min at standard cell culture conditions under light exclusion. Cellular uptake was documented by confocal laser scanning microscopy [CLSM] using a Zeiss Axiovert 200 M microscope coupled to a Zeiss LSM 510 scanning device (Carl Zeiss Co. Ltd., Germany). The inverted microscope was equipped with a Plan-Apochromate 63x objective. Samples were excited with a 514 nm argon laser and fluorescence was detected with a 560 to 615 nm bandpass filter. To attribute for the varying fluorescence properties of the used particle batches and to allow a semiquantitative comparison of the results, images recorded at equivalent microscopic settings were subsequently normalized on the initial fluorescence intensity of the prepared particles by image contrast enhancement.

### **2.2.9 *In-vivo* imaging of fluorescently labelled nanoparticles**

The *in-vivo* behaviour of two differently fluorescently labelled particle types was investigated following intravenous administration in nude, female SKH1-hr mice (25 to 30 g body weight). The *in-vivo* experiments generally complied with the standards for the use of animal subjects as stated in the guideline from the animal care and use committee of the Martin Luther University, Halle-Wittenberg, Germany. All mice were housed under controlled conditions (12 h light/dark schedule at 24 °C). During the imaging process the mice were placed on a 35 °C temperature controlled heating plate to prevent cooling out under the anaesthesia. The used narcotic system was an inhalation anaesthesia system with a gas mixture of isoflurane/oxygen with an initial flow of 4 % isoflurane (3.0 L/min O<sub>2</sub>) and a steady state flow of 1.8 % isoflurane (1.5 L/min O<sub>2</sub>). Following re-dispersion of

an aliquot (nanoparticles lyophilisate in purified water) the dispersion was isotonized with sorbitol and about 100  $\mu$ l of the dispersion were slowly injected into the tail vein.

Measuring and imaging of the particles fluorescence signal *in-vivo* was performed with a Maestro<sup>TM</sup> *in-vivo* fluorescence imaging system (Cambridge Research & Instrumentation, Woburn, MA), equipped with a Cermex<sup>®</sup>-type 300 Watt Xenon lamp with 5600 K. Experimental settings differed slightly depending on the used fluorescence dye (**Tab. 2**).

**Tab. 2:** Instrumental settings for *in-vivo* fluorescence measurements

Particulate system	Excitation filter / nm	Emission filter / nm	Spectral range / nm	Exposure time / ms
PLGA/Nile red	503-555	Long-pass 580	550-800	1000
PEG <sub>2</sub> PLA <sub>20</sub> /DiR	710-760	Long-pass 800	780-950	800

The reference spectra were obtained from aqueous dispersions of dye loaded nanoparticles and the *in-vivo* background spectra were determined using an untreated mouse. Analysis and image generation was performed using the Maestro software supplied with the instrument (version 2.10). The stepwise generation of a representative unmixed picture is demonstrated in **figure 1**. In a first step fluorescence signals of the mice were recorded in 10 nm steps over the whole spectral range (**Tab. 2**). This series is composed to the so-called cube image. Unmixing of these cubes was done by allocating the signal of each pixel either to the background or the desired fluorescent probe. The obtained corresponding images were subsequently saved in monochrome format. The generated greyscale fluorescence images are then displayed using an intensity weighted colour system, where high fluorescence concentrations are displayed in dark red and low fluorescence intensity in blue. In between there is an incremental colour gradient from red to blue.

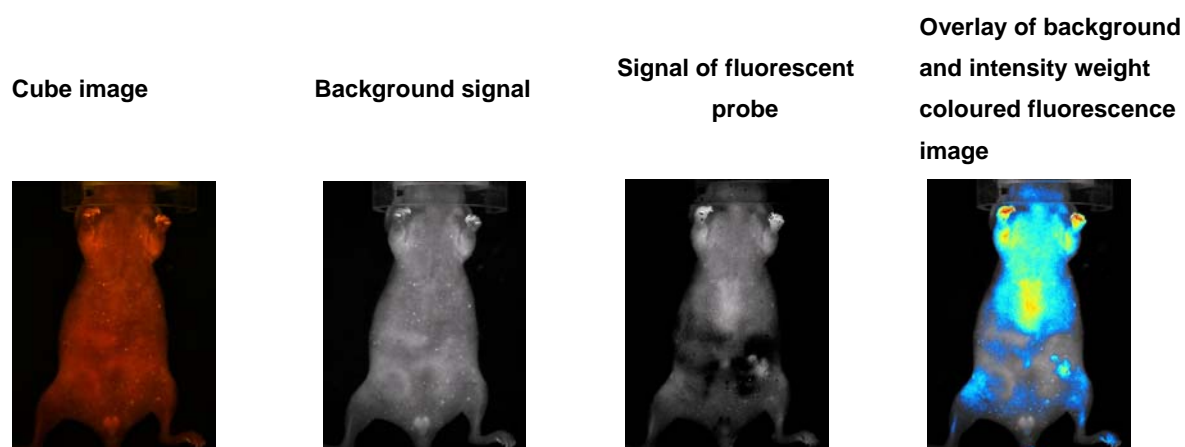


**Fig. 1:** *In-vivo* fluorescence images displayed the step-wise picture analysis procedure

To allow the comparison and evaluation of the time-dependent processes of particle distribution, fluorescence intensities of the obtained images at different time-points after NP administration (p.a.) were normalized on the maximum intensity of all pictures. Results will be presented using these so-called compare images.

### 3. Results

Fluorescently labelled nanoparticles were prepared using different biodegradable polymers. Factors potentially influencing the particles properties (e.g. polymer type, precipitation system and loading) were investigated for the Nile red loaded particles. Both, Nile red and DiR loaded nanoparticles were used as fluorescing marker system either in cellular context or for small animal imaging.

#### 3.1 Nile red loaded nanoparticles – PLGA

##### 3.1.1 Effect of Nile red loading

Following the non-aqueous precipitation method, loading of the lipophilic PLGA nanoparticles with the lipophilic fluorescence dye Nile red was successful over a wide loading range, from 0.05 % up to about 2.5 % dye per polymer weight (**Fig. 2, left**). Only in case of highest intended loading with 5 % preparation failed due to particles' flocculation during dialysis.

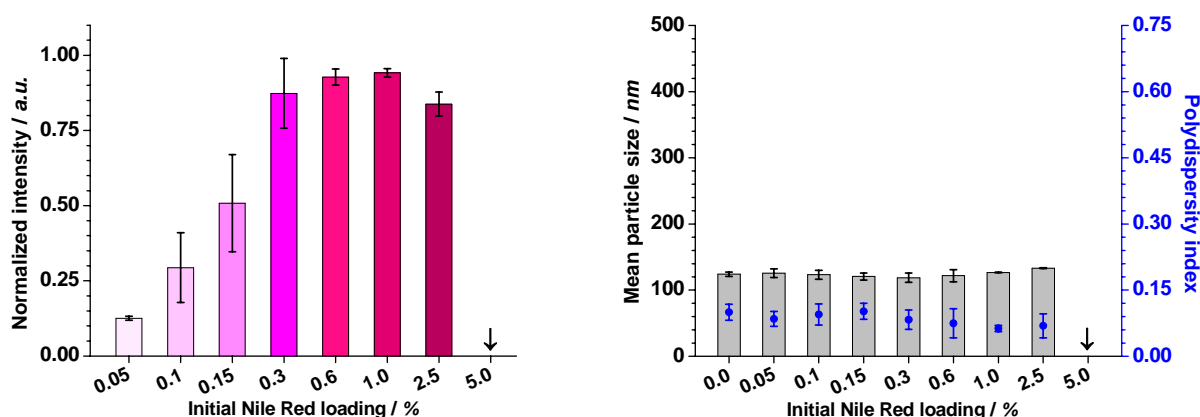


**Fig. 2:** PLGA nanoparticles prepared by nanoprecipitation using ethanol and chloroform, loaded with increasing amounts of Nile red – (*left*) development of maximum fluorescence intensity; (*right*) development of mean particle sizes [nm] and polydispersity index; arrows indicate a failure in particle preparation

Fluorescence intensities were found to increase steadily with increasing Nile red loadings up to 0.3 % and then kept constant with further increase of added dye. Additionally, also the maximum emission wavelength shifted from 590 nm to about 608 nm with increasing loadings of Nile red. However, neither the mean particle sizes nor the size distributions, indicated by the PI of the particles, were affected by the different amounts of added dye molecules (**Fig. 2, right**).



### 3.1.2 Effect of the nanoprecipitation system

In case of the PLGA particles, only a limited impact of the precipitation system on the properties of the obtained particles was found (**Fig. 3**). Both systems resulted in particles, with fluorescence intensities far below the values expected based on the intensity of the used organic stock solution. Furthermore, even a constant fluorescence for different loadings was found in case of the aqueous precipitation system (**Fig. 3, left**).

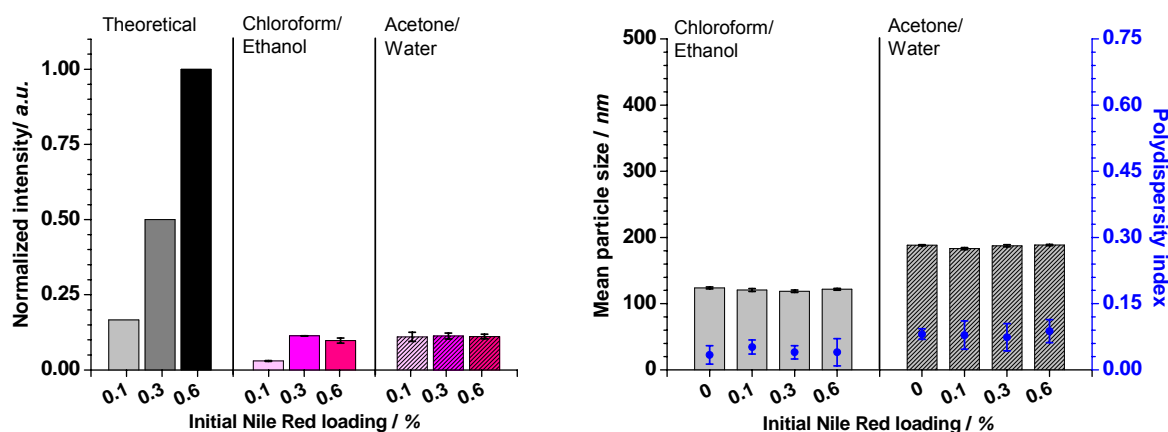


**Fig. 3:** PLGA particles prepared by nanoprecipitation using differing systems, loaded with increasing amounts of Nile red – (*left*) development of maximum fluorescence intensity; (*right*) development of mean particle sizes [nm] and polydispersity index

Particle sizes again were almost independent of the absolute dye loading and the precipitation system. The obtained polydispersity indices indicate very small, nearly monodisperse size distributions (**Fig. 3, right**).

## 3.2 Nile red loaded nanoparticles – diblock copolymers

The impact of different process parameters on the properties of particles prepared from PEG containing diblock copolymers was exemplarily demonstrated using PEG<sub>2</sub>PLA<sub>40</sub>, as the effects were found to be similar for all used amphiphilic diblock copolymers. Comparable to the results obtained with PLGA, fluorescence intensities of particles were far below the expected values, independent of the used precipitation system (**Fig. 4, left**). However, the impact of the absolute loading was found to be higher for the amphiphilic polymers, since intensity steadily increased with higher loadings (**Fig. 4, right**). Additionally, the obtained fluorescence intensities, achieved using the non-aqueous system, were generally lower than the respective values of the aqueous system.

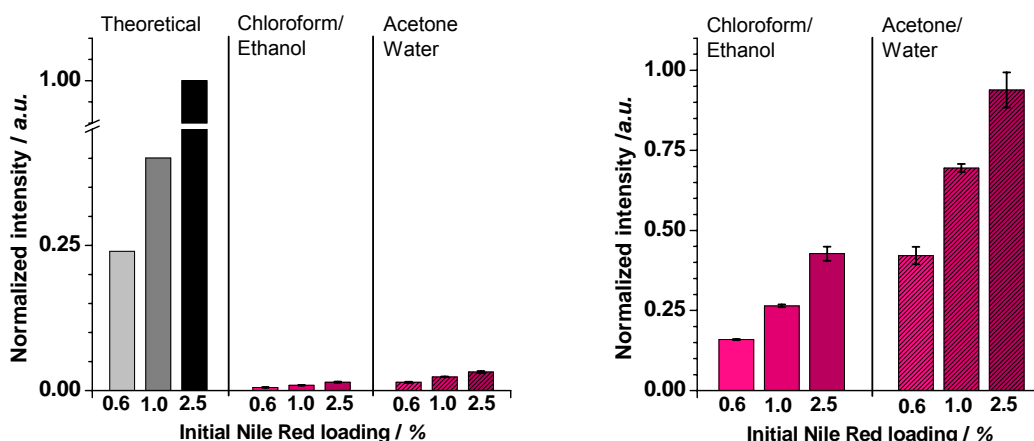


**Fig. 4:** PEG<sub>2</sub>PLA<sub>40</sub> particles prepared by nanoprecipitation using differing systems, loaded with increasing amounts of Nile red – (*left*) development of maximum fluorescence intensity normalized on theoretical maximum value; (*right*) development of maximum fluorescence intensity normalized on real maximum value

Particle sizes were predominantly affected by the used precipitation system (**Fig. 5**). Independent of the Nile red loading particles, prepared by the aqueous route were about 100 nm in diameter. In contrast, the non-aqueous procedure led to clearly higher particle sizes, above 200 nm, which additionally slightly increased with increasing dye load. Indeed, both processes resulted in still very narrow size distributions, indicated by PIs below 0.1.

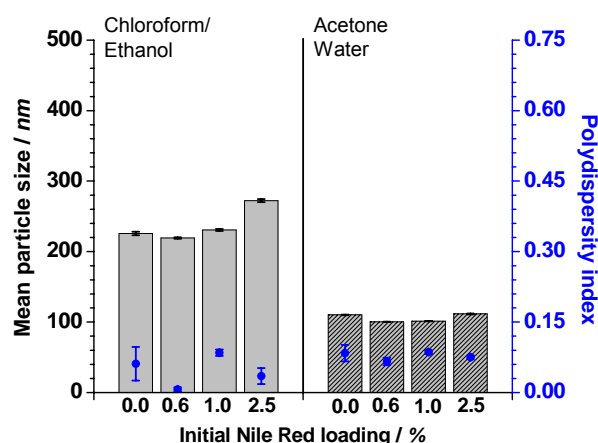


**Fig. 5:** Mean particle sizes [nm] and polydispersity indices of PEG<sub>2</sub>PLA<sub>40</sub> particles loaded with increasing amounts of Nile red prepared by nanoprecipitation using different systems

### 3.3 Biocompatibility of fluorescently labelled nanoparticles

Biocompatibility of fluorescently loaded nanoparticles was tested using different cell lines. Prior to application, tests were usually performed using L929 and CHO cells. Independent of the dye loading (either with Nile red or DiR), cytotoxicity generally was found to be very low, which is expressed by high relative cell viabilities around 100 %.

In case of PLGA particles, loaded with increasing amounts of Nile red (**Fig. 6**), only the batch with 2.5 % loading showed a significant toxicity in CHO cells at the highest concentration (**Fig. 6, right**).

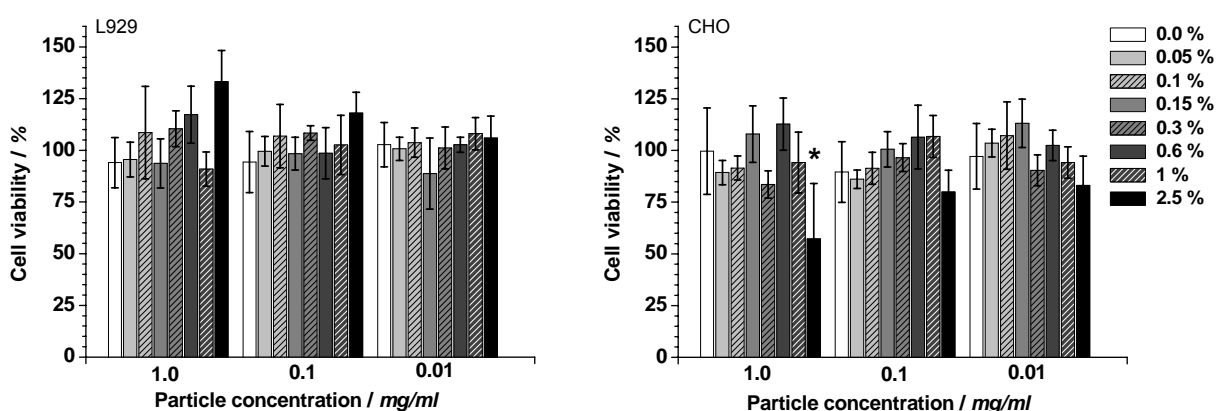


**Fig. 6:** Viability of (*left*) L929 cells and (*right*) CHO cells after incubation (4 h) with PLGA nanoparticles loaded with increasing amounts of Nile red, prepared via the non-aqueous system; star indicate significant toxicity compared to the respective negative control ( $p < 0.05$ ); legend applicable for both diagrams

Since MCF-7 cells were used for the cellular uptake studies, cytotoxicity in this cell line was also tested for the used particles (all loaded with 0.15 % Nile red). Statistically different toxicity was found only in for highest concentrations of PEG<sub>2</sub>PLA<sub>20</sub> particles with still remaining viability over 85 % (**Fig. 7**).

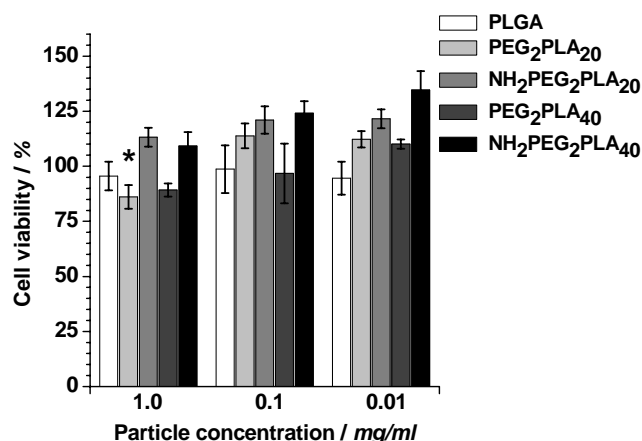


**Fig. 7:** Viability of MCF-7 cells after incubation (4 h) with nanoparticles prepared of different polymers loaded with 0.15 % Nile red; star indicates significant toxicity compared to the respective negative control ( $p < 0.05$ )

PEG<sub>2</sub>PLA<sub>40</sub> particles, loaded with 1 % DiR and prepared following the aqueous procedure, which have been used for the small animal imaging, also caused statistically significant toxicity (again with remaining viability still above 80 %) in CHO cells but not in L929 cells (**Fig. 8**).

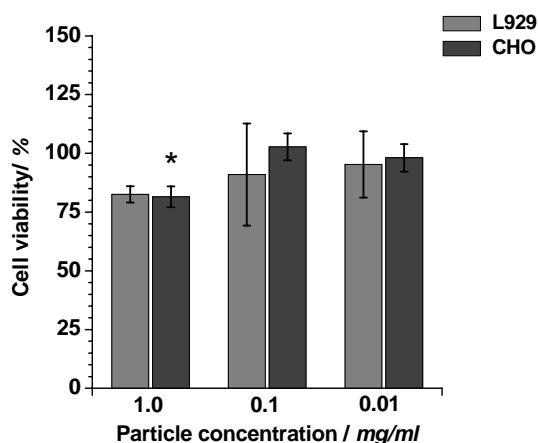


**Fig. 8:** Viability of L929 cells and CHO cells after incubation (4 h) with PEG<sub>2</sub>PLA<sub>40</sub> nanoparticles loaded with 1 % DiR, prepared via the aqueous precipitation route; star indicates significantly reduced viability compared to the respective negative control ( $p < 0.05$ )

### 3.4 Imaging of cellular uptake

The behaviour of nanoparticles prepared from different biodegradable polymers was investigated by imaging their cellular uptake in MCF-7 cells. The used particles differed in their polymer matrix, but also in basic particle properties, such as size and fluorescence intensity, as summarized in **table 3**.

**Tab. 3:** Properties of Nile red loaded particles used for cellular uptake experiments

Polymer	Precipitation system	Initial loading / %	Fluorescence intensity	Mean particle size ( $\pm$ SD) / nm	Zeta potential ( $\pm$ SD) / mV
PLGA	Chloroform/ethanol	0.15	323	123.3 (0.6)	-53.2 (0.9)
PEG <sub>2</sub> PLA <sub>20</sub>	Acetone/water	0.15	304	79.6 (0.3)	-25 (2.1)
NH <sub>2</sub> PEG <sub>2</sub> PLA <sub>20</sub>	Chloroform/ethanol	0.15	132	123.7 (0.7)	-41 (1.7)
PEG <sub>2</sub> PLA <sub>40</sub>	Acetone/water	0.15	683	99.5 (0.6)	-32 (5.3)
NH <sub>2</sub> PEG <sub>2</sub> PLA <sub>40</sub>	Chloroform/ethanol	0.15	110	101.2 (0.2)	-40 (1.7)

Polydispersity indices for all used particles were well below 0.1, indicating overall very small size distributions.

Originally obtained CLSM images have been normalized on the fluorescence intensity of the used particle batch to contribute the mentioned differing optical properties and to allow an estimation of the particle immanent factors affecting the results of the interaction of particles with the cells. Indicated by the thereof obtained different intensities in the pictures, extent of intracellular accumulation of the fluorescence differed depending on the used polymer type (**Fig. 9**).

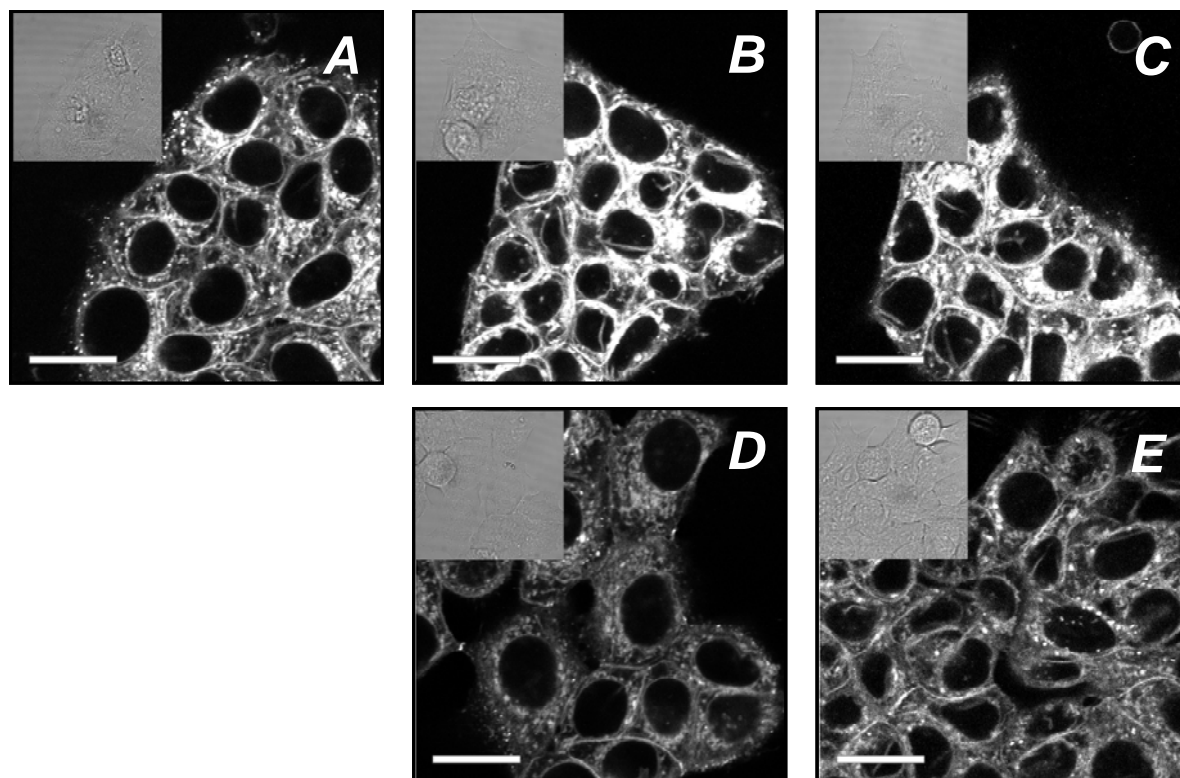


**Fig. 9:** CLSM images of MCF-7 cells after incubation (30 min) with Nile red loaded particles prepared of (A) PLGA; (B) PEG<sub>2</sub>PLA<sub>20</sub>, (C) NH<sub>2</sub>PEG<sub>2</sub>PLA<sub>20</sub>, (D) PEG<sub>2</sub>PLA<sub>40</sub> and (E) NH<sub>2</sub>PEG<sub>2</sub>PLA<sub>40</sub>; inserts represent corresponding brightfield images; scale bars correspond to 20 μm

Based on optical evaluation, highest intensities were found for cells incubated with PEG<sub>2</sub>PLA<sub>20</sub> and NH<sub>2</sub>PEG<sub>2</sub>PLA<sub>20</sub> particles, followed by PLGA nanoparticles and lowest values appeared in case of PEG<sub>2</sub>PLA<sub>40</sub> and NH<sub>2</sub>PEG<sub>2</sub>PLA<sub>40</sub>. Overall no fluorescence was apparent in the cell nuclei (dark round areas within the cells). However, the cellular membranes between neighbouring cells seem to be clearly stained for all used polymers.

### 3.5 *In-vivo* imaging

Small animal imaging was performed after i.v. injection of the particles suspended in isotonic dispersions. Basically two different particle systems were compared – PLGA particles loaded with 0.3 % Nile red (mean particle size of 135 nm) and PEG<sub>2</sub>PLA<sub>40</sub> particles loaded with 1 % DiR (mean particle size of 150 nm). Time-dependent distribution behaviour was investigated by repeated imaging over a certain time and the obtained results are presented as compare images, obtained as described in 2.2.9.

Following the intravenous application fluorescence signal of Nile red was rapidly distributed within the whole animal body (**Fig. 10**) and starts to accumulate predominantly in the gall bladder. Within 15 and 37 min after injection fluorescence intensity in gall bladder reached almost maximum values, followed by an accumulation in the urinary bladder. 55 min after injection Nile red signal is detectable in urinary bladder only.

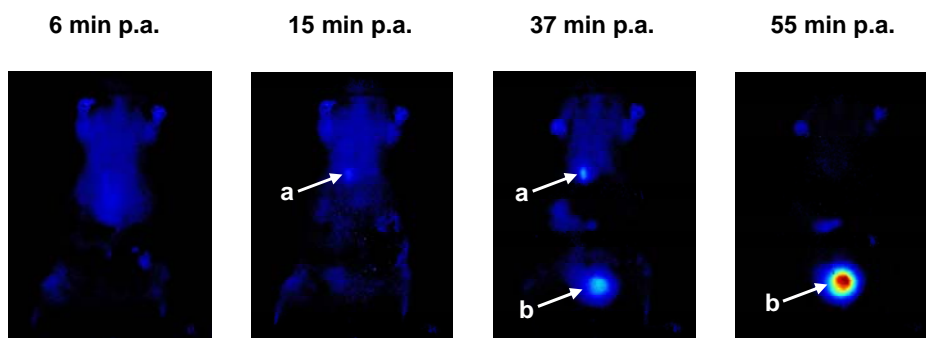


**Fig. 10:** *In-vivo* fluorescence images of nude female mice at certain time points after i.v. administration (p.a.) of PLGA nanoparticles loaded with 0.3 % Nile red; arrows indicate distinct organs: (a) gall bladder and (b) urinary bladder

In case of the DiR loaded PEG<sub>2</sub>PLA<sub>40</sub> particles differing result were obtained (**Fig. 11**). Following an initial rapid distribution phase, accumulation, apparent within 7 min after injection, is almost restricted to the liver during the first 40 min and then fluorescence could be also detected in the spleen. Nevertheless, circulating particles could be detected even 24 h after injection in regions outside spleen and liver, indicated by the blue staining of the animal's body.

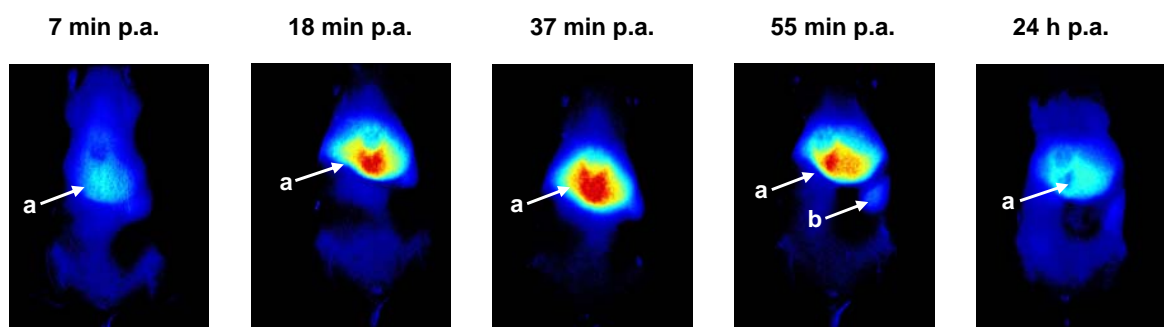


**Fig. 11:** *In-vivo* fluorescence images of female nude mice at certain time points after i.v. administration (p.a.) of PEG<sub>2</sub>PLA<sub>40</sub> nanoparticles loaded with 1 % DiR; arrows indicate distinct organs: (a) liver and (b) spleen

## 4. Discussion

Nanoparticles gain more and more attention in biomedical applications and are also widely used for imaging applications, either for diagnostic purposes or as model systems to visualize the distribution of their respective drug loaded equivalents.

The main focus of this chapter was the evaluation of the established nanoparticulate system with respect to a potential application for fluorescence imaging purposes. Focussed on plain particles several impact factors already have been thoroughly investigated to allow tailoring of suitable particles with desired properties (**chapter 2**). However, also the encapsulation of different dye compounds could alter the particles properties and obviously needs to be evaluated before each application. Respective fluorescence labelling of particles was done by encapsulation of the lipophilic fluorescent dye Nile red, and various dye loadings were investigated with respect to their impact on the particles properties and for identification of optimal conditions for *in-vitro* and *in-vivo* imaging.

Generally, the encapsulation of the lipophilic Nile red was successful in all used polymers and almost independent of the used solvent – non-solvent system. However, the properties of the obtained particles differed depending on the applied preparation conditions. First of all, the effect of Nile red loading on particle size was almost negligible over a wide range of concentrations (**Fig. 2, right; Fig. 3, right; Fig. 5**). The differences observed using different polymers and varying precipitation systems (**Fig. 3, right; Fig. 5**) were almost equal to the behaviour of unloaded nanoparticles, as presented in **chapter 2**. In general the effect of substance load on particles size varied due to the properties of the used compound, the matrix material and also the chosen preparation method [24-27]. Indeed, the initial absolute drug load is usually not among the main factors influencing the resulting particles size. This could deal as indication for a very homogenous distribution of the lipophilic Nile red dye within the used polymeric matrices already in the polymer solution due to intense interactions between the polymer and the dye. Principally it could be expected that nanoparticles with encapsulated compounds, which are well dissolved in the polymer matrix, are less affected by increased loadings compared to systems containing particulate substances in solid state, which obviously require a higher space during the particle formation.

In this context also the encapsulation efficiency of the dye needs to be considered, which obviously determines the particles fluorescence intensity, and therefore might deal as indicator for the amount of encapsulated dye. At first, it is remarkable that the overall fluorescence intensities of Nile red loaded particles are far below the values expected from comparisons with organic stock solutions containing equal concentrations of the dye (**Fig. 3, left; Fig. 4, left**). This would mean overall very bad encapsulation efficiencies of



about only 3 % in the best case, which was unexpected considering the lipophilic nature of both the dye and the matrix polymer. Additionally, at least the used aqueous nanoprecipitation method has been reported to be well-suited for the processing of lipophilic substances [22; 27; 28]. Indeed, the low fluorescence intensities following the encapsulation might be attributed to a quenching of the solid polymer matrix as well as a “self”-quenching of neighbouring dye molecules due to the high loading density [29-31]. Considering both of these possible effects, the determined intensities could hardly be used as measure for the absolute amount of encapsulated compound. However, an estimation of relative values is still possible, allowing the comparison of different batches and particle types. The results obtained also show a differing behaviour of lipophilic PLGA and the amphiphilic copolymers. While PLGA matrices seem to be dye saturated, if the initial loading exceeds 0.3 % (**Fig. 2, left**, **Fig. 3, left**), and no further increase in fluorescence intensity could be observed. The loading and the resulting fluorescence intensity increased in case of the PEG<sub>2</sub>PLA<sub>40</sub> particles with theoretical loadings up to 2.5 % without reaching a plateau of the fluorescence. Comparing the absolute measured intensities it was found that the overall highest values were reached for PEG<sub>2</sub>PLA<sub>40</sub> particles prepared by the aqueous solvent – non-solvent system (**Tab. 4**). However, this does not necessarily mean that also the highest dye amounts are encapsulated in these particles, since the various polymeric matrices could significantly differ in their optical behaviour.

**Tab. 4:** Mean fluorescence intensities ( $\pm$  SD) of Nile red loaded nanoparticles in aqueous dispersion (1 mg/ml)

PLGA			PEG <sub>2</sub> PLA <sub>40</sub>					
Chloroform/ethanol			Chloroform/ethanol			Acetone/water		
0.6 %	1 %	2.5 %	0.6 %	1 %	2.5 %	0.6 %	1 %	2.5 %
873.37 (22.25)	781.88 (11.90)	695.70 (33.55)	232.17 (2.18)	385.35 (5.8)	622.68 (32.08)	614.00 (39.31)	1011.78 (18.08)	1366.70 (80.33)

Considering the absolute values, encapsulation efficiency and resulting fluorescence intensity is not only affected by the polymer type, but moreover also by the used solvent non-solvent system. The decrease in intensity in the non-aqueous environment could be attributed to the higher solubility of Nile red in the ethanolic external phase, leading to a pronounced dye loss from precipitated particles during the evaporation of chloroform. This is in line with reports on a nearly 1000fold increase in Nile red’s solubility by changing the dissolution medium from aqueous to organic (i.e. acetone) [14]. Interestingly this effect was much higher in case of the amphiphilic copolymers, as the intensities of differently loaded PLGA based particles prepared in the different solvent – non-solvent systems

showed only minute differences (**Fig. 3, left**). This additional impact of the polymer matrix may be explained by the softer and more sponge-like structure of the diblock copolymer nanoparticles, already discussed in **chapter 2**. It allows the penetration of ethanol and subsequent enhanced dissolution of dye from the particles, leading to a higher loss of fluorescence in the non-aqueous system.

Although only a limited part of the different process steps was investigated, the obtained results clearly demonstrate the complex nature of the nano-encapsulation processes, whose results are a product of numerous interactions, for example between dye and matrix materials as well as between dye and the different solvents or liquids used. Usually such factors have to be thoroughly investigated in case of drug loaded systems in order to successfully optimize the results for each investigated drug compound. Furthermore, such factors also will have to be considered, if an appropriate model system for imaging purposes is requested. Here an optimal transfer of the imaging results would ideally require identical properties of both the original drug loaded particles and the investigated dye loaded model systems.

Despite the high variability in the resulting particle fluorescence, the particles with initial loadings ranging between 0.15 and 0.6 % were found to be sufficiently bright for all intended imaging purposes, which were subsequently performed with individual batches. Additionally, all investigated batches demonstrated a high biocompatibility of the Nile red loaded nanoparticles in various tested cell types (**Fig. 6; Fig. 7**) independent of used matrix, the loading or the applied solvent – non-solvent system, which obviously allows their universal use as imaging tool in various cellular contexts.

The performance of the polymeric nanoparticles in cellular context was investigated using a human breast cancer cell line, MCF-7 cells, which is a well-established system for evaluation of the efficiency of various antitumor drugs and their respective delivery systems, including various nanoparticulate formulations [10; 32-34]. Uptake of the nanoparticles prepared from differing matrix materials by MCF-7 cells has been already reported [32-35] and could also be demonstrated for all five polymer types investigated herein. The batches were chosen with respect to the obtained particle size based on PCS measurements, which should be around 100 nm for all polymers, which explains the different used preparation procedures (**Tab. 3**). This approach should minimize additional effects of differing particles sizes and only the impact of particle nature or polymer type should be observed. Following the incubation of cells with the different Nile red loaded nanoparticles (for 30 min), the dye fluorescence could be detected for all polymers. It was localized within the cytoplasm or in the region of the cellular membranes (**Fig. 9**). The fluorescence observed in the cytoplasm was attributed to individual or aggregated nanoparticles and the observed intensities differed largely depending on the particle types

(complete *in-vitro* properties are summarized in **table 3**). Observed differences in the normalized fluorescence intensity could not be allocated to one certain factor, as the particles taken up to the highest extent, were prepared from PEG<sub>2</sub>PLA<sub>20</sub> and NH<sub>2</sub>PEG<sub>2</sub>PLA<sub>20</sub> and these particles differed in two properties, their particle size (about 40 nm) as well as their zeta potential (about 10 mV).

Various investigations about factors influencing the cellular uptake of drug loaded nanoparticles can be found in literature [36-41]. The there discussed key parameters include the particle size, the surface charge and the surface decoration with other coatings (e.g. the amount of stabilizers and/or targeting sequences). In summary it could be said that the here observed particle behaviour could hardly be attributed to one specific factor, moreover several parameters were responsible to varying extents.

Focussing on the impact of zeta potential, it was reported to be more important for smaller particles (comparing 250 nm and 100 nm species) [42], whereas further studies also reported almost no impact of the zeta potential [33]. Focussing on the particle size, usually smaller particles are taken up to a higher extent, however, the differences between the investigated sizes were usually more prominent comparing particles with sizes of 150 nm and several micrometer [37; 41; 43]. Also the molecular weight of the surface decorating PEG block in case of PEGylated nanoparticles was found to change the specific cellular response in certain cell types [44], but this is not applicable for the current results, where only one PEG type (2 kDa) was investigated. Additionally, it has to be mentioned that both used types of diblock copolymers probably differ significantly in the PEG surface density, which is indicated by their zeta potentials. This effect has to be attributed to differing preparation methods, which were used in order to prepare similar sized particles. In line with the discussion in **chapter 2** and as mentioned above, the NH<sub>2</sub>PEG<sub>2</sub>PLA<sub>γ</sub> based particles (prepared with the non-aqueous route) were found to exhibit an even more negative surface potential than the respective mPEG-derivatives (prepared via the aqueous procedure). This could deal as an indication for a reduced interaction of the NH<sub>2</sub>PEG with the ethanolic environment, which consequently did not favour the outward orientation of the PEG chains, leading to a reduced shielding of the negative zeta potential.

Overall it was demonstrated that the cellular uptake is a very complex process and its elucidation still is in the focus of ongoing research. Furthermore, the limited results presented herein allow no thorough discussion of all obvious impact factors, which would necessitate a more comprehensive investigation of cellular uptake for different polymer types and also preparation methods as performed in **chapter 2** for the particles sizes and fluorescence properties, which is obviously out of the scope of this work.

As mentioned above also the cell membranes were strongly fluorescing (**Fig. 9**), which could eventually be attributed to a high density of nanoparticles in the outer region of the cytoplasm. However, a very recently published work also used Nile red for the investigation of the *in-vitro* transfer of lipophilic compounds between different lipid particles [45]. Considering that similar phenomena are rather likely to occur also in cellular context, this would lead to a pronounced accumulation of the free dye in the double layer of the lipid cell membrane, which additionally hampers the discussion of the uptake results.

The limitations of the dye Nile red as marker substance for imaging of drug delivery systems became even more obvious by the results obtained from *in-vivo* imaging (**Fig. 10**). Generally the Nile red fluorescence was initially very well distributed within mouse body following i.v. administration of the PLGA nanoparticles. However, since a significant release of the fluorescence dye was already observed *in-vitro*, it is questionable whether the obtained signal could be attributed to the Nile red loaded nanoparticles or to released dye molecules in lipophilic cellular contexts or tissues. Both have to be critically discussed in the following.

First of all the time-dependent distribution of the *in-vivo* fluorescence signal in circulation is comparable to other investigations of polymeric nanoparticles with unmodified surfaces [46-48]. Additionally Nile red is almost exclusively fluorescing in lipophilic environments [14] Therefore, at the first glance, the fraction of the detected fluorescence might be very well attributed to Nile red still incorporated in lipophilic PLGA particles. In that case, the very fast elimination of fluorescence, occurring within 1 h after administration, could be attributed to an strong activation of the reticuloendothelial system [RES] following opsonisation of the unmodified ('naked') particles [46]. However, there are two main factors/observations weakening this assumption: the spectral properties of the fluorescence signal and the observed fluorescence' body distribution. At first, the Nile red fluorescence spectrum extracted from *in-vivo* data is not similar to the respective *in-vitro* curves (**Fig. 12**). This indicates an alteration of the dye loaded particles or a leakage of the dye to different lipophilic areas, since Nile red is known for its pronounced solvatochromatic properties with changing fluorescence depending on the hydrophobicity of its environment [14]. Additionally the observed blue-shift of the maximum emission wavelength ( $\Delta\lambda_{em} \sim 20$  nm) complicates the separation of measured fluorescence from the background signal, which obviously further hampers the image processing.

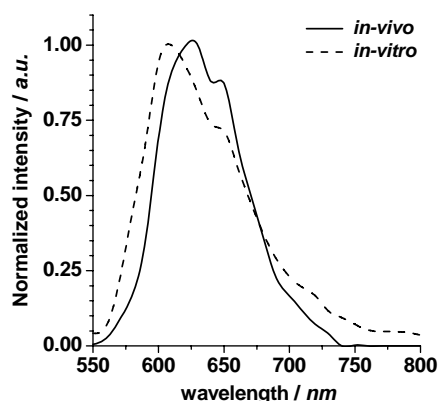


**Fig. 12:** Normalized fluorescence spectra of Nile red loaded PLGA nanoparticles measured either *in-vitro* or *in-vivo*

As mentioned above also the observed tissue distribution of the fluorescence has to be taken into consideration for the final evaluation. Obviously there is pronounced accumulation of the fluorescence also in the bladder. Keeping in mind the renal filtration threshold [49], an accumulation of solid PLGA particles (sizes above 100 nm) will be rather unlikely. Therefore the results might also indicate a significant dye loss during the investigation, which becomes either bound to endogenous substances with significant renal filtration or the dye even gets metabolized.

Additionally, it is very remarkable that no fluorescence at all could be detected in the liver or spleen (**Fig. 10**), which is in contrast to the above mentioned participation of the RES in the elimination of unmodified particles [46]. However, the observed lack of particle accumulation in the liver can also be attributed to other hurdles for the detection. Considering the Nile red fluorescence spectrum, it is very likely that the particles could not be visualized as the main fluorescence will be absorbed by the extraordinary high amounts of haemoglobin present in these RES organs, which exhibit their maximum absorption in the spectral range of Nile red's  $\lambda_{em}$  (**Fig. 13**). Overall, this discussion points out the numerous of factors, which need to be considered during the development of appropriate imaging systems and furthermore show the limited applicability of Nile red as fluorescence marker for *in-vivo* investigations.

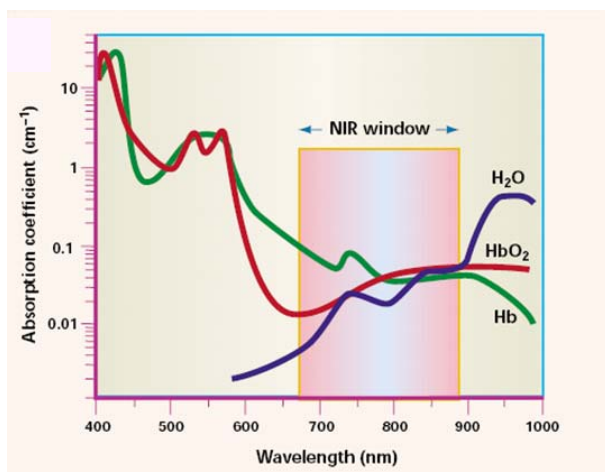


**Fig. 13:** Wavelength dependent absorption coefficient of haemoglobin (Hb), oxyhaemoglobin (HbO<sub>2</sub>) and water; demonstration of the near-infrared window appropriate for *in-vivo* imaging [50]

In general the alternatively used near infrared [NIR] light is much better suited for the non-invasive *in-vivo* imaging, furthermore allowing also the imaging of deeper tissue regions (>500  $\mu\text{m}$ ) [50]. Therefore the second nanoparticulate system was loaded with DiR as lipophilic marker, exhibiting a  $\lambda_{em}$  of about 788 nm. For this dye the partition between lipophilic phases, as observed with Nile red, was expected to occur to a much lower extent. For example, due to the higher lipophilicity of the DiR ( $\log P_{\text{Nile red}} \sim 5$  [16];  $\log P_{\text{DiR}} \sim 18$  [51]) a transfer between lipophilic areas with bridging of hydrophilic barriers should be rather unlikely and additionally no shift in the  $\lambda_{em}$  was detectable during the experiment, when comparing the DiR spectra obtained either *in-vivo* or *in-vitro* (data not shown). PEG<sub>2</sub>PLA<sub>40</sub> particles loaded with 1 % DiR were successfully used to demonstrate an *in-vivo* particle distribution and their improved fluorescence properties even allowed the visualization of individual blood vessels near the animal's skin during the first 4 h following i.v. injection (**Fig. 14**).



**Fig. 14:** Inverted grey-scale fluorescence image of a female nude mouse 30 min p.a. of DiR loaded PEG<sub>2</sub>PLA<sub>40</sub> nanoparticles; dark regions indicate areas with high fluorescence intensity

The time-dependent results differed significantly from the above described Nile red observations (**Fig. 11**). Following a fast distribution phase a pronounced accumulation could be observed in the liver, which was somehow surprising as particles with a PEG layer on the surfaces have been reported to reduce the activation of RES due to a reduced opsonisation, leading to reduced liver uptake, although this can be never completely avoided [44; 46; 52]. Nevertheless, a typical increase in circulation time compared to uncoated particles, could be observed by a significant fluorescence in the circulation (outside the liver) also 24 h after administration of the particles. This inconsistency may be attributed to an inhomogeneous PEG distribution on the particles surfaces, here particles with only partial and imperfect coating would be identified by the RES and eliminated immediately [53] and the perfectly coated ones would be able to circulate up to several days. An identification of the surface coating or a separation of the different particle species would obviously be of utmost importance here to elucidate the observed differences between the eliminated and long circulating particles species.

## 5. Summary and Conclusion

The previously established nanoprecipitation method was successfully applied for the encapsulation of two lipophilic organic fluorescence dyes in order to provide fluorescing nanoparticles. Dealing as a lipophilic label or model drug, Nile red was found to have only limited impact on the resulting particle size or surface characteristics, as the obtained particles were quite similar to unloaded control particles. This probably indicates a homogenous distribution of the dye or even its complete dissolution in the polymer matrix. Although the adjustment of the fluorescence intensity with varying dye loading was limited to a certain extent, the nanoparticles, in general were found to be suitable for different imaging purposes. However, several observed drawbacks might limit their common applicability: A “bleeding” of dye, leading to a decrease in signal intensity, accompanied by a transfer to other surrounding lipophilic areas hampers an image based allocation of the obtained fluorescence signal to the investigated nanoparticulate system. During *in-vivo* imaging applications, moreover, the fluorescence of Nile red might be quenched by endogenous compounds, like haemoglobin, wherefore an assessment of the nanoparticle’s fate would be rather unreliable.

These dye inherent limitations were successfully overcome by exchanging Nile red for the even more lipophilic near-infrared dye DiR. The DiR loaded nanoparticles proved to be an ideal tool, especially for *in-vivo* applications, allowing the imaging of whole body particle distributions as well as the imaging of deeper tissue regions.

Application of the nanoprecipitation method for the encapsulation of other compounds, either marker or drug substances, will require a careful assessment and in general the investigation of particles’ properties in each single case, as the complex interaction of matrix material, the precipitation system and the encapsulated compound will always determine the properties of the final product. In case of the DiR particles the impact of the processing factors were assumed to be very similar to Nile red as both exhibit comparable solubilities.

Fluorescence labelling of nanoparticles by nanoprecipitation could be easily achieved and the results obtained in cell culture and during *in-vivo* imaging generally demonstrate their potential for the evaluation of different nanoparticulate systems. Indeed, the interpretation of the obtained results will be strongly dependent on the choice of an appropriate label, which is especially apparent from the results for the Nile red labelled systems.



## 6. References

- [1] Andersson-Engels, S. et al.: "In Vivo Fluorescence Imaging for Tissue Diagnostics", ***Physics in Medicine and Biology***, 42 (1997) pp. 815.
- [2] Salata, O.V.: "Applications of nanoparticles in biology and medicine", ***Journal of Nanobiotechnology*** 2 (2004) p. 3.
- [3] Fishbein, I. et al.: "Formulation and Delivery Mode Affect Disposition and Activity of Tyrphostin-Loaded Nanoparticles in the Rat Carotid Model", ***Arteriosclerosis, Thrombosis, and Vascular Biology*** 21 (2001) pp. 1434-1439.
- [4] Rancan, F. et al.: "Investigation of Polylactic Acid (PLA) Nanoparticles as Drug Delivery Systems for Local Dermatotherapy", ***Pharmaceutical Research*** 26 (2009) pp. 2027-2036.
- [5] Bilati, U. et al.: "Poly(D,L-lactide-co-glycolide) protein-loaded nanoparticles prepared by the double emulsion method--processing and formulation issues for enhanced entrapment efficiency", ***Journal of Microencapsulation*** 22 (2005) pp. 205-214.
- [6] Brunner, A. et al.: "Labelling peptides with fluorescent probes for incorporation into degradable polymers", ***European Journal of Pharmaceutics and Biopharmaceutics*** 45 (1998) pp. 265-273.
- [7] Jiang, H.L. et al.: "Novel Fluorescent Copolyanhydrides As Potential Visible Matrices for Drug Delivery", ***Biomaterials*** 23 (2002) pp. 2345-2351.
- [8] Lamprecht, A. et al.: "Visualization and quantification of polymer distribution in microcapsules by confocal laser scanning microscopy (CLSM)", ***International Journal of Pharmaceutics*** 196 (2000) pp. 223-226.
- [9] Panyam, J. et al.: "Fluorescence and electron microscopy probes for cellular and tissue uptake of poly(,-lactide-co-glycolide) nanoparticles", ***International Journal of Pharmaceutics*** 262 (2003) pp. 1-11.
- [10] Chawla, J.S. et al.: "Biodegradable poly(epsilon-caprolactone) nanoparticles for tumor-targeted delivery of tamoxifen", ***International Journal of Pharmaceutics*** 249 (2002) pp. 127-138.
- [11] Nguyen, C.A. et al.: "Cell interaction studies of PLA-MePEG nanoparticles", ***International Journal of Pharmaceutics*** 254 (2003) pp. 69-72.
- [12] White, N.S. et al.: "Fluorescence techniques for drug delivery research: theory and practice", ***Advanced Drug Delivery Reviews*** 57 (2005) pp. 17-42.
- [13] Teeranachaideekul, V. et al.: "Influence of oil content on physicochemical properties and skin distribution of Nile red-loaded NLC", ***Journal of Controlled Release*** 128 (2008) pp. 134-141.
- [14] Greenspan, P. et al.: "Spectrofluorometric studies of the lipid probe, nile red", ***Journal of Lipid Research*** 26 (1985) pp. 781-789.
- [15] Greenspan, P. et al.: "Nile red: a selective fluorescent stain for intracellular lipid droplets", ***The Journal of Cell Biology*** 100 (1985) pp. 965-973.
- [16] Horobin, R. et al.: "Interactions of molecular probes with living cells and tissues. Part 1. Some general mechanistic proposals, making use of a simplistic Chinese box model", ***Histochemistry and Cell Biology*** 94 (1990) pp. 205-209.

- [17] Pietzonka, P. et al.: "Transfer of Lipophilic Markers from PLGA and Polystyrene Nanoparticles to Caco-2 Monolayers Mimics Particle Uptake", **Pharmaceutical Research** 19 (2002) pp. 595-601.
- [18] De Jaeghere, F. et al.: "Formulation and Lyoprotection of Poly(Lactic Acid-Co-Ethylene Oxide) Nanoparticles: Influence on Physical Stability and In Vitro Cell Uptake", **Pharmaceutical Research** 16 (1999) pp. 859-866.
- [19] Lombardi Borgia, S. et al.: "Lipid nanoparticles for skin penetration enhancement--correlation to drug localization within the particle matrix as determined by fluorescence and piezoelectric spectroscopy", **Journal of Controlled Release** 110 (2005) pp. 151-163.
- [20] Bourges, J.L. et al.: "Ocular Drug Delivery Targeting the Retina and Retinal Pigment Epithelium Using Polylactide Nanoparticles", **Investigative Ophthalmology Visual Science** 44 (2003) pp. 3562-3569.
- [21] Ballou, B. et al.: "Noninvasive Imaging of Quantum Dots in Mice", **Bioconjugate Chemistry** 15 (2004) pp. 79-86.
- [22] Fessi, H. et al.: "Nanocapsule formation by interfacial polymer deposition following solvent displacement", **International Journal of Pharmaceutics** 55 (1989) pp. R1-R4.
- [23] Westedt, U. et al.: "Poly(vinyl alcohol)-graft-poly(lactide-co-glycolide) nanoparticles for local delivery of paclitaxel for restenosis treatment", **Journal of Controlled Release** 119 (2007) pp. 41-51.
- [24] Dong, Y. et al.: "Methoxy poly(ethylene glycol)-poly(lactide) (MPEG-PLA) nanoparticles for controlled delivery of anticancer drugs", **Biomaterials** 25 (2004) pp. 2843-2849.
- [25] Govender, T. et al.: "PLGA nanoparticles prepared by nanoprecipitation: drug loading and release studies of a water soluble drug", **Journal of Controlled Release** 57 (1999) pp. 171-185.
- [26] Lamprecht, A. et al.: "Biodegradable monodispersed nanoparticles prepared by pressure homogenization-emulsification", **International Journal of Pharmaceutics** 184 (1999) pp. 97-105.
- [27] Barichello, J.M. et al.: "Encapsulation of Hydrophilic and Lipophilic Drugs in PLGA Nanoparticles by the Nanoprecipitation Method", **Drug development and industrial pharmacy** 25 (1999) pp. 471-476.
- [28] Bilati, U. et al.: "Development of a nanoprecipitation method intended for the entrapment of hydrophilic drugs into nanoparticles", **European Journal of Pharmaceutical Sciences** 24 (2005) pp. 67-75.
- [29] Makarova, O.V. et al.: "Adsorption and Encapsulation of Fluorescent Probes in Nanoparticles", **The Journal of Physical Chemistry B** 103 (1999) pp. 9080-9084.
- [30] Penzkofer, A. et al.: "Fluorescence quenching of rhodamine 6G in methanol at high concentration", **Chemical Physics** 103 (1986) pp. 399-405.
- [31] Melhuish, W. H.: "Quantum Efficiencies of Fluorescence of Organic Substances: Effect of Solvent and Concentration of the Fluorescent Solute", **The Journal of Physical Chemistry** 65 (1961) pp. 229-235.
- [32] Miglietta, A. et al.: "Cellular uptake and cytotoxicity of solid lipid nanospheres (SLN) incorporating doxorubicin or paclitaxel", **International Journal of Pharmaceutics** 210 (2000) pp. 61-67.

- 
- [33] Brigger, I. et al.: "Tamoxifen encapsulation within polyethylene glycol-coated nanospheres. A new antiestrogen formulation", **International Journal of Pharmaceutics** 214 (2001) pp. 37-42.
  - [34] Yi, Y. et al.: "A Polymeric Nanoparticle Consisting of mPEG-PLA-Toco and PLMA-COONa as a Drug Carrier: Improvements in Cellular Uptake and Biodistribution", **Pharmaceutical Research** 22 (2005) pp. 200-208.
  - [35] Chawla, J. et al.: "Cellular uptake and concentrations of tamoxifen upon administration in poly( $\epsilon$ -caprolactone) nanoparticles", **The AAPS Journal** 5 (2003) pp. 28-34.
  - [36] Prabha, S. et al.: "Critical Determinants in PLGA/PLA Nanoparticle-Mediated Gene Expression", **Pharmaceutical Research** 21 (2004) pp. 354-364.
  - [37] Prabha, S. et al.: "Size-dependency of nanoparticle-mediated gene transfection: studies with fractionated nanoparticles", **International Journal of Pharmaceutics** 244 (2002) pp. 105-115.
  - [38] Sahoo, S.K. et al.: "Residual polyvinyl alcohol associated with poly (D,L-lactide-co-glycolide) nanoparticles affects their physical properties and cellular uptake", **Journal of Controlled Release** 82 (2002) pp. 105-114.
  - [39] Zhang, Yong et al.: "Surface modification of superparamagnetic magnetite nanoparticles and their intracellular uptake", **Biomaterials** 23 (2002) pp. 1553-1561.
  - [40] Chavanpatil, M.D. et al.: "Nanoparticles for Cellular Drug Delivery: Mechanisms and Factors Influencing Delivery", **Journal of Nanoscience and Nanotechnology** 6 (2006) pp. 2651-2663.
  - [41] Desai, M.P. et al.: "The Mechanism of Uptake of Biodegradable Microparticles in Caco-2 Cells Is Size Dependent", **Pharmaceutical Research** 14 (1997) pp. 1568-1573.
  - [42] Nomura, T. et al.: "Effect of Particle Size and Charge on the Disposition of Lipid Carriers After Intratumoral Injection into Tissue-isolated Tumors", **Pharmaceutical Research** 15 (1998) pp. 128-132.
  - [43] Panyam, J. et al.: "Biodegradable nanoparticles for drug and gene delivery to cells and tissue", **Advanced Drug Delivery Reviews** 55 (2003) pp. 329-347.
  - [44] Gref, R. et al.: "'Stealth' corona-core nanoparticles surface modified by polyethylene glycol (PEG): influences of the corona (PEG chain length and surface density) and of the core composition on phagocytic uptake and plasma protein adsorption", **Colloids and Surfaces B: Biointerfaces** 18 (2000) pp. 301-313.
  - [45] Petersen, S. et al.: "Flow Cytometry as a New Approach To Investigate Drug Transfer between Lipid Particles", **Molecular Pharmaceutics** 7 (2010) pp. 350-363.
  - [46] Owens III, D.E. et al.: "Opsonization, biodistribution, and pharmacokinetics of polymeric nanoparticles", **International Journal of Pharmaceutics** 307 (2006) pp. 93-102.
  - [47] Panagi, Z. et al.: "Effect of dose on the biodistribution and pharmacokinetics of PLGA and PLGA-mPEG nanoparticles", **International Journal of Pharmaceutics** 221 (2001) pp. 143-152.
  - [48] Beletsi, A. et al.: "Biodistribution properties of nanoparticles based on mixtures of PLGA with PLGA-PEG diblock copolymers", **International Journal of Pharmaceutics** 298 (2005) pp. 233-241.
-

- [49] Choyke, P. et al.: "Functional magnetic resonance imaging of the kidney using macromolecular contrast agents", ***Abdominal Imaging*** 31 (2006) pp. 224-231.
- [50] Weissleder, R.: "A clearer vision for in vivo imaging", ***Nature Biotechnology*** 19 (2001) pp. 316-317.
- [51] Rashid, F. et al.: "Interaction of molecular probes with living cells and tissues. Part 2", ***Histochemistry and Cell Biology*** 94 (1990) pp. 303-308.
- [52] Gref, R. et al.: "Biodegradable long-circulating polymer nanospheres", ***Science*** 263 (1994) pp. 1600-1603.
- [53] Dunn, S.E. et al.: "Polystyrene-Poly (Ethylene Glycol) (PS-PEG2000) Particles as Model Systems for Site Specific Drug Delivery. 2. The Effect of PEG Surface Density on the in Vitro Cell Interaction and in Vivo Biodistribution", ***Pharmaceutical Research*** 11 (1994) pp. 1016-1022.

# **Chapter 4**

**Synthesis and characterization of  
CdSe Quantum Dots as stable  
particulate fluorescence markers**



# 1. Introduction

Quantum dots, semiconductor nanocrystals in sizes ranging from 3 to 15 nm, are characterized by their unique optical properties resulting from the so-called quantum confinement [1; 2]. Their composition and size tuneable, bright fluorescence accompanied by narrow emission spectra, broad absorbance spectra and high quantum yields made them desirable fluorescent probes, which outclass organic fluorescence dyes also due to their high photostability [3; 4]. Besides their application in optoelectronic devices or lasers [5-7] tremendous work has been done establishing their use as stable and secure fluorescence labels in bio-imaging or diagnostics, which can also be attributed to their particulate character that allows the attachment of several, also differing, ligands to a single fluorophor [8-12]. Various types of such nanocrystals are available differing in composition, shape or surface characteristics, all determining their exact properties and subsequent potential applications (**Fig. 1**).

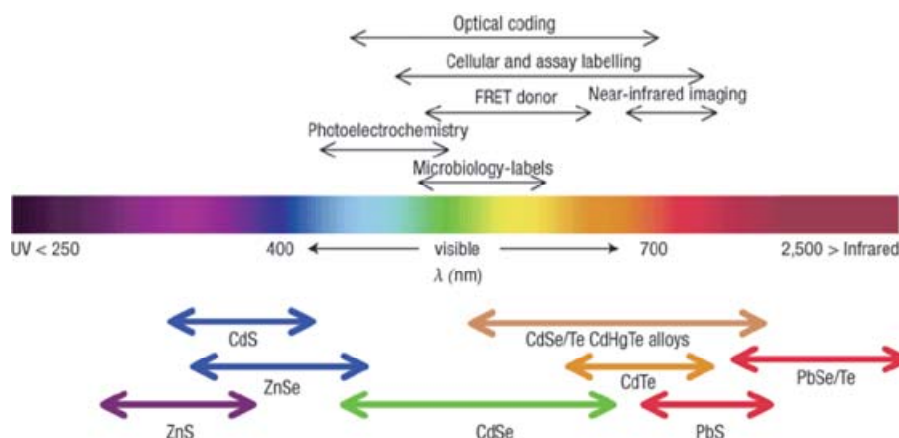


**Fig. 1:** Overview about light emitting properties of differently composed quantum dots and respective area of application [13]

In the present work CdSe quantum dots have been chosen, as they are easy to synthesize with maximum emission wavelengths spanning a broad range of the visible spectrum. Therefore they could allow detection with commonly available fluorescence and confocal laser scanning microscopes applied for *in-vitro* investigations [9; 14], but furthermore might also be used for *in-vivo* small animal imaging [15; 16], which is only limited by the tissue interaction of the exciting and the emitted light [17; 18]. Besides focusing on the reproducible synthesis and purification of the CdSe quantum dots with emission wavelengths above 600 nm, also possibilities for the further stabilization or even increase of their initial photoluminescence [PL] properties have been investigated. This was essential since their application as particulate labels requires further processing

steps, including mechanical stress to the crystal surface or encapsulation into optical denser materials, which most likely will be at the expense of their initial photoluminescence and therefore reducing the later achievable detection limits. Several approaches to improve the luminescence stability have been described in literature. The most commonly used one, is the on-growth of an additional inorganic shell of a wide-band gap semiconductor, usually ZnS, on the primary CdSe core [19]. However, in the current work first attempts using these core/shell systems failed during initial screening experiments due to the immanent complexity of the two step synthesis, wherefore further effort was spent on modifying simple CdSe quantum dots with additional organic capping ligands, which should also ease the subsequent encapsulation of the inorganic nanocrystals in the polymeric particles due to a better interaction with the polymeric matrix. By using capping ligands with a hydrophilic character [20-22] this is an usually done process to obtain water dispersible quantum dots or allow the further attachment of targeting ligands [13; 23]. Herein the performed ligand exchange experiments were focussed on mainly lipophilic coating agents since the prepared CdSe quantum dots are later encapsulated into lipophilic or at least amphiphilic polymer matrices. Using an established synthesis route, CdSe quantum dots were investigated and modified to identify the most promising candidates allowing further processing.



## 2. Materials and Methods

### 2.1 Materials

Cadmiumoxide [CdO] (99.99+ %), anhydrous cadmium chloride, elemental selenium (99.5 %, 100 mesh), oleic acid (techn.), trioctylphosphine [TOP] (90 %), octadecene (90 %), 2-mercaptoethanol, allylamine (>99 %), dodecylamine (>98 %) and oleylamine (70 %) were obtained from Sigma-Aldrich (Sigma-Aldrich Chemie GmbH, Taufkirchen, Germany). Chloroform (p.a.), hexane (p.a.) and acetone (p.a.) were obtained from Acros (Acros Organics, Fischer scientific GmbH, Nidderau, Germany). Ethanol (p.a.), methanol (p.a.), isopropanol (p.a.) and nitric acid (65 %) were provided from Merck (Merck KGaA, Darmstadt, Germany).

### 2.2 Methods

#### 2.2.1 Synthesis of CdSe Quantum Dots

Unmodified CdSe quantum dots were synthesized according a simple organometallic route described in literature using precursor solutions of Cd and Se in hot, coordinating organic solvents [24-26].

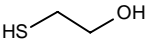
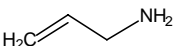
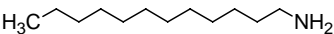
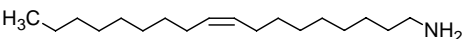
The Se-precursor was prepared by mixing 16 mg (0.203 mmol) Se powder with 0.72 ml TOP under agitation until a clear colourless solution was obtained. For the second, the Cd-precursor 51 mg (0.397 mmol) CdO, 20 ml octadecene and 2 ml oleic acid were mixed in a three neck flask. Under N<sub>2</sub> atmosphere the mixture was heated up to 230 °C using a heating mantle with controller (Isopad TD 2000; Tyco Thermal Controls GmbH, Heidelberg, Germany) until all substances were dissolved. Afterwards the Se–TOP was injected at once to initiate the CdSe crystal nucleation, temperature of the heating mantle was decreased to 220 °C and crystals were allowed to grow for certain time, 60 min standard, and then finally cooled down to room temperature.

Crystal growth kinetic was monitored by determination of their sizes (derived from their absorption wavelengths) as well as the quantum yields [QY] every 5 min during synthesis.

#### 2.2.2 Coating of CdSe Quantum Dots

After their synthesis original CdSe quantum dots were treated with several organic ligands. By comparing different ligands, described in literature [19; 27; 28], standard coating conditions were determined with respect to each kind of coating, namely the coating temperature and the duration of coating, as summarized in **table 1**.

**Tab. 1:** Lipophilic ligands and applied conditions used for coating of CdSe Quantum Dots

Ligand	Temperature	Atmosphere	Max. coating duration
2-Mercaptoethanol	room temperature	normal	24 h
	60 °C	N <sub>2</sub>	24 h
Allylamine	room temperature	N <sub>2</sub>	24 h
	--	--	
Dodecylamine	room temperature	N <sub>2</sub>	24 h
	85 °C	N <sub>2</sub>	24 h
Oleylamine	room temperature	N <sub>2</sub>	24 h
	100 °C	N <sub>2</sub>	24 h

In brief, an aliquot of the unpurified CdSe dispersions derived from synthesis was put in a three neck flask. The five-fold volume of the respective ligand was added under N<sub>2</sub> atmosphere (if applicable). In the case of increased temperatures the systems were heated up to the desired temperature and temperature was kept over 24 h. Temperature was controlled using a heating mantle with controller. The coating process was monitored by determination of the quantum yields during the coating process.

### 2.2.3 Purification of the Quantum Dot dispersion

Prior to analysis or further application, the CdSe raw dispersions were purified, unless otherwise stated. Different literature described methods [29-31] were compared with respect to their effect on PL properties and recovery. An aliquot of the coated quantum dot raw dispersion was mixed with an at least 30-fold excess of a polar organic solvent (e.g. acetone, ethanol, isopropanol/methanol, methanol) to induce the precipitation of the lipophilic nanocrystals. Each solvent was tested either alone or in combination with the quantum dot compatible solvent hexane as stabilizer, according a procedure previously introduced at the Department of Pharmaceutical Technology. After centrifugation (10,000 g, 20 min, 10 °C) using a high-speed centrifuge (Avanti JE centrifuge; Beckman Coulter GmbH, Krefeld, Germany) the supernatant was discarded and the obtained sediment was re-dispersed in CHCl<sub>3</sub> for all preparations.

### 2.2.4 Spectroscopic analysis

All quantum dot batches were characterized regarding their absorbance, maximum emission wavelength  $\lambda_{em}$  and quantum yield prior and after their purification. Measurements were performed in chloroform dispersions using 1 cm path length quartz cuvettes.

Absorbance spectra of the quantum dots (380 to 700 nm) were determined with a two-beam spectrophotometer (UVIKON 941; Kontron Instruments, Germany). Fluorescence emission spectra were recorded using a LS 55 spectrophotometer (PerkinElmer, Waltham, USA) over the range of 500 to 700 nm with an excitation wavelength of 400 nm. The relative quantum yield  $\Phi$  generally was determined by comparing wavelength integrated fluorescence intensity of an unknown sample to that of a well known standard [32]. The fluorescence standard used was oxazine 170 perchlorate in ethanolic solution ( $\Phi_{St} = 0.6$ ) [33]. Calculation was based on the following equation [33]:

$$\Phi = \Phi_{St} * \frac{A}{A_{St}} * \frac{F_{St}}{F} * \left( \frac{n}{n_{St}} \right)^2; \quad (1)$$

with the integrated area under the corrected fluorescence spectrum  $A$ , the fraction of light absorbed at excitation wavelength  $F$  (applied: 400 nm) and the refractive index  $n$  of the solvent or dispersion medium respectively. The subscript “ $St$ ” denotes the values of the used fluorescence standard. Optical density of the investigated samples was set within the range of 0.01 to 0.1 to avoid inner filter effects.

### 2.2.5 Determination of nanocrystals size and molar concentration

Size and absorbance coefficient of uncoated and coated CdSe quantum dots in dispersion were determined based on the lowest energy excitonic peak at  $\lambda_a$  in their absorbance spectra (**Fig. 2**).

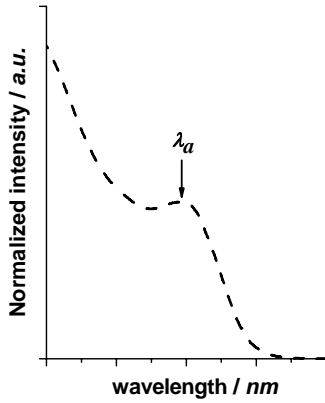


**Fig. 2:** Exemplary UV absorbance spectrum of CdSe quantum dots and definition of  $\lambda_a$

The relationship between the achieved particle diameter  $d$  and its  $\lambda_a$ , as well as the dependence of the absorbance coefficient  $\varepsilon_{ab}$  on the particle sizes was reported in literature based on the evaluation of particles using TEM as well as absorbance spectroscopy. The following empirically derived equations are generally used for the calculation of the particle size and absorbance coefficient of CdSe quantum dots, respectively [34]:

$$d_{CdSe} = (1.6112 \cdot 10^{-9})\lambda_a^4 - (2.6575 \cdot 10^{-6})\lambda_a^3 + (1.6242 \cdot 10^{-3})\lambda_a^2 - (0.4277)\lambda_a + 41.57 \quad (2)$$

$$\varepsilon_{ab} = 5867 * d^{2.56}; \quad (3)$$

with the mean diameter of CdSe quantum dots  $d_{CdSe}$  [nm], the lowest energy excitonic peak  $\lambda_a$  [nm] and the decadic molar absorbance coefficient  $\varepsilon_{ab}$  [L/mol\*cm].

The subsequent molar concentration of CdSe quantum dots in dispersion was calculated based on Lambert Beer's law using the determined absorbance coefficient and the measured absorbance of the samples [35]:

$$c = \frac{A}{\varepsilon_{ab} * d}; \quad (4)$$

with the absorbance of the sample  $A$ , the concentration of quantum dots in the sample  $c$  [mol/L], the length of penetrated medium  $d$  [cm] and decadic molar absorbance coefficient  $\varepsilon_{ab}$  [L/mol\*cm].

### 2.2.6 Calculation of theoretical – UV-based amount of Cd and Se

Based on the mean size of the synthesized CdSe quantum dots determined using their characteristic UV absorbance (see 2.2.5) the molar amount of Cd and Se atoms per mol nanocrystals was calculated assuming their preferential crystallisation in the wurzite structure [24; 34], which is described by the typical elementary cell ( $a=b=4.298 \text{ \AA}$ ,  $c=6.716 \text{ \AA}$ ) containing four atoms of each element.

### 2.2.7 Determination of real elemental Quantum Dot composition

Inductively coupled plasma optical emission spectroscopy [ICP-OES] was used to determine absolute concentrations and elemental ratios of the quantum dot components (Cd and Se). Sample solutions were prepared by oxidative disintegration of the nanocrystals. An aliquot, between 50 and 200  $\mu\text{l}$ , of the purified quantum dot dispersion was dried under atmosphere pressure at room temperature and disintegrated by addition of 500  $\mu\text{l}$  nitric acid and 2 to 3 drops of ethanol. Subsequently, samples were diluted to 10 ml using a volumetric flask. The final concentration of  $\text{HNO}_3$  was about 2 to 3 %.

The standard solutions, prepared of cadmium chloride and selenium, contained 100 ppm, 10 ppm and 1 ppm of Cd and Se in 2 to 3 % nitric acid. Measurements were performed using a Jobin Yvon 70 Plus (S+S) ICP-OE spectrophotometer (Horiba, Jobin Yvon, France) in the sequential analysis mode. Instrumental settings and element characteristics are given in **tables 2 and 3**.

**Tab. 2:** Instrumental settings for ICP-OES measurements

Instrumental setting	
Plasma gas (temperature and flow rate)	Argon (~8000 K; 10-20 L/min)
Transport gas	Argon (0.6-1 L/min)
Sample flow rate	1 ml/min

**Tab. 3:** Element characteristics for ICP-OES measurements

Element	Detection wavelength / nm	Nominal detection limit / ppb
Cadmium	226.502	23
Selen	196.090	75

### **2.2.8 Investigation of Quantum Dot morphology**

The morphologic analysis of uncoated and coated CdSe quantum dots was done by transmission electron microscopy [TEM]. Samples were prepared by dropping diluted organic dispersions on 3.05 mm formvar/carbon coated copper grids (300 mesh) followed by drying under vacuum. Images were taken using a Zeiss EM C/CR (Carl Zeiss AG, Jena, Germany) with 60 kV operating voltage.

### 3. Results

#### 3.1 Synthesis and characterization of CdSe Quantum Dots

CdSe quantum dots have been prepared following a simple organometallic route. Immediately after combination of both pre-cursor solutions nucleation of fluorescing crystals occurred indicated by the resulting absorption and emission properties of the synthesis mixture (30 s value) (**Fig. 3**). The following time of synthesis is characterized by a continuous red-shift in both, first excitonic peak ( $\lambda_a$ ) and maximum emission wavelengths ( $\lambda_{em}$ ), ranging from 509 and 527 nm, respectively, after 30 s, to 603 and 617 nm after 90 min of synthesis duration.

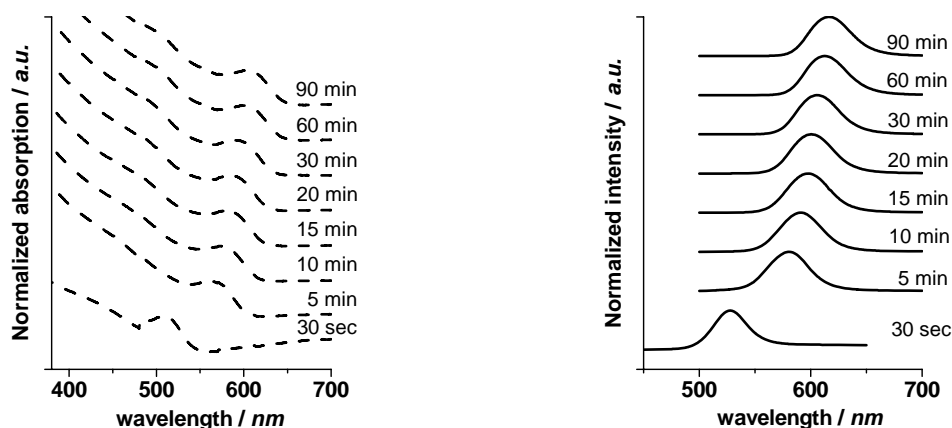


**Fig. 3:** Development of (*left*) normalized absorption and (*right*) fluorescence spectra during CdSe quantum dots synthesis over 90 min

With increasing  $\lambda_{em}$  also the mean diameter  $d$  of the nanocrystals increased by continuous incorporation of both, Cd and Se, to the once nucleated crystals, indicated by the growing amounts of both elements per 0.1 mmol of disintegrated quantum dots over the synthesis duration (**Fig. 4**). Generally the ratio of Cd to Se is influenced by the synthesis route and herein the amount of incorporated Cd was always slightly higher, indicated by a Cd/Se ratio of at least 1.7 during the whole synthesis.

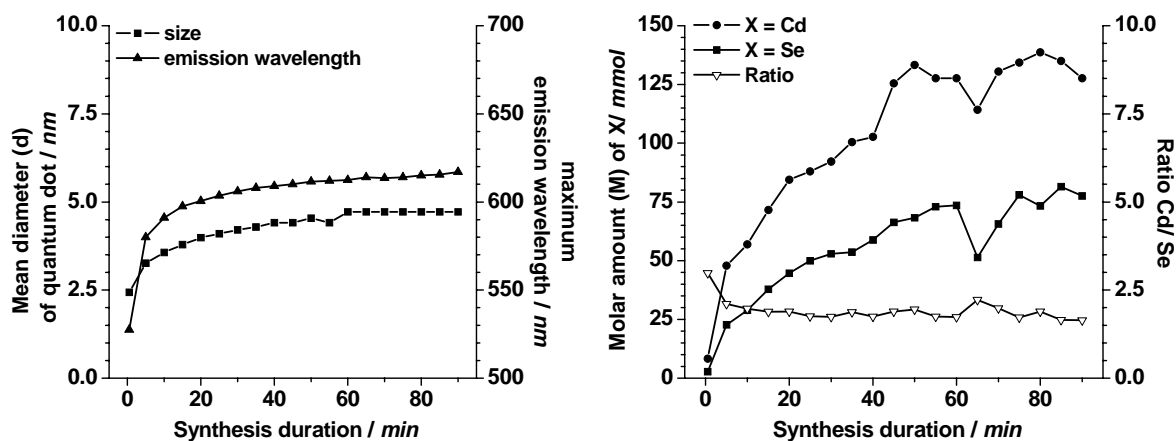


**Fig. 4:** Development of (*left*) nanocrystals size [nm] with increasing maximum emission wavelength and (*right*) of elemental composition of CdSe quantum dots [mmol / 0.01 mmol QDs] during synthesis over 90 min

Morphological investigations of the as prepared quantum dots, determined by TEM proved the formation of narrowly size distributed crystals (**Fig. 5**), which however, did not appear exactly round (dot-shaped).

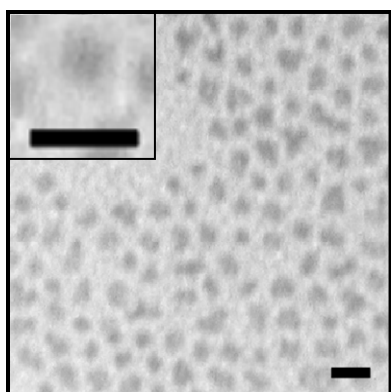


**Fig. 5:** TEM images of CdSe quantum dots; magnification 63,000 x; scale bars correspond to 10 nm

The optical properties of the quantum dots were displayed by their QY, which decreased from the initial maximum value of 16 % to about 9 % within 15 min and kept almost stable over the following 70 min of synthesis (**Fig. 6**).



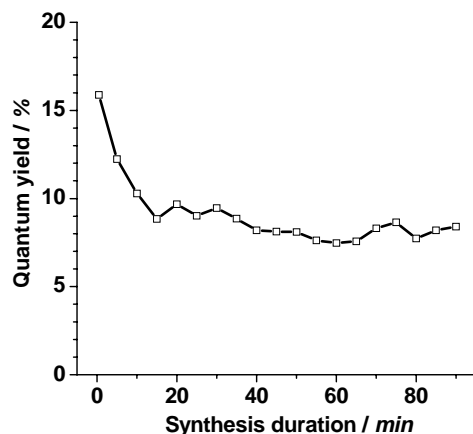


Fig. 6: Development of quantum yield of CdSe quantum dots during synthesis over 90 min

### 3.2 Purification of CdSe Quantum Dots

Several solvents and solvent mixtures, as summarized in **table 4**, were compared especially with respect to their impact on QY (**Fig. 7**) and their precipitation efficiency (**Fig. 8**).

Tab. 4: Organic liquids used for precipitation of CdSe quantum dots

Method	Solvent / Solvent mixture
A	Ethanol
B	Ethanol + Hexane (5:1)
C	Acetone
D	Acetone + Hexane (5:1)
E	Methanol
F	Methanol + Hexane (5:1)
G	Methanol/Isopropanol (75/25)
H	Methanol/Isopropanol + Hexane (5:1)

To attribute for the already high initial QY variability of the different batches, the investigations were conducted using four different starting batches of CdSe quantum dots. Even following identical synthesis protocols without noticeable obvious failures (e.g. pronounced fluctuation in the nucleation- or growth temperature) the conducted QD synthesis is highly sensitive, resulting in batches with significant differences in quality. However, the general effects of the used purification method on the PL properties seem to be almost independent of the initial quality of the quantum dots (**Fig. 7**). Interestingly all

methanol containing precipitation mixtures resulted in the lowest QYs (**E-F**), whereas the highest QY stability was found for acetone both with and without the addition of hexane (**C+O**). For all investigated polar solvents, the addition of hexane generally led to slightly higher values of obtained QY.

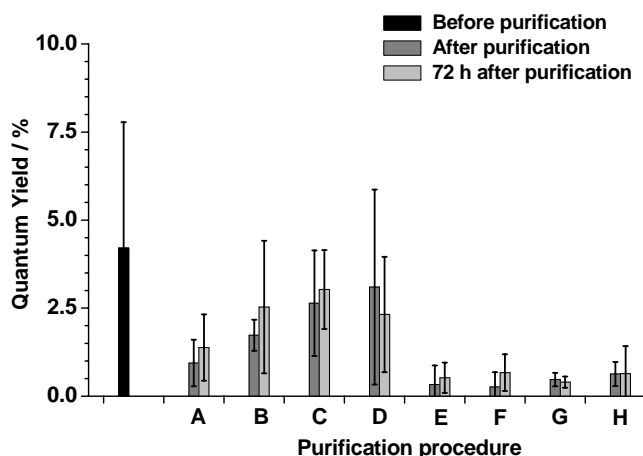


**Fig. 7:** Influence of purification procedure on quantum yield of CdSe quantum dots; given as means ( $\pm$ SD) of four separately synthesized QD batches; explanation of different procedures represented by capital letters given in **table 2**

The precipitation efficiency, herein dealing as a measure for the recovery of the initial amount of quantum dots after re-dispersion following purification (**Fig. 8**), on the other hand was found to be the best in case of the methanol based solvents, whereas only 50 % or even 25 % were recovered in case of acetone based precipitation solvent mixtures.

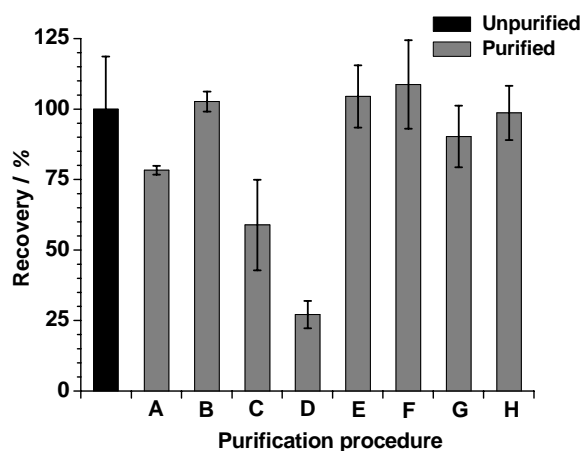


**Fig. 8:** Recovery of CdSe quantum dots following purification with different procedures; explanation of different procedures represented by capital letters given in **table 4**

### 3.3 Lipophilic coating of CdSe Quantum Dots

Surface modification of original CdSe quantum dots was performed by exchanging the surface ligands resulting from the synthesis either by several primary alkylamines differing in chain length or 2-mercaptoethanol under various conditions, as summarized in **table 5**.

**Tab. 5:** Lipophilic coatings and coating conditions

Method	Conditions
a	Oleylamine/ room temperature
b	Oleylamine/ 100 °C
c	Dodecylamine/ 40 °C
d	Dodecylamine/ 85 °C
e	2-Mercaptoethanol/ 60 °C
f	2-Mercaptoethanol/ room temperature
g	Allylamine/ room temperature

Using the identical CdSe starting batch the development of the QY was found to be strongly influenced by both the coating material and moreover the temperature (**Fig. 9, left**).

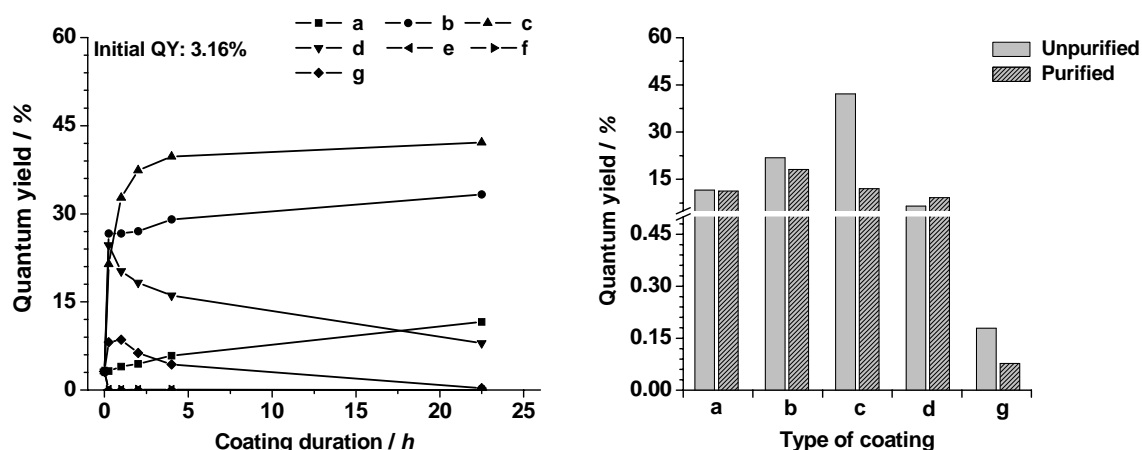


**Fig. 9:** Quantum yield of CdSe quantum dots (*left*) during coating with different lipophilic ligands and (*right*) its stability during purification using acetone/hexane; explanation of coating procedure represented by lowercase letters given in **table 5**

The different procedures improved the initial PL properties in the following order: dodecylamine/ 40 °C > oleylamine/ 100 °C > dodecylamine/ 85 °C > oleylamine/ room temperature. No positive effect at all was found for allylamine and 2-mercaptoethanol.

Regardless of the initially achieved QY after coating, the following purification step again decreased the QY to about 15 % in the case of the oleylamine and dodecylamine derivatives, independent of the used coating procedure, which however still is a multiple of the pre-coating value of about 3 % (**Fig. 9, right**). Indeed, aborting the coating process during the first hour, which was characterized by the strongest increase in QY (**Fig. 9, left**), again led to a substantial loss of QY during purification. This then equates almost the pre-coating value (**Fig. 10**).

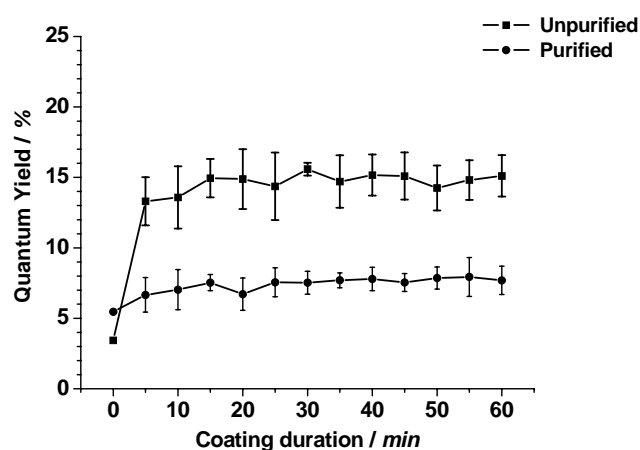


**Fig. 10:** Quantum yield of CdSe quantum dots during coating with oleylamine at 100 °C over 60 min and its respective stability during purification using acetone/hexane

### 3.4 Quantification of CdSe Quantum Dots

Basically there are two different methods to determine the concentration of quantum dots in dispersion. The molar concentration of quantum dots can be determined based on their absorbance spectrum, which includes the maximum absorption wavelength as well as the absorbance (see equation (3)). On the other hand it is possible to quantify the molar amounts of the quantum dot forming elements, herein Cd and Se, after disintegration of the nanocrystals, using ICP-OES. In order to answer the question of their relative proportion for different quantum dot species, the apparent Se concentration, as determined by ICP-OES, was compared to the theoretical molar concentration of Se, calculated from the respective nanocrystals' light absorbance (**Fig. 11**).

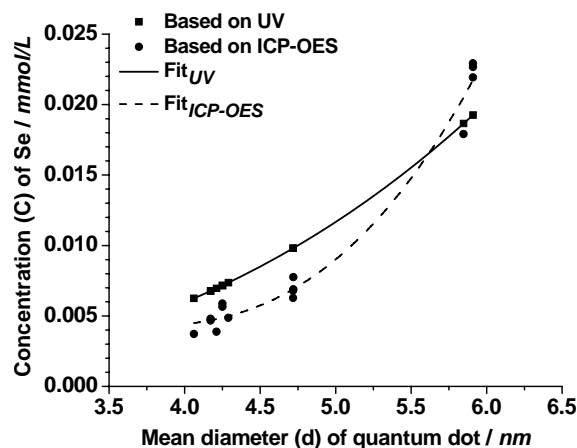


**Fig. 11:** Relation between Se concentration based quantification of uncoated CdSe quantum dots using either UV-based or ICP-OES-based calculation dependent on quantum dot size; mathematical fits (solid and dashed line) inserted for explanation only

As expected, the amount of Se steadily increases with increasing quantum dot diameter, but on the other hand the apparent concentration of Se is slightly lower than the theoretically expected one for crystal sizes of 4 to almost 5 nm and the observed differences are constant within this size range. With further increasing size, the ICP-OES results are characterized by a steady increase in Se amounts whereas the UV-based calculation followed an almost linear relation.

In case of further surface modified quantum dots the relation between UV-based and ICP-OES-based Se concentrations was also investigated, but only starting from one single quantum dot batch, which consequently possesses only one single average crystal size (**Fig. 12**).

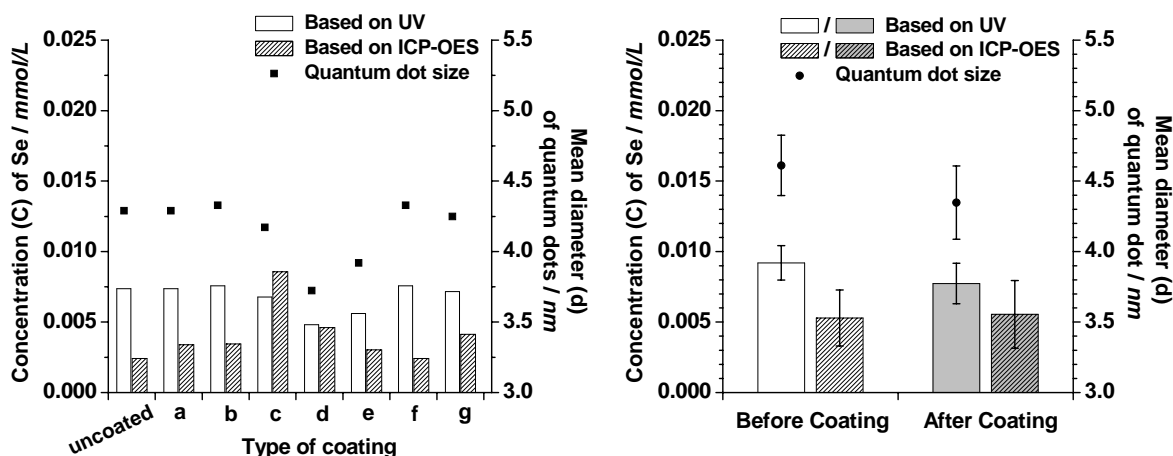


**Fig. 12:** Relation between Se concentration based quantification of CdSe quantum dot using either UV-based or ICP-OES-based calculation – (*left*) after coating with different lipophilic ligands and (*right*) focused on oleylamine-coated quantum dots; explanation of coating procedure represented by lowercase letters given in table 5

Except after coating with dodecylamine, which also showed the most pronounced impact on the earlier investigated PL properties, the same general trend (UV-based concentrations higher than the ICP-OES-based ones) was obtained, but here strongly varying absolute differences were observed. The initial ratio of “UV concentrations” to “ICP-OES concentrations” before coating of this batch has been about 3.5. Following coating the ratios range from 0.78 to 4 for the different investigated coating procedures. However, a good reproducibility was found for the afterwards commonly used coating scheme with oleylamine, which was conducted in triplicate.

## 4. Discussion

Several synthesis procedures for fluorescing semiconductor nanocrystals have been described in literature, predominantly differing in the used pre-cursor substances, solvents or stabilizing ligands [24; 36-41]. However, independent of the used synthesis scheme they can be separated into two major steps: (1) nucleation and (2) growth of nanocrystals [42]. The continuous red-shift in both, the absorbance ( $\lambda_{ab}$ ) and maximum emission wavelengths ( $\lambda_{em}$ ), (**Fig. 3**) act as a direct indicator for the typical size tuneable optical properties of quantum dots. Since both, the emission and the absorbance of CdSe quantum dots, span a broad range of the visible spectrum, changes of the emission and absorbance are observable by the formation of the yellow particle dispersion immediately after nucleation and thereafter a stepwise change to a deep-red colour of the dispersion. In parallel the formed particles also show a constant alteration of their fluorescence colour under excitation with UV-light to longer wavelengths as indicated in **figure 13**.

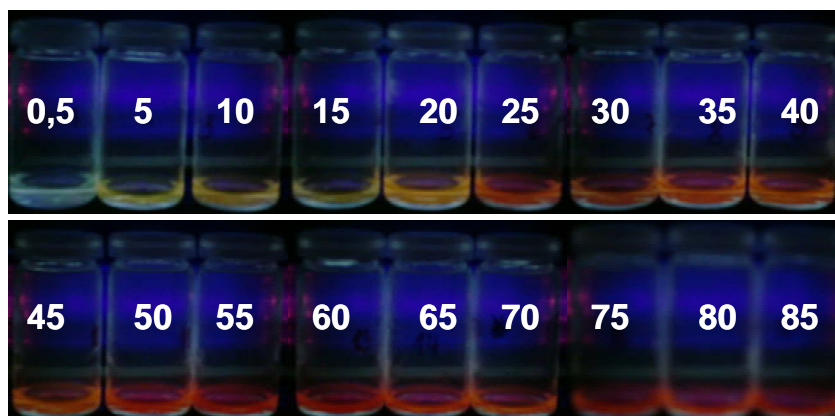


**Fig. 13:** Images of development of emission wavelength of CdSe quantum dots during synthesis under UV-excitation at 355 nm; numbers indicate time points of sampling in minutes

The resulting shape of the synthesized nanocrystals is predominantly driven by thermodynamic processes and thus understandably sensitive towards thermal or kinetic fluctuations [42; 43], wherefore the deviation in crystal morphology (**Fig. 5**) from the expected perfect dot-shape is not surprising. However, the shape of quantum dots on the other hand could have pronounced impact on the crystal quality also regarding the optical properties, which are for example also affected by defects in the quantum dot surfaces [43; 44]. The optical quality of the quantum dots is primarily defined by their quantum yield (also known as quantum efficiency), determining the radiative energy transition, represented by the amount of emitted light per amount of absorbed light [45]. In case of the CdSe quantum dots, QYs did not exceed 10 to 15 % during the whole synthesis (**Fig. 6**), which is in line with results previously described in literature [46].

Considering all characterized parameters, it is obvious that the most pronounced changes in composition and fluorescence occur during the first minutes of crystal growth. Within five minutes  $\lambda_{em}$  shifts about more than 50 nm into the red range and the diameter increases about one third of the initial size, which is also accompanied with increased elemental concentrations determined after crystals disintegration. However, in the following, initially measured QY of 16 % decreases steadily, which could be attributed to occurring surface defects of the growing crystals. Compared to that initial shift, changes in the following growth appear almost marginal and quantum dot properties seem to be almost fixed after the first 15 minutes of reaction. Focusing on the fluorescence intensity, the “best” quantum dots therefore would be available after only a few minutes of synthesis. However, for the optimal duration of the reaction the overall photoluminescence properties are crucial, of course including the QY but also the maximum emission wavelength  $\lambda_{em}$ , which should be as high as possible, to allow a detection also in cells, tissues or even small animals. Thus, CdSe batches have been prepared with a standard growth time of 60 min, essential to achieve the long emission wavelengths typical for bigger quantum dots, but consequently with lower overall QY.

After synthesis quantum dots are dispersed in a mixture containing unreacted pre-cursors and several other organic compounds resulting from the synthesis. Prior to their further application purification is essential, preferable without too detrimental effect on the quantum dots' PL properties. The investigated purification methods (**Tab. 4**) differed significantly regarding their impact on QY as well as their precipitation efficiency (**Fig. 7; Fig. 8**). Interestingly, all methanol containing precipitation mixtures, which are most commonly described in literature [30; 47] resulted in the lowest quantum yields (**Fig. 7, E-F**), but the best precipitation efficiencies (**Fig. 8, E-F**). The obvious relationship between a method's precipitation efficiency and the QY of the purified quantum dots can be explained, considering the mechanistic background of the purification process. The interactions of the polar solvent (added in excess) with the surface capping ligands (e.g. TOP, oleic acid) lead to a destabilization of the capping layer, followed by a temporary aggregation of the particles, which allows their centrifugation. Stronger interactions, as in the case of methanol therefore lead to strong destabilization and good precipitation, but, also to an increased surface destruction, demonstrated by the low obtained QY. In contrast, the most gentle purification methods, using pure acetone or acetone with hexane, are accompanied with only low precipitation efficiencies, indicating the limited interaction with the surface ligands. Unlike previously reported for CdTe-based quantum dots [44], no significant regeneration of the fluorescence could be observed during storage over 72 h following purification (**Fig. 7**).



Conclusively, none of the investigated methods fulfilled all desired properties, i.e. quantitative precipitation (and re-dispersion) and a maintained high quantum yield. Indeed, focusing on the PL would increase the loss of initial quantum dots by magnitudes, which is not desirable for the intended applications. Therefore, one has to compromise and choose the purification method depending on the intended application of the QDs. In the case of a QD characterization, if only less amounts are sufficient, method D (acetone + hexane) will be used, whereas in the cases where more QDs are required (e.g. for encapsulation into polymeric particles) method B (ethanol + hexane) will be used, accepting a significantly reduced QY.

Capping ligands, which are bound to the surface of nanocrystals, have been identified to be essential for their desired optical properties. By passivation of dangling lone pairs (partially coordinated surface atoms) they prevent a non-radiative energy loss and additionally they might play an active role in surface reconstitution [48]. Lots of effort already has been spent to investigate ligand effects either during synthesis [38] or during post-treatment ligand exchange experiments [27; 49; 50]. As discussed above the initial quantum yield of the custom-made CdSe quantum dots is already highly variable, hardly exceeds 10 to 15 % and furthermore is sensitive to post-preparative procedures, like for example purification. Surface passivation therefore would offer an attractive option to improve quantum dot stability and moreover, their photoluminescence properties. Considering the results obtained from coating with different primary alkylamines and 2-mercaptoethanol no clear trends could be determined, neither regarding the alkyl chain length nor the applied coating temperature (**Fig. 9**). In general effects found in literature could not be confirmed for the here used system, except the obvious quenching of CdSe fluorescence by the thiol ligand, once established for stabilizing CdTe quantum dots [51]. Quite contrary to literature, no improvement at all was found for the short allylamine, which has been described to increase QY up to 50 % [47].

The impact of the coating time can be easily understood considering that the coating procedures generally are described as dynamic processes [49]. Thus they need a certain time until their equilibrium state is reached, which however is not characterized by the highest increase in QY but moreover in the highest stability of the newly attached ligands towards removal during purification (**Fig. 9, right; Fig. 10**). Successful coating processes have been described to last between 12 to 96 h [27; 51]. Thus for particles used in further experiments coating times of at least 12 h were applied. The diversity of the obtained results and the information, derived from literature, which are also partially inconsistent, indicate that the involved processes during surface modification of quantum dots are still not completely elucidated. Numerous factors influencing either the coating process or the outcome have been identified, including – quantum dot type, size and concentration, initial

PL properties, original surface ligands and therefore the overall synthesis route, the proportion of crystals to ligand, the dispersing solvents, the coating temperature, length of the alkyl chain, type of amine (primary, secondary, tertiary), surface coverage or the ligand, and ligand's classification regarding the Lewis acid-base theory [27; 38; 42; 50; 51]. The establishment of an optimal coating procedure for all these factors actually seems to be a mostly empirical process, which is furthermore hampered by an unsatisfying reproducibility of the modification steps.

For the further encapsulation experiments an exact knowledge of the current quantum dot concentration is essential as the PL properties of a fluorescent probe are strongly depending on their absolute concentration. The molar concentrations of quantum dots in dispersions are commonly determined based on their absorbance following an empirical relationship as introduced in **2.2.5**, which was already described in literature for a certain type of quantum dots [34]. This relationship, obtained from TEM and spectroscopy studies, has also been used in this work, if the quality of different quantum dot batches should be determined or compared with each other. However, one has to keep in mind that this method it is not applicable in cases where the measurement of the absorbance spectra is not possible or where it might be disturbed by the presence of other light absorbing substances (e.g. when quantum dots are mixed with or encapsulated in other organic materials). In such cases it is only possible to quantify the amounts of the quantum dot forming chemical elements, herein Cd and Se, after disintegration of the particles and subsequent quantification using for example ICP-OES. During the later investigated encapsulation of the quantum dots (**Chapters 5 and 6**) both methods have been used: Prior to encapsulation the PL properties and the molar concentrations of CdSe in the stock solution were determined and the intended loading was calculated based on the non destructive UV measurements. In contrast, the effective loading (real amount of encapsulated nanocrystals) subsequently was determined based on the Se concentration measured by ICP-OES of an aliquot before and after encapsulation.

Comparing the results of both methods, focusing on the Se concentration, there is an apparent deviation of the two concentrations (**Fig. 11**), which may be due to the restriction to the mean diameter of the nanocrystals in order to calculate the theoretical Se concentration. However, the used quantum dots are obviously not monodisperse and the actual broadness of the current size distribution can especially account for the deviation of the ICP-OES measurements, which even changes with the investigated particle sizes. Nevertheless the observed differences kept almost constant within the size range of 4 to almost 5 nm and therefore the results of the UV-measurements could still be used as reliable indicator of the quantum dot concentration during encapsulation into particles.

The evaluation of the relationship in case of different coatings of quantum dots was also essential, since the mentioned empirical equations (2.2.5; equations (2-4)) were initially used for the determination of molar concentrations of simple uncoated CdSe quantum dots without further processing and modifications. Since it was demonstrated earlier that coating and purification could dramatically change the optical properties of quantum dots (absorbance as well as emission), it is quite obvious, that using an absorbance based calculation for coated quantum dots could lead to more or less pronounced errors of calculated particle sizes and concentrations. A similar general trend (UV-based concentrations higher than ICP-OES-based ones) was obtained for most investigated coatings (**Fig. 12**). The strongly varying differences are understandable, but the available data are certainly not sufficient at all to discuss the individual effects of the coatings. Nevertheless, for the afterwards commonly used oleylamine coating the obtained ratio and also its reproducibility was very satisfying and this is why no further elucidation of the involved processes was performed.

Generally the observed differences in the calculation can therefore be considered as constant and will not disturb the obtained absolute concentration values, since for the encapsulation efficacy always the ICP-OES measurements were directly compared and for comparisons of purifications procedures (etc.) always the same starting particle concentrations were directly compared in the subsequent experiments.

## 5. Summary and Conclusion

Following a simple organometallic approach CdSe quantum dots with the desired maximum emission wavelengths  $\lambda_{em}$  of about 610 nm were successfully synthesized. While the obtained crystal size and composition are predominantly responsible for their  $\lambda_{em}$ , the surface properties (e.g. presence of crystal defects and attached surface ligands) were found to contribute significantly to the quantum dots optical quality, especially their quantum yield. Generally the PL of these nanocrystals was found to be highly sensitive towards deviations in the synthesis or generally towards all processes, which potentially lead to a destruction of their delicate surface structure. Besides a sufficient initial stability, especially the reproducibility of all preparation steps is essential with respect to a potential application of these QD as fluorescent marker substances. Therefore standardised methods were defined for the synthesis conditions, purification of the QD dispersions and furthermore a post-synthesis surface modification. Following the same synthesis protocol over 60 min, purification procedures differed depending on the intended application of the respective quantum dots. Characterization and comparison of different batches was done after precipitation with a mixture of acetone and hexane, which were found to be less aggressive to the crystal surface. However, due to a resulting low recovery of QDs this method was not appropriate in cases where larger amounts of purified crystals are required. For these applications the purification was done with a mixture of ethanol and hexane, taking into account the reduced optical quality of the obtained nanocrystals.

An exchange of the original surface capping ligands, derived from the synthesis, for primary alkylamines (chain lengths of C<sub>12</sub> or C<sub>18</sub>) led to an improvement of the initial QY by multiples. Moreover the PL stability of the obtained nanoparticles was also enhanced during aggressive process steps, like for example the purification. Coating with oleylamine at elevated temperatures was consequently used as standard coating method for further work using the CdSe quantum dots as particulate fluorescence markers.

## 6. References

- [1] Klimov, V. "Semiconductor and metal nanocrystals - Synthesis and electronic and optical properties"; Marcel Dekker Inc., New York, 2004.
- [2] Bawendi, M.G. et al.: "The Quantum Mechanics of Larger Semiconductor Clusters ("Quantum Dots")", **Annual Review of Physical Chemistry** 41 (1990) pp. 477-496.
- [3] Smith, A.M. et al.: "Chemical analysis and cellular imaging with quantum dots", **The Analyst** 129 pp. 672-677.
- [4] Resch-Genger, U. et al.: "Quantum dots versus organic dyes as fluorescent labels", **Nature Methods** 5 (2008) pp. 763-775.
- [5] Mueller, A.H. et al.: "Multicolor Light-Emitting Diodes Based on Semiconductor Nanocrystals Encapsulated in GaN Charge Injection Layers", **Nano Letters** 5 (2005) pp. 1039-1044.
- [6] Schaefer, J. et al.: "Quantum Dot Microdrop Laser", **Nano Letters** 8 (2008) pp. 1709-1712.
- [7] Tang, S.K. Y. et al.: "A multi-color fast-switching microfluidic droplet dye laser", **Lab on a Chip** 9 pp. 2767-2771.
- [8] Arya, H. et al.: "Quantum dots in bio-imaging: Revolution by the small", **Biochemical and Biophysical Research Communications** 329 (2005) pp. 1173-1177.
- [9] Bruchez, M.J. et al.: "Semiconductor Nanocrystals as Fluorescent Biological Labels", **Science** 281 (1998) pp. 2013-2016.
- [10] Ornberg, R.L. et al.: "Western blot analysis with quantum dot fluorescence technology: a sensitive and quantitative method for multiplexed proteomics", **Nature Methods** 2 (2005) pp. 79-81.
- [11] Rosenthal, S.J. et al.: "Targeting Cell Surface Receptors with Ligand-Conjugated Nanocrystals", **Journal of the American Chemical Society** 124 (2002) pp. 4586-4594.
- [12] Geho, D. et al.: "Pegylated, Steptavidin-Conjugated Quantum Dots Are Effective Detection Elements for Reverse-Phase Protein Microarrays", **Bioconjugate Chemistry** 16 (2005) pp. 559-566.
- [13] Medintz, I.L. et al.: "Quantum dot bioconjugates for imaging, labelling and sensing", **Nature Materials** 4 (2005) pp. 435-446.
- [14] Jaiswal, J.K. et al.: "Long-term multiple color imaging of live cells using quantum dot bioconjugates", **Nature Biotechnology** 21 (2003) pp. 47-51.
- [15] Ballou, B. et al.: "Noninvasive Imaging of Quantum Dots in Mice", **Bioconjugate Chemistry** 15 (2004) pp. 79-86.
- [16] Gao, X. et al.: "In vivo molecular and cellular imaging with quantum dots", **Current Opinion in Biotechnology** 16 (2005) pp. 63-72.
- [17] Richards-Kortum, R. et al.: "Quantitative optical spectroscopy for tissue diagnosis", **Annual Review of Physical Chemistry** 47 (1996) pp. 555-606.
- [18] Mourant, J.R. et al.: "Mechanisms of Light Scattering from Biological Cells Relevant to Noninvasive Optical-Tissue Diagnostics", **Applied Optics** 37 (1998) pp. 3586-3593.

- [19] Talapin, D.V. et al.: "Highly Luminescent Monodisperse CdSe and CdSe/ZnS Nanocrystals Synthesized in a Hexadecylamine-Trioctylphosphine Oxide-Trioctylphosphine Mixture", **Nano Letters** 1 (2001) pp. 207-211.
- [20] Yildiz, I. et al.: "Biocompatible CdSe-ZnS Core-Shell Quantum Dots Coated with Hydrophilic Polythiols", **Langmuir** 25 (2009) pp. 7090-7096.
- [21] Anderson, R.E. et al.: "Systematic Investigation of Preparing Biocompatible, Single, and Small ZnS-Capped CdSe Quantum Dots with Amphiphilic Polymers", **ACS Nano** 2 (2008) pp. 1341-1352.
- [22] Pradhan, N. et al.: "Efficient, Stable, Small, and Water-Soluble Doped ZnSe Nanocrystal Emitters as Non-Cadmium Biomedical Labels", **Nano Letters** 7 (2006) pp. 312-317.
- [23] Goldman, E.R. et al.: "Avidin: A Natural Bridge for Quantum Dot-Antibody Conjugates", **Journal of the American Chemical Society** 124 (2002) pp. 6378-6382.
- [24] Peng, Z.A. et al.: "Formation of High-Quality CdTe, CdSe, and CdS Nanocrystals Using CdO as Precursor", **Journal of American Chemical Society** 123 (2001) pp. 183-184.
- [25] William, Y. et al.: "Formation of High-Quality CdS and Other II-VI Semiconductor Nanocrystals in Noncoordinating Solvents: Tunable Reactivity of Monomers", **SO: Angewandte Chemie International Edition** 41 (2002) pp. 2368-2371.
- [26] Vasiliev, R.B. et al.: "Synthesis and optical properties of PbSe and CdSe colloidal quantum dots capped with oleic acid", **Mendeleev Communications** 14 (2004) pp. 169-171.
- [27] Comparelli, R. et al.: "Improved optical properties of CdS quantum dots by ligand exchange", **Materials Science and Engineering: C** 23 (2003) pp. 1083-1086.
- [28] Fei, D. et al.: "Study on the interaction between 2-mercaptoethanol, dimercaprol and CdSe quantum dots", **SO: Luminescence** 23 (2008) pp. 321-326.
- [29] Qu, L. et al.: "Control of Photoluminescence Properties of CdSe Nanocrystals in Growth", **Journal of American Chemical Society** 124 (2002) pp. 2049-2055.
- [30] Querner, C. et al.: "Size and ligand effects on the electrochemical and spectroelectrochemical responses of CdSe nanocrystals", **Phys Chem Chem Phys** 7 (2005) pp. 3204-3209.
- [31] Schmelz, O. et al.: "Supramolecular Complexes from CdSe Nanocrystals and Organic Fluorophors", **Langmuir** 17 (2001) pp. 2861-2865.
- [32] Lakowicz, J.R. "*Principles of fluorescence spectroscopy*"; 2nd Edition Edition, Kluwer Academic/ Plenum Publisher, New York, (1999).
- [33] Sens, R. et al.: "Fluorescence quantum yield of oxazine and carbazine laser dyes", **Journal of Luminescence** 24-25 (1981) pp. 709-712.
- [34] Yu, W.W. et al.: "Experimental Determination of the Extinction Coefficient of CdTe, CdSe, and CdS Nanocrystals", **Chemistry of Materials** 15 (2003) pp. 2854-2860.
- [35] Leuenberger, H.: "*Martin - Physikalische Pharmazie*"; 4th Edition, Wissenschaftliche Verlagsgesellschaft, Stuttgart, (2002).
- [36] Mekis, I. et al.: "One-Pot Synthesis of Highly Luminescent CdSe/CdS Core-Shell Nanocrystals via Organometallic and "Greener" Chemical Approaches", **Journal of Physical Chemistry B** 107 (2003) pp. 7454-7462.

- [37] Qu, L. et al.: "Alternative Routes toward High Quality CdSe Nanocrystals", **Nano Letters** 1 (2001) pp. 333-337.
- [38] Pradhan, N. et al.: "Surface Ligand Dynamics in Growth of Nanocrystals", **Journal of the American Chemical Society** 129 (2007) pp. 9500-9509.
- [39] Green, M.: "Organometallic based strategies for metal nanocrystal synthesis", **Chemical Communications (Cambridge, United Kingdom)** (2005).
- [40] Wu, D. et al.: "A New Class of Capping Ligands for CdSe Nanocrystal Synthesis", **Chemistry of Materials** 17 (2005) pp. 6436-6441.
- [41] Murray, C. B. et al.: "Synthesis and Characterization of Nearly Monodisperse CdE (E= S, Se, Te) Semiconductor Nanocrystallites", **Journal of American Chemical Society** 115 (1993) pp. 8706-8715.
- [42] Yin, Y. et al.: "Colloidal nanocrystal synthesis and the organic-inorganic interface", **Nature** 437 (2005) pp. 664-670.
- [43] Peng, X. et al.: "Shape control of CdSe nanocrystals", **Nature** 404 (2000) pp. 59-61.
- [44] Hezinger, A.F.E.: "*Biocompatible inorganic nanocrystals for fluorescence and CT imaging*"; University of Regensburg (2010)
- [45] Grabolle, M. et al.: "Determination of the Fluorescence Quantum Yield of Quantum Dots: Suitable Procedures and Achievable Uncertainties", **Analytical Chemistry** 81 (2009) pp. 6285-6294.
- [46] Dabbousi, B.O. et al.: "(CdSe)ZnS Core-Shell Quantum Dots: Synthesis and Characterization of a Size Series of Highly Luminescent Nanocrystallites", **Journal of Physical Chemistry** 101 (1997) pp. 9463-9475.
- [47] Talapin, D.V. et al.: "Highly Luminescent Monodisperse CdSe and CdSe/ZnS Nanocrystals Synthesized in a Hexadecylamine - Trioctylphosphine Oxide - Trioctylphosphine Mixture", **Nano Letters** 1 (2001) pp. 207-211.
- [48] Wuister, S.F. et al.: "Temperature antikenquenching of luminescence of capped CdSe quantum dots", **Angewandte Chemie, International Edition** 43 (2004) pp. 3029-3033.
- [49] Ji, X. et al.: "Ligand Bonding and Dynamics on Colloidal Nanocrystals at Room Temperature: The Case of Alkylamines on CdSe Nanocrystals", **Journal of the American Chemical Society** 130 (2008) pp. 5726-5735.
- [50] Bullen, C. et al.: "The Effects of Chemisorption on the Luminescence of CdSe Quantum Dots", **Langmuir** 22 (2006) pp. 3007-3013.
- [51] Munro, Andrea M. et al.: "Quantitative Study of the Effects of Surface Ligand Concentration on CdSe Nanocrystal Photoluminescence", **The Journal of Physical Chemistry C** 111 (2007) pp. 6220-6227.





# **Chapter 5**

**Non-aqueous nanoprecipitation**

**—**

**A promising technique for the  
encapsulation of lipophilic Quantum  
Dots?**



## 1. Introduction

The current research in life sciences using quantum dots as fluorescent markers has grown tremendously since these fluorescent nanocrystals, have been identified as promising tools for imaging applications, based on their extraordinary optical properties compared to the commonly used organic fluorescent dyes [1]. Actually, cellular diagnostics or molecular imaging would be hardly possible in some cases without the application of quantum dots.

Bearing predominantly non-biocompatible, lipophilic organic ligands at their inorganic core surface and with the suitable optical properties, which are restricted to crystals in smallest nano-dimensions [2], usually a post-synthesis processing is required in order to increase their biocompatibility and allow their use in biological systems [3; 4]. Depending on the intended application there is a variety of modifications described in literature, which can be roughly separated into three main groups of processing techniques: (1) direct modification of single quantum dot surfaces by conjugation with biomolecules or polymers [5; 6], (2) embedding of quantum dots in micelles or liposomes [7; 8] or (3) their encapsulation into solid biocompatible matrices [9-11]. Such quantum dot conjugates have been widely used for in vitro cell-based assays [12], targeting and imaging of certain tissues [13], identification of different cell types [8; 14] or intracellular trafficking [15]. Furthermore they could also deal as an alternative to common organic fluorescence dyes frequently used during development and characterization of drug delivery systems. However, each here described modification of the quantum dots could lead to an alteration in their physicochemical and optical characteristics [3] and possibly results in a loss of their desired optical properties [16]. To gain a better understanding of available processing methods, essential for further optimization, occurring processes and critical parameters need to be characterized focused on one single system, which was the main intention of the current work.

The encapsulation of quantum dots into solid polymeric matrices by so-called nanoprecipitation has been chosen since this is a simple method offering several advantages. Characterized by overall narrow size distributions, the particle size can be easily tailored by various factors, thoroughly discussed in **chapter 2**. Furthermore other commonly applied procedures in preparation of nanoparticles (e.g. solvent evaporation, polymerization [6; 9; 17]) use aggressive emulsification steps or require radicals or UV irradiation to initiate the polymerization of monomers of the matrix, which obviously limit their applicability to encapsulate sensitive substances. In comparison with this, nanoprecipitation appears as gentle method and therefore seems to be appropriate for the encapsulation of quantum dots, known to be very sensitive against their environment and different processing steps, in order to preserve their desired optical properties.

In the present work the applicability of the non-aqueous nanoprecipitation method for the encapsulation of lipophilic quantum dots was investigated. The impact of loading, properties of the quantum dot surface or matrix material was determined, primarily focusing on the resulting fluorescence properties of the obtained polymeric nanoparticles.

## 2. Materials and Methods

### 2.1 Materials

PLGA 75:25 (Resomer<sup>®</sup> 756) was a kind gift of Boehringer Ingelheim (Boehringer Ingelheim AG, Biberach, Germany). Biodegradable copolymers (mPEG<sub>2</sub>PLA<sub>40</sub> and NH<sub>2</sub>PEG<sub>2</sub>PLA<sub>40</sub>) were synthesized following an established method as described in **chapter 2**. Unmodified CdSe quantum dots and oleylamine-coated (OA-coated) CdSe quantum dots were synthesized as described in **chapter 4**. QDot<sup>®</sup>800 were purchased from Molecular Probes (Invitrogen, Goettingen, Germany). Oxazine 170 perchlorate (95 %), Pluronic<sup>®</sup> F68, elemental selenium (100 mesh) and anhydrous cadmium chloride (p.a.) were obtained from Sigma-Aldrich (Sigma-Aldrich Chemie GmbH, Taufkirchen, Germany). Sucrose, ethanol (p.a.), methanol (p.a.), isopropanol (p.a.) and nitric acid (65 %) were purchased at Merck (Merck KGaA, Darmstadt, Germany). Chloroform (p.a.), hexane (p.a.) and acetone (p.a.) were obtained from Acros (Acros Organics, Fischer scientific GmbH, Nidderau, Germany).

### 2.2 Methods

#### 2.2.1 Preparation and characterization of CdSe Quantum Dot stock dispersion

Prior to encapsulation raw dispersions of custom-made CdSe quantum dots were purified following a procedure established in **chapter 4**. Briefly, an aliquot, usually 1 to 2 ml of the dispersion were mixed with a 30-fold excess of a mixture of ethanol and hexane (5:1), followed by centrifugation (10,000 g, 30 min, 10 °C; Avanti JE centrifuge; Beckman Coulter GmbH, Krefeld, Germany), discarding the supernatant and subsequent re-dispersion of the sediment in chloroform.

Photoluminescence [PL] properties and molar concentrations of nanocrystals were determined following methods described in **chapter 4 (2.2.4 & 2.2.5)**.

#### 2.2.2 Preparation and characterization of the QDot<sup>®</sup> 800 stock dispersion

The commercially available QDots<sup>®</sup> 800 were purified following the method recommended by the supplier. An aliquot of the QDot<sup>®</sup> raw dispersion was mixed with a 4-fold excess of a solvent mixture of methanol and isopropanol (ratio=3:1). After centrifugation (3,000 g, 5 min, 10 °C) the supernatant was discarded and the sediment was re-dispersed in CHCl<sub>3</sub>. The molar concentration of the QDots<sup>®</sup> in the stock dispersion could not be calculated based on the commonly used UV absorption due to the unknown composition of the

particles, and therefore was estimated assuming a quantitative precipitation and re-dispersion. PL properties basically were determined following the same procedure as for the CdSe quantum dots; however, with changed instrumental settings, for the measurement of the fluorescence emission spectra a red-sensitive R928 photomultiplier was additionally used. In contrary to custom-made quantum dots, QDot® 800 were excited at 460 nm and spectra were recorded over the range of 500 to 900 nm.

### **2.2.3 Precipitation of Quantum Dot loaded nanoparticles**

Polymeric nanoparticles were prepared following a modified nanoprecipitation method [18], introduced in detail in **chapter 2**, using chloroform and ethanol as solvent – non-solvent system. If not otherwise stated the preparation followed the standard conditions described there. Briefly, a 1 % solution of the polymer (PLGA, mPEG<sub>2</sub>PLA<sub>40</sub> or NH<sub>2</sub>PEG<sub>2</sub>PLA<sub>40</sub>) was prepared in CHCl<sub>3</sub> and a respective amount of the quantum dot stock dispersion was added (depending on the determined quantum dot concentration and intended loading). The final volume of this organic phase was then adjusted to 5 ml. Afterwards this polymer solution was added dropwise to 40 ml of the non-solvent, while the formation of particles occurred immediately. Either pure ethanol or an ethanolic solution of Pluronic F68 (0.1 to 0.5 %) were used as external non-solvent phase. Avoiding further agitation of the particle dispersion, the CHCl<sub>3</sub> was allowed to evaporate over at least three days at room temperature. The ethanol was subsequently removed via dialysis against water containing 0.1 % Pluronic F68 using a Nadir® dialysis membrane (cut-off of 10-20 kDa; Carl ROTH GmbH, Karlsruhe, Germany). Recovery of the nanoparticles from the aqueous dispersion was performed by centrifugation (12,500 g, at least 30 min, 10 °C) and subsequent re-dispersion in 5 % sucrose solution. Formed microparticles and other artefacts were removed via filtration (< 1 µm). Subsequently, the nanoparticles were freeze-dried using a lab-scale freeze-dryer (Martin Christ Gefriertrocknungsanlagen, Osterode am Harz; Germany).

Preparation of unloaded nanoparticles, dealing as negative control, followed same procedure except the addition of the quantum dots.

### **2.2.4 Determination of particle concentration**

Analysis of the PL properties of the quantum dot loaded nanoparticles required knowledge about their concentration in dispersion, which usually was estimated semiquantitatively based on the solid content in a certain aliquot of dispersion, depending on the investigated production step. Within particle preparation, 0 % loss of material during the initial precipitation step was assumed, and the particle concentration was obtained from the

initial weight of polymer in relation to the actually apparent present volume of the particle dispersion. To determine the concentration in the final, purified, dispersion an aliquot (usually 500 to 1000 µl) was centrifuged (15,000 g, 45 min, 10 °C) and the residual sediment was freeze-dried and again weighed to obtain the solid content of the aliquot.

### 2.2.5 Fluorescence spectroscopic analysis of the nanoparticles

Fluorescence properties of quantum dot loaded nanoparticles were determined at different steps during particle preparation. Therefore fluorescence spectra (500 to 750 nm; 500 to 900 nm) of the polymer particles either dispersed in ethanolic or aqueous solutions were measured using a LS 55 spectrophotometer (PerkinElmer, Waltham, USA), equipped with a red-sensitive R928 photomultiplier in the case of the QDot® 800 loaded samples, following excitation with either 488 nm or 460 nm and a photomultiplier voltage of 750 V. To allow comparison of different process steps or particle batches, measured intensities were subsequently normalized on the pre-determined particle concentration.

### 2.2.6 Determination of particles loading with CdSe Quantum Dots

Inductively coupled plasma optical emission spectrophotometry [ICP-OES] was used to determine the elemental concentrations of the quantum dot components Cd and Se. For sample preparation an aliquot of the final lyophilisate was disintegrated in 2 ml ethanol containing HNO<sub>3</sub> (65 %). 50 to 100 µl of the initial organic quantum dot dispersion used in the respective experiment dealt as reference for the determination of the maximum achievable amounts of Cd and Se. Subsequently all samples were diluted up to 10 ml in a volumetric flask and the final concentration of HNO<sub>3</sub> was about 2 to 3 %.

The standard solutions, prepared of cadmium chloride and selenium, contained 100 ppm, 10 ppm and 1 ppm of Cd and Se in 2 to 3 % HNO<sub>3</sub>. Measurements were performed using a Jobin Yvon 70 Plus (S+S) ICP-OE spectrophotometer (Horiba, Jobin Yvon, France) in the sequential analysis mode. Instrumental settings and element characteristics are given in **chapter 4 (2.2.7)**.

The CdSe loading of the nanoparticles was calculated based on the following equations:

$$\text{Loading} / \% = \frac{100 * C(\text{Se})_{\text{real}}}{C(\text{Se})_{\text{initial}}} ; \quad (1)$$

$$C(\text{Se})_{\text{real}} = \frac{M(\text{Se})_{\text{ICP-Sample}}}{m_{\text{ICP-Sample}}} ; \quad (2)$$

$$C(Se)_{initial} = \frac{M(Se)_{QD-Reference} * f_{QD-Reference}}{m_{Polymer}} ; \quad (3)$$

with the real concentration of Se in the nanoparticles  $C(Se)_{real}$  [nmol/mg], the molar amount of Se in degraded particles measured via ICP-OES  $M(Se)_{ICP-Sample}$  [nmol], the weight of the particles used for the preparation of the ICP-sample  $m_{ICP-Sample}$  [mg], the theoretical required concentration of Se in the nanoparticles given at 100 % encapsulation  $C(Se)_{Initial}$  [nmol/mg], the molar amount of Se in the QD-reference measured with ICP-OES  $M(Se)_{QD-Reference}$  [nmol], the multiple of the volume of the QD-reference used for encapsulation  $f_{QD-Reference}$  and the weight of polymer used for particle preparation  $m_{Polymer}$  [mg].

### 2.2.7 Determination of particle sizes

Photon correlation spectroscopy [PCS] was used to determine the hydrodynamic diameters and polydispersity indices of the prepared nanoparticles usually dispersed in 5 % sucrose. Measurements were performed at 20 °C with a Zetasizer 3000 A (Malvern Instruments Inc., Herrenberg; Germany). Results are presented as mean and relative standard deviation of three independent measurements.

### 2.2.8 Morphologic analysis of Quantum Dot loaded nanoparticles

The morphology of quantum dot loaded nanoparticles as well as the spatial distribution of quantum dots within the polymeric matrix was imaged by transmission electron microscopy [TEM]. Samples were prepared by dropping diluted aqueous dispersions on 3.05 mm formvar/carbon coated copper grids (300 mesh) followed by negative staining with phosphotungstic acid (2 % in water) for 30 s and subsequent drying under vacuum. Images were taken using a Zeiss EM C/CR (Carl Zeiss AG, Jena, Germany) with 60 kV operating voltage.



### 3. Results

The characterization of the quantum dot loaded nanoparticles was primarily focused on their photoluminescence properties, to prove their suitability as potential imaging systems. Besides the mere effect of quantum dot loading, also the optimization by using surface modified quantum dots as well as different matrix materials was investigated. Additionally, the results of the custom-made nanocrystals were compared with commercially available quantum dots (QDots® 800).

#### 3.1 PLGA based nanoparticles – the effect of loading

The preparation of stable PLGA based nanoparticles was only possible by supplementing 0.5 % Pluronic F68 to the ethanolic external phase, otherwise particles agglomeration occurred already during the precipitation process. PLGA particles were prepared with increasing amounts of initially added quantum dots over the range of 0.023 to 0.75 nmol per milligram of polymer. The quantum yield of the used quantum dot stock dispersions was about 3 %. Immediately following the precipitation, all quantum dot containing samples clearly showed a detectable fluorescence; however, no dependency on the initial loading with quantum dots was observed (**Fig. 1, left**). Considering all three main process stages (precipitation, dialysis and lyophilisation) a dramatic loss in the particles' fluorescence could be observed for all batches with different amount of encapsulated quantum dot (**Fig. 1, right**) and similar trends were obtained in three control experiments.

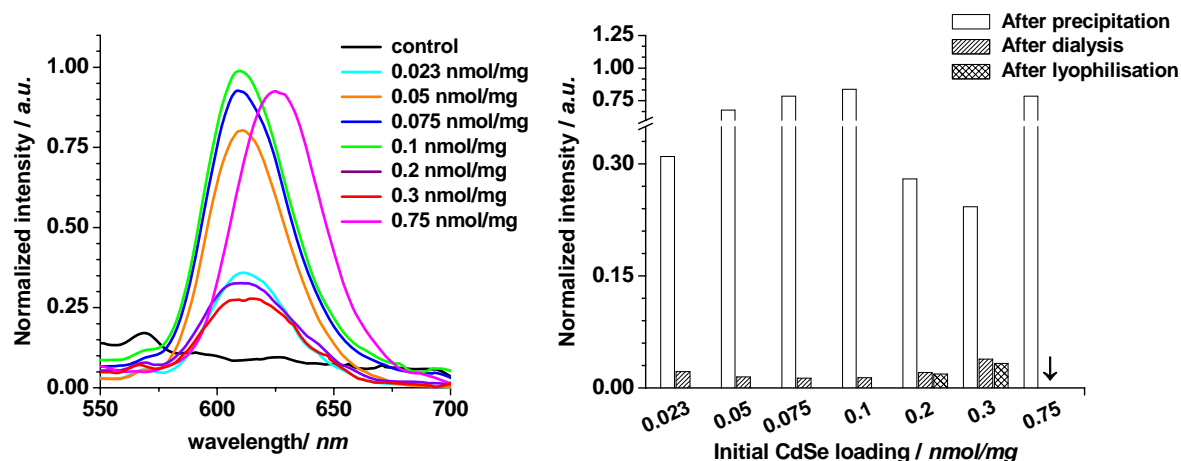


**Fig. 1:** PLGA based nanoparticles with increasing loadings of uncoated CdSe quantum dots given in nmol/mg – (*left*) normalized fluorescence spectra taken immediately after nanoprecipitation; (*right*) development of fluorescence intensity during the whole preparation process (displayed by values of three fundamental preparation stages); arrow indicates failure in particle preparation; intensity of samples with equal particle concentrations (1 mg/ml) normalized on maximum fluorescence intensity

The particles with loadings up to 0.1 nmol/mg were initially characterized by the highest luminescence intensities directly following precipitation. However, the final dispersion did not show any fluorescence at all. In contrast, the batches with lowest post-precipitation intensities were finally the only two exhibiting a detectable fluorescence of the final product, which however, was only a tenth of the initially observed value. Thus, the post-precipitation value was not considered an adequate indicator for the properties of the final product. Interestingly, no particles could be obtained in the case of the highest intended quantum dot loading. Following a successful precipitation almost complete aggregation occurred within the first hours of evaporation.

An increasing amount of encapsulated quantum dots was also found to affect the resulting size of the polymeric nanoparticles (**Fig. 2**).

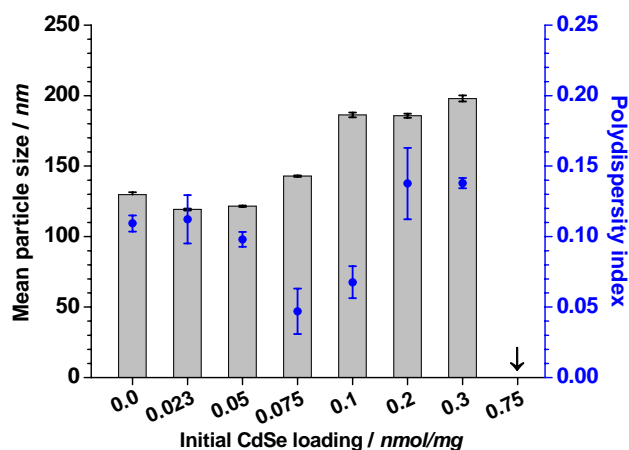


**Fig. 2:** Particle sizes [nm] and polydispersity indices of PLGA nanoparticles with increasing loadings of uncoated CdSe quantum dots given in nmol/mg; arrow indicates failure of particle preparation

Keeping almost the size of the unloaded control until a quantum dot loading of 0.075 nmol/mg, the nanoparticle size escalated about almost 50 nm, followed by negligible further increase, when loading exceeded 0.1 nmol/mg of polymer. Indicated by overall very low polydispersity indices, all batches prepared have narrow size distributions.

No significant impact of the quantum dot concentration on the encapsulation efficiency could be determined, which was found to range generally between 92 and 100 %.

An overall increase in the number of encapsulated nanocrystals with increasing loading was further proved by TEM, exemplarily shown for loadings of 0.1 and 0.2 nmol/mg (**Fig. 3**). Quantum dots were found to be randomly distributed within the polymeric matrices.

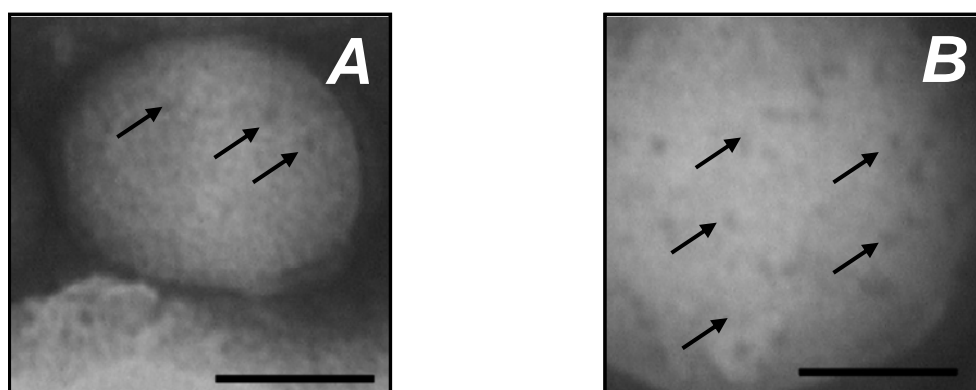


**Fig. 3:** TEM images of PLGA based nanoparticles loaded with either **(A)** 0.1 nmol/mg uncoated CdSe quantum dots or **(B)** 0.2 nmol/mg uncoated CdSe quantum dots; arrows indicate single nanocrystals; scale bars correspond to 50 nm

### 3.2 PLGA based nanoparticles – the effect of Quantum Dot coating

Post-synthesis surface modification of CdSe quantum dots was found to partially increase their initial PL characteristics and is discussed to increase stability during further processing (**Chapter 4**). Therefor the fluorescence characteristics of PLGA nanoparticles loaded with increasing amounts of oleylamine-coated (OA-coated) CdSe quantum dots were compared to that obtained with uncoated quantum dots at the main process stages (**Fig. 4**).

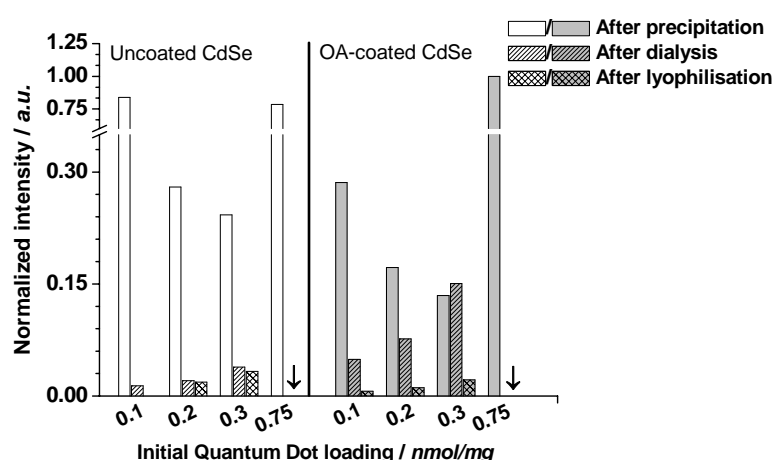


**Fig. 4:** Normalized fluorescence intensity of PLGA nanoparticles loaded with increasing amounts of either uncoated CdSe or OA-coated CdSe quantum dots; intensity of samples with equal particle concentrations (1 mg/ml) normalized on maximum intensity; arrows indicate failures of particle preparation

By far highest post-precipitation values were measured with particles containing the highest quantum dot loadings of 0.75 nmol/mg. However, independent of the surface properties of the encapsulated QDs, preparation finally failed in both cases due to polymer aggregation. For all other the loading also the within preparation intensities increased with increasing quantum dot loadings; however, again fluorescence of the final particle dispersions was very low.

OA-coated CdSe also showed bigger effects on the polymeric nanoparticles size, which increased stepwise up to 230 nm in the case of the 0.3 nmol/mg of polymer loading (**Fig. 5**). Also for the surface modified quantum dots loaded nanoparticles polydispersity indices were very low, indicating a narrow size distribution.

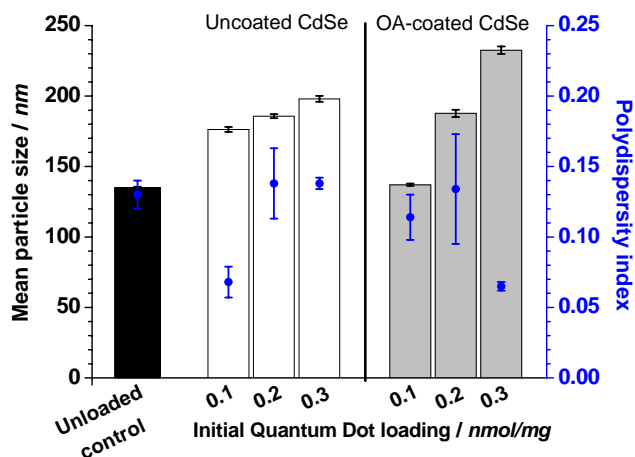


**Fig. 5:** Particle sizes [nm] and polydispersity indices of PLGA nanoparticles loaded with increasing amounts of either uncoated or OA-coated CdSe quantum dots given in nmol/mg

### 3.3 The effect of matrix material

Three different materials, the lipophilic PLGA and two amphiphilic diblock copolymers ( $\text{PEG}_2\text{PLA}_{40}$  and  $\text{NH}_2\text{PEG}_2\text{PLA}_{40}$ ) were used to investigate the possible impact of the matrix material on the final polymeric nanoparticles' PL properties using similar initial loadings of both uncoated and OA-coated quantum dots. First of all it should be noted that the used precipitation systems differed depending on the applied polymer. While the addition of 0.5 % Pluronic F68 to the external phase was a pre-condition for precipitation in case of PLGA, no further stabilization is required in the case of the amphiphilic polymers. Moreover, the presence of even small amounts of the surfactant in the external phase (e.g. 0.1 %) led to stepwise aggregation of the precipitated polymer during the evaporation step. Thus particles made of  $\text{PEG}_2\text{PLA}_{40}$  and  $\text{NH}_2\text{PEG}_2\text{PLA}_{40}$  were generally prepared using surfactant-free ethanol as external phase.

The matrix forming polymer was found to have a pronounced effect on the optical quality of the prepared particles in case of both coated and uncoated quantum dots (**Fig. 6, left**).

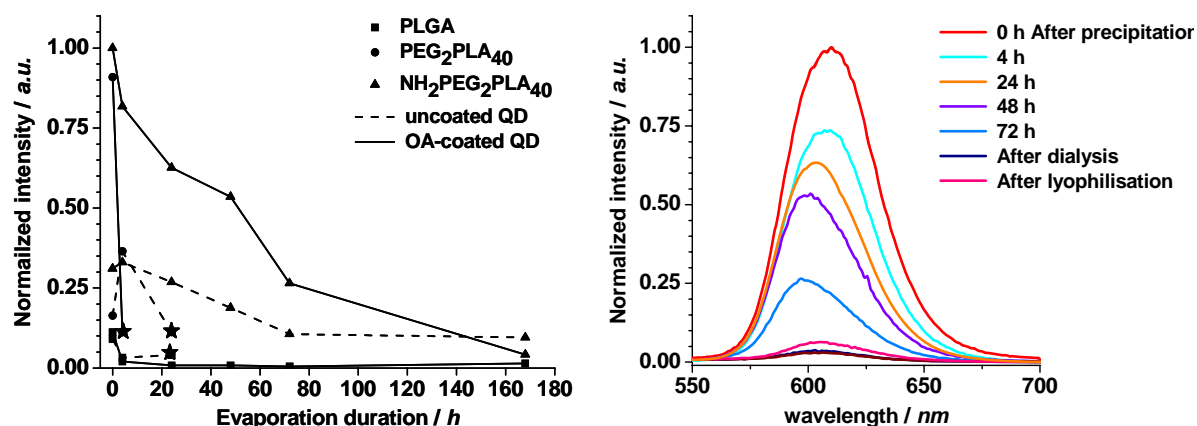


**Fig. 6:** (*left*) Development of normalized (maximum) fluorescence intensity of nanoparticles loaded either with uncoated (dashed line) or OA-coated CdSe quantum dots (solid line) during evaporation phase; symbols represent the type of polymer used as matrix; stars indicate time-point of failure and abortion; (*right*) normalized fluorescence spectra of nanoparticles based on NH<sub>2</sub>PEG<sub>2</sub>PLA<sub>40</sub> loaded with OA-coated CdSe quantum dots at various stages of the preparation process; initial loading with quantum dots was 0.75 nmol/mg; intensity of samples with equal particle concentrations (1 mg/ml)

As already demonstrated above no particles at all were obtained using PLGA loaded with uncoated CdSe quantum dots and aggregation or moreover a film formation also occurred during evaporation for PEG<sub>2</sub>PLA<sub>40</sub> based batches independent of the used quantum dot type. Highest stability was found in case of NH<sub>2</sub>PEG<sub>2</sub>PLA<sub>40</sub> based systems. The development of fluorescence spectra during the whole preparation process is exemplarily presented for NH<sub>2</sub>PEG<sub>2</sub>PLA<sub>40</sub> loaded with OA-coated quantum dots (**Fig. 6, right**).

NH<sub>2</sub>PEG<sub>2</sub>PLA<sub>40</sub> particles loaded either with unmodified or OA-coated quantum dots remained fluorescing over the complete process (**Fig. 7, left**). However, only in case of the nanoparticles loaded OA-modified nanocrystals the fluorescence signal could be allocated to the typical quantum dot fluorescence (**Fig. 7, right**).

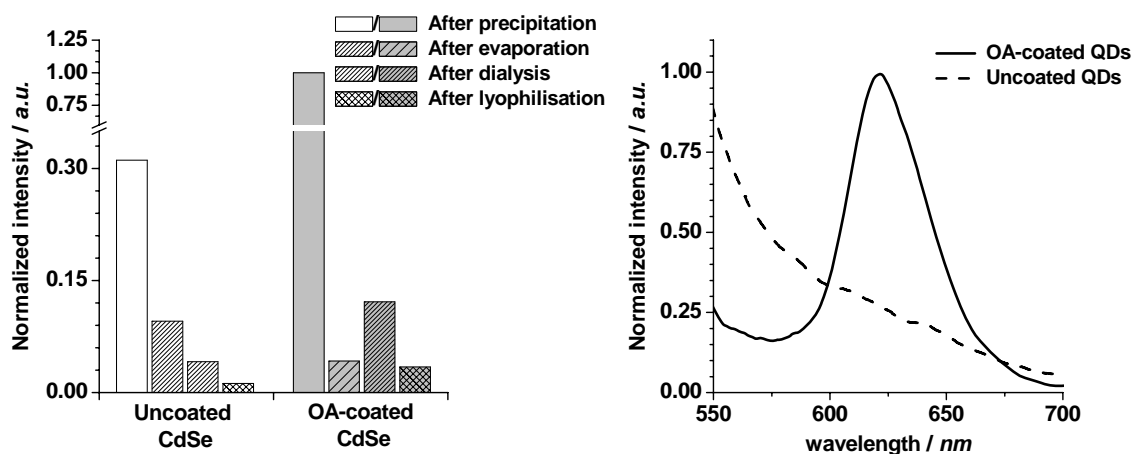


**Fig. 7:** (*left*) Development of fluorescence intensity of nanoparticles based on  $\text{NH}_2\text{PEG}_2\text{PLA}_{40}$  during the whole preparation process (displayed by values of four fundamental preparation stages); initial loading of either uncoated or OA-coated CdSe quantum dots was 0.75 nmol/mg, intensity of samples with equal particle concentrations (1 mg/ml) normalized on maximum intensity; (*right*) comparison of normalized fluorescence spectra recorded following lyophilisation and re-dispersion in water

Compared to the negative control a pronounced increase in particle size was observed for such  $\text{NH}_2\text{PEG}_2\text{PLA}_{40}$  based particles if loaded with 0.75 nmol/mg, which were slightly higher if uncoated CdSe were encapsulated (**Fig. 8, left**).

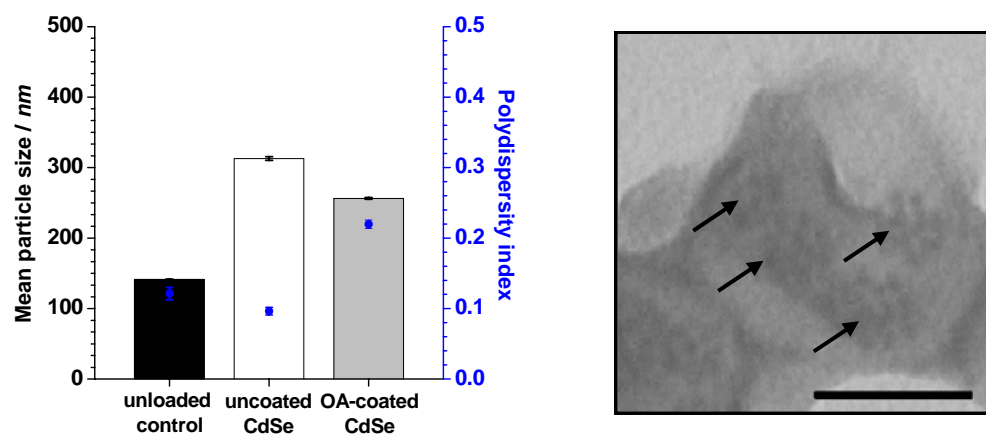


**Fig. 8:** (*left*) Particle sizes [nm] and polydispersity indices of  $\text{NH}_2\text{PEG}_2\text{PLA}_{40}$  nanoparticles either unloaded or loaded with uncoated or OA-coated CdSe quantum dots respectively (initial loading 0.75 nmol/mg); (*right*) TEM image of  $\text{NH}_2\text{PEG}_2\text{PLA}_{40}$  nanoparticles loaded with OA-coated quantum dots, arrows indicate quantum dot clusters; scale bar corresponds to 50 nm

Within the solid particles the OA-coated quantum dots were not further randomly distributed, as in case of PLGA particles with lower loadings, moreover crystals were

found to be arranged in cluster like structures and several clusters were apparent per nanoparticle (**Fig. 8, right**).

### 3.4 Encapsulation of QDot® 800

Commercially available quantum dots with an emission wavelength of about 790 nm were encapsulated to additionally offer an imaging tool with enhanced *in-vivo* detectability. PLGA was used as matrix material and the initial loading was estimated to be about 0.02 nmol/mg. Following high initial maximum fluorescence intensity after precipitation, the values mainly decreased in two steps of the preparation process – during first hours of evaporation and during dialysis (**Fig. 9**).

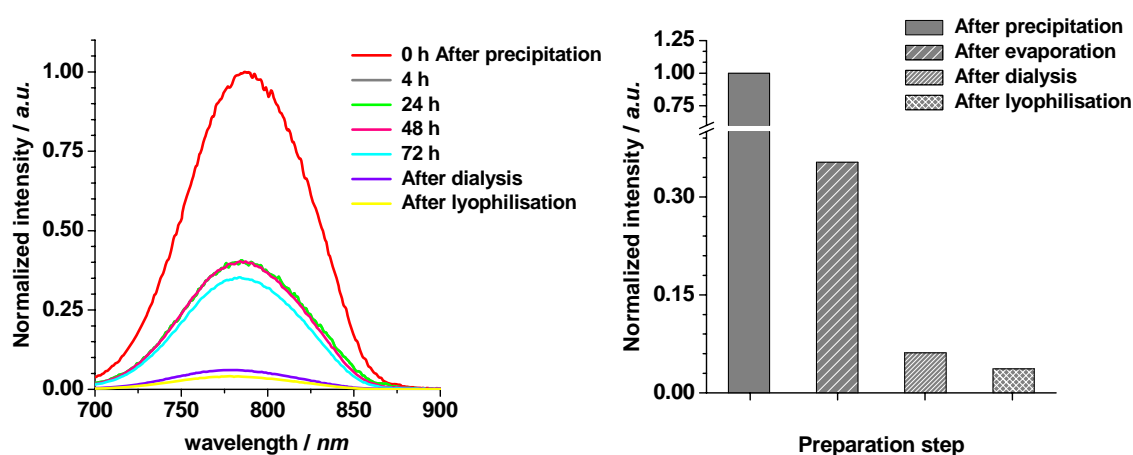


**Fig. 9:** (*left*) Normalized fluorescence spectra and (*right*) development of maximum fluorescence intensity of PLGA nanoparticles loaded with QDot® 800 quantum dots during the whole preparation process; initial loading 0.02 nmol/mg; intensity of samples with equal particle concentrations (1 mg/ml) normalized on maximum intensity

The maximum fluorescence intensity of nanoparticles in final dispersion was only a tenth of the post-precipitation value, which is comparable to the results presented for the encapsulation of custom-made quantum dots. With a mean diameter of 150 nm the QDot® containing particles are similar sized as the unloaded control.



## 4. Discussion

Nanoprecipitation generally serves as appropriate method for the preparation of polymeric nanoparticles. Varying process parameters were found to allow tailoring of particle sizes ranging from 50 to 300 nm with narrow size distributions. Compared to typically used solvent evaporation procedures [10; 14] no emulsification step (e.g. sonication) is required and due to the resulting lack of mechanical stress to the quantum dot surface, nanoprecipitation was expected to stabilize or moreover protect quantum dot photoluminescence properties during the encapsulation process. However, this expected behaviour could not be proved at all by the conducted experiments, most likely due to the effect of the used solvents and matrix materials on the surfaces of the encapsulated quantum dots.

Principally, independent of the exact polymer/quantum dot system, nanoprecipitation was found to result in quantum dot loaded nanoparticles, whose final fluorescence intensities were multitudes below the values expected based on the initial PL of the used quantum dots. There is an apparent loss in the intensity signal throughout the whole preparation process (**Fig. 1; Fig. 4; Fig. 6; Fig. 7; Fig. 9**). Generally three critical steps could be identified and will be discussed in the following (1) the precipitation, (2) the evaporation of chloroform and (3) the final dialysis against water.

The impact of precipitation was determined by comparing intensities of both, the pure organic quantum dot stock dispersion and the dispersions of nanoparticles, immediately after precipitation, providing equal quantum dot concentrations in both. Considering the initial QY of the organic stock preparation there was a loss in quantum dots fluorescence intensity of about 99.9 % during the precipitation step. For evaluation of the loaded nanoparticles the initial post-precipitation intensity was defined as 100 %. During evaporation over at least three days this post-precipitation intensity decreased by about 50 to 90 %, followed by an almost negligible further loss of 5 to 10 % during final dialysis. Independent of the respective preparation stage there are very few reasons, which can provide an explanation of these phenomena. Since quantum dots have been reported to be sensitive to their environment [19-21] the loss in intensity is discussed to result predominantly from a destabilization or destruction of the quantum dot surface. This is supported by reports in literature whereupon a loss in QDs fluorescence intensity results of a depletion of surface ligands [13]. Both, the matrix polymer itself or the organic non-solvent ethanol, which also was found to gradually diffuse into the polymeric nanoparticles during chloroform evaporation (**Chapter 2**), can interact with the crystal surface or the surface capping ligands. This could lead either to a change in the spatial arrangement of the ligands or even their partial detachment. Additionally results also suggest that spontaneous solidifications of the particle matrix can cause mechanical

stress to the quantum dot surface, which also reduces their photoluminescence. Keeping in mind the extraordinary impact of surface integrity and ligands on the optical properties of the quantum dots [22], after all these negative effects are not surprising. In this context also an apparent quenching of the quantum dots fluorescence by the polymer matrix has to be considered. This phenomenon was even found to take place in solution, depending on both the polymer type and its applied concentration (**Fig. 10**).

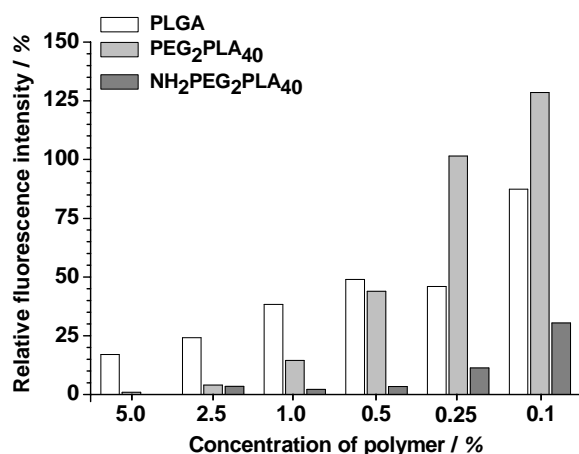


**Fig. 10:** Relative maximum fluorescence intensity of CdSe quantum dots after addition of organic solutions containing different amounts of different biodegradable polymers

For concentrations of 1 % as used for nanoparticles preparation in the present work already the dissolved polymers caused a decrease in fluorescence ranging between 50 and 90 %. After precipitation, in the solid particle state, the impact can be expected to be even higher due to a locally much higher concentration of the polymer around the quantum dots and an also increased optical density of the solid polymer matrix as compared to the polymer solution.

Based on PLGA as matrix polymer and unmodified quantum dots, several factors were investigated with respect to their impact/contribution on the fluorescence properties of the labelled nanoparticles.

The preparation of stable fluorescing PLGA based nanoparticles generally was successful by increasing the quantum dot loading (**Fig. 1**), proved by overall high encapsulation efficiencies from 0.023 to 0.3 nmol/mg, and the nanocrystals were found randomly distributed (**Fig. 3**). The fluorescence intensities of these QD loaded PLGA nanoparticles, however, would hardly allow their application as an imaging tool. Indeed, a further increase in loading up to 0.75 nmol/mg was very limited since aggregation of the PLGA nanoparticles occurred immediately after precipitation. This effect might be due to space requirements of the nanocrystals dispersed in the polymeric matrix. During the

establishment of the nanoprecipitation, it was determined, that the here applied process parameters (non-aqueous system, 1 % PLGA, ratio of solvent and non-solvent phase of 1:8) usually lead to particles smaller than 200 nm (**Chapter 2**). Considering the limited impact of the quantum dot loading on final size of PLGA particles (**Fig. 2**) and, in addition, the relative large space required by the nanocrystals determined in case of highly loaded  $\text{NH}_2\text{PEG}_2\text{PLA}_{40}$  particles (~280 nm) (**Fig. 8, left**) the loading capacity of PLGA particles is expected to be limited predominantly by spatial factors of the incorporated particulate substances. The larger amounts of solid crystals obviously lead to the formation of inhomogeneous polymer matrices with insufficient surface stabilization and subsequently the formation of precipitating polymer aggregates.

In case of the PLGA particles, an exchange of the unmodified nanocrystals by oleylamine-coated quantum dots, which were found to stabilize QDs optical properties (**Chapter 4**), could not level the overall impact of the preparation process on the fluorescence properties within the investigated loading range of 0.1 to 0.75 nmol/mg (**Fig. 4**). There is almost no protective effect of the OA ligand during precipitation. This is indicated by similar post-precipitation intensities of two particle batches containing QDs with initial QY (about 3 %) but different surface ligands (unmodified or OA-coated) (**Fig. 4**). The above discussed fluorescence quenching by the polymer (**Fig. 10**) also occurred in case of the OA-coated quantum dots (data not shown), but was slightly lower ranging between 60 and 40 % for solutions containing 1 % polymer. Nevertheless results indicate similar sensitivity of the oleylamine ligand to rearrangement or detachment as the original ligands resulting from the synthesis. Following precipitation intensities firstly suggest an increased stability of the OA-coated quantum dots, indicated by enhanced within preparation values ("after dialysis"). Indeed this is afterwards levelled by a higher sensitivity towards the lyophilisation and the final product has no improved fluorescence intensities compared to particles prepared with uncoated CdSe.

The particles sizes were found to be even more influenced by the surface properties of the encapsulated quantum dots than by the initial loading (**Fig. 5**). This may be due to the bigger surface ligand and additionally its interaction with the lipophilic PLGA, which may lead to matrices with a more spongy structure and therefore larger particles.

The choice of the nanoparticle forming matrix material by far had the most pronounced impact on the nanoparticles, as indicated by the comparison of the lipophilic PLGA and the two amphiphilic diblock copolymers  $\text{PEG}_2\text{PLA}_{40}$  and  $\text{NH}_2\text{PEG}_2\text{PLA}_{40}$  (**Fig. 6**). At first, as reported for PLGA particles also the preparation of  $\text{PEG}_2\text{PLA}_{40}$  particles failed with the high QD loading of 0.75 nmol/mg. In contrast, the  $\text{NH}_2\text{PEG}_2\text{PLA}_{40}$  polymer resulted in stable particles with the best optical properties of all prepared systems, despite its similarity of the chemical structure (**Fig. 7**). Again also the space requirements of the

nanocrystals could contribute to the observed destabilization. However, contrary to the above discussed PLGA, PEG<sub>2</sub>PLA<sub>40</sub> by far resulted in highest particle sizes if precipitated in the non-aqueous system (**Chapter 2**) and therefore could offer sufficient space. Moreover the differences between both types of diblock copolymers suggest a partition of the respective PEG part (either mPEG or NH<sub>2</sub>-PEG). In case of the mPEG<sub>2</sub>PLA<sub>40</sub> an interaction of the PEG-block with the quantum dots generally is very likely as similar polymers already have been used for the surface modification of quantum dots [23]. A hence resulting preferential orientation of the PEG block to interior of the particle would lead to an inadequate surface decoration of the polymeric nanoparticles with PEG, which is essential as steric barrier for the forming nanoparticles [24], subsequently resulting in particle aggregation and coalescence. Indeed, considering this, it was surprising that the addition of further emulsion stabilizers (e.g. Pluronic F68) to the non-solvent phase as in the case of PLGA particles could not successfully prevent the aggregation of the forming PEG<sub>2</sub>PLA<sub>40</sub> particles.

A general similar destabilization of the polymer nanoparticles would be expected also in case of the NH<sub>2</sub>PEG<sub>2</sub>PLA<sub>40</sub>, especially since an interaction of other primary amines with quantum dots has been already demonstrated [25] (also see **Chapter 4**). The enhanced PL properties of the final dispersion (**Fig. 7**), compared to all other batches, may deal as additional proof for a crystal surface stabilizing activity of the amine group. Thus, a re-orientation of the NH<sub>2</sub>-PEG to the particle interior would be expectable. Nevertheless no aggregation of the forming nanoparticles occurred for this polymer. This suggest that the number of amine groups interacting with the quantum dots are small enough to still ensure sufficient presence of NH<sub>2</sub>-PEG on nanoparticles surface, acting as steric barrier for the polymer particles. This might be explained with respect to the spatial distribution of quantum dots within the polymeric matrix with was found to be cluster-like (**Fig. 8, right**), assuming that only few crystals in the outer area of the clusters will interact with the amine groups. Overall the exact processes of particle stabilization could not be explained so far. In this context it should be noted that nanoprecipitation initially was successful in case of all three materials and aggregation and coalescence occurred only within several hours following preparation. This clearly suggests an initially sufficient steric stabilization of the nanoparticle surfaces. However, in contrast to the aqueous procedure particles precipitated in ethanol, as in the current case, were found to harden only incompletely after precipitation due to a continuously swelling and uptake of ethanol (**Chapter 2**). Therefore it may be possible that there is dynamic change in the initial polymer orientation which could lead to continuous destabilization of the particles.

As mentioned above for the PLGA nanoparticles, also in case of the diblock copolymers the OA-coated quantum dots showed no superiority compared to the uncoated quantum

dots. The ratio in fluorescence of polymeric nanoparticles within preparation was found to be 0.35 which is almost the same as determined for the both used QD stock dispersions with initial QYs of 3.42 % and 10 % respectively. The positive effect on the fluorescence properties of the final product (**Fig. 7**) would then primarily be based on the initial higher quantum yield of the OA-coated quantum dots.

Compared to the custom-made CdSe quantum dots commercially available nanocrystals were found to show pronounced differences in the PL properties of the prepared nanoparticles. Even with loadings as low as 0.02 nmol/mg, similar to the lowest investigated loading of the custom-made quantum dots, nanoparticles exhibit a low, but still detectable fluorescence. The generally similar profiles of signal loss following the precipitation (**Fig. 1**; **Fig. 9**) indicate comparable sensitivities of both quantum dot types. But several factors can contribute to the observed superiority of the commercial quantum dots over the custom-made nanocrystals. On the one hand QDots® 800 exhibit a higher initial quantum yield of more than 20 % (compared to 3 to 10 % in case of CdSe used within this work). Additionally a higher stability during the precipitation step was observed, since the post-precipitation intensity was only 5 % below the intensity of the stock solution containing same amounts of QDots®. In addition the conflicts of the polymers' optical properties and the near-infrared emitting QDots® will be certainly different due to different absorption wavelengths.

## 5. Summary and Conclusion

Basically the here investigated preparation of quantum dot loaded nanoparticles using the nanoprecipitation method provided a simple tool for the production of monodisperse fluorescently labelled nanoparticles, with high encapsulation efficiencies and only limited impact of the load on the resulting particle sizes. However, the finally achieved fluorescence intensities of the resulting polymeric nanoparticles actually would be insufficient for an application of the prepared particles for most imaging purposes.

The investigation of the encapsulation process allowed the identification of main impact factors, which are essential for further optimization of this labelling procedure. Since the overall achieved high encapsulation efficiencies of quantum dots confirm the assumption of an effective fluorescence label, only the complex interference of the used quantum dots with the used solvents and polymeric matrices, together with the particle formation steps, can be made responsible for the poor optical properties of the final products. Namely three critical process steps have been identified, whereas the biggest impact was found during initial evaporation phase, predominantly due to the interaction of the quantum dot coating with the non-solvent ethanol. Nevertheless, based on the current results, nanoprecipitation can still be considered a promising method for the preparation of monodisperse quantum dot loaded polymeric nanoparticles. Application of quantum dot batches with initially higher optical quality would be a first step towards an improved fluorescence.

However, keeping in mind the numerous impact factors and the limited stability of most of these nanocrystals, optimization of the system will still be a very empirical process, to find the ideal combination of QDs surface modification, matrix material and solvent system used for the precipitation.

## 6. References

- [1] Resch-Genger, U. et al.: "Quantum dots versus organic dyes as fluorescent labels", ***Nature Methods*** 5 (2008) pp. 763-775.
- [2] Klimov, V. "Semiconductor and metal nanocrystals - Synthesis and electronic and optical properties"; Marcel Dekker Inc., New York, 2004.
- [3] Hoshino, A. et al.: "Physicochemical Properties and Cellular Toxicity of Nanocrystal Quantum Dots Depend on Their Surface Modification", ***Nano Letters*** 4 (2004) pp. 2163-2169.
- [4] Tan, W.B. et al.: "Surface modification of gold and quantum dot nanoparticles with chitosan for bioapplications", ***Journal of Biomedical Materials Research, Part A*** 75A (2005) pp. 56-62.
- [5] Cai, W. et al.: "Peptide-Labeled Near-Infrared Quantum Dots for Imaging Tumor Vasculature in Living Subjects", ***Nano Letters*** 6 (2006) pp. 669-676.
- [6] Lee, Y.D. et al.: "Encapsulation of CdSe/ZnS Quantum Dots in Poly(ethylene glycol)-Poly(D,L-lactide) Micell for Biomedical Imaging and Detection", ***Macromolecular research*** 15 (2007) pp. 330-336.
- [7] Schroeder, J.E. et al.: "Folate-mediated tumor cell uptake of quantum dots entrapped in lipid nanoparticles", ***Journal of Controlled Release*** 124 (2007) pp. 28-34.
- [8] Stroh, M. et al.: "Quantum dots spectrally distinguish multiple species within the tumor milieu in vivo", ***Nature Medicine*** 11 (2005) pp. 678-682.
- [9] Cao, X. et al.: "Fabrication of Strongly Fluorescent Quantum Dot-Polymer Composite in Aqueous Solution", ***Chemistry of Materials*** 19 (2007) pp. 3773-3779.
- [10] Pan, J. et al.: "Targeting and imaging cancer cells by Folate-decorated, quantum dots (QDs)- loaded nanoparticles of biodegradable polymers", ***Biomaterials*** 30 (2009) pp. 1176-1183.
- [11] Chen, Y. et al.: "Synthesis of Glyconanospheres Containing Luminescent CdSe-ZnS Quantum Dots", ***Nano Letters*** 3 (2003) pp. 581-584.
- [12] Bruchez, M.P.: "Turning all the lights on: quantum dots in cellular assays", ***Current Opinion in Chemical Biology*** 9 (2005) pp. 533-537.
- [13] Gao, X. et al.: "In vivo cancer targeting and imaging with semiconductor quantum dots", ***Nature Biotechnology*** 22 (2004) pp. 969-976.
- [14] Gao, X. et al.: "In vivo molecular and cellular imaging with quantum dots", ***Current Opinion in Biotechnology*** 16 (2005) pp. 63-72.
- [15] Derfus, A.M. et al.: "Intracellular Delivery of Quantum Dots for Live Cell Labeling and Organelle Tracking", ***SO: Advanced Materials*** 16 (2004) pp. 961-966.
- [16] Medintz, I.L. et al.: "Quantum dot bioconjugates for imaging, labelling and sensing", ***Nature Materials*** 4 (2005) pp. 435-446.
- [17] Yin, W. et al.: "Fluorescent Quantum Dot-Polymer Nanocomposite Particles by Emulsification/Solvent Evaporation", ***Chemistry of Materials*** 19 (2007) pp. 2930-2936.
- [18] Fessi, H. et al.: "Nanocapsule formation by interfacial polymer deposition following solvent displacement", ***International Journal of Pharmaceutics*** 55 (1989) pp. R1-R4.

- [19] Wuister, S.F. et al.: "Temperature anti-quenching of luminescence of capped CdSe quantum dots", **Angewandte Chemie, International Edition** 43 (2004) pp. 3029-3033.
- [20] Kalyuzhny, G. et al.: "Ligand Effects on Optical Properties of CdSe Nanocrystals", **The Journal of Physical Chemistry B** 109 (2005) pp. 7012-7021.
- [21] Bullen, C. et al.: "The Effects of Chemisorption on the Luminescence of CdSe Quantum Dots", **Langmuir** 22 (2006) pp. 3007-3013.
- [22] Meulenberg, R.W. et al.: "Effects of Alkylamine Chain Length on the Thermal Behavior of CdSe Quantum Dot Glassy Films", **The Journal of Physical Chemistry B** 106 (2002) pp. 7774-7780.
- [23] Ballou, B. et al.: "Noninvasive Imaging of Quantum Dots in Mice", **Bioconjugate Chemistry** 15 (2004) pp. 79-86.
- [24] Peracchia, M.T. et al.: "PEG-coated nanospheres from amphiphilic diblock and multiblock copolymers: Investigation of their drug encapsulation and release characteristics", **Journal of Controlled Release** 46 (1997) pp. 223-231.
- [25] Munro, A.M. et al.: "Quantitative Study of the Effects of Surface Ligand Concentration on CdSe Nanocrystal Photoluminescence", **The Journal of Physical Chemistry C** 111 (2007) pp. 6220-6227.



# **Chapter 6**

**Quantum Dots as fluorescent marker  
for microparticulate drug delivery  
systems**



## 1. Introduction

Fluorescence imaging is a frequently used and well-established method to gain insight in the preparation and application of larger as well as smaller particulate drug delivery systems [DDS] (e.g. implants, micro- and nanoparticles) and thereby increase the knowledge of these systems with respect to their formation and fate at the application site, allowing further development and optimization. Compared to other imaging methods based for example on radioactivity [1; 2], radiocontrast [3] or magnetic properties [4; 5] fluorescence imaging enables a detection with relatively low technical effort and costs both *in-vitro* and *in-vivo*. Despite these advantages, the introduction of a fluorescent probe in the delivery system is essential to allow its detection and consequently the choice of an appropriate label strongly depends on the intended investigation. Labelling can commonly be achieved either by incorporation of small molecular weight organic fluorescence dyes, eventually also the fluorescently labelled drug molecule of interest, or by fluorescent modification of the used matrix material forming the particles. In the most studies labelling of a small molecules is preferred, since the interest is focused on the fate of the incorporated drug substance, investigation of the distribution within the particle [6; 7] and its behaviour during the release or the degradation of the carrier [8; 9]. In contrast, imaging of a whole system is useful either for the investigation of the composition and fabrication of so-called hybrid DDS, containing for example microparticles embedded in other carriers [10], or for the tracking of particles paths or drug release *in-vitro* or *in-vivo* [11; 12]. While the investigation of small molecular weight labels is characterized by a continuous loss of the marker substance in case of their release or particle degradation [13; 14], chemical and especially photochemical stability is by far the biggest hurdle for all applications, where a long term tracking of particles is intended. Possible strategies to fulfil these requirements could be a particle loading with increased amounts of the fluorophor or only slowly released fluorescent dyes. Alternatively, only the covalent attachment of the fluorophor to the matrix can yield a stable particle fluorescence, which just depends on the degradability of the matrix material [7; 15]. However, all these approaches struggle with the limited photostability of common organic fluorophores [16; 17] and moreover, an extended loading or chemical alteration of the polymer structure could result in altered properties of the produced particles, probably hindering a transfer of the results to the investigated drug delivery system.

With all these prerequisites for an ideal labelling procedure, quantum dots are an attractive alternative towards a more permanent labelling of drug delivery systems. Besides their well-known optical properties, including the tuneable emission wavelength and their high photostability, these inorganic fluorescent nanocrystals are expected to stay within the surrounding particle matrix as they are dispersed as solid crystals and very

unlikely to be degraded, dissolved or eluted, which would be essential for long-term imaging [17-19]. Introduced as fluorescence labels more than 10 years ago [20; 21], numerous works have been performed using them as probes in biomedical imaging [20; 22; 23]. Surprisingly no reports are available about substituting common organic fluorophores during the development and investigation of new drug delivery systems. Various micro-scaled systems, containing quantum dots either in polystyrene or polylysine matrices, have been described in literature. However, their intended application was generally limited to bioassays or sensorics [24-28].

Therefore quantum dots were investigated as promising candidates to label microparticles, which could be either intended for parenteral use or also further processing in hybrid DDS. In combination with well-established degradable matrix materials and commonly applied encapsulation methods the microparticles should deal as satisfying models also for drug loaded derivatives possibly allowing a transfer of the obtained results to the later drug delivery application. In the here presented work lipophilic CdSe quantum dots containing microparticles have been prepared by loading lipophilic and amphiphilic matrix materials using a lab-scale emulsion based encapsulation method. Main interest was focused on the establishment of the microparticulate system, identification of potential impact factors and an evaluation of the applicability of the prepared labelled particles.

## 2. Materials and Methods

### 2.1 Materials

#### 2.1.1 Preparation and characterization of microparticles

PLGA 75:25 (Resomer<sup>®</sup> 756) was a kind gift of Boehringer Ingelheim (Boehringer Ingelheim AG, Biberach, Germany). The biodegradable diblock copolymer, PEG<sub>2</sub>PLA<sub>40</sub>, was custom made following an established method described in **chapter 2**. Glycerol tripalmitate (Dynasan 116) was obtained from Sasol (Sasol Germany GmbH, Witten, Germany). Oligo(poly(ethylene glycol)fumarate [OPF] 6K was custom made in the Department of Pharmaceutical Technology by Matthias Henke following an adapted method previously described by Jo et al. [29]. Uncoated and oleylamine-coated [OA-coated] CdSe quantum dots were synthesized as described in **chapter 4**. Nile red (nile blue A oxazone), oxazine 170 perchlorate [oxazine], fluorescein, poly(vinylalcohol) [PVA] (Mowiol 40-88), Pluronic F68, Igepal<sup>®</sup> CA-630 (Octylphenyl-poly(ethylene glycol)), N,N,N',N'-Tetramethylethylenediamine [TEMED] and ammonium persulfate [APS] were purchased from Sigma-Aldrich (Sigma-Aldrich Chemie GmbH, Taufkirchen, Germany). 1,2-dipalmitoyl-sn-glycero-3-phosphocholine (Lipoid<sup>®</sup> PC 16:0/16:0) was obtained from Lipoid (Lipoid GmbH, Ludwigshafen, Germany). Methylene chloride (p.a.) [CH<sub>2</sub>Cl<sub>2</sub>] and chloroform [CHCl<sub>3</sub>] were obtained from Acros (Acros Organics, Fischer scientific GmbH, Nidderau, Germany). Ethanol (p.a.), methanol (p.a.), isopropanol (p.a.) and nitric acid (65 %) [HNO<sub>3</sub>] were provided from Merck (Merck KGaA, Darmstadt, Germany).

#### 2.1.2 Cell culture

The L929 mouse fibroblast cell line was a kind gift of the Department of Pharmaceutical Chemistry, University of Regensburg. Fetal bovine serum [FBS] was purchased from Biochrom (Biochrom KG, Berlin, Germany). Trypsin-EDTA 0.25 % and Dulbecco's phosphate buffered saline [PBS] were obtained from Invitrogen (Invitrogen GmbH, Karlsruhe, Germany). 3-[4,5-Dimethylthiazol-2-yl]-2,5-diphenyltetrazolium bromide [MTT] was purchased from AppliChem (AppliChem GmbH, Darmstadt, Germany). Eagle's minimum essential medium [EMEM], was obtained from Sigma-Aldrich (Sigma-Aldrich Chemie GmbH, Taufkirchen, Germany). Triton-X (p.a.) was obtained from Merck (Merck KGaA, Darmstadt, Germany).

## **2.2 Methods**

### **2.2.1 Preparation and characterization of CdSe Quantum Dot stock dispersion**

Prior to encapsulation raw dispersions of the custom-made CdSe quantum dots were purified following a procedure established in **chapter 4**. Briefly an aliquot, usually 1 to 2 ml of the dispersion were mixed with a 30-fold excess of a mixture of ethanol and hexane (5:1), followed by centrifugation (10,000 g, 30 min, 10 °C; Avanti JE centrifuge; Beckman Coulter GmbH, Krefeld, Germany), discarding of the supernatant and subsequent re-dispersion of the sediment in CH<sub>2</sub>Cl<sub>2</sub>.

Photoluminescence [PL] properties and molar concentrations of nanocrystals were determined following methods described in **chapter 4 (2.2.4 & 2.2.5)**.

### **2.2.2 Standard preparation of polymeric microparticles**

Polymeric microparticles generally were prepared following an established emulsion based solvent evaporation method [30]. If not otherwise stated following standard procedure was used for encapsulation of lipophilic quantum dots dispersed in methylene chloride. 200 mg of the polymer (PLGA or Peg<sub>2</sub>PLA<sub>40</sub>) were dissolved in methylene chloride. After addition of an aliquot of the marker containing solution the final volume of the organic phase was adjusted to 4 ml (concentration of polymer in solution was 5 %). 8 ml of an aqueous solution containing 0.5 % PVA were added and thereafter the mixture was homogenized via vortexing at maximum speed for either 10 s in the case of PLGA or 30 s in the case of the copolymer. Subsequently, the as prepared primary emulsion was poured into 100 ml of an aqueous solution containing 0.1 % PVA and the organic solvent was allowed to evaporate over night under permanent stirring at 550 rpm.

Plain microparticles were prepared in the same way, but without addition of the quantum dot dispersion.

For particle recovery the microparticle dispersions were centrifuged (5,000 g, 15 min, 10 °C), the supernatant was discarded and the particles were washed three times with a solution containing 0.1 % of Pluronic F68 in order to prevent their aggregation. Afterwards the particles were freeze-dried using a lab-scale freeze-dryer (Martin Christ Gefriertrocknungsanlagen GmbH, Osterode am Harz, Germany) and dried particles were stored under vacuum or at -20 °C until further application.

### **2.2.3 Standard preparation of lipid microparticles**

The preparation of lipid microparticles followed an adapted melt dispersion method [31]. In a 50 ml round-bottom flask 500 mg of the triglyceride (Dynasan® 116) were dissolved in chloroform. In case of the quantum dot loaded particles the organic quantum dot dispersion was added, otherwise pure chloroform was added as control. Under reduced pressure the organic solvent was removed at 60 °C followed by complete melting of the left lipid or lipid/QD mixture at 70 °C. A pre-heated solution containing 0.1 % phosphatidylcholine (PC 16/16) in 70 % ethanol was added. Afterwards the mixture was homogenized via shaking and poured, under agitation, into 100 ml of ice-cooled water, for immediate hardening of the particles. Particles were collected by filtration, washed three times with water and subsequently dried under vacuum over night.

### **2.2.4 Particle size determination**

Particle size distributions of the polymeric particles were determined based on laser diffraction using a Mastersizer 2000 equipped with the Hydro 2000 $\mu$  dispersion unit (both Malvern Instruments, Herrenberg, Germany). Measurements were done in water containing Igepal® CA-630 as non-foaming surfactant under mild agitation at 300 rpm. Results are given as d10, d50 and d90 values describing the size distributions. All data were expressed as mean of quadruplicate measurements.

Scanning electron microscopic images (2.2.5) were used to determine the mean diameter of the lipid particles. Size was determined by manual measuring the diameter of 100 particles. Results are presented as mean and relative standard deviation.

### **2.2.5 Imaging of particles surface morphology**

Scanning electron microscopy [SEM] was used for imaging of microparticles' surface morphology. Prior to the investigation the original material was mounted on aluminium stubs and sputtered with a thin gold film (4 x 20 s). Images were obtained using a JSM 840 scanning electron microscope (Jeol GmbH, Echting, Germany) with 3 kV operating voltage.

### **2.2.6 Determination of loading with Quantum Dots**

Inductively coupled plasma optical emission spectrophotometry [ICP-OES] was used to determine the elemental concentrations of the quantum dot components Cd and Se. Sample preparation differed between polymeric and lipid microparticles. An aliquot, usually about 100 mg, of the lyophilisate of quantum dot containing polymeric

microparticles was degraded under increased temperatures in 2 ml, ethanol containing HNO<sub>3</sub> (65 %) over 12 h. In the case of the lipid microparticles the particles were melted prior to the addition of HNO<sub>3</sub> and ethanol. At least three melting and concealing cycles were performed to ensure quantitative isolation and disintegration of the quantum dots. Thereafter the remaining lipid phase was removed via filtration.

50 to 100 µl of the organic quantum dot dispersion used in the respective experiment deal as reference for the determination of the initial amounts of Cd and Se. After drying at room temperature under atmospheric pressure nanocrystals were oxidatively disintegrated. Subsequently all samples were diluted up to 10 ml in a volumetric flask. The final concentration of HNO<sub>3</sub> was about 2 to 3 %. Plain particles served as negative control.

The standard solutions, prepared of cadmium chloride and selenium, contained 100 ppm, 10 ppm and 1 ppm of Cd and Se in 2 to 3 % nitric acid. Measurements were performed using a Jobin Yvon 70 Plus (S+S) ICP-OE spectrophotometer (Horiba, Jobin Yvon, France) in the sequential analysis mode. Instrumental settings and element characteristics are given in **chapter 4 (2.2.7)**.

The CdSe loading of the microparticles was calculated based on the following equations:

$$Loading / \% = \frac{100 * C(Se)_{real}}{C(Se)_{initial}} ; \quad (1)$$

$$C(Se)_{real} = \frac{M(Se)_{ICP-Sample}}{m_{ICP-Sample}} ; \quad (2)$$

$$C(Se)_{initial} = \frac{M(Se)_{QD-Reference} * f_{QD-Reference}}{m_{Polymer}} ; \quad (3)$$

with the real concentration of Se in the microparticles  $C(Se)_{real}$  [nmol/mg], the molar amount of Se in degraded particles measured via ICP-OES  $M(Se)_{ICP-Sample}$  [nmol], the weight of the particles used for the preparation of the ICP sample  $m_{ICP-Sample}$  [mg], the theoretically required concentration of Se in the microparticles given at 100 % encapsulation  $C(Se)_{Initial}$  [nmol/mg], the molar amount of Se in the QD-reference measured with ICP-OES  $M(Se)_{QD-Reference}$  [nmol], the multiple of the volume of the QD-reference used for encapsulation  $f_{QD-Reference}$  and the initial weight of polymer used for particle preparation  $m_{Polymer}$  [mg].



### 2.2.7 Confocal imaging of Quantum Dot loaded microparticles

Spatial distribution of fluorescence within the polymeric and lipid microparticles loaded with quantum dots was determined by confocal laser scanning microscopy using a Zeiss Axiovert 200 M microscope coupled to a Zeiss LSM 510 scanning device (Carl Zeiss Co. Ltd., Germany). The inverted microscope was equipped with a C-Apochromat 40x and a Plan-Apochromate 63x objective. Particles were excited at 488 nm using an argon laser and fluorescence was detected using a long pass 560 nm filter. Unloaded microparticles served as negative control at same conditions and were used for determination of the auto fluorescence of the matrix materials.

### 2.2.8 Fluorescence spectroscopic analyses

The fluorescence properties were determined with respect to the fluorescence intensity and the maximum emission wavelength ( $\lambda_e$ ). Microparticles were investigated in solid state using a custom made sample holder (**Fig. 1**) and after dissolving an aliquot of the particles (either 25 or 50 mg in 1 ml  $\text{CHCl}_3$ ) using quartz glass cuvettes (1 cm path length).

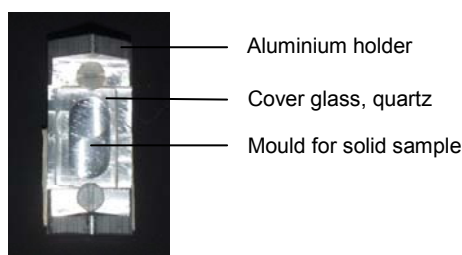


**Fig. 1:** Sample holder for fluorescence measurements of solid state samples

All experiments were performed with a LS 55 spectrophotometer (PerkinElmer, Waltham, USA) equipped with the FL WinLab V4.00.03 software. After excitation with 488 nm fluorescence spectra were recorded over the range of 500 to 700 nm, with a photomultiplier voltage of either 775 or 900 V.

### 2.2.9 Microparticles embedded in polymeric hydrogels

The OPF 6k hydrogels were prepared via thermally induced free radical polymerization using TEMED and APS as initiator system. Quantum dot loaded microparticles were embedded prior to cross-linking by addition of the dry particles and subsequent stirring avoiding the incorporation of additional air bubbles.

Spatial distribution of the microparticles within the hydrogels was imaged with z-stacks obtained with CLSM using a Zeiss Axiovert 200 M microscope, equipped with a Plan-

Neofluar 10x and a Plan-Apochromate 40x objective, coupled to a Zeiss LSM 510 scanning device (Carl Zeiss Co. Ltd., Germany). Samples were excited at 488 nm using an argon laser and fluorescence was detected using a long pass 560 nm filter.

#### **2.2.10 Cell culture**

The L929 cell line was cultured in EMEM medium supplemented with 10 % FBS at standard cell culture conditions (37 °C; 95 % relative humidity and 5 % CO<sub>2</sub>). Growth medium was changed every third day.

#### **2.2.11 Biocompatibility of polymeric microparticles**

Investigation of biocompatibility of the prepared particulate systems followed a procedure adapted from ISO 10993/EN 30993 [32] using the colorimetric MTT assay for quantitative assessment. Microparticles were investigated using an extraction procedure [33]. In brief, 100 mg of each microparticle batch were incubated in 10 ml medium (without FBS) for 24 h at 37°C. After removing the solid particles 10 % FBS were added and the stock extracts were diluted serially with medium (+ 10 % FBS) prior to addition to the cells. General parameters of the assay in detail have been given in **chapter 2**. However, in case of the microparticles incubation of cells with test extracts took 24 h.

All data were expressed as mean (N=4) and relative standard deviation. Statistic significance was assessed by one-way analysis of variances (ANOVA) in conjunction with Tukey's studentized range test using SigmaStat software.

### 3. Results

#### 3.1 Tailoring the particle size

The easy controllable preparation step of the primary emulsion was investigated with respect to its effect on the resulting particle size distributions, which was also found to strongly depend on the used polymer type (**Tab. 1**).

**Tab. 1:** Summary of characteristics of particle size distributions of PLGA and PEG<sub>2</sub>PLA<sub>40</sub> microparticles depending on the pre-emulsification step

	PLGA microparticles			PEG <sub>2</sub> PLA <sub>40</sub> microparticles		
Pre-emulsion	d10 / $\mu\text{m}$	d50 / $\mu\text{m}$	d90 / $\mu\text{m}$	d10 / $\mu\text{m}$	d50 / $\mu\text{m}$	d90 / $\mu\text{m}$
Vortex 5 s	29.04	58.60	119.12	41.58	150.18	506.77
Vortex 10 s	24.82	42.39	67.42	30.48	82.13	351.12
Vortex 30 s	18.03	34.82	70.12	11.37	28.13	53.75
Vortex 60 s	17.31	33.43	75.65	10.61	32.135	66.90
Vortex 90 s	17.81	34.81	76.23	9.17	32.8	73.11
Vortex 120 s	16.68	31.94	53.90	13.35	49.30	95.30
Ultrasonic 10 s	1.44	4.53	24.51	4.40	27.00	283.30
Ultrasonic 30 s	1.43	2.23	97.11	8.34	28.45	226.13
Ultrasonic 60 s	1.27	2.64	83.95	4.06	16.32	117.06
Ultrasonic 90 s	1.37	3.24	83.95	3.77	10.46	118.42

Overall, changing the emulsification method (vortexing or sonication) showed the strongest impact on mean particle size in contrast to alterations of the treatment times. Comparing the results obtained with different agitation forces of the Vortex and the ultrasound treatment indicate that longer treatment times generally only led to a narrowing of size distribution for the particles without further significant reduction of the particle size. Additionally, the observed effects are only limited to a certain size range and no submicron particles were obtained, regardless of the applied emulsification time.

The effects of similarly altered process parameters in case of lipid based microparticles was not investigated due to the hardly controllable time and especially strength of the shaking process in the round bottom flask. However, following the described standard preparation procedure a mean particle size was found of about 124  $\mu\text{m}$  ( $\pm 16 \mu\text{m}$ ) as determined from SEM investigations.

### 3.2 Determination of encapsulation efficiency

Encapsulation efficiency of the CdSe quantum dots generally was found to be very high (all above 75 %), indicated by the microparticles' Se content as determined by ICP-OES (**Tab. 2**). In case of OA-coated quantum dots efficiency seems to slightly decrease with increasing initial loading independent of the used matrix material.

**Tab. 2:** Encapsulation efficiencies of microparticles loaded either with uncoated or OA-coated Quantum Dots

	uncoated CdSe			Oleylamine-coated CdSe		
	1 nmol/200mg	5 nmol/200mg	10 nmol/200mg	1 nmol/200 mg	5 nmol/200mg	10 nmol/200mg
PLGA	105.74 %	106.92 %	101.92 %	105.93 %	87.65 %	74.93 %
PEG <sub>2</sub> PLA <sub>40</sub>	118.10 %	117.03 %	107.52 %	108.25 %	99.39 %	82.33 %
Triglyceride	104.77 %	105.00 %	122.00 %	107.99 %	98.56 %	95.06 %

### 3.3 Optical properties of Quantum Dot loaded microparticles

Optical properties of quantum dot loaded particles were determined both in solid state and after dissolving of the particles in chloroform, and the evaluation was done with respect to the impact of quantum dots surface modification (either uncoated or OA-coated) and the initial loading.

Fluorescence spectra of the microparticles loaded with uncoated CdSe quantum dots (**Fig. 5**) were slightly broadened when measured in solid state, with highest impact of the matrix material PEG<sub>2</sub>PLA<sub>40</sub>. However, the effect of the matrix state (solid or dissolved) on the maximum emission wavelength was almost negligible.

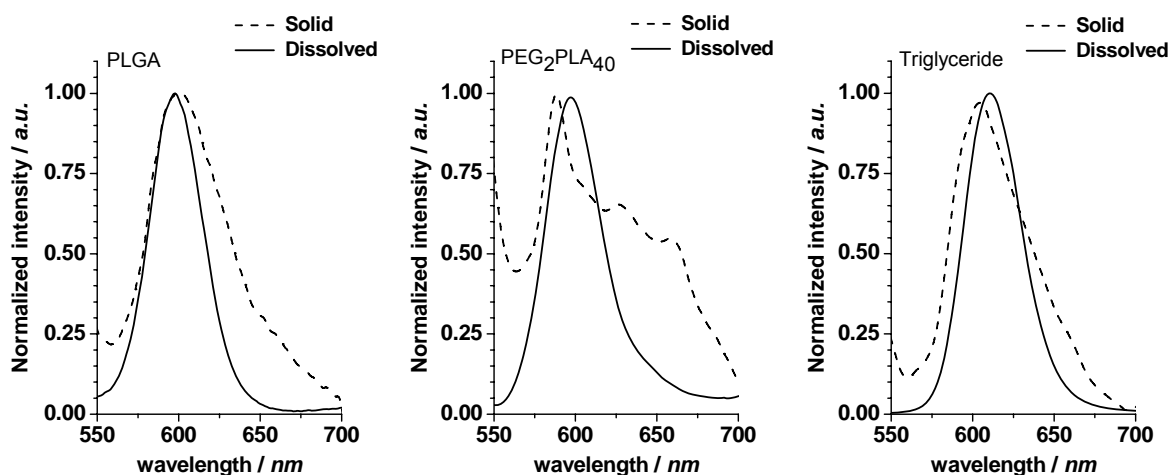


**Fig. 5:** Normalized fluorescence spectra of microparticles prepared of PLGA, PEG<sub>2</sub>PLA<sub>40</sub> and glycerol tripalmitate, loaded with uncoated quantum dots; each measured both in solid state and after dissolving in CHCl<sub>3</sub>

After encapsulation of quantum dots with an initial quantum yield of 6 %, the solid matrix was found to lead to a pronounced loss in fluorescence intensity for all three types but with the highest impact for the lipid particles (**Fig. 6, left**). Indeed, despite the higher fluorescence quenching of the solid triglyceride, indicated by the measured fluorescence increase upon dissolving of the particles (**Fig. 6, left**), solid lipid microparticles were found to exhibit the best fluorescing properties of all matrix materials, followed by PLGA and PEG<sub>2</sub>PLA<sub>40</sub> (**Fig. 6, right**).

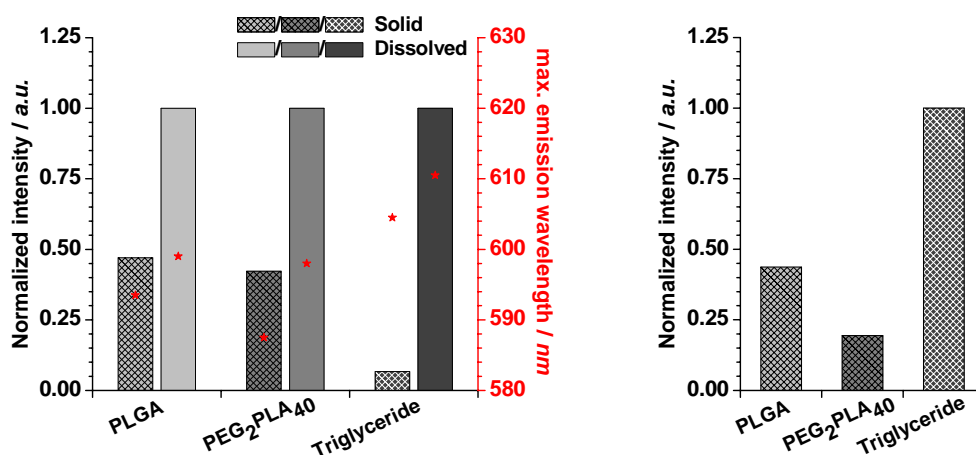


**Fig. 6:** Normalized fluorescence intensities of microparticles loaded with uncoated CdSe quantum dots (initial loading of 6 nmol/200 mg) - (**left**) comparison of maximum fluorescence intensity in solid state and after dissolving same particle amounts in CHCl<sub>3</sub>, each material normalized on its maximum intensity; (**right**) comparison of maximum fluorescence intensities of solid particles measured; normalized on maximum intensity of all materials

Both, the effect of increasing initial loading of CdSe quantum dots and of modified quantum dots, were found to differ depending on the used matrix material (**Fig. 7**). In case of the polymeric particles increasing amounts of quantum dots generally resulted in improved optical properties (**Fig. 7, left**). In case of PLGA this was only detectable for the dissolved samples since none of the solid particles showed any detectable fluorescence. In contrary the PEG<sub>2</sub>PLA<sub>40</sub> particles, although loaded with quantum dots of very poor initial quality, even a fluorescence of the solid particles could be detected. However, their overall fluorescence was very low, which certainly can be attributed to the bad quality of the here encapsulated quantum dots.

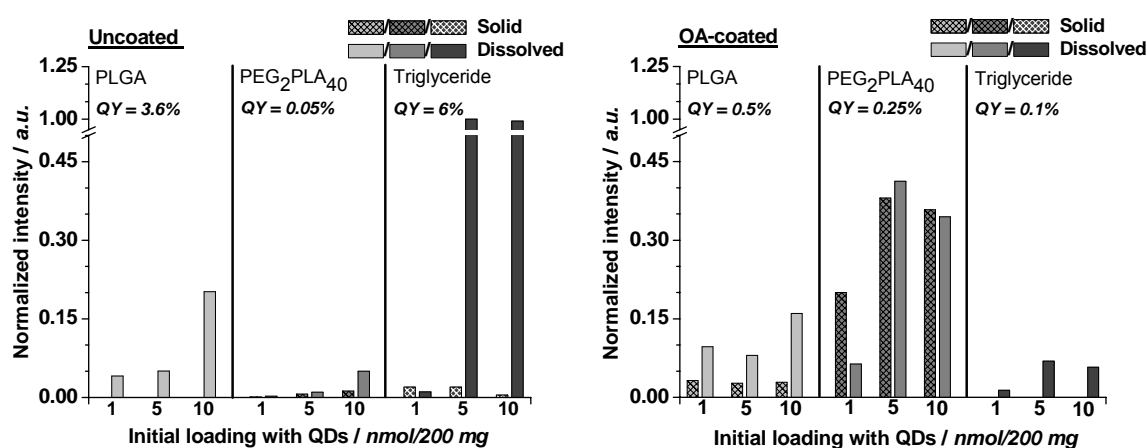


**Fig. 7:** Normalized fluorescence intensities of microparticles prepared of different materials loaded with increasing amounts of either (*left*) uncoated CdSe quantum dots or (*right*) OA-coated quantum dots; all normalized on overall maximum of all materials

Glycerol tripalmitate again showed the highest impact of the solid matrix on the particles' fluorescence intensity and moreover no detectable improvement in quality of the solid particles could be achieved by increasing the loading with quantum dots.

Results obtained with the OA-coated quantum dots indicate dramatically improved fluorescence properties of polymer based microparticles despite the much lower initial quantum yield of the used quantum dots (**Fig. 7, right**). Lowest intensities, however, were obtained in case of the lipid matrix system, which also could not be detected in the solid state. No obvious effect of increasing quantum dot loadings could be determined. Interestingly, the quenching effect of the solid matrix was even levelled in case of PEG<sub>2</sub>PLA<sub>40</sub> microparticles, if loaded with OA-coated quantum dots.

### 3.4 Morphologic characterization of Quantum Dot loaded microparticles

Depending on the used matrix materials, quantum dot loaded microparticles differed significantly in their surface morphology and also in the spatial distribution of the detectable fluorescence, which could act as indicator of varying internal distributions of the nanocrystals in polymeric or lipid particles. In case of the uncoated quantum dots (**Fig. 8, left**) both lipophilic matrices PLGA and glycerol tripalmitate exhibit smooth particle surfaces (**Fig. 8, A+C**) and a homogeneous distribution of fluorescence (**Fig. 8, a+c**) over the whole cross section of the particles. In contrast, the particles prepared of the amphiphilic PEG<sub>2</sub>PLA<sub>40</sub> (**Fig. 8, B+b**) is characterized by a spongy surface morphology and its fluorescence is only restricted to an inner area or core of the particle, which is surrounded by a non-fluorescing corona.

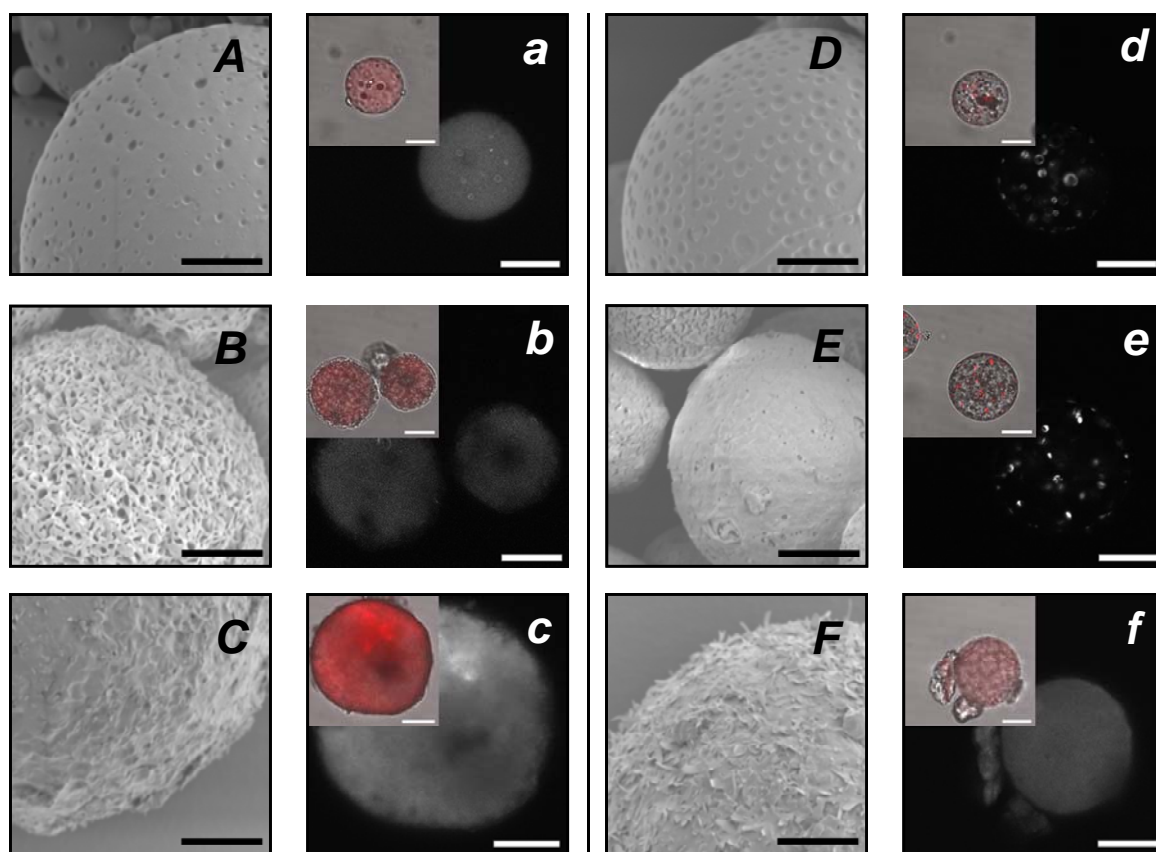


**Fig. 8:** (*left*) Microparticles loaded with uncoated CdSe quantum dots prepared of (**A/a**) PLGA, (**B/b**) PEG<sub>2</sub>PLA<sub>40</sub> and (**C/c**) glycerol tripalmitate; (*right*) microparticles loaded with OA-coated CdSe quantum dots prepared of (**D/d**) PLGA, (**E/e**) PEG<sub>2</sub>PLA<sub>40</sub> and (**F/f**) glycerol tripalmitate; **capital letters:** SEM images; magnification 2,500x, scale bars correspond to 10  $\mu$ m; **lower case letters:** corresponding grey-scale CLSM images, inserts represent coloured overlays of CLSM- and brightfield images; magnification 63x, scale bars correspond to 20  $\mu$ m

After encapsulation of OA-coated quantum dots (**Fig. 8, right**) no changes could be observed in case of the lipid microparticles (**Fig. 8, F/f**). PEG<sub>2</sub>PLA<sub>40</sub> based particles lost their rough surface morphology (**Fig. 8, E**) and in both polymeric matrices fluorescence appears to be restricted to individual, clearly defined small areas randomly distributed over the whole particle (**Fig. 8, d+f**).

### 3.5 Biocompatibility of Quantum Dot loaded microparticles

Biocompatibility of the polymeric microparticles was tested using a standard cell line for the evaluation of biomaterials (L929 mouse fibroblasts). There was no significant toxicity (tested against negative control) of either PLGA or PEG<sub>2</sub>PLA<sub>40</sub> microparticles loaded with uncoated CdSe quantum dots even in case of the highest quantum dot loadings (**Fig. 9**). Measured cell viabilities were generally above 75 % for all investigated dilutions and quantum dot loadings.

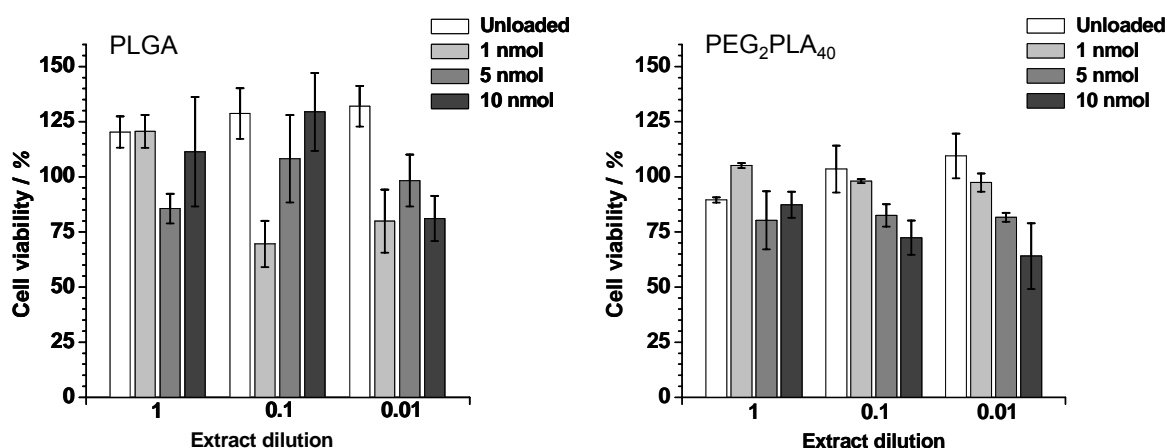


**Fig. 9:** Viability of L929 cells after incubation (24 h) with extracts of microparticles prepared of (**left**) PLGA or (**right**) PEG<sub>2</sub>PLA<sub>40</sub>; both loaded with increasing amounts of uncoated CdSe quantum dots; star indicate significant toxicity compared to the respective negative control ( $p < 0.05$ )

In contrast, the particles loaded with the OA-coated quantum dots showed a significant toxicity (compared to negative control) if loading increased up to 10 nmol/200 mg independent of the used type of polymer (**Fig. 10**). The here obtained viabilities decreased down to about 50 % for the high quantum dot loading.



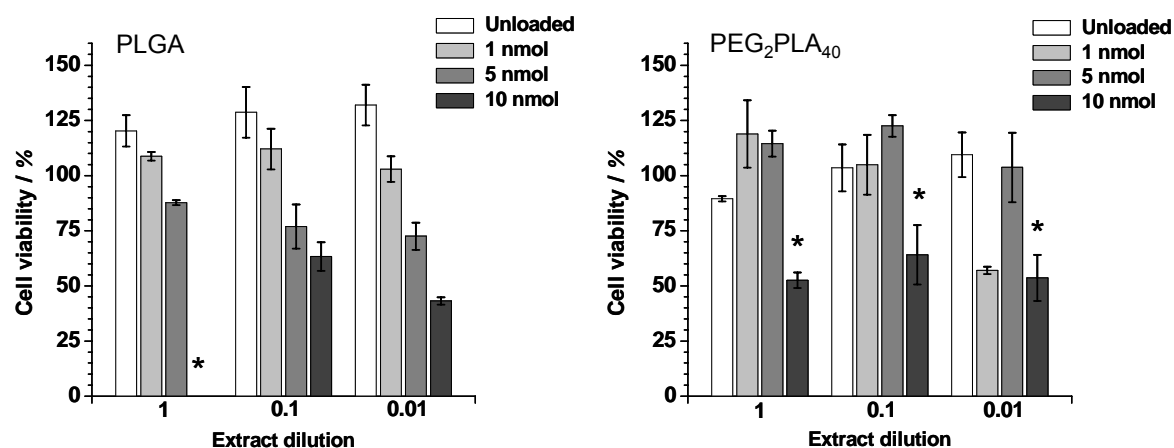


**Fig. 10:** Viability of L929 cells after incubation (24 h) with extracts of microparticles prepared of (*left*) PLGA or (*right*) PEG<sub>2</sub>PLA<sub>40</sub>; both loaded with increasing amounts of OA-coated CdSe quantum dots; star indicate significant toxicity compared to the respective negative control (p<0.05)

## 4. Discussion

Various methods for the preparation of micro-scaled drug delivery systems have been described in literature [34-39], but the solvent evaporation methods are the most frequently used ones for encapsulation of both hydrophilic as well as lipophilic substances [40-43]. Therefore this method was chosen to be appropriate for an easy preparation of polymeric microparticles in the current work. Varying only a single process parameter, namely the preparation of the primary emulsion, allows the adaption of particles size within a certain range (**Tab. 1**). The desired particle sizes, between 50 and 75  $\mu\text{m}$ , could be prepared by emulsification with 10 s vortexing in case of PLGA and respectively 30 s in case of PEG<sub>2</sub>PLA<sub>40</sub>. These standard conditions have been used for production of all further polymeric microparticles. Since the lipid based particle approach has been used primarily for the investigation of the potential impact of the differing processing and matrix material on the optical properties of the obtained particles and since particles were not intended for further applications, no optimization of the originally found particle size was performed.

Quantum dots, which were identified as attractive alternative to label particulate systems, have been successfully encapsulated using a single emulsion method and generally behaved very similar to other lipophilic marker substances, if compared with commonly used organic fluorescence dyes, exemplarily shown for the PEG<sub>2</sub>PLA<sub>40</sub> based particles (**Fig. 11**).

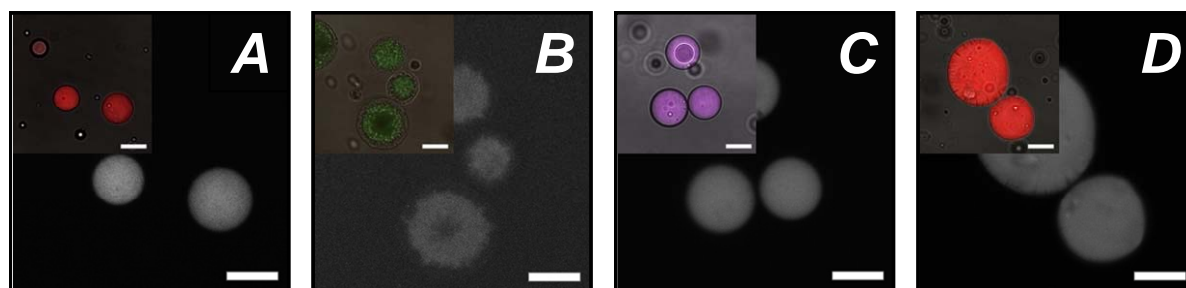


**Fig. 11:** CLSM Images of PEG<sub>2</sub>PLA<sub>40</sub> microparticles loaded with (**A**) uncoated CdSe quantum dots ( $\lambda_{\text{ex}}$ =488 nm/ LP 560 nm), (**B**) fluorescein ( $\lambda_{\text{ex}}$ =488 nm/ BP 530-600 nm), (**C**) oxazine ( $\lambda_{\text{ex}}$ =633 nm/ LP 650 nm) and (**D**) Nile red ( $\lambda_{\text{ex}}$ =488 nm/ LP 650 nm); inserts show overlay of CLSM- and brightfield images, magnification 63x; scale bars correspond to 20  $\mu\text{m}$

Encapsulation of the lipophilic particulate markers always resulted in high encapsulation efficiencies as shown in **table 2**, which is generally reported for lipophilic substances used in the emulsion based microencapsulation [44].

Since quantum dots are known to be very sensitive to different processing steps and it was the goal to reproducibly produce high quality fluorescing microparticles, an

investigation of potential impact factors on the resulting optical properties of the particles was essential. The prepared microparticles were evaluated focusing on the type of used matrix material, the quantum dot loading and the surface properties of the used quantum dots.

Comparison of the finally obtained fluorescence intensities of the particles made from the three materials (**Fig. 6, right**) at the first glance suggests a protective effect of the triglyceride on the quantum dots PL. However, although assuming a higher stability in the lipophilic matrix material, this effect can also result from the slightly differing preparation process of lipid microparticles, where the emulsion was prepared only by manual shaking and not by vortexing at obviously higher frequency. The resulting lower agitation forces in combination with an increased viscosity of the melted pure lipid compared to the organic polymer solutions will lead to reduced shear forces on the quantum dot surfaces and therefore a much lower destruction of the surface coating, which proved to be beneficial for the particles' fluorescence intensity. This positive effect of the triglyceride matrix is somewhat diminished by the materials higher optical density, obviously reducing the amount of penetrating and emitted light. The loss in the overall fluorescence intensity of the particles due to the matrix solidification for lipid matrices was found to be nearly twice as much as in case of both investigated polymer matrices (**Fig. 6, left**).

Improvement of the particles' optical properties was intended by both increasing the initial loading of quantum dots and also by encapsulation of OA-coated quantum dots. Such surface modified quantum dots were found to exhibit improved optical properties and were expected to show enhanced stability during encapsulation. Focusing on the mere fluorescence intensity of the solid particles the impact of the changed quantum dot type clearly exceeds the effect of an increased loading (**Fig. 7**), which is especially surprising, since the used batches of OA-coated quantum dots showed the overall lowest initial QY. The most significant improvement was found for the diblock copolymer, which suggests a contribution of the PEG-part. An interaction of the polymers PEG-blocks with the OA-coated quantum dots could result in a further stabilization of their surface. The change in the microparticle morphology in the SEM (**Fig. 8, B+E**) could deal as an additional proof for this assumption. Following the solvent evaporation and freeze drying, the particles made of PEG containing block polymers are usually characterized by a very spongy structure, which can result from the predominant orientation of the PEG-chains towards the particle surface, due to an increased interaction with the surrounding aqueous environment in the emulsion [45]. Following encapsulation of OA-coated quantum dots, the microparticle surface appeared more or less smooth due to a possible preferential orientation of the PEG chains to the inside of the particles. A consequent internal enrichment of the hydrophilic polymer compound may result in the development of a

porous internal structure, also found for other PEG containing block copolymers [46]. A subsequently resulting decrease in the materials' optical density could furthermore explain the significantly reduced impact of the matrix state (solid or dissolved) on the particles' fluorescence intensity (**Fig. 7**).

In contrast, the effect of OA-coating appeared almost negligible in case of PLGA particles and was found to even impair the optical quality in case of lipid microparticles. No alteration in surface morphology could be observed for both of these lipophilic materials. However, there is a significant alteration of the internal fluorescence distribution using OA-coated quantum dots. Originally the fluorescence is almost homogeneously distributed in the lipophilic core, if particles are loaded with unmodified quantum dots (**Fig. 8, a+b**). For the OA-coated quantum dots the fluorescence, as indicator for the distribution of the nanocrystals, is now restricted to several small areas (**Fig. 8, d+e**), which were found to be comparable to the reports on the encapsulation of hydrophilic drug substances [47]. The distribution of an encapsulated material is usually a result of its interaction with the surrounding polymer matrix, which is especially apparent, when hydrophilic and lipophilic compounds are compared [48]. Although both types of used quantum dots (native and OA-coated) bear a lipophilic capping, these results suggest a reduced interaction of PLA and PLGA with oleylamine, which consequently leads to an accumulation of quantum dots in pores or hollows, instead of a homogeneous distribution within the polymer matrix. A resulting lower shear stress for the crystal surface could additionally account for the also improved optical properties. Due to these obvious differences in the internal distribution of the fluorescence, using the fluorescing area as indicator for the apparent particle size during imaging would only be possible in case of particles loaded with unmodified and consequently well dispersed quantum dots.

However, a final concluding evaluation of the various impact factors on the particles' quality could hardly be done as the fluorescence was also found to regenerate or restore during the extended storage of the particles. After 8 months, the fluorescence intensity of the solid particles again increased more than 900 % for some of the particles (**Fig. 12**), which indicate a still possible "healing" of the damaged quantum dot surfaces.

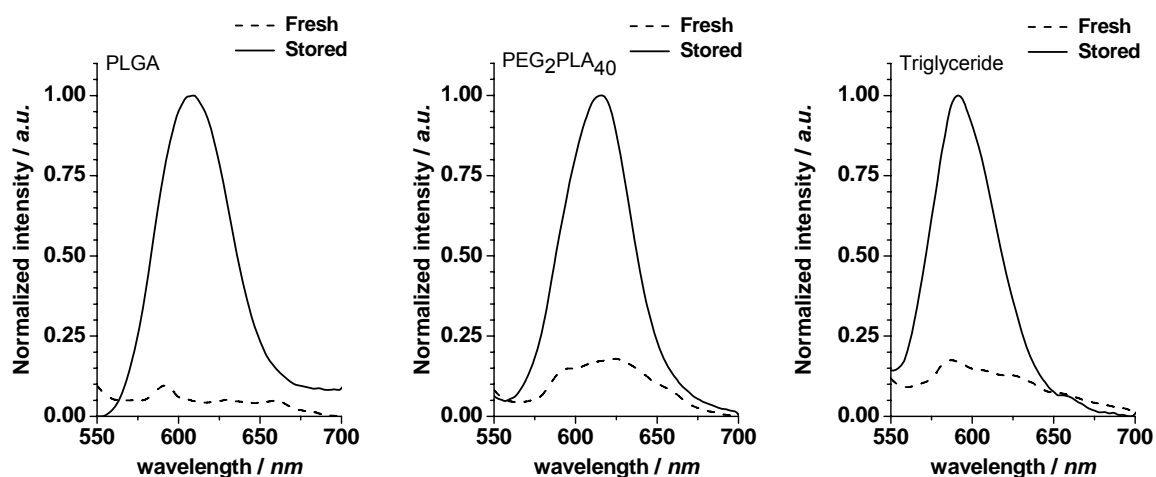


**Fig. 12:** Normalized fluorescence spectra of microparticles prepared of PLGA, PEG<sub>2</sub>PLA<sub>40</sub> and glycerol tripalmitate loaded with OA-coated CdSe quantum dots (initial loading 5 nmol/200 mg) measured in solid state, directly after preparation and after storage for 8 months

Indeed, independent of the used polymer material this regeneration was only observed in case of the particles loaded with OA-coated CdSe quantum dots, suggesting a participation of the primary amine ligand on the surface reconstitution of the nanocrystals. Although exhibiting the best intensities directly after preparation no superiority of the amphiphilic diblock copolymer could be determined after this “healing” period.

Despite the diverse results and an originally only moderate optical quality, the prepared particles of both quantum dots types were successfully applied as fluorescent labels for the investigation of a hybrid drug delivery system. The above discussed differences in internal spatial arrangement of the fluorescing areas were found to be almost irrelevant in case of the imaging at lower magnifications, even using confocal microscopy. Therefore both types of labelled particles are suited for observations in a three-dimensional context. This is exemplarily demonstrated for PLGA microparticles (either loaded with uncoated or OA-coated QDs) embedded in transparent OPF hydrogels (**Fig. 13**). Despite very similar particle sizes and particle loadings the spatial distribution of the microparticles within the hydrogel differed, which already might affect the release characteristics in case of drug loaded delivery systems.

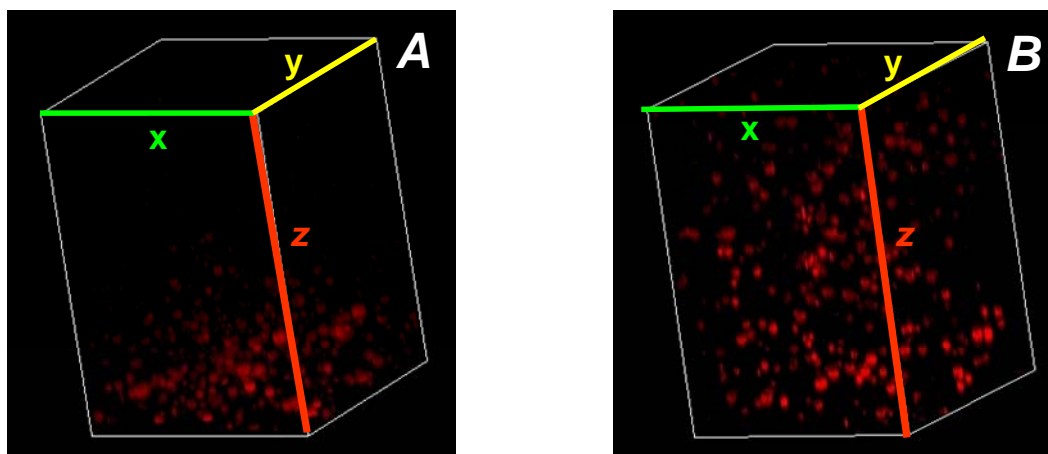


**Fig. 13:** CLSM images (z-stacks) of OPF 6k hydrogels loaded with PLGA microparticles fluorescently labelled with either (**A**) uncoated CdSe quantum dots or (**B**) OA-coated quantum dots; magnification 10x; stack size:  $x=y=824\ \mu\text{m}$ ,  $z=1210\ \mu\text{m}$

The additionally envisioned application of quantum dot labels to track particulate systems in a cellular context or even during *in-vivo* applications requires biocompatibility of the used imaging system, which was tested using a common cell line used for biomaterial testing [32]. Independent of the used polymeric matrix no toxicity was found for particles loaded with uncoated CdSe quantum dots (**Fig. 9**), whereas particles containing increasing amounts of OA-coated quantum dots led to a statistical significant reduction in cell viability (**Fig. 10**). This may be due to a more likely leakage of quantum dots during extraction of microparticles, which could be enhanced due to the porous particle structure or an also possible solubilisation of released oleylamine, possibly acting as cell damaging surfactant. Further studies are necessary here to identify the cause of toxicity and take suitable counteractions.

## 5. Summary and Conclusion

Fluorescence labelling of microparticulate systems using lipophilic quantum dots was successfully established using commonly available particle preparation methods and therefore could serve as an alternative to the commonly used organic fluorescence dyes (e.g. Nile red, Rhodamine dyes). The final characteristics of the obtained labelled particles strongly depend on the initial optical quality of the used quantum dots, but moreover on the interaction of the used matrix material and the quantum dot surface ligands. However, the obtained results could hardly be generalized, keeping in mind the numerous different synthesis routes to produce the fluorescing nanocrystals. As synthesis routes are usually differing in the composition of reaction solvents and added stabilizing ligands, the surface decoration of the prepared or even of different commercially obtained quantum dots will be highly variable. Focusing on one intended application it is therefore essential to choose an appropriate model system and to improve its encapsulation process with respect to the photoluminescence and quantum yield. Especially if the quantum dots should be used as model compounds for crystalline drug substances, which are similarly only dispersed within the microparticles, a careful adaption of their surface characteristics would be required to allow transferring the obtained results on their behaviour during encapsulation and particle degradation on the later applied drug substances.

Besides the already presented investigations on hybrid drug delivery systems, the prepared microparticles could also be used as differently sized probes to investigate the macroporosity and interconnectivity of pores, which are of special interest in hydrogel foams or solid scaffolds applied in tissue engineering applications.

## 6. References

- [1] Gupta, R.K. et al.: "In vivo distribution of radioactivity in mice after injection of biodegradable polymer microspheres containing <sup>14</sup>C-labeled tetanus toxoid", **Vaccine** 14 (1996) pp. 1412-1416.
- [2] Kissler, S. et al.: "Uterine contractility and directed sperm transport assessed by hysterosalpingoscintigraphy (HSSG) and intrauterine pressure (IUP) measurement", **Acta Obstetrica et Gynecologica Scandinavica** 83 (2004) pp. 369-374.
- [3] Leander, P.: "A New Liposomal Contrast Medium for CT of the Liver", **Acta Radiologica** 37 (1996) pp. 63-68.
- [4] Chen, H.H. et al.: "MR imaging of biodegradable polymeric microparticles: A potential method of monitoring local drug delivery", **SO: Magnetic Resonance in Medicine** 53 (2005) pp. 614-620.
- [5] Brunner, A. et al.: "pH and Osmotic Pressure Inside Biodegradable Microspheres During Erosion", **Pharmaceutical Research** 16 (1999) pp. 847-853.
- [6] Yang, Y.Y. et al.: "Morphology, drug distribution, and in vitro release profiles of biodegradable polymeric microspheres containing protein fabricated by double-emulsion solvent extraction/evaporation method", **Biomaterials** 22 (2001) pp. 231-241.
- [7] Lamprecht, A. et al.: "Structural analysis of microparticles by confocal laser scanning microscopy", **AAPS PharmSciTech** 1 (2000) pp. 10-19.
- [8] Li, L. et al.: "Mapping neutral microclimate pH in PLGA microspheres", **Journal of Controlled Release** 101 (2005) pp. 163-173.
- [9] Kang, J. et al.: "Pore Closing and Opening in Biodegradable Polymers and Their Effect on the Controlled Release of Proteins", **Molecular Pharmaceutics** 4 (2007) pp. 104-118.
- [10] Brannon-Peppas, L.: "Recent advances on the use of biodegradable microparticles and nanoparticles in controlled drug delivery", **International Journal of Pharmaceutics** 116 (1995) pp. 1-9.
- [11] Doiron, A. et al.: "Poly(Lactic-co-Glycolic) Acid as a Carrier for Imaging Contrast Agents", **Pharmaceutical Research** 26 (2009) pp. 674-682.
- [12] Delie, F.: "Evaluation of nano- and microparticle uptake by the gastrointestinal tract", **Advanced Drug Delivery Reviews** 34 (1998) pp. 221-233.
- [13] Suh, H. et al.: "Cellular Uptake Study of Biodegradable Nanoparticles in Vascular Smooth Muscle Cells", **Pharmaceutical Research** 15 (1998) pp. 1495-1498.
- [14] Pietzonka, P. et al.: "Transfer of Lipophilic Markers from PLGA and Polystyrene Nanoparticles to Caco-2 Monolayers Mimics Particle Uptake", **Pharmaceutical Research** 19 (2002) pp. 595-601.
- [15] Hu, Y. et al.: "Controlled Release from Coated Polymer Microparticles Embedded in Tissue-engineered Scaffolds", **Journal of Drug Targeting** 9 (2001) pp. 431-438.
- [16] Molecular Probes: "The Handbook - A Guide to fluorescent probes and labeling technologies",
- [17] Jaiswal, J.K. et al.: "Potentials and pitfalls of fluorescent quantum dots for biological imaging", **Trends in Cell Biology** 14 (2004) pp. 497-504.



- 
- [18] Jaiswal, J.K. et al.: "Long-term multiple color imaging of live cells using quantum dot bioconjugates", **Nature Biotechnology** 21 (2003) pp. 47-51.
- [19] Ballou, B. et al.: "Noninvasive Imaging of Quantum Dots in Mice", **Bioconjugate Chemistry** 15 (2004) pp. 79-86.
- [20] Bruchez, M.J. et al.: "Semiconductor Nanocrystals as Fluorescent Biological Labels", **Science** 281 (1998) pp. 2013-2016.
- [21] Chan, W.C. et al.: "Quantum Dot Bioconjugates for Ultrasensitive Nonisotopic Detection", **Science** 281 (1998) pp. 2016-2018.
- [22] Arya, H. et al.: "Quantum dots in bio-imaging: Revolution by the small", **Biochemical and Biophysical Research Communications** 329 (2005) pp. 1173-1177.
- [23] Medintz, I.L. et al.: "Quantum dot bioconjugates for imaging, labelling and sensing", **Nature Materials** 4 (2005) pp. 435-446.
- [24] Nolan, J.P. et al.: "Multiplexed and microparticle-based analyses: Quantitative tools for the large-scale analysis of biological systems", **SO: Cytometry Part A** 69A (2006) pp. 318-325.
- [25] Han, M. et al.: "Quantum-dot-tagged microbeads for multiplexed optical coding of biomolecules", **Nature Biotechnology** 19 (2001) pp. 631-635.
- [26] Cao, Y.C. et al.: "Preparation of silica encapsulated quantum dot encoded beads for multiplex assay and its properties", **Analytical Biochemistry** 351 (2006) pp. 193-200.
- [27] Wang, H.Q. et al.: "Multi-color encoding of polystyrene microbeads with CdSe/ZnS quantum dots and its application in immunoassay", **Journal of Colloid and Interface Science** 316 (2007) pp. 622-627.
- [28] Liu, S. et al.: "Synthesis and characterization of iron oxide/polymer composite nanoparticles with pendent functional groups", **Colloids and Surfaces B: Biointerfaces** 51 (2006) pp. 101-106.
- [29] Jo, S. et al.: "Synthesis and Characterization of Oligo(poly(ethylene glycol) fumarate) Macromer", **Macromolecules** 34 (2001) pp. 2839-2844.
- [30] Brunner, A. et al.: "Labelling peptides with fluorescent probes for incorporation into degradable polymers", **European Journal of Pharmaceutics and Biopharmaceutics** 45 (1998) pp. 265-273.
- [31] Reithmeier, H. et al.: "Lipid microparticles as a parenteral controlled release device for peptides", **Journal of Controlled Release** 73 (2001) pp. 339-350.
- [32] International Organisation of Standardisation: "ISO 10993, Biocompatibility of medical devices. Part 5. Test for cytotoxicity: in vitro methods"; Geneva, (1992)
- [33] Torrente, M.: "*Biomaterial-Cell interactions of hydrogelas and particulate delivery systems*"; University of Padua (2008)
- [34] Kang, Y. et al.: "Characterization and Biological Evaluation of Paclitaxel-Loaded Poly(L-lactic acid) Microparticles Prepared by Supercritical CO<sub>2</sub>", **Langmuir** (2008).
- [35] Katti, D.: "Preparation of albumin microspheres by an improved process", **Journal of Microencapsulation** 16 (1999) pp. 231-242.
- [36] Mallarde, D. et al.: "PLGA-PEG microspheres of teverelix: influence of polymer type on microsphere characteristics and on teverelix in vitro release", **International Journal of Pharmaceutics** 261 (2003) pp. 69-80.
-

- [37] Sato, T. et al.: "Porous Biodegradable Microspheres for Controlled Drug Delivery. I. Assessment of Processing Conditions and Solvent Removal Techniques", **Pharmaceutical Research** 5 (1988) pp. 21-30.
- [38] Mok, H. et al.: "Water-free microencapsulation of proteins within PLGA microparticles by spray drying using PEG-assisted protein solubilization technique in organic solvent", **European Journal of Pharmaceutics and Biopharmaceutics** 70 (2008) pp. 137-144.
- [39] Carrasquillo, K.G. et al.: "Non-aqueous encapsulation of excipient-stabilized spray-freeze dried BSA into poly(lactide-co-glycolide) microspheres results in release of native protein", **Journal of Controlled Release** 76 (2001) pp. 199-208.
- [40] O'Donnell, P.B. et al.: "Preparation of microspheres by the solvent evaporation technique", **Advanced Drug Delivery Reviews** 28 (1997) pp. 25-42.
- [41] Wischke, C. et al.: "Principles of encapsulating hydrophobic drugs in PLA/PLGA microparticles", **International Journal of Pharmaceutics** 364 (2008) pp. 298-327.
- [42] Blanco, D. et al.: "Protein encapsulation and release from poly(lactide-co-glycolide) microspheres: effect of the protein and polymer properties and of the co-encapsulation of surfactants", **European Journal of Pharmaceutics and Biopharmaceutics** 45 (1998) pp. 285-294.
- [43] Herrmann, J. et al.: "Biodegradable, somatostatin acetate containing microspheres prepared by various aqueous and non-aqueous solvent evaporation methods", **European Journal of Pharmaceutics and Biopharmaceutics** 45 (1998) pp. 75-82.
- [44] Hombreiro Pérez, M. et al.: "The preparation and evaluation of poly([epsilon]-caprolactone) microparticles containing both a lipophilic and a hydrophilic drug", **Journal of Controlled Release** 65 (2000) pp. 429-438.
- [45] Chung, Y.Y.H.: "Microencapsulation of gentamicin in biodegradable PLA and/or PLA/PEG copolymer", **Journal of Microencapsulation** 18 (2001) pp. 457-465.
- [46] Ruan, G. et al.: "Preparation and characterization of poly(lactic acid)-poly(ethylene glycol)-poly(lactic acid) (PLA-PEG-PLA) microspheres for controlled release of paclitaxel", **Biomaterials** 24 (2003) pp. 5037-5044.
- [47] Rafati, H. et al.: "Protein-loaded poly(-lactide-co-glycolide) microparticles for oral administration: formulation, structural and release characteristics", **Journal of Controlled Release** 43 (1997) pp. 89-102.
- [48] Berkland, C. et al.: "Microsphere size, precipitation kinetics and drug distribution control drug release from biodegradable polyanhydride microspheres", **Journal of Controlled Release** 94 (2004) pp. 129-141.

# **Chapter 7**

## **Overall summary and conclusions**



## 1. Overall summary

Covering a wide range of different sizes and structures particulate drug carriers represent highly sophisticated systems, which are designed to enable control of the carriers' biodistribution, its targeting abilities and also its release kinetics or mechanisms, thereby improving the overall performance in therapeutic or diagnostic issues. Despite the fact that particulate systems are in the focus of research since several decades, there is still a tremendous further development going on in order to get deeper insight in particle formation and distribution. In this context fluorescence based analyses offer an irreplaceable analytical tool to gain more insight into the characteristics and underlying mechanisms, which is essential for the adaption of the particle preparation and their further improvement.

Main focus of this thesis was to provide a versatile pool of particulate systems, which proved to be applicable in different fluorescence imaging applications ranging from *in-vitro* investigations to cell culture testing or small animal applications.

Based on a simple and very gentle phase separation method, the nanoprecipitation, a system for the reproducible production of polymeric nanoparticles within the size range of 50 to 250 nm was established (**Chapter 2**). A thorough evaluation of several impact factors on particle formation, allowed to provide a toolbox, which was suitable to adjust the desired particle properties (i.e. size and surface characteristics) by choosing a certain biodegradable polymer (either PLGA, mPEG-PLA or NH<sub>2</sub>PEG-PLA) in combination with definite preparation parameters, e.g. the polymers' molecular weight, polymer concentration, solvent and non-solvent system and the used solvents' volume ratio. Generally, the influence of the different impact factors differed significantly for different polymers, which certainly requires similar investigations for every new polymer. In addition to the most commonly used aqueous preparation route (acetone/water) also a non-aqueous procedure (chloroform/ethanol) was established and thoroughly characterized, overcoming the limitations of nanoprecipitation for the encapsulation of lipophilic compounds.

The as prepared polymeric nanoparticles were furthermore successfully applied for *in-vitro* as well as *in-vivo* imaging purposes, following an encapsulation of lipophilic fluorescence dyes, using either Nile Red or DiR as model compounds (**Chapter 3**). Interestingly, the impact of 'drug' loading on particles' properties was found to be almost negligible, indicating a very homogenous distribution or even dissolution of the dye within the polymer matrix.

A comparison of the imaging results obtained with these differing systems (Nile red vs. DiR loading), however, indicates the limitations of the Nile red loaded system (a "bleeding"

of dye into other surrounding lipophilic areas and the strong quenching of Nile reds' *in-vivo* fluorescence by endogenous compounds). These dye inherent limitations were successfully overcome by exchanging Nile Red for the much more lipophilic near-infrared dye DiR. The DiR loaded nanoparticles proved to be an ideal tool, especially for *in-vivo* applications, allowing the imaging of whole body particle distributions as well as the imaging of deeper tissue regions due to the much higher tissue penetration of the near-infrared light.

The second part of the thesis was focused on the establishment of quantum dots as alternative solid crystalline marker substances for the fluorescence imaging of particulate drug delivery systems.

At first, CdSe quantum dots with desirable maximum emission wavelengths of about 610 nm were synthesized (**Chapter 4**). Their native optical properties as well as stability were successfully improved by adapting the synthesis duration, the purification methods or by addition of a post-synthesis surface coating of a lipophilic organic ligand. These improvements provided a bright fluorescing stable marker system, which should be applicable for further processing or encapsulation steps. Standardised synthesis methods were defined, which were dependent on the intended application of the respective quantum dots.

The established non-aqueous nanoprecipitation process in general was found to be also an appropriate method for the preparation of small, monodisperse, quantum dot loaded nanoparticles (**Chapter 5**). Actually, their applicability as fluorescent imaging system was limited due to a high loss in their optical quality, like quantum yield and the subsequent fluorescence intensity. However, critical process steps could be identified and the problematic interference of the used solvents and matrix materials with the QD surface coatings was discussed, now allowing a constant further improvement of this promising system. Especially the application of quantum dot batches with initially much higher optical quality and different surface coating, as proven by commercially obtained nanocrystals, would be an initial step towards an enhanced fluorescence of the labelled nanoparticles.

Finally, also the fluorescence labelling of microparticulate systems with custom-made lipophilic quantum dots was successfully established. Here the commonly available particle preparation methods, solvent evaporation and melt dispersion techniques, were investigated (**Chapter 6**). The characteristics of the labelled particles, especially the morphology and intraparticulate QD distribution, were found to strongly depend on the initial optical quality and coating of the used quantum dots, but moreover on the interaction of the used matrix material with the applied quantum dot surface ligands. Besides the application of QDs as a model compound for crystalline non-soluble drug

compounds the accordingly labelled microparticles could be successfully used as stable fluorescence marker system for long-term investigations of hybrid drug delivery systems or eventually *in-vivo* applications of microparticulate carriers.

## 2. Conclusions and Outlook

In conclusion, the developed particulate drug delivery systems could be successfully applied for differing fluorescence imaging purposes. However, it also was demonstrated that the development and preparation of ideally monodisperse, fluorescently labelled particles for the investigation of *in-vivo* transport phenomena is a quite difficult task, which has to overcome several still persisting obstacles.

Starting from the establishment of uniform nanoparticles and their loading with lipophilic dyes it became obvious that their permanent fixation within the small nanoparticles is especially challenging in cellular context and *in-vivo* environment. Once sufficiently optimized, the nanoparticulate systems established within this thesis, were successfully applied for investigation of passive drug targeting processes in small animals (**Fig. 1**).

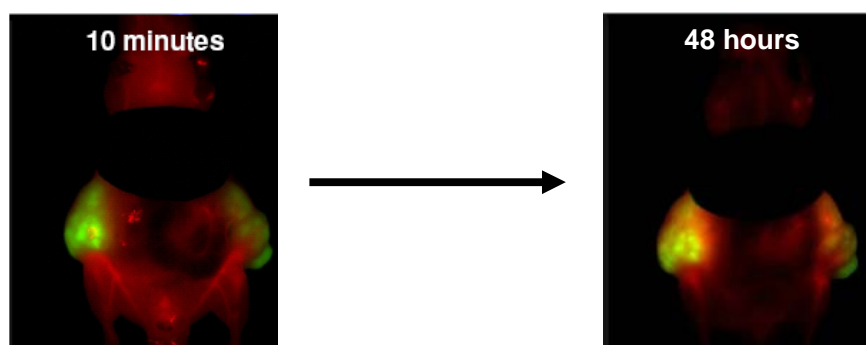


**Fig. 1:** Co-localization fluorescence signal of a DsRed<sub>2</sub> expressing subcutaneous coloncarcinoma (green fluorescence) and DiR (red fluorescence) after 48 h following i.v. administration of DiR loaded NPs in mice

An alternative set of particles (nano- and microscaled) was prepared, exchanging the low molecular weight dyes for inorganic fluorophores, the quantum dots. Quantum dots in general are known to be attractive alternatives for most commonly used organic fluorescence dyes and are already established in the field of diagnostics or diagnostical imaging. This work demonstrates their great potential also for future applications in the development of sophisticated and complex particulate drug delivery systems.

However, despite their described advantages, like the optical properties and the particulate character, one has to keep in mind the still to overcome photolability during the performed encapsulation processes and their intrinsic toxicity, which certainly hampers *in-vivo* diagnostics. There is a tremendous need for “high-quality” quantum dots with

improved surface coatings to guarantee increased photostability and reduced or better eliminated toxicity, which certainly can be achieved by adapted synthesis parameters or additional post-synthesis treatments, as demonstrated in a recently finished PhD thesis [1].

Adaption or even tailoring of the QDs surface properties would furthermore allow using them as a versatile model for different hydrophilic and lipophilic drug compounds to be incorporated in the particulate systems. At least the *in-vitro* investigation of low-soluble or in-soluble compounds might provide a deeper insight in the formation and also the release of newly developed drug delivery systems. Thus the quantum dots can participate in the development of better drug delivery systems and more successful therapy, even during non-toxic *in-vitro* studies.

Besides the potential perspectives of the established delivery systems, the obtained results point out the necessity for each researcher to pay special attention to the careful interpretation of experimental data and the choice of an appropriate set-up of analytical methods. It was found especially for the particulate DDS that they are quite sensitive to even slight changes in their preparation (e.g. within the preparation method or encapsulated compound). Therefore, once obtained results for the encapsulation of one specific drug compound could hardly be generalized, and need to be verified with every change to a new system. Overall, the investigation of model compounds provide only a small assistance on the way to improved drug delivery systems, but certainly help to better visualize and understand the formation and performance of particulate delivery systems.



### **3. References**

- [1] Hezinger, A. F. E.: "Biocompatible inorganic nanocrystals for fluorescence and CT imaging"; University of Regensburg (2010).



# **Appendix A**

## **Characterization of biodegradable copolymers**



## 1. Methods

### 1.1 $^1\text{H}$ -NMR Spectroscopy

About 30 mg of each synthesized polymer were dissolved in 1 ml  $\text{CDCl}_3$ . The  $^1\text{H}$ -NMR spectra were taken at 250.13 MHz with tetramethylsilane (TMS) as internal standard using a Bruker AC250 spectrometer with dual sample head and an autosampler (Bruker, Rheinstetten, Germany). For the detection of the primary amine group of the polymer spectra were taken after addition 100  $\mu\text{l}$  TFA to allow acylation of the amine and hydroxyl end group.

### 1.2 Gel permeation chromatography

Gel permeation chromatography was used for estimation of the molecular weight of the synthesized polymers. Samples were prepared by dissolving about 10 mg of each polymer in 2 ml chloroform followed by filtration through a 0.2  $\mu\text{m}$  chloroform resistant regenerated nitrocellulose membrane filter to remove particulate impurities. As stationary phase served a combination of a 5  $\mu\text{m}$  particle size Phenogel<sup>®</sup> pre-column (50 x 7.8 mm) with an analytical column Phenogel<sup>®</sup> Linear(5) (separation range 100 to 10.000 kDa; both Phenomenex, Torrance, CA).  $\text{CHCl}_3$  with a flow rate of 1.0 ml/min was used a mobile phase. Chromatograms were recorded on a 10A<sup>VP</sup> HPLC system (Shimadzu, Duisburg, Germany). The columns were kept at 35 °C using a CTO-10AC<sup>VP</sup> column oven (Shimadzu, Duisburg, Germany). After injection of 50  $\mu\text{l}$  sample solution, signals were recorded by a RID 10A refractive index detector (Shimadzu, Duisburg, Germany).

Molecular weight of the polymer sample were calculated from the retention time of polystyrene standards with narrow size distribution (Polymer laboratories, Darmstadt, Germany) using the Class VP software version 5.0.

### 1.3 Modulated differential scanning calorimetry

Thermal behaviour of all used polymers, expressed by their glass transition temperature ( $T_G$ ), was investigated by modulated differential scanning calorimetry [MDSC] on a DSC 2920 equipped with refrigerated cooling system and an autosampler (TA Instruments, Alzenau, Germany). Samples were prepared by weighing of about 3 mg of each polymer in aluminium sample pans, which were afterwards sealed using the TA Instruments sample encapsulating press. An empty sealed pan served as reference.

For determination of  $T_G$  the following protocol was used: first, both sample and reference were equilibrated at -45 °C for 5 min. Samples were heated up from -40 °C to 80 °C at a

heating rate of 2 °C/min, using a sinusoidal temperature modulation with a period of 60 s and temperature amplitude of 0.32 °C. After retaining the temperature at 80 °C for 5 min, the sample were cooled to -45 °C at a cooling rate of 2 °C/min. As relaxation phenomena are less pronounced after the first heating and cooling cycle, the  $T_G$  was determined from a second heating run, which was carried out using the same sinusoidal temperature modulation. After 5 min isothermal phase the temperature was raised at a rate of 2 °C/min to heat sample and reference from -45 to 80 °C. Thermograms were analyzed for  $T_G$  (obtained as half height of the transition) with the Thermal Advantage software provided with the MDSC system.

## 2. Results

### 2.1 $^1\text{H}$ NMR Spectroscopy

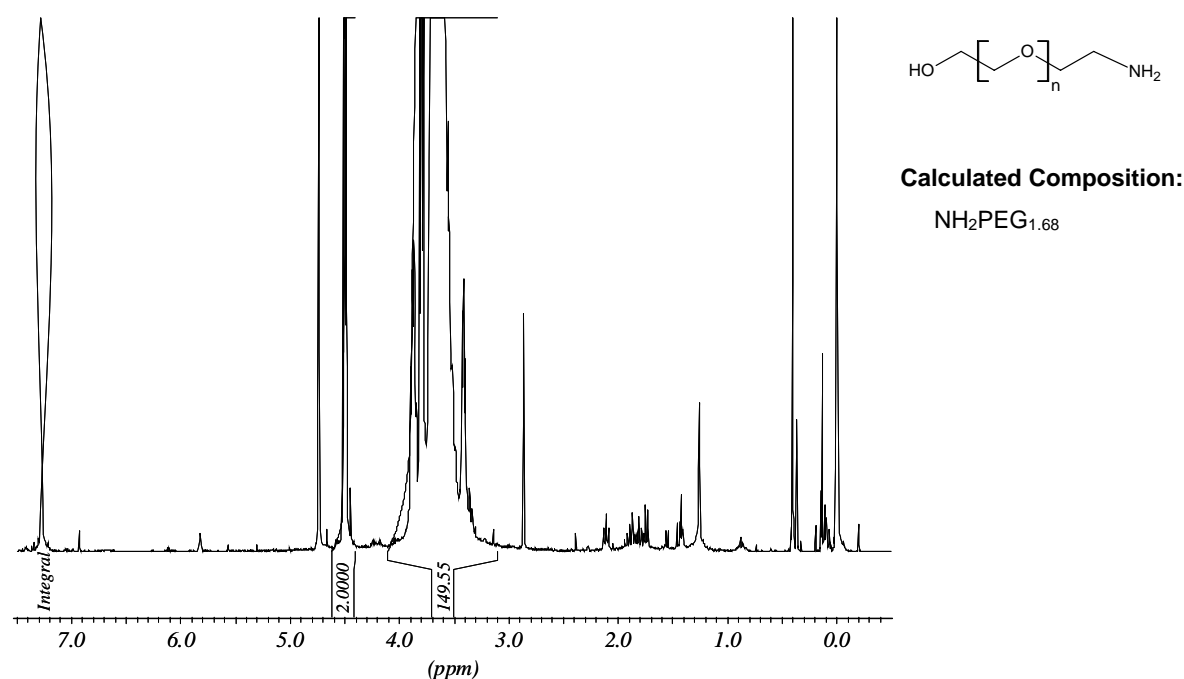


Fig. 1:  $^1\text{H}$ -NMR spectrum of  $\text{NH}_2\text{PEG}_{2000}$  in  $\text{CDCl}_3$  after acylation with TFA

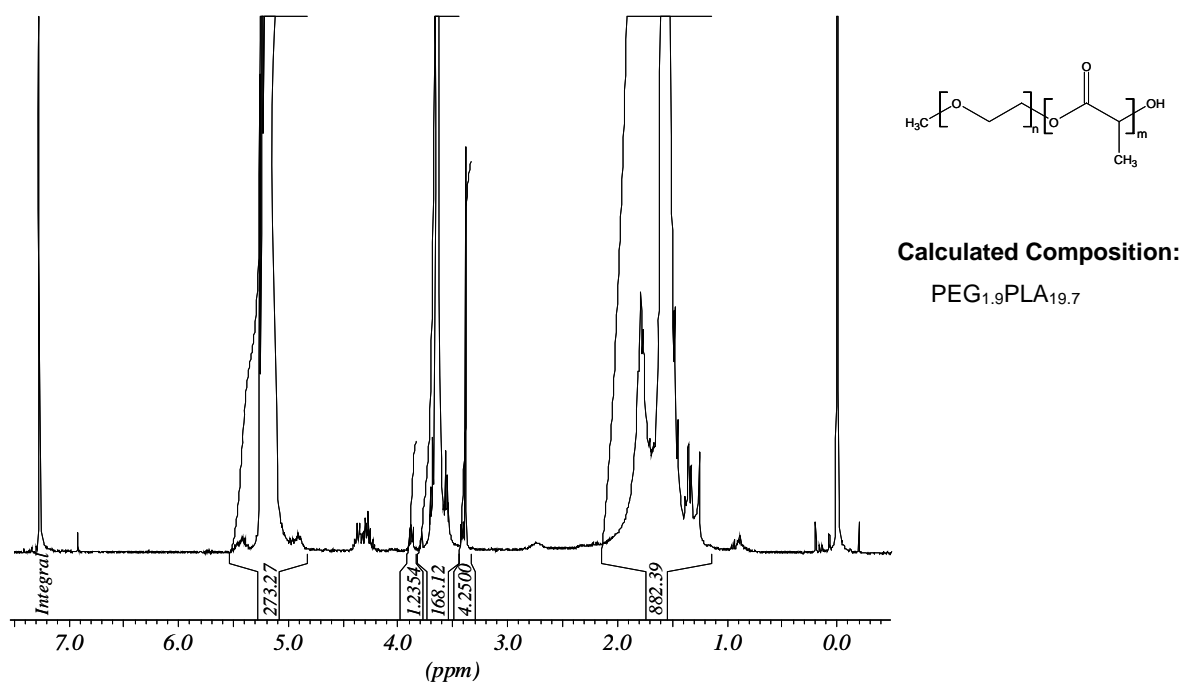


Fig. 2: <sup>1</sup>H-NMR spectrum of PEG<sub>2</sub>PLA<sub>20</sub> in CDCl<sub>3</sub>

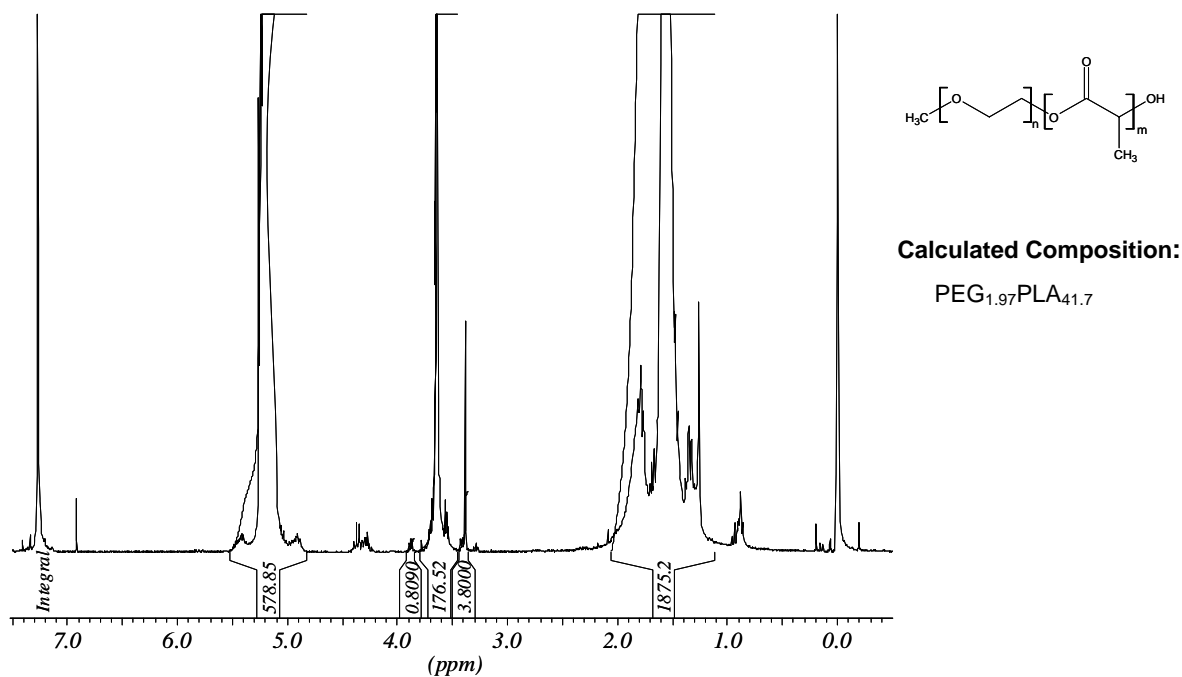


Fig. 3: <sup>1</sup>H-NMR spectrum of PEG<sub>2</sub>PLA<sub>40</sub> in CDCl<sub>3</sub>

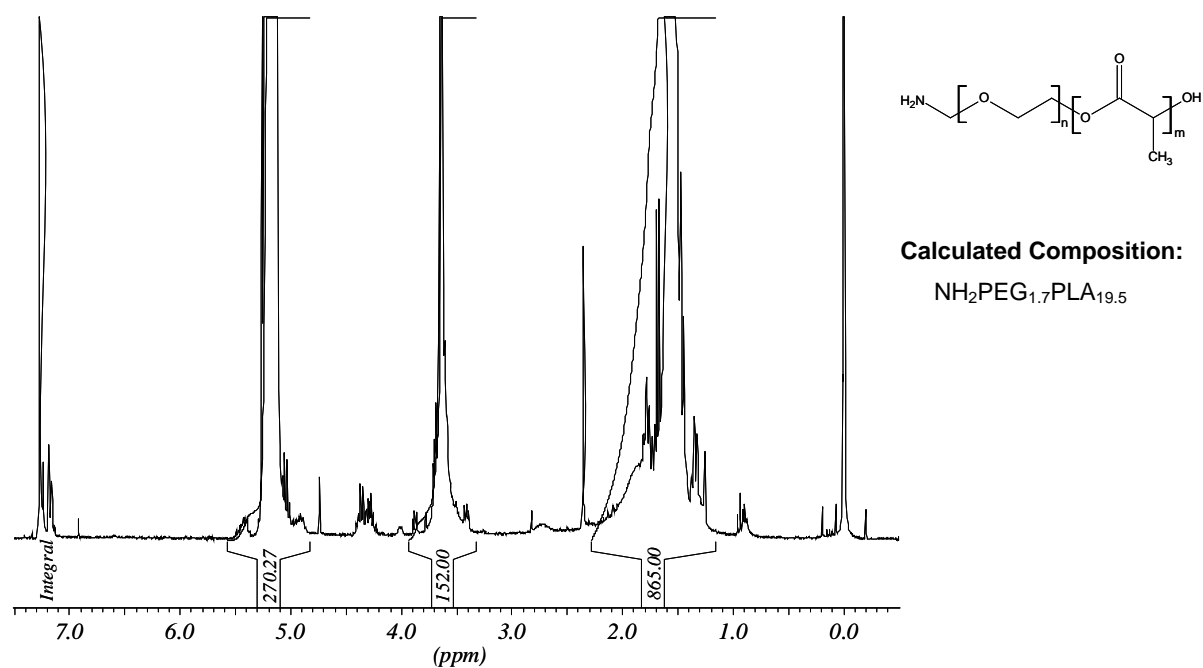


Fig. 4:  $^1\text{H}$ -NMR spectrum of  $\text{NH}_2\text{PEG}_2\text{PLA}_{20}$  in  $\text{CDCl}_3$

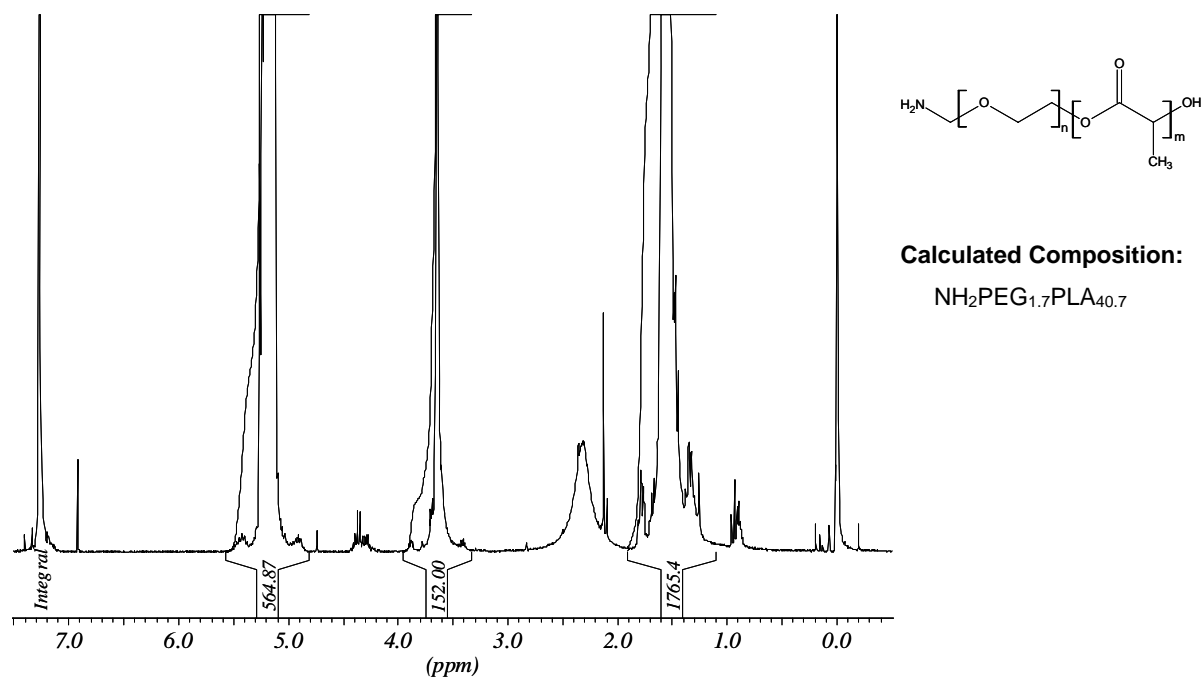
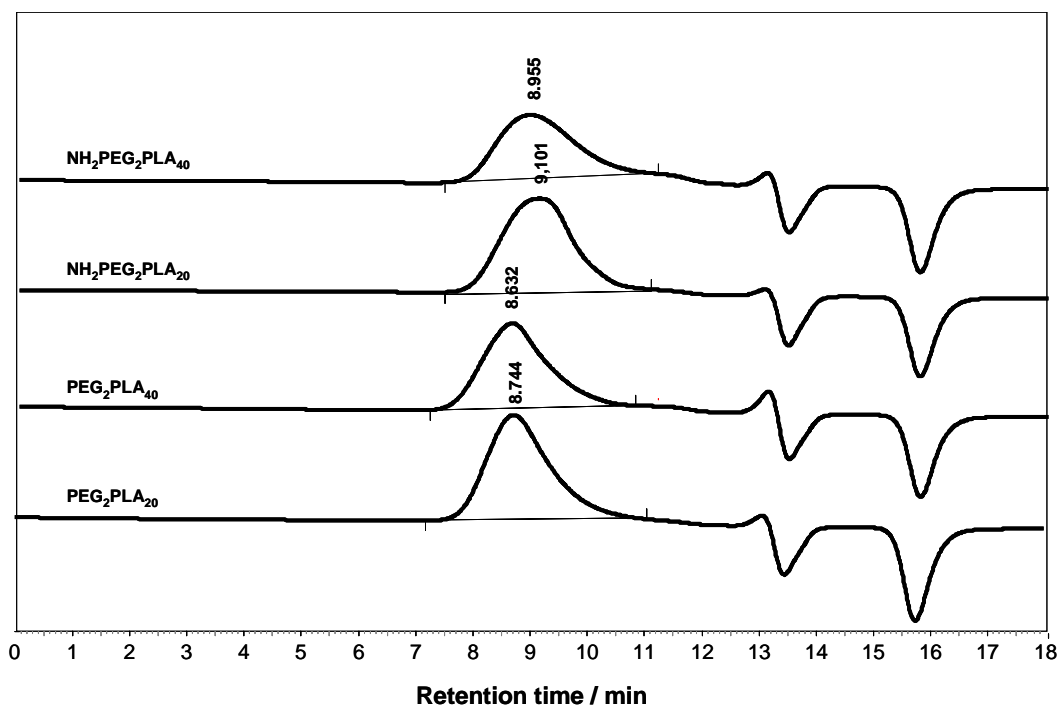


Fig. 5:  $^1\text{H}$ -NMR spectrum of  $\text{NH}_2\text{PEG}_2\text{PLA}_{40}$  in  $\text{CDCl}_3$



## 2.2 Gel permeation chromatography



**Fig. 6:** GPC chromatograms and retention times of custom-made diblock copolymers

**Tab. 1:** Molecular weights of custom-made polymers – calculated based on retention times

Polymer	Retention time / min	expected MW / kDa	calculated MW / kDa
NH <sub>2</sub> PEG <sub>2000</sub>	10.272	2	2.07
PEG <sub>2</sub> PLA <sub>20</sub>	8.744	22	23.77
PEG <sub>2</sub> PLA <sub>40</sub>	8.632	42	45.33
NH <sub>2</sub> PEG <sub>2</sub> PLA <sub>20</sub>	9.101	22	16.83
NH <sub>2</sub> PEG <sub>2</sub> PLA <sub>40</sub>	8.955	42	23.16

## 2.3 Modulated differential scanning calorimetry

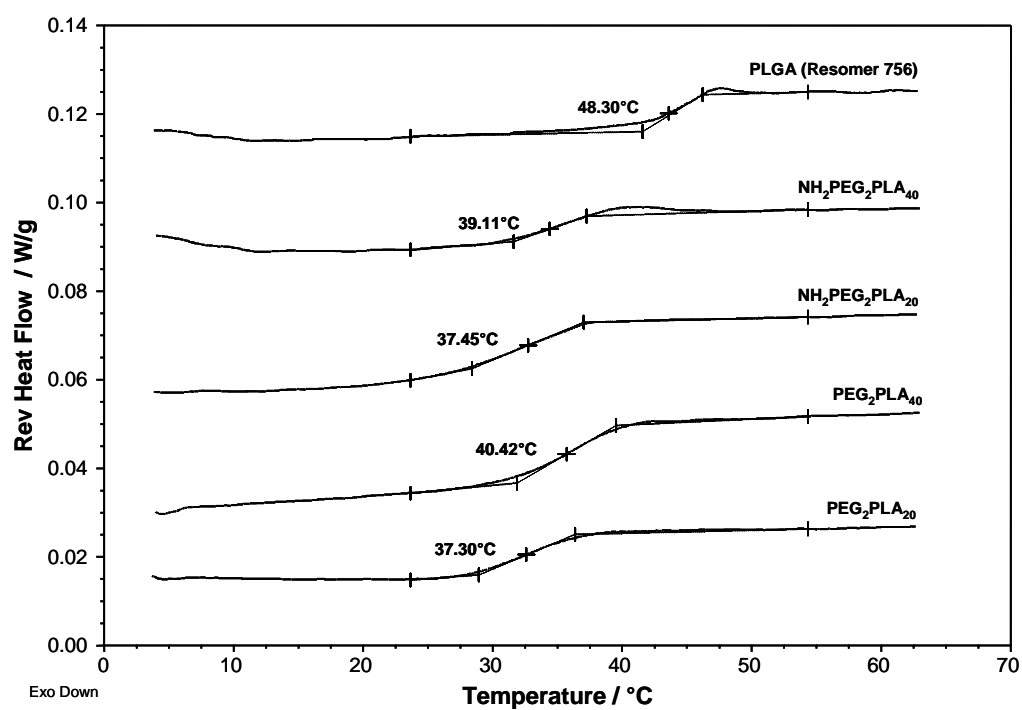


Fig. 7: Reversed heat flow thermograms of used/ synthesized polymers with calculated  $T_G$

# **Appendix B**

## **Characterization of dispersion media**



## 1. Methods

### 1.1 Preparation of dispersion media

At first stock solutions of all stabilizing agents (sucrose, glucose, Pluronic F68 and PVA) in purified water were prepared. The media with exact concentrations over the intended concentration range were prepared by appropriate dilution with purified water. For all investigations media were pre-conditioned to 20 °C.

### 1.2 Determination of refractive index

Refractive indices  $n$  were determined at 20 °C using a temperature-controlled Abbé refractometer. Purified water, with a refractive index of 1.33 was used as control liquid. Results will be given at mean values of triplicate measurements.

### 1.3 Determination of density

Densities of solutions (at 20 °C) were determined using calibrated glass pycnometers. Calibration volumes  $V_c$  of the used pyknometers were given with 51.712 cm<sup>3</sup> and 51.870 cm<sup>3</sup>. Pyknometer weight was determined in empty (clean and dry) and filled state and density was calculated according to the following equation:

$$\rho \left[ \frac{\text{g}}{\text{cm}^3} \right] = \frac{m_f - m_n}{V_c};$$

with density  $\rho$  [g/cm<sup>3</sup>], the pyknometers weight filled with the respective medium  $m_f$  [g]; the pyknometers' net weight  $m_n$  [g] and its calibrated volume  $V_c$  [cm<sup>3</sup>].

### 1.4 Dynamic viscosity

Kinematic viscosity  $\nu$  of solutions of sucrose, glucose and Pluronic F68 was measured using an Ubbelodhe capillary viscosimeter (PVS®; LAUDA DR. R. Wobser GmbH & CO. KG, Lauda-Königshofen, Germany), equipped with an capillary No. I (nominal capillary constant=0.01). During the measurement temperature was maintained at 20 °C using a temperature controlled water-bath (Lauda E 100; LAUDA DR. R. Wobser GmbH & CO. KG, Lauda-Königshofen, Germany).

Dynamic viscosity  $\eta$  of each solution was subsequently calculated according to the following equation:

$$\eta = \nu * \rho;$$

with the dynamic viscosity  $\eta$  [cP=mPas], the kinematic viscosity  $\nu$  [cSt=mm<sup>2</sup>/s] and the solutions' density  $\rho$  [g/cm<sup>3</sup>]. The results will be given mean of quadruplicate measurements

Dynamic viscosity of solutions of the high molecular weight polymer PVA (Mowiol® 40-88) was calculated based on the following empirical equation [1]:

$$\eta = 1.4197 * e^{0.8455 * c};$$

with the dynamic viscosity  $\eta$  [cP=mPas] and the concentration of the PVA in solution  $c$  [%].

## 2. Results

Dispersion medium Concentration	Refractive index $n$	Density $\rho$ / g/cm <sup>3</sup>	Dyn. viscosity $\eta$ /cP
Sucrose			
0.5 %	1.330	0.999 (~1)	1.00
5.0 %	1.337	1.018	1.13
10 %	1.345	1.025	1.30
20 %	1.359	1.084	1.90
Glucose			
0.5 %	1.330	0.996 (~1)	1.00
5.0 %	1.336	1.014	1.12
10 %	1.343	1.033	1.27
20 %	1.357	1.069	1.69
Pluronic F68			
0.1 %	1.330	0.997	1.00
0.5 %	1.330	0.998	1.00
1.0 %	1.331	0.977	1.16
1.5 %	1.332	0.999	1.28
PVA			
1 %	1.331	-	3.31
1.5 %	1.332	-	5.05
2.5 %	1.333	-	11.75

### 3. References

- [1] Kuraray Europe GmbH: "*Mowiol - Technical data sheet*"; (2007)





# Appendix C



## Curriculum Vitae

Name	Cornelia Rose
Date of birth	November 21 <sup>st</sup> , 1980
Place of birth	Bad Salzungen / Thuringia
Nationality	German
Marital status	Single

---

### Work experience

Since 11/2009	SocraTec CSC GmbH/ Oberursel Research assistant and project manager
10/2005-10/2009	PhD thesis at University of Regensburg, Department of Pharmaceutical Technology Thesis: <b><i>“Particulate systems for fluorescence imaging and drug delivery”</i></b>
02/2005 – 09/2005	Hospital pharmacy of “Südharz-Krankenhaus”, Nordhausen

---

### University

01/2005	License as pharmacist
06/2004 – 11/2004	Traineeship at pharmacy, “Arcisapotheke”/ Munich
07/2004	Degree of “Diplom Pharmazeut”
11/2003 – 05/2004	Diploma thesis at Ernst-Moritz-Arndt University, Greifswald, Department of Pharmaceutical Technology Thesis: <b><i>„Untersuchung zu Erosions- und Quellungsfront in HPMC-basierten Tabletten“</i></b>
1999-2004	Studies of pharmacy at Ernst-Moritz-Arndt University/ Greifswald

---

### School education

1999	Diploma from German secondary school qualifying for university admission or matriculation
1991 – 1999	„Wilhelm von Humboldt - Gymnasium“/ Nordhausen



## List of Publications

### Poster Presentations

A. Schädlich, C. Rose, J. Kuntsche, H. Caysa, T. Müller, A. Göpferich, K. Mäder: "In vivo and ex vivo studies of PEG-PLA block copolymer nanoparticles for tumor visualization and treatment" **DPHG Joint Meeting**, Braunschweig (D), (2010).

A. Schädlich, C. Rose, J. Kuntsche, T. Müller, A. Göpferich and K. Mäder: "In vivo studies of PEG - PLA block copolymer nanoparticles for the visualisation of colon carcinoma". **8<sup>th</sup> International Symposium on Polymer Therapeutics: From Laboratory to Clinical Practice**, Valencia (Sp), (2010).

A. Schädlich, C. Rose, J. Kuntsche, T. Mueller, A. Göpferich, K. Mäder: "In vivo fate and tumor targeting studies of new synthesized PEG - PLA blockcopolymer nanoparticles using non invasive fluorescence imaging" **7<sup>th</sup> World Meeting on Pharmaceutics and Biopharmaceutics and Pharmaceutical Technology**, Malta (M), (2010)

M. Henke, C. Rose, A. Goepferich, J. Tessmar: "Covalently cross-linked hydrogel foams as 3D-mounting media for particles or cells". **22<sup>nd</sup> European Conference of Biomaterials**, Lausanne (CH), (2009).

J. Tessmar, A.F.E. Hezinger, G. Zayed, B. Kosog, C. Rose, A.M. Göpferich: "Nanoparticulate detection systems for the evaluation of New Drug Delivery Approaches and Drug Targeting principles". **World Congress on Medical Physics and Biomedical Engineering**, Munich (D), (2009).

C. Rose, A.Goeperich, and J.K.Tessmar: "Establishment of an anhydrous preparation method for polymeric nanoparticles loaded with fluorescent dyes and nanocrystals". **36<sup>th</sup> Annual Meeting of the Controlled Release Society**, Copenhagen (DK), (2009).

W. Hild, K. Zenger, C. Rose, A. Hezinger, J. Teßmar, A. Göpferich: „Towards the optimization of quantum dot preparation for use in biological systems". **NaNaX 3**, Lecce (I), (2008).

C. Rose, A. Hezinger, C. Becker, J. Teßmar, A. Göpferich: "Imaging of particulate delivery systems - Quantum dots as sensitive fluorescent probes". **DPHG Joint Meeting**, Erlangen (D), (2007).

C. Rose, A. Hezinger, C. Becker, J. Teßmar, A. Göpferich: „Quantum Dots as tool for the long-term imaging of particulate drug delivery systems". **34<sup>th</sup> Annual Meeting of the Controlled Release Society**, Long Beach (California), (2007).

C. Rose, J. K. Tessmar, A. M. Goepferich: "Investigation of nanoparticle distribution inside formed microparticles using Quantum Dots". **PARTEC**, Nürnberg (D), (2007).

### Oral presentations

C. Rose, A. Hezinger, C. Becker, J.Tessmar, A. Goepferich: "Quantum Dots – fluorescent markers for particulate delivery systems." **German Chapter of the Controlled Release Society**, Freiburg i. Brsg. (D), (2007).



## Acknowledgements

At this point I would like to thank all persons supporting me and thus contributing to the success of this thesis.

First of all, I wish to express my gratitude to **Prof. Dr. Achim Göpferich** for offering the opportunity to prepare this thesis at his department, for ongoing discussions, the permanent encouragement to challenge once obtained results and for his support to present own results at national and international conferences.

I am deeply indebted to my supervisor **Dr. Jörg Teßmar** for almost everything – the ongoing discussions during the practical work, his patience, his continued encouragement and support, especially during the “hard times” of writing and for knowing at least something about nearly everything.

I would like to thank **Dr. Torsten Blunk** for continued discussions and his ongoing effort in changing the point of view of a very critical person.

I am very grateful to **Dr. Harald Huber** (Department for Microbiology, University of Regensburg) for offering the opportunity for ICP-OES measurements and his support in all related concerns and problems and to **Angelika Kühn** (Department of Zoology, University of Regensburg) for providing the TEM equipment.

I will sincerely thank **Klaus Pollinger** for the support during cellular uptake studies and **Matthias Henke** for providing the OPF hydrogels for investigation of complex DDS.

Special thanks go to **Andreas Schädlich** and **Prof. Dr. Karsten Mäder** (Department of Pharmaceutical Technology, Martin-Luther University, Halle-Wittenberg) for many fruitful discussions and the performance of small animal fluorescence imaging making me “see and not just believe”.

Just for being the best lab colleagues one could have I want to thank **Anna Hezinger** and **Annina Seitz** – for all scientific and non-scientific discussions and the time spent together inside and outside the lab.

I want to thank all technical assistants of the department for simplifying our everyday life, providing ongoing support and sharing their long-time experiences. Special thanks go to **Angelika Berié** for spending hours of life together with me during fascinating ICP-OES and SEM measurements.

Although not mentioned in detail, I am very grateful to all my former and present colleagues at the department creating an atmosphere of friendship, open to ongoing discussions and support. – One do not need to know everything, but who to ask for.

Finally I wish to thank my family and all my friends for providing never-ending support, believing and reminding me of the life besides and after the thesis.

This thesis has partly been supported by the **BMBF “NanoforLife”** project “*Nanogel*” and the **Bayer Schering Pharma AG**. Their support is gratefully acknowledged.



## Erklärung

Ich versichere, dass ich die vorliegende Dissertation mit dem Titel "*Particulate systems for fluorescence imaging and drug delivery*" selbstständig verfasst und keine anderen Hilfsmittel als die angegeben verwendet habe. Die Stellen, die anderen Werken dem Wortlaut oder Sinn nach entnommen sind, habe ich in jedem Fall durch Angabe der Quelle kenntlich gemacht.

Regensburg, den

---

Cornelia Rose



